Electroweak Input Schemes in the Standard Model Effective Field Theory

SMITH, TOMMY

Electroweak Input Schemes in the Standard Model Effective Field Theory

Tommy Smith

A Thesis presented for the degree of
Doctor of Philosophy

Institute for Particle Physics Phenomenology
Department of Physics
Durham University
United Kingdom

May 2024

Electroweak Input Schemes in the Standard Model Effective Field Theory

Tommy Smith

Submitted for the degree of Doctor of Philosophy

May 2024

Abstract: We consider the use of different electroweak input schemes in the Standard Model Effective Field Theory (SMEFT). First, we provide a review of the implementation of three commonly used input schemes in the literature, detailing the definitions of counterterms and present analytic formulas. An analysis of these three schemes follows, where we discuss general features and provide benchmark numerical results for heavy boson decays in each of the schemes at next-to-leading order (NLO) in the dimension-six SMEFT. Exploring the sensitivity to Wilson coefficients and perturbative convergence of different schemes, we show that the pattern of convergence is more complicated than in the Standard Model, yet the large-m_t limit provides a valid approximation to the largest corrections. Using a benchmark process of the W boson decay to leptons, a set of universal corrections are defined on the leading order results. Remaining NLO corrections thus become of a similar size between schemes.

Secondly, we develop the necessary theoretical machinery to define two new input schemes for the SMEFT. These involve the effective weak mixing angle as an input parameter. Again, we provide definitions and formulas for the counterterms. We analyse a set of precision observables to find an attractive feature of the two schemes

is that large correction from top loops appearing in other schemes are absorbed into the definition of the weak mixing angle. Conversely, this same renormalisation condition undesirably introduces numerous flavour specific couplings between the Z boson and charged leptons, motivating a need for flavour assumptions for any practical application. Once more, a large-m_t analysis provides a good approximation, in most instances, to the full NLO results, allowing for the largest scheme dependent corrections to be understood. However, the non-trivial pattern of perturbative convergence across all the schemes is remarked on, and examples of prefactors multiplying different Wilson coefficients in multiple schemes are given, highlighting the influence and importance of the scheme choice in precision electroweak calculations.

Contents

Abstract **iii**

List of Figures **ix**

List of Tables **xi**

List of Abbreviations **xv**

1 The Standard Model **1**

1.1 The Standard Model Lagrangian 1

1.1.1 Gauge 2

1.1.2 Higgs 3

1.1.3 Fermion 7

1.1.4 Assumptions on the Lagrangian 11

1.2 Calculations in the Standard Model 12

1.2.1 Loop Diagrams 14

1.2.2 UV Renormalisation 16

1.2.3 IR safety 20

1.2.4 Renormalisation Group 21

2 The Standard Model Effective Field Theory 25

2.1 Effective Field Theories 25

2.1.1 Introduction to Effective Field Theories 26

2.2 The Standard Model Effective Field Theory 29

2.2.1 Changes to SM Electroweak parameters 32

2.2.2 Operator renormalisation 36

3 Preliminary Information 41

3.1 Motivation 41

3.2 Assumptions and Work Flow 44

3.2.1 Lagrangian Assumptions and Flavour Scenarios 44

3.2.2 Work Flow 47

4 Schemes in the SMEFT Literature 49

4.1 The α Scheme 50

4.2 The α_μ Scheme 53

4.2.1 Relation to the α scheme 59

4.3 The LEP Scheme 60

5 Analysis of Schemes in the Literature 65

5.1 Numerical Values of Inputs 66

5.2 Number of Wilson coefficients 66

5.3 Perturbative convergence 71

5.4 Derived Parameters 77

5.5 Heavy Boson Decays 81

5.5.1 $W \to \ell\nu$ decays 83

5.5.2 $h \to b\bar{b}$ decays . . . 87

5.5.3 $Z \to \ell\ell$ decays . . . 90

5.6 Universal corrections in SMEFT . . . 96

6 Introduction to the v_σ^{eff} Schemes in the SMEFT **107**

6.1 Introduction to $\sin\theta^\ell_{\text{eff}}$ . . . 108

6.2 The v_μ^{eff} Scheme . . . 109

6.3 The v_α^{eff} Scheme . . . 114

6.3.1 Relation to the v_μ^{eff} scheme . . . 116

6.3.2 Relation to the α and α_μ schemes . . . 118

7 Numerical Analysis of the v_σ^{eff} schemes **121**

7.1 Numerical Values of Inputs . . . 121

7.2 Number of Wilson coeffficients . . . 122

7.3 Numerical Analysis . . . 126

7.3.1 Derived parameters . . . 126

7.3.2 Heavy boson decays at NLO . . . 131

8 Conclusions **135**

A Appendix **139**

A.1 Warsaw Basis . . . 139

A.2 Phase Space Integrals . . . 142

A.2.1 Two-body phase space . . . 143

A.2.2 Three-body phase space . . . 144

A.3 Comparison with previous literature . . . 146

A.4 Numerical results for the decay rates 147

A.4.1 $W \to \tau\nu$ decay 147

A.4.2 $h \to b\bar{b}$ decay 149

A.4.3 $Z \to \tau\tau$ decay 152

A.5 Numerical results using universal corrections in SMEFT 154

Bibliography **157**

List of Figures

1.1 Feynman diagram contributing to the decay of the Z boson to electrons at one loop and with a QED correction. 14

5.1 Representative Feynman diagrams contributing to the WW, ZZ, γZ, and $\gamma\gamma$ two-point functions in SMEFT. 69

5.2 Representative Feynman diagrams contributing to the decay of the muon at one loop and involving four-fermion operators. 70

5.3 Representative virtual corrections for W decay into leptons at NLO. 83

5.4 LO and NLO corrections $\Delta^{\mathrm{s}(i,j)}_{W\tau\nu}$, as defined in Eq. (5.5.2), for the decay $W \to \tau\nu$ in the three schemes. Note that "NLO" in the legends only refers to the NLO corrections and that we write superscripts in the Wilson coefficient names as $C_{Hq3} \equiv C^{(3)}_{Hq}$. The flavour indices i and j run over values $j \in 1, 2$, and $i \in 1, 2, 3$. Operators which appear only through counterterms in a particular scheme are shown on the right. The dashed lines indicate the large-m_t limit of the NLO corrections. For operators appearing at LO the orange triangles indicate if the sign of the NLO correction is the same as (triangle pointing up) or different from (triangle pointing down) the sign of the LO contribution. 104

5.5 As in Figure 5.4, but for the decay $h \to b\bar{b}$. 105

5.6 As in Figure 5.4, but for the decay $Z \to \tau\tau$. 106

7.1 Representative Feynman diagrams contributing to the decay of a Z boson via a four fermion operator. 123

7.2 SMEFT corrections to the W boson mass in the v_μ^{eff} (top) and v_α^{eff} (bottom) schemes, with Δs_w determined from $Z \to ee$ decay, so that $\ell = 1$. The Wilson coefficients are evaluated at $C_i = 1/v_\sigma^2$. The flavour indices i and j run over values $j \in 1, 2$, and $i \in 1, 2, 3$. . . . 129

List of Tables

4.1 Nomenclature for the Electroweak (EW) input schemes considered in this work. 50

5.1 Input parameters employed throughout this section. Note that v_α is a derived parameter. 67

5.2 Number of Wilson coefficients introduced in the dimension-six counterterms for the bare M_W, M_Z and v_T at LO and NLO, as well as the number of unique coefficients between them. 68

5.3 NLO corrections to prefactors of LO Wilson coefficients in the three schemes. Negative corrections indicate a reduction in the magnitude of the numerical coefficient of a given Wilson coefficient. The flavour index j refers to $j \in 1, 2$. 86

5.4 NLO corrections to prefactors of LO Wilson coefficients in the three schemes, split into QCD and EW corrections. The flavour index j refers to $j \in 1, 2$. 87

5.5 NLO corrections to prefactors of LO Wilson coefficients in the three schemes. Negative corrections indicate a reduction in the magnitude of the numerical coefficient of a given Wilson coefficient, while $< 0.1\%$ indicates changes below 0.1%, both positive and negative. The flavour index j refers to $j \in 1, 2$. 95

5.6 SM results in the α and LEP schemes. For each process, the results are normalised to the SM NLO results in the α_μ scheme. 100

5.7 The numerical prefactors of the Wilson coefficients in the α scheme appearing in $K_W^{(6,1,\alpha)}$ for various perturbative approximations. The tree-level decay rate as well as v_α^2 have been factored out and the results have been evaluated at the scale of the process. We show the results for W decay (top), h decay (center) and Z decay (bottom). 102

5.8 The numerical prefactors of the Z decay SMEFT Wilson coefficients in the α_μ scheme appearing leading to dominant corrections at various perturbative approximations. The tree-level decay rate as well as v_μ^2 have been factored out and the results have been evaluated at the scale of the process. 103

7.1 Input parameters employed throughout this section. Note that v_α^{eff} is a derived parameter. 122

7.2 Number of Wilson coefficients appearing in the derived parameters of each scheme under general flavour assumptions and $U(2)^2 \times U(3)^3$. The LO row represents the (6,0) piece of the corresponding quantity, whereas NLO represents the (6,1) piece. 124

7.3 Number of Wilson coefficients appearing in heavy boson decay rates under general flavour assumptions and $U(2)^2 \times U(3)^3$. Note that assuming $U(2)^2 \times U(3)^3$ the number of operators appearing in $\Gamma_{Z\tau\tau}$ and Γ_{Zee} is the same and hence only one value is given. 125

7.4 Nomenclature for the EW input schemes considered in this work. . 126

7.5 SM results for derived parameters in scheme s relative to the experimental values in table 7.1. 126

7.6 The numerical prefactors of the Wilson coefficients in the v_μ^{eff} and v_α^{eff} schemes contributing to Δ_W for the LO, NLO and NLO$_t$ (large-m_t limit) perturbative approximations. The SM tree-level approximation along with v_μ^2 has been factored out. The results have been evaluated at $\mu = M_Z$ and varied up and down by a factor of 2 to give the uncertainties. Only Wilson coefficients whose numerical prefactor is greater than 1% at NLO have been included. 130

7.7 Deviations of the SM predictions for $Z \to \ell\ell$ and $W \to \ell\nu$ decay rates in scheme s from the experimental measurements of $\Gamma_{Z\ell\ell}^{\text{exp}} = 83.98$ MeV and $\Gamma_{W\ell\nu}^{\text{exp}} = 226.4$ MeV [10]. 132

7.8 Selected SMEFT contributions to the $Z \to \tau\tau$ decay rate including scale variation in the five schemes. 133

A.1 The 59 independent baryon number conserving dimension-six operators built from Standard Model fields, in the notation of [45]. The subscripts p, r, s, t are flavour indices, and σ^I are Pauli matrices. . . 141

A.2 The numerical prefactors of the Wilson coefficients in the α_μ scheme appearing in $K_W^{(6,1,\mu)}$ for various perturbative approximations. The tree-level decay rate as well as v_μ^2 have been factored out and the results have been evaluated at the scale of the process. We show the results for W decay (left) and Higgs decay (right). 155

A.3 The numerical prefactors of the Wilson coefficients in the LEP scheme appearing in $K_W^{(6,1,\mu)}$ and $\hat{\Delta}_{W,t}^{(6,1,\mu)}$ for various perturbative approximations. The tree-level decay rate as well as v_μ^2 have been factored out and the results have been evaluated at the scale of the process. We show the results for W decay (top) and Z decay (bottom). . . . 156

List of Abbreviations

EFT	Effective Field Theory
EM	Electromagnetism
EW	Electroweak
EWPO	Electroweak Precision Observable
IR	Infra Red
LO	Leading-Order
MS	Minimal Subtraction
$\overline{\textbf{MS}}$	modified Minimal Subtraction
NLO	Next-to-Leading-Order
NNLO	Next-to-Next-to-Leading-Order
QCD	Quantum Chromo Dynamics
QED	Quantum Electro Dynamics
QFT	Quantum Field Theory
RG	Renormalisation-Group
SM	Standard Model
SMEFT	Standard Model Effective Field Theory

UV Ultra Violet

VEV Vacuum Expectation Value

Declaration

The work in this thesis is based on research carried out in the Department of Physics at Durham University. No part of this thesis has been submitted elsewhere for any degree or qualification.

The ideas presented in some of this thesis are based on work undertaken by the author and collaborators with the following approximate splitting as follows.

Chapters 4 and 5, which concerns a review of three common electroweak input schemes in the SMEFT, are based on the work of the author in collaboration with Anke Biekötter, Benjamin D. Pecjak, and Darren J. Scott.

Electroweak input schemes and universal corrections in SMEFT
Anke Biekötter, Benjamin D. Pecjak, Darren J. Scott, Tommy Smith
JHEP 07 (2023), 115

Chapters 6 and 7, which involves the introduction of two new electroweak input schemes for the SMEFT involving the weak mixing angle, are based on the work of the author in collaboration with Anke Biekötter, and Benjamin D. Pecjak

Using the effective weak mixing angle as an input parameter in SMEFT
Anke Biekötter, Benjamin D. Pecjak, Tommy Smith
To be published in JHEP

Acknowledgements

The work of this thesis would not have been possible without the help of numerous people who I have had the pleasure of meeting and working with throughout my time in the IPPP and who I owe a debt of gratitude.

First and foremost, I would like to thank my supervisor, Ben Pecjak. His help, support and enthusiasm has been invaluable to me throughout my PhD, and it would have not been possible without him. I would also like to thank Anke Biekötter for the generosity of her time to help me over the past three years in any which way she could.

I would also like to thank everyone in the IPPP who have made my time here an enjoyable experience, Wendy for the interesting conversations in the office (sorry about the mess) as well as Edwin, Guillaume, Jack, James, Mia and all other patrons of Café 215 for all the laughs and to Joanne and Trudy, and Adam and Paul for all their help along the way. Additionally, I would like to thank Livia, Sofie, and Tim for their help with proofreading parts of this thesis.

Finally, I thank my family. I promise to answer your calls more and reply to messages a bit faster now!

Chapter 1

The Standard Model

We start this thesis with the customary review of the Standard Model (SM). We focus on salient features in order to provide context for what follows.

1.1 The Standard Model Lagrangian

The SM is our best description of the fundamental interactions of the universe. It uses the language of a Quantum Field Theory (QFT), which combines the concepts of Special Relativity and Quantum Mechanics into a single theory.

To delve into the details of the SM, unless otherwise stated, we use [1] as a reference, potentially changing the notation slightly to suit our needs.

The SM is a Gauge Theory, a type of QFT which is invariant under transformations of a gauge group. For the SM, this gauge group [2–7] is

$$SU(3)_c \times SU(2)_L \times U(1)_{\mathcal{Y}}\,, \tag{1.1.1}$$

where the subscripts c, L and $\mathcal{Y}$ correspond to colour, left and hypercharge respectively.[2] The SM Lagrangian[3] is invariant under transformations belonging to the

[2]We shall drop the subscripts from here on.

[3]More precisely, a Lagrangian density. However, we refer to this as a Lagrangian throughout.

gauge group. Despite the complexity of the SM, its Lagrangian can be written in a succinct form, namely,

$$\begin{aligned}\mathcal{L}_{\text{SM}} = &-\frac{1}{4}F^{\mu\nu}F_{\mu\nu} \\ &+\left(D_\mu H\right)^\dagger (D^\mu H) - V(H) \\ &+ i\bar{\Psi}\not{D}\Psi \\ &- Y_{ij}\bar{\Psi}_i H \Psi_j + \text{h.c.}\,,\end{aligned} \tag{1.1.2}$$

where we have used Feynman slash notation such that $\not{D} \equiv \gamma^\mu D_\mu$. The covariant derivative, D_μ, in Eq. (1.1.2), which preserves invariance under transformations of the SM gauge group, takes the form,

$$D_\mu = \partial_\mu - ig_1 \mathcal{Y} B_\mu - ig_2 \tau^a W_\mu^a - ig_s t^A G_\mu^A\,, \tag{1.1.3}$$

where g_1, g_2 and g_s are couplings, $\mathcal{Y}$, τ^a and t^A are generators and B_μ, W_μ^a and G_μ^A are fields of the gauge groups $U(1)$, $SU(2)$ and $SU(3)$ respectively. The group $U(1)$ is an Abelian , whereas $SU(2)$ and $SU(3)$ are non-Abelian therefore their generators are non-commutative.

When describing the SM Lagrangian, we choose to separate it into three parts, where each predominantly contains the information corresponding to certain collections of particles.

1.1.1 Gauge

The first part of the SM Lagrangian we consider is the gauge Lagrangian, which comprises terms given in line one of Eq. (1.1.2). The gauge Lagrangian is named accordingly due to its construction purely from gauge fields. Moreover, the information contained within describes the self interactions and dynamics of those gauge fields. To better understand these interactions and dynamics we write this part of

the SM Lagrangian as a sum of three terms, one for each gauge group,

$$\mathcal{L}_{\text{Gauge}} = -\frac{1}{4}F^{\mu\nu}F_{\mu\nu} = -\frac{1}{4}B^{\mu\nu}B_{\mu\nu} - \frac{1}{4}W^{a\mu\nu}W^{a}_{\mu\nu} - \frac{1}{4}G^{A\mu\nu}G^{A}_{\mu\nu}\,. \tag{1.1.4}$$

Written as above, the gauge Lagrangian is built of field strength tensors. We can express the field strength tensors as a combination of their corresponding gauge fields and structure functions of the gauge groups,

$$\begin{aligned} B_{\mu\nu} &= \partial_\mu B_\nu - \partial_\nu B_\mu\,, \\ W^{a}_{\mu\nu} &= \partial_\mu W^{a}_{\nu} - \partial_\nu W^{a}_{\mu} + g_2 \epsilon^{abc} W^{b}_{\mu} W^{c}_{\mu}\,, \\ G^{A}_{\mu\nu} &= \partial_\mu G^{A}_{\nu} - \partial_\nu G^{A}_{\mu} + g_s f^{ABC} G^{B}_{\mu} G^{C}_{\mu}\,, \end{aligned} \tag{1.1.5}$$

where B_μ is the gauge field for $U(1)$, W^a_μ are the gauge fields for $SU(2)$ and G^A_μ are the gauge fields for $SU(3)$. Furthermore, ϵ^{abc} and f^{ABC} are the structure constants for the gauge groups $SU(2)$ and $SU(3)$ respectively. We see that for the Abelian gauge field, B_μ, the gauge part of the Lagrangian consists of only a dynamical term whereas for the non-abelian gauge fields, W^a_μ and G^A_μ, we additionally produce self interactions of the gauge fields, a feature of non-abelian gauge theories.

1.1.2 Higgs

The following part of the SM Lagrangian is the Higgs Lagrangian, given in line two of Eq. (1.1.2),

$$\mathcal{L}_{\text{Higgs}} = \left(D_\mu H\right)^\dagger \left(D^\mu H\right) - V(H). \tag{1.1.6}$$

The Higgs field H takes the form of an $SU(2)$ doublet of complex scalar fields with hypercharge $\mathcal{Y} = \frac{1}{2}$ [8, 9],

$$H = \begin{pmatrix} \phi^+ \\ \phi^0 \end{pmatrix} = \frac{1}{\sqrt{2}} \begin{pmatrix} \phi_1 + \phi_2 \\ \phi_3 + \phi_4 \end{pmatrix}\,. \tag{1.1.7}$$

This part of the Lagrangian describes the interaction and dynamics of the Higgs fields and, as we will shortly see, through the process of spontaneous symmetry

breaking, it gives rise to the masses of the particles in the SM [8,9]. To see how this occurs, we consider the Higgs potential,

$$V(H) = \mu^2 H^\dagger H + \lambda \left(H^\dagger H\right)^2 , \tag{1.1.8}$$

where we have $\lambda > 0$ and $\mu^2 < 0$ such that the minimum of the Higgs potential occurs for a non-zero value of the Higgs doublet. The minimum of the Higgs potential occurs at the Vacuum Expectation Value (VEV), v, of the field,

$$\langle H^\dagger H \rangle \equiv \frac{v^2}{2} = -\frac{\mu^2}{2\lambda}. \tag{1.1.9}$$

Eq. (1.1.9) defines an infinite continuum of degenerate minima which are invariant under $SU(2)$ rotations. We are free to choose that the minimum occurs at H_0,

$$H_0 = \frac{1}{\sqrt{2}} \begin{pmatrix} 0 \\ v \end{pmatrix} , \tag{1.1.10}$$

where the VEV has the value of 246 GeV, [10]. The process of VEV generation has consequences for the gauge bosons of the theory. Consider the action of the following linear combinations of generators on H_0,

$$\begin{aligned} Q H_0 &= \left(\tau^3 + \mathcal{Y}\right) H_0 = 0 \,, \\ K H_0 &= \left(\tau^3 - \mathcal{Y}\right) H_0 \neq 0 \,, \\ \tau^1 H_0 &\neq 0 \,, \\ \tau^2 H_0 &\neq 0 \ . \end{aligned} \tag{1.1.11}$$

The first generator is unbroken, whereas the subsequent three are broken. Thus, as will be demonstrated soon, we will have one massless gauge boson, and three massive gauge bosons in the theory whose mass is generated via the Higgs mechanism.

Goldstones theorem dictates that for each broken generator of a symmetry, there is a resultant massless Goldstone boson in the spectrum [11, 12]. These would be Goldstone bosons are then said to be "eaten" by the gauge fields, and in doing so, the gauge fields acquire a mass and the required longitudinal degree of freedom.

The remianing unbroken generator Q corresponds to the electric charge. The Higgs field, and therefore the vacumm, is uncharged as demonstrated by the annihalation of the vacuum by the generator. The generator Q corresponds to a symmetry of the vacuum, $U(1)_{\text{QED}}$, which the guage group of the SM has been spontaneously broken down to

$$SU(2)_L \times U(1)_{\mathcal{Y}} \to U(1)_{\text{QED}}. \tag{1.1.12}$$

After choosing a VEV, we wish to determine the dynamics of the Higgs field around it. For small fluctuations around the vacuum, we can write the Higgs doublet as

$$H = \frac{1}{\sqrt{2}} \begin{pmatrix} 0 \\ v + h \end{pmatrix}, \tag{1.1.13}$$

whereby we have again used the fact that full Higgs Lagrangian is invariant under $SU(2)$ rotations and have "rotated" the doublet into this form. This procedure is called choosing a gauge, and we have chosen what is known as the unitary gauge, the basis in which the Goldstone components of the Higgs fields are set to zero. The field h is the small fluctuation around the VEV and is what we take to be the physical Higgs boson.

This form of the Higgs doublet as in Eq. (1.1.13), when substituting into the Lagrangian in Eq. (1.1.8), enables us to identify the Higgs mass as

$$m_H^2 = 2\lambda v^2. \tag{1.1.14}$$

Furthermore, to demonstrate the generation of the gauge boson masses, we can expand the kinetic part of the Higgs Lagrangian in unitary gauge,

$$\left(D_\mu H\right)^\dagger \left(D^\mu H\right) \supset \frac{v^2}{8} \left[g_2^2 \left(W_\mu^1\right)^2 + g_2^2 \left(W_\mu^2\right)^2 + \left(g_2 W_\mu^3 - g_1 B_\mu\right)^2 \right]. \tag{1.1.15}$$

The fields W_μ^1 and W_μ^2 are mass-diagonal, but W_μ^3 and B_μ are not. To diagonalise

these, we perform the field rotations

$$\begin{pmatrix} W_\mu^3 \\ B_\mu \end{pmatrix} = \begin{pmatrix} \cos\theta_w & \sin\theta_w \\ -\sin\theta_w & \cos\theta_w \end{pmatrix} \begin{pmatrix} Z_\mu \\ A_\mu \end{pmatrix}, \tag{1.1.16}$$

where θ_w is the weak mixing angle given by

$$\tan\theta_w = \frac{g_1}{g_2}, \tag{1.1.17}$$

and

$$\begin{aligned} \sin\theta_w &= \frac{g_1}{\sqrt{g_1^2 + g_2^2}}, \\ \cos\theta_w &= \frac{g_2}{\sqrt{g_1^2 + g_2^2}}. \end{aligned} \tag{1.1.18}$$

We identify that Z_μ and A_μ are the physical degrees of freedom given by the Z boson and photon respectively.

Additionally, experimentally we measure the charges of the W bosons to be ± 1. To match this, we define

$$W_\mu^\pm = \frac{1}{\sqrt{2}} \left(W_\mu^1 \pm i W_\mu^2 \right). \tag{1.1.19}$$

Therefore, to identify the masses of the gauge bosons we express Eq. (1.1.15) in terms of the physical fields,

$$\left(D_\mu H\right)^\dagger \left(D^\mu H\right) \supset \left[M_W^2 W_\mu^+ W^{\mu-} + \frac{1}{2} M_Z^2 \left(Z_\mu\right)^2 + \frac{1}{2} M_A^2 \left(A_\mu\right)^2 \right], \tag{1.1.20}$$

with

$$\begin{aligned} M_A &= 0, \\ M_W &= g_2 \frac{v}{2}, \\ M_Z &= \sqrt{g_1^2 + g_2^2} \frac{v}{2}. \end{aligned} \tag{1.1.21}$$

As expected, we have one massless boson and three massive ones. Finally, for completeness, using all notation set forth thus far, we express the covariant derivative

in the EW sector as

$$D_\mu = \partial_\mu - i\frac{g_2}{\sqrt{2}}\left(W_\mu^+\tau^+ + W_\mu^-\tau^-\right) - i\frac{g_2}{\cos\theta_w}Z_\mu\left(\tau^3 - \sin^2\theta_w Q\right) - ieA_\mu Q, \quad (1.1.22)$$

where we have defined, $\tau_\mu^\pm = \frac{1}{\sqrt{2}}\left(\tau_\mu^1 \pm i\tau_\mu^2\right)$ and e is the electric charge,

$$e = \frac{g_1 g_2}{\sqrt{g_1^2 + g_2^2}}. \quad (1.1.23)$$

1.1.3 Fermion

The final two lines of Eq. (1.1.2) are the last part of the SM Lagrangian. The fermion part, as our name suggests, describes the dynamics and interactions of the fermions. Line three is a kinetic term for massless fermions and line four, after the spontaneous symmetry breaking, gives rise to the fermion masses through the Higgs mechanism. In what is to follow, we split the fermions up into the leptons and quarks and discuss each separately.

Leptons

The kinetic term for the leptons reads,

$$\mathcal{L}_{\text{lep,kin}} = i\bar{\ell}_L^i \not{D}\delta_{ij}\ell_L^j + i\bar{\ell}_R^i \not{D}\delta_{ij}\ell_R^j, \quad (1.1.24)$$

where

$$\ell_L^i = \left\{\begin{pmatrix}\nu_{e_L}^i \\ e_L^i\end{pmatrix}\right\}, \quad \ell_R^i = \left\{e_R^i\right\}, \quad (1.1.25)$$

and $i = \{1, 2, 3\}$ represents the three flavour generations. The fields ℓ_L^i are an $SU(2)$ doublet whereas the fields ℓ_R^i are an $SU(2)$ singlet. As the operator $\not{D}$ is the identity in leptonic flavour space, which we have made explicit in Eq. (1.1.24) via the inclusion of the flavour space delta function δ_{ij}, ℓ_L and ℓ_R form a triplet representation of a global symmetry group, $U(3)_{\ell_L}$ and $U(3)_{\ell_R}$ respectively.[1]

[1] This is an approximate symmetry as it is broken by the Yukawas.

The final line of Eq. (1.1.2) is the Yukawa Lagrangian, and for the leptons we have

$$\begin{aligned}\mathcal{L}_{\text{lep,Yuk}} &= -Y^e_{ij}\bar{\ell}^i_L H e^j_R + \text{h.c.} \\ &= -Y^e_{ij}\bar{e}^i_L e^j_R \frac{v+h}{\sqrt{2}} + \text{h.c.}\,,\end{aligned} \tag{1.1.26}$$

where in the second line we have chosen unitary gauge for the Higgs doublet. The matrix Y^e is the Yukawa matrix for leptons which does not need to be Hermitian and may be complex.

In the form as written, the fields are expressed in what is labelled as the weak basis, so called as it is the basis for weak interactions. However, we are not restricted to this basis and have the freedom to redefine the lepton fields,

$$e_L \to L_e e_L, \quad e_R \to R_e e_R\,, \tag{1.1.27}$$

where L_e and R_e are unitary matrices. Therefore, we can choose a frame in which we are diagonal in flavour space, labelled as the mass basis. In the mass basis, the Yukawa Lagrangian takes the form

$$\mathcal{L}_{\text{lep,Yuk}} = -M^e_{ij}\bar{e}^i_L e^j_R \frac{v+h}{\sqrt{2}} + \text{h.c.}\,, \tag{1.1.28}$$

where

$$M^e = L_e^\dagger Y^e R_e = \text{diag}\left(y_e, y_\mu, y_\tau\right). \tag{1.1.29}$$

Hence, we have rotated the fields into mass eigenstates, giving justification for the name of the basis. The masses of the leptons are read off as

$$m_l = y_l \frac{v}{\sqrt{2}}. \tag{1.1.30}$$

The presence of the Yukawa interaction breaks the global symmetry of the leptons,

$$U(3)_{\ell_L} \times U(3)_{\ell_R} \to U(1)_e \times U(1)_\mu \times U(1)_\tau\,, \tag{1.1.31}$$

to the symmetry group of lepton family number conservation, which is exact in the SM. Therefore, the number of leptons of each species N_e, N_μ and N_τ are

separately conserved in each interaction [13]. Consequently, total lepton number is also conserved.

Quarks

The other fermionic fields in the SM are the quarks. Their kinetic terms are

$$\mathcal{L}_{\text{quark,kin}} = i\bar{q}_L^i \not{\partial} \delta_{ij} q_L^j + i\bar{u}_R^i \not{\partial} \delta^{ij} u_R^j + i\bar{d}_R^i \not{\partial} \delta^{ij} d_R^j + \text{h.c.}\,, \tag{1.1.32}$$

where

$$q_L^i = \left\{ \begin{pmatrix} u_L^i \\ d_L^i \end{pmatrix} \right\}, \quad u_R^i = \left\{ u_R^i \right\}, \quad d_R^i = \left\{ d_R^i \right\}, \tag{1.1.33}$$

with $i = \{1, 2, 3\}$ for the three generation of quarks. Here, q_l, u_R and d_R again form triplet representations of the global symmetry groups $U(3)_{q_L}$, $U(3)_{u_R}$ and $U(3)_{d_R}$. Analogous to leptons, this is an approximate symmetry as it is broken by the presence of the Yukawa term for quarks,

$$\begin{aligned} \mathcal{L}_{\text{quarks,Yuk}} &= -Y_{ij}^u \bar{q}_L^i \tilde{H} u_R^j - Y_{ij}^d \bar{q}_L^i H d_R^j + \text{h.c.} \\ &= -Y_{ij}^u \bar{u}_L^i u_R^j \frac{v+h}{\sqrt{2}} - Y_{ij}^d \bar{d}_L^i d_R^j \frac{v+h}{\sqrt{2}} + \text{h.c.}\,, \end{aligned} \tag{1.1.34}$$

where in the second line we have chosen the unitary gauge and

$$\tilde{H} = i\sigma_2 H\,, \tag{1.1.35}$$

where σ_2 is the second Pauli matrix

$$\sigma_2 = \begin{pmatrix} 0 & -i \\ i & 0 \end{pmatrix}. \tag{1.1.36}$$

Again, we have the freedom to perform the field redefinitions,

$$\begin{aligned} u_L \to L_u u_L, \quad u_R \to R_u u_R, \\ d_L \to L_d d_L, \quad d_R \to R_d d_R, \end{aligned} \tag{1.1.37}$$

which take us from the weak basis for the quarks into the mass basis. In doing so, the Yukawa terms for quarks in unitary gauge become,

$$\mathcal{L}_{\text{quarks,yuk}} = -M^u_{ij}\bar{u}^i_L u^j_R \frac{v+h}{\sqrt{2}} - M^d_{ij}\bar{d}^i_L d^j_R \frac{v+h}{\sqrt{2}} + \text{h.c.}\,, \tag{1.1.38}$$

where

$$\begin{aligned} M^u &= L_u^\dagger Y^u R_u = \text{diag}\,(y_u, y_c, y_t)\,, \\ M^d &= L_d^\dagger Y^d R_d = \text{diag}\,(y_d, y_s, y_b)\,. \end{aligned} \tag{1.1.39}$$

We can therefore read off the masses of the quarks as

$$m_q = y_q \frac{v}{\sqrt{2}}. \tag{1.1.40}$$

The field redefinitions of Eq. (1.1.27) and Eq. (1.1.37) have some interesting consequences for the kinetic terms of the Lagrangian for the fermions. In the weak basis, the covariant derivative can be expanded such that part of the kinetic terms read,

$$\begin{aligned} \mathcal{L}_{\text{fer,kin}} \supset \frac{e}{\sqrt{2}\sin\theta_w}\Big(&\bar{e}^i_L \gamma^\mu W^+_\mu \nu^i_{e_L} + \bar{\nu}^i_{e_L}\gamma^\mu W^-_\mu e^i_L \\ &+\bar{u}^i_L \gamma^\mu W^+_\mu d^i_L + \bar{d}^i_L \gamma^\mu W^-_\mu u^i_L\Big). \end{aligned} \tag{1.1.41}$$

After performing the redefinitions of Eq. (1.1.27) and Eq. (1.1.37) we have the freedom to keep the leptonic current flavour diagonal by redefining ν_{e_L} which was previously untouched. This freedom is not available for the quarks. Consequently, in the mass basis, the terms in the equation above for quarks are written as

$$\begin{aligned} \mathcal{L}_{\text{quarks,kin}} \supset& \frac{e}{\sqrt{2}\sin\theta_w}\Big([L^u]^\dagger_{ik}[L^d]_{kj}\bar{u}^i_L\gamma^\mu W^+_\mu d^j_L + [L^d]^\dagger_{ik}[L^u]_{kj}\bar{d}^i_L\gamma^\mu W^-_\mu u^j_L\Big) \\ =& \frac{e}{\sqrt{2}\sin\theta_w}\Big(V_{ij}\bar{u}^i_L\gamma^\mu W^+_\mu d^j_L + V^\dagger_{ij}\bar{d}^i_L\gamma^\mu W^-_\mu u^j_L\Big)\,, \end{aligned} \tag{1.1.42}$$

where we have defined

$$V \equiv L_u^\dagger L_d = \begin{pmatrix} V_{ud} & V_{us} & V_{ub} \\ V_{cd} & V_{cs} & V_{cb} \\ V_{td} & V_{ts} & V_{tb} \end{pmatrix}\,, \tag{1.1.43}$$

which is known as the CKM matrix [14, 15], named after Cabibbo, Kobayashi and, Maskawa. In the SM, the CKM matrix is the only source of interactions between fermions of different generations, so-called flavour violating interactions. The Wolfenstein parameterisation [16] can approximate the CKM matrix using a single parameter

$$V \approx \begin{pmatrix} 1-\frac{\lambda^2}{2} & \lambda & \lambda^3 \\ -\lambda & 1-\frac{\lambda^2}{2} & \lambda^2 \\ \lambda^3 & -\lambda^2 & 1 \end{pmatrix} \tag{1.1.44}$$

where experimentally, it is found that $\lambda \approx 0.23$ [10]. This parameterisation of the CKM matrix gives us an approximate strength of the flavour violating interactions, where we see that these interactions are significantly suppressed as compared to the flavour conserving interactions.

1.1.4 Assumptions on the Lagrangian

In the previous sections, we have described the bulk of the SM, mentioning all fields and couplings relevant for this thesis, with remaining aspects being discussed in detail in reference texts [1, 17, 18]. Going forward, we need to understand how calculations in the SM are performed, detailing specifics to navigate potential road blocks along the way. As is apparent from the numerous particles and interactions present in the SM, any calculations we pose will have significant complexity when, as we wish to do, quantum corrections are discussed. Consequently, we therefore apply a few simplifications and assumptions on the Lagrangian to reduce the computational ordeal we have to undertake. These assumptions, although not at the cutting edge of our ability in SM precision calculations, nonetheless are common practice for the field of work considered in this thesis and more than suffice for this application.

The first assumption we make is taking the massless limit of all fermions except the top quark. The quark masses we have set to zero range from the lightest being the electron having a mass of 0.5 MeV, up to the bottom quark of mass 4.2 GeV.

In comparison to the W boson of mass 80.4 GeV, which is approximately 20 times heavier than that of the bottom quark, the light fermions masses are insignificant and can be ignored. The main desirable consequence of this assumption affects the loop integrals introduced in Section 1.2.1. We have reduced the number of massive scales appearing inside the integrals, greatly simplifying them.

Secondly, we set the CKM matrix to the identity. From the Wolfenstein parameterisation, Eq. (1.1.44), we can see that this simplification, although not perfect, is a good approximation of the underlying physics as we only neglect terms subleading in the small parameter λ. The importance of this assumption is found again when considering the loop corrections to a process. Removing the source of flavour changing interactions results in a significantly reduced set of Feynman diagrams one must consider when computing loop corrections. Hence, fewer loop integrals must be computed.

1.2 Calculations in the Standard Model

It is at this point we wish to demonstrate how calculations in the SM are performed, in particular, Next-to-Leading-Order (NLO) EW calculations, which contribute the main calculational workload of this thesis. We will focus on the problem of loop level calculations and the difficulties that emerge which we must overcome. We will discover how Ultra Violet (UV) divergences arise, how they are regularised and ultimately renormalised to return finite predictions once a sufficiently inclusive observable is considered.

To highlight all the intricacies of an NLO calculation in the SM, there is no better way than that of an example. An important process in the discussion of input schemes is the decay of the Z boson to leptons. Specifically, here we choose to consider the decay to the first generation of charged leptons, the electron, and its anti-particle, the positron. To make our point in the most succinct way, we choose

a slightly simplified version of the problem and only consider the Quantum Electro Dynamics (QED) corrections to the process.

The first port of call is to use the Feynman rules, which can be derived from the Lagrangian (with details found in [1] and a full list can be found in [19]), to write down the matrix element for the process. Using the SM Feynman rules, the bare amplitude, denoted by the subscript 0, thus reads

$$\mathcal{A}_0\left(Z \to ee\right) = \frac{e_0}{2c_{w,0}s_{w,0}}\left(\mathcal{A}_{L,0}S_L + \mathcal{A}_{R,0}S_R\right) , \tag{1.2.1}$$

where we have defined

$$s^2_{w,0} = 1 - c^2_{w,0} , \quad c^2_{w,0} = \frac{M^2_{W,0}}{M^2_{Z,0}} . \tag{1.2.2}$$

We have introduced the spinor structures

$$S_L = \left[\bar{u}(p_{e^-})\gamma^\nu P_L v(p_{e^+})\right]\epsilon^*_\nu(p_Z) , \quad S_R = \left[\bar{u}(p_{e^-})\gamma^\nu P_R v(p_{e^+})\right]\epsilon^*_\nu(p_Z) , \tag{1.2.3}$$

with $P_L = (1-\gamma_5)/2$ and $P_R = (1+\gamma_5)/2$ being the left and right projection operators. The expansion for the bare amplitude can be written as

$$\mathcal{A}_{L/R,0} = \mathcal{A}^{(4,0)}_{L/R,0} + \mathcal{A}^{(4,1)}_{L/R,0} + \dots , \tag{1.2.4}$$

where the superscript (i,j) of $\mathcal{A}^{(i,j)}_{L/R,0}$ labels the operator dimension[1], i, and the order in the perturbative series, j. The Leading-Order (LO) terms are simple to write down,

$$\mathcal{A}^{(4,0)}_{L,0} = -1 + 2s^2_{w,0} , \quad \mathcal{A}^{(4,0)}_{R,0} = 2s^2_{w,0} , \tag{1.2.5}$$

At LO the amplitude is now complete, we could square it, perform the spin sum/average and integrate over the two body phase space to obtain a prediction for this decay rate - see Appendix A.2. However, the NLO corrections to the amplitude, $\mathcal{A}^{(4,1)}_{L/R,0}$, have features which we must discuss further.

[1] In the SM this is redundant as it is always four, but we introduce it with the foresight of what is to come.

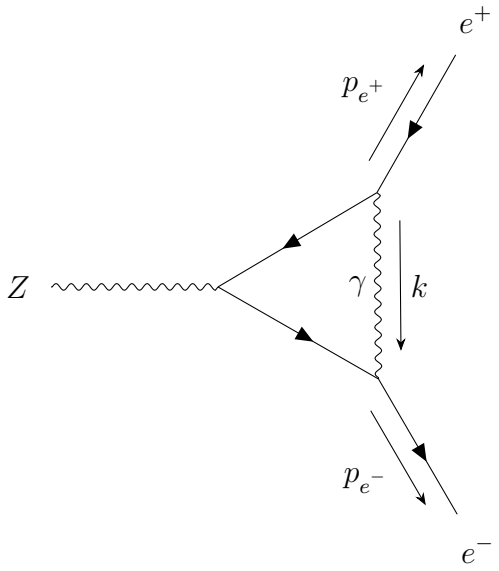

Figure 1.1: Feynman diagram contributing to the decay of the Z boson to electrons at one loop and with a QED correction.

1.2.1 Loop Diagrams

In many instances, an NLO calculation in the SM, or any QFT, will involve a loop integral which is infinite. In our example of $Z \to ee$, this is no different. Consider the virtual QED correction to the process: the graph where a photon connects the two outgoing electrons, as seen in Figure 1.1.

The calculation of this diagram involves the loop integral

$$\int \frac{d^4k}{(2\pi)^4}\gamma^\mu \frac{\left(\not{p}_{e^-} - \not{k}\right)}{\left(p_{e^-} - k\right)^2}\gamma^\sigma \left(P_L\mathcal{A}_L^{(4,0)} + P_R\mathcal{A}_R^{(4,0)}\right) \frac{\left(\not{p}_{e^+} + \not{k}\right)}{\left(p_{e^+} + k\right)^2}\gamma_\mu \frac{1}{k^2}\,, \tag{1.2.6}$$

where, as per our assumptions, we have set the electron mass to zero.

In four space-time dimensions, this integral is infinite. The integral infinite as we integrate up as $k \to \infty$, which we call a UV divergence. This can easily be seen by a counting exercise, giving the number of powers of loop momenta in the problem as zero, which then when integrated to infinity diverges. Moreover, the integral diverges as we integrate $k \to 0$, labelled an Infra Red (IR) divergence [20]. This occurs as the inegrand itself diverges in this limit. These divergences are dealt with separately to achieve a finite result. UV divergences are cancelled in the renormalisation process,

whereby counterterms are introduced which exactly match the divergences of the amplitude. On the other hand, to NLO in perturbation theory, the IR divergences of the virtual corrections are cancelled by considering an IR safe observable. An IR safe observable is one in which we also include diagrams with an extra particle such that if it goes soft or collinear to another particle, the result will look identical to the desired process. In the case of $Z \to ee$, the process including an additional photon in the final state should also be considered. The $Z \to ee\gamma$ decay rate will also have IR divergences which will exactly cancel with those appearing in the virtual correction. This cancellation, or more generally the fact that the SM is IR finite as a whole when a sufficiently inclusive observable is considered, is called the KLN theorem [21, 22].

In order to cancel both UV and IR divergences, we first need a method to mathematically define the divergences arising from the Feynman integrals, we need to regularise them. One method of regularisation, but not the only, is that of dimensional regularisation [23]. Dimensional regularisation involves moving the integral away from four spacetime dimensions, where it is infinite, to $d = 4 - 2\epsilon$ spacetime dimensions, with ϵ being a small positive parameter, where it is finite. This enables a Laurent series around $\epsilon = 0$ to be taken. The resulting expansion contains poles in ϵ providing an explicit, analytic expression of the divergences upon recovering the four dimensional space-time result.

An interesting consequence of moving away from four space-time dimensions is that the mass dimension of the fields and couplings shift. However, to maintain integer coupling mass dimensions, we can factor out some function of the parameter μ, which has mass dimension one, as

$$g \to \mu^{\frac{4-d}{2}} g, \tag{1.2.7}$$

where g is an arbitrary coupling.

Returning to our example, after regularising the integral, UV and IR singularities are made manifest as poles in ϵ which enabling explicit cancellation through the

renormalisation procedure or when considering an IR safe observable. We find the diagram (figure 1.1) evaluates to

$$\mathcal{M}^{\text{QED}}_{\text{loops}} \sim \left(\frac{1}{\epsilon_{\text{UV}}} - \frac{2}{\epsilon^2_{\text{IR}}} - \frac{2}{\epsilon_{\text{IR}}}\left(2 + \log\frac{-\mu^2}{M_Z^2}\right)\right) \times \frac{e^3}{32\pi^2 c_w s_w}\left(\mathcal{A}_L^{(4,0)} S_L + \mathcal{A}_R^{(4,0)} S_R\right) + \dots\,, \tag{1.2.8}$$

where μ is the renormalisation scale and the ellipsis represents finite terms. For convenience, we have dropped the subscript 0 denoting that these are bare parameters. Additionally, we have identified the source of the divergence, either UV or IR in nature, with a subscript on the epsilon, even though strictly speaking in dimensional regularisation $\epsilon_{\text{UV}} = \epsilon_{\text{IR}} = \epsilon$. To move forward in our calculation, we require a method to remove these divergences.

1.2.2 UV Renormalisation

Renormalisation is the method we use to deal with UV divergences. This constitutes redefining the bare parameters and fields in the Lagrangian. This allows the infinite shifts, introduced by quantum corrections to relations between the Lagrangian parameters and the experimentally measured quantities, to be absorbed into additional terms called counterterms. Therefore, the counterterms themselves are divergent; the use of dimensional regularisation manifests the divergences as poles in ϵ.

A full review of the renormalisation in the EW SM is given in [24], but briefly, the renormalisation procedure follows the following format. We write the bare Lagrangian parameters or fields in terms of the renormalised quantities as,

$$X_0 = X Z_X = X(1 + \delta X)\,, \tag{1.2.9}$$

where Z_X is a renormalisation constant, which we then expand in perturbation theory to define the counterterm δX. A renormalisation condition defines the exact form of the counterterm with different conditions giving a differing finite structure but a necessarily identical pole structure. Calculations using the renormalised Lagrangian

then involve additional diagrams, with counterterm insertions, which cancel UV divergences of the loop integrals.

We will demonstrate this procedure with a subset of the SM parameters and fields relevant for our example of $Z \to ee$ and the additional calculations presented hereinafter. We will focus on quantities which are renormalised on-shell, whereby the renormalisation conditions are such that the pole of a propagator is at the physical mass whilst also requiring that the resudue of a propagator is unity when evaluated at this mass. Furthermore, it is required that higher order vertex corrections vanish in the limit of zero momnetum transfer. The set of quantities we renormalise here are: the wavefunction of the W and Z bosons, and the fermions as well as the W-bosons and Z-bosons masses and the QED coupling α.

As a side note, as the main focus of this thesis is renormalisation of different input schemes in the Standard Model Effective Field Theory (SMEFT), it is important to state at this point that these are not the only way to perform the renormalisation nor the only parameters we can define renormalisation conditions for. For example, the Minimal Subtraction (MS) renormalisation scheme defines the counterterms to be solely the poles in ϵ. Alternatively, modified Minimal Subtraction ($\overline{\text{MS}}$) also includes factors of γ_E and $\log 4\pi$ which are associated with the pole structure. Furthermore, the on-shell scheme, which we discuss here, includes finite corrections in counterterms from two point functions in their definition. Moreover, we could use the Fermi constant G_F as our coupling parameter as opposed to α and thus a renormalisation condition for this must be defined - see Section 4.2.

Nonetheless, to begin the determination of the on-shell counterterms we first relate the bare parameters to the renormalised ones as,

$$
\begin{aligned}
e_0 &= eZ_e = e(1 + \Delta e^{(4,1)}) \,, \\
M^2_{W,0} &= M^2_W Z_{M^2_W} = M^2_W(1 + 2\Delta M^{(4,1)}_W) \,, \\
M^2_{Z,0} &= M^2_Z Z_{M^2_Z} = M^2_Z(1 + 2\Delta M^{(4,1)}_Z) \,, \\
f^i_{L,0} &= f^i_L \sqrt{Z^L_{f^i}} = f^i_L(1 + \frac{1}{2}\Delta Z^{L(4,1)}_{f^i}) \,,
\end{aligned}
$$

$$
\begin{aligned}
f^i_{R,0} &= f^i_R\sqrt{Z^R_{f^i}} = f^i_R(1+\frac{1}{2}\Delta Z^{R(4,1)}_{f^i})\,,\\
W^\pm_0 &= W^\pm\sqrt{Z_W} = W^\pm(1+\frac{1}{2}\Delta Z^{(4,1)}_W)\,,\\
\begin{pmatrix} Z_0 \\ A_0 \end{pmatrix} &= \begin{pmatrix} \sqrt{Z_{ZZ}} & \sqrt{Z_{ZA}} \\ \sqrt{Z_{AZ}} & \sqrt{Z_{AA}} \end{pmatrix}\begin{pmatrix} Z \\ A \end{pmatrix} = \begin{pmatrix} 1+\frac{1}{2}\Delta Z^{(4,1)}_{ZZ} & \frac{1}{2}\Delta Z^{(4,1)}_{ZA} \\ \frac{1}{2}\Delta Z^{(4,1)}_{AZ} & 1+\frac{1}{2}\Delta Z^{(4,1)}_{AA} \end{pmatrix}\begin{pmatrix} Z \\ A \end{pmatrix}\,. \qquad (1.2.10)
\end{aligned}
$$

For succinctness of expression and to reduce the number of equations, we have changed the notation slightly from that of Section 1.1 and written a general fermion as f. The renormalised one-particle irreducible two point functions in Feynman gauge are then given by

$$
\begin{aligned}
\Gamma^W_{\mu\nu}(k) &= -ig_{\mu\nu}\left(k^2-M^2_W\right) - i\left(g_{\mu\nu}-\frac{k_\mu k_\nu}{k^2}\right)\Sigma^W_T(k^2) - i\frac{k_\mu k_\nu}{k^2}\Sigma^W_L(k^2)\,,\\
\Gamma^{ab}_{\mu\nu}(k) &= -ig_{\mu\nu}\left(k^2-M^2_a\right) - i\left(g_{\mu\nu}-\frac{k_\mu k_\nu}{k^2}\right)\Sigma^{ab}_T(k^2) - i\frac{k_\mu k_\nu}{k^2}\Sigma^{ab}_L(k^2)\,,\\
\Gamma^f_{ij}(p) &= i\delta_{ij}\left(\not{p}-m_i\right) + i\left[\not{p}P_L\Sigma^{f,L}_{ij}(p^2) + \not{p}P_R\Sigma^{f,R}_{ij}(p^2) + \left(m_{f,i}P_L + m_{f,j}P_R\right)\Sigma^{f,S}_{ij}(p^2)\right]\,.
\end{aligned} \qquad (1.2.11)
$$

where $a,\ b = A,\ Z$ and remembering $M_A = 0$. The self energies $\Sigma(k^2)$ are in general defined as in 1.2.12 where we have reproduced the figures from [25]. The self energies are constructed from 1PI diagrams $\Sigma_{\rm 1PI}(k^2)$, a 2-point tadpole counterterm $\Sigma_{t,2}$, tadpole loop diagrams $\Sigma_{\rm tad}$ and one point tadpole counterterms $\Sigma_{t,1}$,

$$
\Sigma(k^2) \;=\; \Sigma_{\rm 1PI}(k^2) \;+\; \Sigma_{t,2} \;+\; \Sigma_{\rm tad} \;+\; \Sigma_{t,1}\,. \qquad (1.2.12)
$$

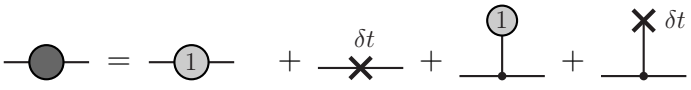

Specifically, here in this thesis we use the Fleischer Jegerlehner (FJ) tadpole scheme [26] where the tadpole counterterms $\Sigma_{t,1}$ and $\Sigma_{t,2}$ cancel exactly. What remains is therefore just the contribution from the 1PI diagrams and the direct tadpole loop diagrams. Invoking the renormalisation condition, for which an explicit mathematical constraint can be found in [24], gives the gauge boson counterterms

to be

$$\begin{aligned}
\Delta M_W^{(4,1)} &= \frac{1}{2}\,\mathrm{Re}\,\frac{\Sigma_T^W(M_W^2)}{M_W^2}\,, & \Delta M_Z^{(4,1)} &= \frac{1}{2}\,\mathrm{Re}\,\frac{\Sigma_T^{ZZ}(M_Z^2)}{M_Z^2}\,,\\
\Delta Z_{ZZ}^{(4,1)} &= -\,\mathrm{Re}\,\frac{\partial\Sigma_T^{ZZ}(k^2)}{\partial k^2}\bigg|_{k^2=M_Z^2}\,, & \Delta Z_{ZA}^{(4,1)} &= 2\frac{\Sigma_T^{AZ}(0)}{M_Z^2}\,,\\
\Delta Z_{AZ}^{(4,1)} &= -2\,\mathrm{Re}\,\frac{\Sigma_T^{ZA}(M_Z^2)}{M_Z^2}\,, & \Delta Z_{AA}^{(4,1)} &= -\,\mathrm{Re}\,\frac{\partial\Sigma_T^{AA}(k^2)}{\partial k^2}\bigg|_{k^2=0}\,.
\end{aligned} \tag{1.2.13}$$

While the fermion wavefunction counterterms are given by

$$\begin{aligned}
\Delta Z_{f^i}^{L(4,1)} &= -\,\mathrm{Re}\,\Sigma_{ii}^{f,L}(m_{f,i}^2) - m_{f,i}^2\frac{\partial}{\partial p^2}\,\mathrm{Re}\left[\Sigma_{ii}^{f,L}(p^2)+\Sigma_{ii}^{f,R}(p^2)+2\Sigma_{ii}^{f,S}(p^2)\right]\Big|_{p^2=m_{f,i}^2}\,,\\
\Delta Z_{f^i}^{R(4,1)} &= -\,\mathrm{Re}\,\Sigma_{ii}^{f,R}(m_{f,i}^2) - m_{f,i}^2\frac{\partial}{\partial p^2}\,\mathrm{Re}\left[\Sigma_{ii}^{f,R}(p^2)+\Sigma_{ii}^{f,R}(p^2)+2\Sigma_{ii}^{f,S}(p^2)\right]\Big|_{p^2=m_{f,i}^2}\,.
\end{aligned} \tag{1.2.14}$$

It is important to remember that although we have made the simplification of setting the light fermion masses to zero, this limit must be made after taking the derivative with respect to momentum in the fermion wavefunction counterterms. Finally, the electric charge renormalisation is given by

$$\Delta e^{(4,1)} = -\frac{1}{2}\Delta Z_{AA} - \frac{s_w}{c_w}\Delta Z_{ZA}. \tag{1.2.15}$$

It should be made clear that the mass dimension and loop number of the two point functions on the right-hand side of the above equations should match that of the left-hand side, so in all the cases given here we have a mass dimension four and one loop. This is important when it comes to renormalising the SMEFT, in the second half of this thesis, where the mass dimension for counterterms needed is six.

Moving back to our example, calculation of the counterterms gives the following,

$$\mathcal{M}_{\mathrm{CT}}^{\mathrm{QED}} \sim \left(\frac{1}{\epsilon_{\mathrm{IR}}} - \frac{1}{\epsilon_{\mathrm{UV}}}\right)\frac{e^3}{32\pi^2 c_w s_w}\left(\mathcal{A}_L^{(4,0)}S_L + \mathcal{A}_R^{(4,0)}S_R\right) + \dots\,, \tag{1.2.16}$$

where again the ellipsis represents finite terms. As expected, the UV divergences cancel exactly with those in Eq. (1.2.8) ,

$$\mathcal{M}_{\mathrm{loops}}^{\mathrm{QED}} + \mathcal{M}_{\mathrm{CT}}^{\mathrm{QED}} \sim \left(-\frac{2}{\epsilon_{\mathrm{IR}}^2} - \frac{1}{\epsilon_{\mathrm{IR}}}\left(3 + \log\frac{-\mu^2}{M_Z^2}\right)\right)$$

$$\times \frac{e^3}{32\pi^2 c_w s_w} \left(\mathcal{A}_L^{(4,0)} S_L + \mathcal{A}_R^{(4,0)} S_R\right) + \dots . \tag{1.2.17}$$

The amplitude is now UV finite, however, IR divergences remain which we handle next.

1.2.3 IR safety

From the UV renormalised matrix element, we are now in the position to calculate the decay rate for $Z \to ee$. However, naively following the procedure to calculate a decay rate for a two body decay returns a result which is not IR safe,

$$\Gamma^{\text{QED}}_{Z\to ee} = \frac{M_Z e^2}{96\pi c_w^2 s_w^2}\left(5 - 12c_w^2 + 8c_w^4\right)(1 - \frac{e^2}{8\pi^2}\left(\frac{2}{\epsilon_{IR}^2} + \frac{1}{\epsilon_{IR}}\left(5 + 4\log\frac{\mu^2}{M_Z^2}\right) + \dots\right). \tag{1.2.18}$$

There remains IR divergences which we need to remove. IR divergences can be classified into two categories, soft and collinear. Soft divergences occur when, at the amplitude level, loop momenta of a massless particle tends to zero, as we have seen in Eq. (1.2.8) or when a singular massless external particles' energy tends to zero. Collinear divergences occur when two massless particles occupy the same region in phase space.

The KLN theorem [21, 22] states that the SM is finite when an IR safe observable is considered to a given expansion level in perturbation theory. An IR safe observable is one in which all degenerate states are summed over. For our example, this involves the addition of the decay rate where we have included an additional photon in the final state. As the photon becomes sufficiently soft or collinear, this is indistinguishable from the desired process. The decay rate of this three body final state contains IR singularities as expected,

$$\Gamma^{\text{QED}}_{Z\to ee\gamma} = \frac{M_Z e^2}{96\pi c_w^2 s_w^2}\left(5 - 12c_w^2 + 8c_w^4\right)\frac{e^2}{8\pi^2}\left(\frac{2}{\epsilon_{IR}^2} + \frac{1}{\epsilon_{IR}}\left(5 + 4\log\frac{\mu^2}{M_Z^2}\right) + \dots\right). \tag{1.2.19}$$

The determination of this decay rate involves a three-body phase space integral, for which details can be found in Appendix (A.2) along with those for the two-body phase space. The aggregate of the two decay rates $\Gamma^{\text{QED}}_{Z\to ee}$ and $\Gamma^{\text{QED}}_{Z\to ee\gamma}$ is an IR safe observable at NLO and is therefore finite to NLO in perturbation theory,

$$\Gamma^{\text{QED}}_{Z\to ee(\gamma)} \equiv \Gamma^{\text{QED}}_{Z\to ee} + \Gamma^{\text{QED}}_{Z\to ee\gamma} = \frac{M_Z e^2}{96\pi c_w^2 s_w^2}\left(5 - 12c_w^2 + 8c_w^4\right)(1 + \ldots)\,. \tag{1.2.20}$$

Additionally, the result is independent of the renormalisation scale μ, a feature of the on-shell renormalisation scheme as all inputs are defined from a physical observable.

1.2.4 Renormalisation Group

In our example above, we have chosen to present the on-shell renormalisation scheme. However, this is by no means the only choice. As mentioned, one could use the MS or $\overline{\text{MS}}$ scheme for the coupling to equally achieve a UV finite result. A different renormalisation procedure will however render the UV finite matrix element different. A key difference of the MS or $\overline{\text{MS}}$ scheme is an explicit dependence on the renormalisation scale, μ, which is accompanied by the coupling additionally being dependent on the same scale.

Consider the renormalisation of the electric charge in the $\overline{\text{MS}}$ scheme in $d = 4 - 2\epsilon$ dimensions. We relate the bare and renormalised couplings through an analogous equation to Eq. (1.2.10)

$$e_0 = \mu^\epsilon e(\mu) Z_e(\mu), \tag{1.2.21}$$

where we have now an explicit and implicit dependence on μ. As the unrenormalised Lagrangian has no reference to a renormalisation scale, it is necessarily independent on μ. The same can also be said about any one of the parameters of the Lagrangian. This property must be preserved when expressing the bare parameters in terms of the renormalised ones. Therefore, we take a derivative of Eq. (1.2.21) with respect

to μ,[1]

$$0 = \mu \frac{de_0}{d\mu} = \epsilon \mu^{\epsilon} e(\mu) Z_e(\mu) + \mu^{\epsilon+1} \frac{de(\mu)}{d\mu} Z_e(\mu) + \mu^{\epsilon+1} e(\mu) \frac{dZ_e(\mu)}{d\mu}. \tag{1.2.22}$$

We can then rewrite the right-hand side to read

$$0 = \mu^{\epsilon} Z_e(\mu) \left(\frac{de(\mu)}{d \log \mu} + \epsilon e(\mu) \right) + \mu^{\epsilon} e(\mu) \frac{dZ_e(\mu)}{d \log \mu}, \tag{1.2.23}$$

or when rewriting in terms of $\alpha = \frac{e^2}{4\pi}$, the fine structure constant,

$$Z_e(\mu) \left(\frac{1}{2} \frac{d\alpha(\mu)}{d \log \mu} + \epsilon \alpha(\mu) \right) + \alpha(\mu) \frac{dZ_e(\mu)}{d \log \mu} = 0. \tag{1.2.24}$$

Again, we can rewrite this one last time to identify the QED beta function,

$$\frac{d\alpha(\mu)}{d \log \mu} \equiv \beta(\alpha)\,. \tag{1.2.25}$$

Eq.(1.2.25) and those similar are known as the Renormalisation-Group (RG) equations [27, 28]. These can be solved perturbatively in the coupling,

$$\beta(\alpha) = -2\alpha(\mu) \left(\sum_{n=0} \left(\frac{\alpha(\mu)}{4\pi} \right)^{n+1} \beta_n(\alpha) \right). \tag{1.2.26}$$

The LO solution to Eq.(1.2.26) is the LO QED beta function $\beta_0(\alpha)$. We can compute this in a five flavour QED×QCD theory, where the top quark has been decoupled [29],[2]

$$\beta_0(\alpha) = -\frac{4}{3} \left(N_l Q_l^2 + N_C \left((N_u - 1)\, Q_u^2 + N_d Q_d^2 \right) \right) = -\frac{80}{9}\,, \tag{1.2.27}$$

where N_c is the number of colours and N_f and Q_f, with $f = l, d, u$, are the number and charges of the leptons, down type quarks and up type quarks respectively.

Solving Eq.(1.2.25) to LO we have

$$\alpha(\mu) = \frac{\alpha(\mu_0)}{1 - \alpha(\mu_0) \frac{\beta_0(\alpha)}{2\pi} \log \frac{\mu_0}{\mu}}$$

[1] We multiply through by μ for later convenience.

[2] We choose to use the five flavour theory here to match the calculations presented in Chapters 4 and 5.

$$= \alpha(\mu_0)\left(1 + 2\gamma_e(\mu_0)\log\frac{\mu_0}{\mu}\right), \tag{1.2.28}$$

where in the final line we have again expanded the denominator and written the equation in terms of the electric charge anomalous dimension $\gamma_e(\mu_0) = \frac{\alpha(\mu_0)}{\pi} \times \frac{20}{9}$. Eq. (1.2.28) can be used to perform scale changes of the couplings.

One can analogously play the same game with the QCD couplings or with the quark masses to define the QCD beta function or the quark mass anomalous dimension. In a five flavour QED×QCD theory, this procedure is detailed in [29] along with the additional details on the previous discussion.

A final remark is to mention that any observable should be invariant under a change in scale at a certain order in perturbation theory. Any explicit μ dependence must analytically cancel against the implicit μ dependence of the running of the couplings and masses, such as in Eq. (1.2.28).

Changes in the numerical value of predictions when the scale is varied occur first at the succeeding order in perturbation theory, giving an avenue to make an estimate on theoretical uncertainties.

These so-called scale uncertainties are typically estimated by varying the scale up and down by a factor of two in order to determine the stability of a result under changes in the unphysical renomalisation scale. The uncertainty is thus determined by the variation of the prediction. Scale uncertainties give one advantage of an $\overline{\text{MS}}$ renormalisation scheme over an on-shell one, where parameters do not run.

Chapter 2

The Standard Model Effective Field Theory

In this chapter, we wish to introduce the concept of the Standard Model Effective Field Theory (SMEFT). However, we first start with the general notion of an Effective Field Theory (EFT), using Fermi Theory as a simple example, and progressing the ideas to define the SMEFT. We consider how working with the SMEFT changes the interpretation parameters that also exist in the SM. We conclude in obtaining the first step in relating the Lagrangian parameters to an input scheme.

2.1 Effective Field Theories

An EFT, in the context of particle physics, is a QFT which is only a valid approximation up to a given energy scale. Defining an applicable EFT is dependent on the underlying high energy process having a hierarchy of scales [30], a high "new physics" scale, Λ, and the relatively smaller scale of the experimental process, E, being considered. A general EFT Lagrangian will have the structural form [31–33]

$$\mathcal{L}_{\text{EFT}} = \sum_i \mathcal{C}_i^{(d)} \mathcal{O}_i^{(d)} \,, \tag{2.1.1}$$

where $\mathcal{C}$ is the Wilson coefficient for operator $\mathcal{O}$. When constructing the EFT Lagrangian, there is a systematic procedure to include corrections of higher powers in $\delta \sim \frac{E}{\Lambda}$, which can be achieved in a top-down or bottom-up method. The precision of predictions made in the EFT are determined by the small expansion parameter δ, otherwise called a power counting parameter. For the EFT to be an accurate description of the physics at low orders in the expansion in δ, it needs to be small, i.e. we need the hierarchy of scales. Like any QFT, an EFT is accompanied by a regularisation and renormalisation scheme, which are necessary to obtain finite matrix elements and ultimately make predictions for physical processes.

Given the current limitations of the SM, it can be said that it is the first term of an EFT expansion, valid up to some currently unknown, high energy scale. At energies approaching this scale, the SM would no longer be an accurate description of physics, and a new alternate theory with a different particle content and interactions would be a more apt description.

2.1.1 Introduction to Effective Field Theories

First, in order to demonstrate some of the properties of EFTs, let us consider an EFT where the UV theory, the theory containing the heavy dynamical degrees of freedom, is known. Through the process of integrating-out the heavy degrees of freedom [34,35], we obtain a new EFT, which approximates the UV theory in the low energy limit. The mass scale of the heavy particle integrated-out of the theory gives the energy scale, around which the EFT is no longer a valid approximation. This process of obtaining the EFT from a known, high energy theory is colloquially called the top-down approach. A simple toy example, illustrating how the integrating-out process is applied, is given in [36] where a heavy scalar is integrated-out of a zero dimensional theory, containing the heavy scalar and a light scalar, leaving only a single light scalar in the EFT. Any notion of the heavy particle is lost, but its effects are imprinted on additional operators included in the low energy theory.

Here however, to understand some key features of EFTs, we use a more applicable and probably the most famous example of an EFT, Fermi theory. Fermi theory is a low energy theory of lepton interactions which was first proposed in the 1930s to explain nuclear β-decay [37]. Today, a more fundamental theory is known, the SM, from which Fermi theory can be derived as an EFT.

Consider the process of Muon decay as described in the SM. This process is mediated by the W boson, which couples to a charged lepton and corresponding neutrino via the weak current,

$$j^{\mu}_{W} = (\bar{\nu}_{\ell}\gamma^{\mu}P_{L}\ell) \ , \tag{2.1.2}$$

where ℓ is a generic charged-lepton, ν_{ℓ} is the corresponding neutrino and barred quantities have their usual definitions. The Feynman gauge tree level amplitude for this process in the SM is given by

$$\mathcal{A} = \left(\frac{g_2}{\sqrt{2}}\right)^2 \left[\bar{\nu}_{\mu}\gamma_{\mu}P_{L}\mu\right] \left(\frac{g^{\mu\nu}}{p^2 - M_W^2}\right) \left[\bar{e}\gamma^{\mu}P_{L}\nu_{e}\right] \ , \tag{2.1.3}$$

where $\frac{g_2}{\sqrt{2}}$ is the coupling of the W boson, of which we have two copies; the W propagator connects two lepton currents. Now consider the situation in which there is a low momentum transfer such that we have $p \ll M_W$. In this low energy limit of the problem, we can expand the W propagator in powers of $\frac{p^2}{M_W^2}$,

$$\frac{1}{p^2 - M_W^2} = -\frac{1}{M_W^2}\left(1 + \frac{p^2}{M_W^2} + \left(\frac{p^2}{M_W^2}\right)^2 + \dots\right) \ , \tag{2.1.4}$$

where the $\dots$ represents higher order terms in the expansion. Substituting Eq. (2.1.4) into our muon decay amplitude calculated in the SM, Eq. (2.1.3), and keeping only the leading order term in the expansion of the propagator, we have,

$$\mathcal{A} = -\frac{g_2^2}{2M_W^2}\left[\bar{\nu}_{\mu}\gamma_{\mu}P_{L}\mu\right] \times \left[\bar{e}\gamma^{\mu}P_{L}\nu_{e}\right] \ , \tag{2.1.5}$$

which is the low energy limit of the amplitude in the SM. However, this same low energy approximation for the amplitude could have been obtained by considering

the Effective Lagrangian,

$$\mathcal{L} = -\frac{4G_F}{\sqrt{2}} \left[\bar{\nu}_\mu \gamma_\mu P_L \mu\right] \times \left[\bar{e}\gamma^\mu P_L \nu_e\right] , \tag{2.1.6}$$

where, for the historical reason that G_F was experimentally measured before the idea of electroweak theory, we have made the identification,

$$\frac{G_F}{\sqrt{2}} = \frac{g_2^2}{8M_W^2}. \tag{2.1.7}$$

The EFT Lagrangian in Eq. (2.1.6), is the Lagrangian for Fermi Theory. The W boson has been integrated out of the SM as it is no longer a dynamical degree of freedom in the EFT. The effects of the W boson are captured by the dimension-six four fermion interaction and the associated effective coupling.

Although it is a simple example of an EFT, with only a single term in the Lagrangian, we can explore some of the key aspects and characteristic features of EFTs by studying it.

First, we note that the derivation required the fact that $p \ll M_W$, the mass of the W boson is large compared to other scales in the problem, and so we have a hierarchy of scales as required. Therefore, this implies that the EFT loses validity as we approach this energy scale, $E \sim M_W$, as a defining assumption of the EFT is broken.

The expansion parameter in this theory can be identified as $\delta = \frac{p^2}{M_W^2}$ from Eq. (2.1.4). In this example, we have only kept terms to zeroth order in the expansion parameter, errors are therefore $\mathcal{O}\left(\frac{p^2}{M_W^2}\right)$ as these are the largest terms we have truncated in the series. The truncated terms have the approximate size, $\frac{m_\mu^2}{M_W^2} \sim 10^{-6}$, giving rationalsation for the truncation of the expansion to first order. Nonetheless, to reduce the errors, one could have kept higher order terms in the expansion parameter. At the next order, dimension-eight terms are included, which involve the same fermion bilinears as the dimension-six terms along with two powers of a derivative. Retention of terms $\mathcal{O}(\delta^2)$ implies the errors are now $\mathcal{O}(\delta^3)$. This relation between the order of terms kept, and the precision potentially obtained from a physical prediction, is a general feature of an EFT. Expansion up to order δ^n implies predictions will have

an inherent error of order δ^{n+1}.

The examples of EFTs given so far have been examples of top down EFTs, where the high energy dynamics are known and have been integrated out. What remains are effective operators and an effective coupling constant comprised from known parameters of the UV theory. However, one can consider the same operator, with no mention of the UV theory, and include an unknown effective coupling constant. In the example of Fermi theory,

$$\mathcal{L} = \mathcal{C}\left[\bar{\nu}_\mu \gamma_\mu P_L \mu\right] \times \left[\bar{e}\gamma^\mu P_L \nu_e\right], \tag{2.1.8}$$

is the form of this Lagrangian, with $\mathcal{C}$ being the effective coupling constant, more generally known as a Wilson coefficient. As alluded previously, this was historically the first theory for Muon decay, derived before any knowledge of the W boson, where the Fermi constant G_F was used in place of the more modern terminology of Wilson coefficients.[1]

Building the EFT by starting with a low energy theory and constructing higher dimensional operators from fields in the low energy theory is known as the bottom-up approach.

One can consider the SM as the first term in a low energy EFT. By keeping the method of electroweak symmetry breaking linear and including higher dimensional operators constructed purely from SM fields in a bottom-up approach, one will arrive at the SMEFT. This theory is the topic of discussion for the remainder of this thesis.

2.2 The Standard Model Effective Field Theory

We now focus on the SMEFT [33, 38–40] which, contrary to our initial presentation of Fermi Theory, is an example of a bottom-up EFT. The SMEFT Lagrangian starts from the SM Lagrangian Eq. (1.1.2) and is constructed by the inclusion of additional,

[1] As written, a factor of $-2\sqrt{2}$ is also required.

higher dimensional operators. The introduced operators are built purely from SM fields, so that no new degrees of freedom are introduced. These composite operators, by construction, obey all the symmetries of the SM: the Poincaré symmetries and the gauge symmetries of Eq. (1.1.1). Each operator is accompanied by a corresponding Wilson coefficient, which, as previously mentioned, can be interpreted as an effective coupling coefficient for the corresponding operator. The mass dimension of the Lagrangian must be four. Consequently, Wilson coefficients associated with higher dimensional operators have negative mass dimensions.

Much like Eq. (2.1.1) but specifying that the dimension-four terms are the SM, we can write down a generic structural form of the SMEFT Lagrangian. Making no claim on what the introduced operators are at this point,

$$\begin{aligned}\mathcal{L}_{\text{SMEFT}} &= \mathcal{L}_{\text{SM}} + \sum_{d>4}\sum_{i} \mathcal{C}_i^{(d)}\mathcal{O}_i^{(d)} \\ &= \mathcal{L}_{\text{SM}} + \sum_{d>4}\sum_{i} \frac{\tilde{\mathcal{C}}_i^{(d)}}{\Lambda_{\text{NP}}^{d-4}}\mathcal{O}_i^{(d)}\,, \end{aligned} \tag{2.2.1}$$

where the $\mathcal{O}_i^{(d)}$ are the operators of dimension d and the $\mathcal{C}_i^{(d)}$ are the corresponding Wilson coefficients. The two sums indicate that we are including all possible mass dimensions of operators greater than four and all possible operators of a given mass dimension. In the second line, we have factored out the new physics scale, Λ_{NP}, from the Wilson coefficients to define the dimensionless quantity $\tilde{C}_i^{(d)}$, making manifest the negative mass dimensionality of the Wilson coefficients in the first line.

The most general SMEFT Lagrangian in Eq. (2.2.1) contains a sum over all operators of mass dimension greater than four. However, as the scale of new physics is large, typically $\Lambda_{\text{NP}} \sim \mathcal{O}\,(1\text{ TeV})$ in analyses, the effects of operators of higher mass dimensions become greatly diminished due to an ever-increasing number of inverse powers of this large scale.

From here on in, we truncate the SMEFT Lagrangian to dimension-six in the operator's mass dimension. Consequently, the expressions given are only correct and self-consistent up to dimension-six and should be interpreted accordingly. Written

equations, which may implicitly contain a dimension-eight contribution, should be understood such that the dimension-eight pieces are ignored as the relations are only valid to linear order in the Wilson coefficients.

After truncating the SMEFT Lagrangian to dimension-six, we are left with only the dimension-five and dimension-six operators to add to the SM

At dimension-five, after imposing the SM gauge symmetry constraints and ignoring flavour indices, there is only a single operator to be included into the SMEFT Lagrangian. This is the Weinberg operator [41], which after electroweak symmetry breaking generates neutrino masses and mixing. However, due to this operator playing no role in the Electroweak precision observables, we forgo to mention any further physics implication of the operator and shall remove it from our Lagrangian.

Finally, we are just left with the dimension-six operators. In order to write down the Lagrangian for the SMEFT we first need to identify all the operators. We require a minimal basis of operators, where equations of motion, field redefinitions and Fierz relations have been used to eliminate redundant operators such that no single operator can be rewritten as a linear combination of the others.

A first attempt to derive a minimal basis was completed in [33] where a total of 80 operators were found if one ignores flavour indices. Later, in [40], it was shown that only 59 of these were linearly independent to define what is now known as the Warsaw basis.[1] A full list of these operators can be found in Appendix (A.1) where the operators are categorised into eight distinct classes.

Using the Warsaw basis, we arrive at and can write down the SMEFT Lagrangian used throughout this work as

$$\begin{aligned}\mathcal{L}_{\text{SMEFT}} &= \mathcal{L}^{(4)} + \mathcal{L}^{(6)} \\ &= \mathcal{L}_{\text{SM}} + \sum_i \mathcal{C}_i \mathcal{Q}_i \,, \end{aligned} \tag{2.2.2}$$

where the terms in the second line are in the same order as those on the first. The

[1] If one includes flavour indices there are 2499 independent Wilson coefficients.

sum now runs over all operators in the Warsaw basis. Identically to [40], we choose to represent an operator in the Warsaw basis using a $\mathcal{Q}$ to distinguish from any other basis.

2.2.1 Changes to SM Electroweak parameters

The introduction of the SMEFT operators has consequences for many of the bare parameters as defined in the SM in Section 1.1. Additional operators disrupt the SM relations between parameters. Moreover, fields are no longer canonically normalised due to the presence of these operators.

Field redefinitions can reimpose canonical normalisation, yet in other fundamental relations of the theory, the influence of the operators remains. The work of [42] draws attention to most of these changes, whilst here, with the foresight of studying the Electroweak input parameters, we give a review of the changes to the Higgs VEV and doublet and gauge couplings.

Higgs VEV

We start with the Higgs VEV where in the SM, Section 1.1.2, the VEV takes the form

$$v = \sqrt{\frac{\mu^2}{2\lambda}}. \tag{2.2.3}$$

The Class 2 operator $\mathcal{Q}_H$ is an interaction between Higgs doublets only. As a result, it provides an additional term in the Higgs potential, which now reads,

$$V(H) = \lambda\left(H^\dagger H - \frac{v^2}{2}\right) - \mathcal{C}_H\left(H^\dagger H\right)^3, \tag{2.2.4}$$

where the first term is the usual SM potential, which has been rearranged compared to Eq. (1.1.8).[1] Following the same procedure as for the SM, minimising the VEV

[1] A constant term, which does not change the position of the minimum has also been included.

yields the following after expanding to first order in the Wilson coefficient,

$$\langle H^\dagger H\rangle \equiv \frac{v_T^2}{2} = \frac{v^2}{2}\left(1+\frac{3}{4}\frac{\mathcal{C}_H v^2}{\lambda}\right). \tag{2.2.5}$$

The quantity v_T is the 'true' VEV, which includes a contribution from the SMEFT Wilson coefficient C_H.

Class 3 operators involve the quantity $H^\dagger H$ and its derivatives. These contribute additional kinetic terms to the Higgs field,

$$\begin{aligned}\mathcal{L}_{\text{Higgs, Kin}} &= \left(D_\mu H\right)^\dagger (D^\mu H) + C_{H\Box}\left(H^\dagger H\right)\Box\left(H^\dagger H\right) + C_{HD}\left(H^\dagger D_\mu H\right)^*\left(H^\dagger D_\mu H\right)\\ &= \frac{1}{2}(\partial_\mu h)(\partial^\mu h) - v_T^2 C_{H\Box}(\partial_\mu h)(\partial^\mu h) + \frac{v_T^2}{4}C_{HD}(\partial_\mu h)(\partial^\mu h)\,,\end{aligned} \tag{2.2.6}$$

where in the second line we have chosen to expand the Higgs doublet in unitary gauge. As has been made explicit in Eq. (2.2.6), the dynamic part of the Higgs field is no longer canonically normalised using the SM form of the Higgs doublet, Eq. (1.1.13). Performing the field redefinition,

$$h \to h\left(1 + v_T^2 C_{H\Box} - \frac{v_T^2}{4}C_{HD}\right), \tag{2.2.7}$$

we can reinstate this condition as required. The Higgs doublet is now written, in unitary gauge, as

$$H(x) = \frac{1}{\sqrt{2}}\begin{pmatrix}0\\ h\left(1 + v_T^2 C_{H\Box} - \frac{v_T^2}{4}C_{HD}\right) + v_T\end{pmatrix}, \tag{2.2.8}$$

where the Higgs field is now normalised correctly. For completeness, we note that in R_ξ gauge, while the charged gauge bosons $\phi^\pm$ require no redefinitions from the SM, the neutral Goldstone boson ϕ^0 is redefined to be

$$\phi^0 \to \phi^0\left(1 - \frac{v_T^2}{4}C_{HD}\right). \tag{2.2.9}$$

Again for completeness, combining the kinetic terms with the Higgs potential, the

Higgs mass is obtained to be

$$m_H^2 = 2\lambda v_T^2 \left(1 - \frac{3v_T^2 C_H}{2\lambda} + 2v_T^2 \left(C_{H\Box} - \frac{C_{HD}}{4}\right)\right). \tag{2.2.10}$$

Gauge Couplings

Similar to the Higgs sector, definitions in the gauge sector are affected by the presence of SMEFT operators. In the broken theory, Class 4 operators contribute to kinetic terms of the gauge bosons,

$$\begin{aligned}\mathcal{L}_{\text{Gauge, Kin}} =& -\frac{1}{2}W^+_{\mu\nu}W^{\mu\nu}_- - \frac{1}{4}W^3_{\mu\nu}W_3^{\mu\nu} - \frac{1}{4}B_{\mu\nu}B^{\mu\nu} - \frac{1}{4}G^A_{\mu\nu}G^{A,\mu\nu} \\ &+ \frac{1}{2}v_T^2 C_{HG} G^A_{\mu\nu}G^{A,\mu\nu} + \frac{1}{2}v_T^2 C_{HW} W^a_{\mu\nu}W^{a,\mu\nu} + \frac{1}{2}v_T^2 C_{HB} B_{\mu\nu}B^{\mu\nu} \\ &+ \frac{1}{2}v_T^2 C_{HWB} W^3_{\mu\nu}B^{\mu\nu}\,,\end{aligned} \tag{2.2.11}$$

while the class 3 operator C_{HD} has a contribution to the mass terms,

$$\mathcal{L}_{\text{Gauge, Mass}} = \frac{1}{4}g_2^2 W^+_\mu W^\mu_- + \frac{1}{8}v_T^2\left(g_2 W^3_\mu - g_1 B_\mu\right)^2 + \frac{1}{16}v_T^4 C_{HD}\left(g_2 W^3_\mu - g_1 B_\mu\right)^2. \tag{2.2.12}$$

Again, the direct inclusion of the SMEFT operators into the SM Lagrangian has left us with problems. The final term in Eq. (2.2.11) gives rise to kinetic mixing, while the Lagrangian as a whole is again not canonically normalised. Similar to the Higgs sector, field redefinitions are once again required to regain the desired properties of the Lagrangian.

First, we redefine the gauge fields as,

$$\begin{aligned} B_\mu &= \mathcal{B}_\mu(1 + v_T^2 C_{HB}), \\ W^a_\mu &= \mathcal{W}^a_\mu(1 + v_T^2 C_{HW}), \\ G^A_\mu &= \mathcal{G}^A_\mu(1 + v_T^2 C_{HG}). \end{aligned} \tag{2.2.13}$$

Requiring that the products of gauge fields and corresponding couplings remain

unchanged, we define the modified coupling constants

$$\begin{aligned}\bar{g}_1 &= g_1(1 + v_T^2 C_{HB}),\\ \bar{g}_2 &= g_2(1 + v_T^2 C_{HW}),\\ \bar{g}_s &= g_s(1 + v_T^2 C_{HG}).\end{aligned} \tag{2.2.14}$$

These redefinitions fix the normalisation of the gluon field, however like in the SM, we need a rotation into the mass basis for the electroweak sector. The mass basis rotation, as first written in [43], is

$$\begin{pmatrix}\mathcal{W}_\mu^3\\ \mathcal{B}_\mu\end{pmatrix} = \begin{pmatrix}1 & -\frac{1}{2}v_T^2 C_{HWB}\\ -\frac{1}{2}v_T^2 C_{HWB} & 1\end{pmatrix}\begin{pmatrix}\cos\bar{\theta} & \sin\bar{\theta}\\ -\sin\bar{\theta} & \cos\bar{\theta}\end{pmatrix}\begin{pmatrix}\mathcal{Z}_\mu\\ \mathcal{A}_\mu\end{pmatrix}, \tag{2.2.15}$$

where

$$\begin{aligned}\sin\bar{\theta} &= \frac{\bar{g}_1}{\sqrt{\bar{g}_1^2+\bar{g}_2^2}}\left(1 + \frac{v_T^2}{2}\frac{\bar{g}_2}{\bar{g}_1}\frac{\bar{g}_2^2-\bar{g}_1^2}{\bar{g}_2^2+\bar{g}_1^2}C_{HWB}\right),\\ \cos\bar{\theta} &= \frac{\bar{g}_2}{\sqrt{\bar{g}_1^2+\bar{g}_2^2}}\left(1 - \frac{v_T^2}{2}\frac{\bar{g}_1}{\bar{g}_2}\frac{\bar{g}_2^2-\bar{g}_1^2}{\bar{g}_2^2+\bar{g}_1^2}C_{HWB}\right).\end{aligned} \tag{2.2.16}$$

Writing the Lagrangian in the mass basis allows one to read off the boson masses in terms of $\bar{g}_1$, $\bar{g}_2$ and the two Wilson coefficients C_{HD} and C_{HWB},

$$\begin{aligned}M_A^2 &= 0,\\ M_W^2 &= \frac{\bar{g}_2 v_T^2}{4},\\ M_Z^2 &= \frac{v_T^2}{4}\left(\bar{g}_1^2+\bar{g}_2^2\right) + \frac{1}{8}v_T^4\left(\bar{g}_1^2+\bar{g}_2^2\right)C_{HD} + \frac{1}{2}v_T^4\bar{g}_1\bar{g}_2 C_{HWB}.\end{aligned} \tag{2.2.17}$$

As is to be expected, the photon is massless because the $U(1)_{\mathrm{EM}}$ gauge symmetry is unbroken. In the limit that $\Lambda_{NP} \to \infty$, the masses of the W and Z boson regain the expected form as seen in Section 1.1.2.

From here, one could go further to write the covariant derivative in terms of the barred quantities $\bar{g}_1$, $\bar{g}_2$, $\sin\bar{\theta}$ and $\cos\bar{\theta}$. This would lead to the covariant derivative having the same form as for the SM, where one can directly read off the couplings as is done in [42].

Here however, we opt to show a somewhat inverted relation allowing for the couplings $\bar{g}_1$ and $\bar{g}_2$ to be written in terms of masses and the Higgs VEV, v_T, in addition to Wilson coefficients. This is undertaken with the foreknowledge of requiring the Lagrangian to be written in a standard and convenient form to conduct a study into electroweak input schemes. These relations read,

$$\begin{aligned}\bar{g}_1 &= \frac{2M_W s_w}{c_w v_T}\left[1 - \frac{v_T^2}{4s_w^2}\left(C_{HD} + 4c_w s_w C_{HWB}\right)\right], \\ \bar{g}_2 &= \frac{2M_W}{v_T}, \end{aligned} \tag{2.2.18}$$

where

$$s_w = \sqrt{1 - c_w^2}, \quad c_w = \frac{M_W}{M_Z}. \tag{2.2.19}$$

The use of these equations, at the level of the electroweak Lagrangian, is an important first step in Chapters 4 and 6.

2.2.2 Operator renormalisation

If we wish to calculate quantum corrections in the SMEFT, additional to the renormalisation procedure of Section 1.2.2 applied to the SMEFT, we need to renormalise the local dimension-six operators. We achieve this by introducing counterterms for the associated Wilson coefficients.

We follow the same tack as Section 1.2.2, where we relate the bare operators to the renormalised ones through, what is in this case, a renormalisation constant matrix Z_O defined in an $\overline{\text{MS}}$ scheme. The matrix Z_O allows for operator mixing between the bare and renormalised fields [44],

$$O_i^{(0)} = \left[Z_O(\mu)\right]_{ij} O_j(\mu), \tag{2.2.20}$$

or, for later convenience, inverting and writing in terms of amputated Green's

functions of the operator,

$$\langle O_i \rangle = \left[Z_O^{-1}(\mu) \right]_{ij} \langle O_j \rangle^{(0)} \,. \tag{2.2.21}$$

Taking a derivative of Eq. (2.2.20) with respect to the renormalisation scale μ gives

$$0 = \frac{dO_i^{(0)}}{d\log\mu} = \frac{d\left[Z_O(\mu)\right]_{ij}}{d\log\mu} O_j(\mu) + \left[Z_O(\mu)\right]_{ij} \frac{dO_j(\mu)}{d\log\mu} \,, \tag{2.2.22}$$

where we have made use of the fact that the bare parameters have no dependence on a renormalisation scale. Solving this equation yields,

$$\frac{dO_i(\mu)}{d\log\mu} = -\left[Z_O^{-1}\right]_{ik} \frac{d\left[Z_O(\mu)\right]_{kj}}{d\log\mu} O_j(\mu) = -\gamma_{ij}^{\intercal} O_j(\mu) \,, \tag{2.2.23}$$

where we use this as a definition of the anomalous dimension matrix γ_{ij}. We include the somewhat arbitrary transpose and negative sign at this point for later simplification.

The operator renormalisation constants will provide a way to renormalise the EFT, however, when considering bottom-up EFTs, as is the SMEFT, one usually likes to think in terms of counter terms to Wilson coefficients. To this end, consider a generic renormalised expectation value,

$$\begin{aligned}
\langle \mathcal{H} \rangle &= C_i^{(0)} \langle O_i \rangle^{(0)} \\
&= \left[Z_C(\mu)\right]_{ij} C_j(\mu) \langle O_i \rangle^{(0)} \\
&= C_i(\mu) \langle O_i \rangle^{(0)} + \left(\left[Z_C(\mu)\right]_{ij} - \delta_{ij} \right) C_j(\mu) \langle O_i \rangle^{(0)} \\
&= C_i(\mu) \langle O_i \rangle^{(0)} + \left(\left[\delta Z_C(\mu)\right]_{ij} \right) C_j(\mu) \langle O_i \rangle^{(0)} \\
&= C_i(\mu) \langle O_i \rangle \,.
\end{aligned} \tag{2.2.24}$$

In the first equality we have introduced the renormalisation constant for the Wilson coefficients $\left[Z_C(\mu)\right]_{ij}$. The second term in the third line is identified to be the counterterms resulting in the finite prediction in line five.

To make the connection with the operator renormalisation constants we make use

of Eq. (2.2.21) to find

$$[Z_C(\mu)]_{ij}\, C_i(\mu)\langle O_i\rangle^{(0)} = C_i(\mu)\langle O_i\rangle = C_i(\mu)\left[Z_O^{-1}(\mu)\right]_{ij}\langle O_j\rangle^{(0)} = \left[Z_O^{-1}(\mu)\right]_{ji} C_j(\mu)\langle O_i\rangle^{(0)}, \tag{2.2.25}$$

making it easy to identify that

$$[Z_C(\mu)]_{ij} = \left[Z_O^{-1}(\mu)\right]_{ji}. \tag{2.2.26}$$

This identification of renormalisation constants for operators and Wilson coefficients allows us to write the RG equation in terms of the anomalous dimension matrix. Starting from the Wilson coefficient equivalent of Eq. (2.2.23),

$$\begin{aligned}\frac{dC_i(\mu)}{d\log\mu} &= -\left[Z_C^{-1}\right]_{ik}\frac{d\,[Z_C(\mu)]_{kj}}{d\log\mu}C_j(\mu)\\ &= -\frac{d\left[Z_O^{-1}(\mu)\right]_{jk}}{d\log\mu}\,[Z_O]_{ki}\,C_j(\mu)\\ &= \left(\frac{d\left(\left[Z_O^{-1}(\mu)\right]_{jk}[Z_O(\mu)]_{ki}\right)}{d\log\mu} + \left[Z_O^{-1}\right]_{jk}\frac{d\,[Z_O(\mu)]_{ki}}{d\log\mu}\right)C_j(\mu)\\ &= \gamma_{ij}C_j(\mu),\end{aligned} \tag{2.2.27}$$

where now the previous minus sign and transpose in the definition of γ_{ij} are justified. This equation above describes the running of the Wilson coefficients as the scale at which they are evaluated is changed. In the SMEFT, these runnings are known to one loop [42, 45, 46] and thus, so is the anomalous dimension matrix. Furthermore, computational tools [47, 48] allow for quick implementation.

However, for a specific loop calculation in the SMEFT, we still require the analytic form of the counterterms in order to make finite predictions. In the $\overline{\text{MS}}$ scheme, these can be related to the running of the Wilson coefficients. Consider a renormalised amplitude in the $\overline{\text{MS}}$ scheme,

$$\langle A\rangle \sim \left[\delta_{ij} + A_{ij}\left(\frac{1}{\epsilon} + 2\log\mu\right) + [\delta Z_C]_{ij} + \ldots\right]C_j(\mu)\langle O_i\rangle, \tag{2.2.28}$$

where the ... represents additional finite pieces of the amplitude. We clearly see that we must have,

$$[\delta Z_C]_{ij} = -\frac{1}{\epsilon} A_{ij} \,, \tag{2.2.29}$$

in order for the amplitude to be finite. Therefore, understanding the form of A_{ij} enables the determination of the counterterms. At one loop, the amplitude is independent of the renormalisation scale, therefore we write

$$\begin{aligned} \frac{d\langle A\rangle}{d\log\mu} = 0 &= 2A_{ij}C_j(\mu)\langle O_i\rangle + \frac{dC_j(\mu)}{d\log\mu}\langle O_i\rangle \\ &= \Big(2A_{ij} + \gamma_{ij}\Big)\, C_j(\mu)\langle O_i\rangle, \end{aligned} \tag{2.2.30}$$

hence,

$$A_{ij} = -\frac{1}{2}\gamma_{ij}. \tag{2.2.31}$$

This identification leads simply on to the equality

$$[\delta Z_C]_{ij} = -\frac{1}{\epsilon} A_{ij} = \frac{1}{2\epsilon}\gamma_{ij}, \tag{2.2.32}$$

or in terms of counterterms for individual Wilson coefficients,

$$\delta C_i = \frac{1}{2\epsilon}\gamma_{ij} C_j = \frac{1}{2\epsilon}\frac{dC_i(\mu)}{d\log\mu} \,. \tag{2.2.33}$$

The specific form of the counterterms for the Wilson coefficients are now known in the $\overline{\text{MS}}$ scheme, and we have all we need to calculate quantum corrections in the SMEFT. Interestingly, as a final remark, although we are concerned here with the SMEFT, no part of the lead up to Eq. (2.2.33) relies on specific SMEFT framework, and so it is valid for any EFT.

Chapter 3

Preliminary Information

In this chapter and the following chapters, we begin to focus on the main topic of the thesis; a study into EW input schemes in the dimension-six SMEFT. In Chapter 4 we introduce three schemes which have common use in the SMEFT literature, and we set our notation for what follows. Chapter 5 provides a study into these commonly used input schemes, discussing the salient features and finishing with a set of universal corrections associated with each scheme. In Chapter 6, we introduce two new schemes for the SMEFT, which involve the effective mixing angle $\sin\theta^{\ell}_{\text{eff}}$ as an input and in Chapter 7, we again discuss the features of these new schemes but mainly focus on comparison with the aforementioned schemes which are currently in use.

In order to undertake such a task, we must first motivate why such a study is necessary.

3.1 Motivation

The first step in motivating why a study into electroweak input schemes is necessary, we must clarify what we understand an input scheme to be. We will discuss what it means to choose an input scheme and what are the possible choices that one can make. The link between the choice of input scheme and renormalisation will be

made apparent, allowing the importance of the scheme choice to be highlighted and alluding to how differences between schemes come to pass. Here we tell no specifics about any one scheme, which is left for later chapters.

At the most basic level, an input scheme can loosely be defined as a set of physical, experimentally measurable parameters one uses in a calculation, in order to obtain a numerical prediction. They are the numbers we "input" into the machinery of the theory in order to return predictions. These experimentally measurable parameters can be anything from the theory. In the SM they can consist of, but are not limited to, masses of particles and couplings between particles. If the SM were exact to LO our definition of an input scheme would be complete here. However, this is not the case in the SM or SMEFT, as we work in perturbation theory and relations between potential input parameters at LO do not hold true to NLO and beyond.

Working in perturbation theory beyond LO requires renormalisation to obtain finite predictions for amplitudes. Renormalisation introduces counterterms into the amplitude, cancelling the divergences appearing from the matrix elements of a process. The counterterms introduced are those relating to the potential input parameters appearing in the LO matrix elements.[1]

Although the divergences appearing in the appropriate combination of counterterms must match for all possible scheme choices, as the divergences in the matrix elements remain the same, there is in general no relation between finite pieces. Hence, different schemes will have differing perturbative behaviours as a result of the scheme dependent corrections stemming from the counterterms.

An input scheme is therefore not merely the numbers one plugs into a calculation to return a numerical prediction, but an intrinsic part of the renormalisation procedure and a crucial step in any perturbative calculation.

To fully define an input scheme, one must list the full set of parameters one chooses to replace the Lagrangian parameters with to obtain a numerical result. Further-

[1] Along with those associated with wave-function renormalisation and, in the SMEFT, Wilson coefficients.

more, if renormalisation is needed to produce finite prediction, specification of how counterterms are defined and extracted should be given to leave no ambiguity.

For the simpler case of a purely Quantum Chromo Dynamics (QCD) process[1], the choice of input parameters, to re-express the Lagrangian variables in terms of, is predetermined by the theory. The only available quantities are the strong coupling and the quark masses, and therefore they must be used.

In EW physics, this is not the case due to an over complete basis of possible input parameters. There are, however, a number of choices which are customary to use, for example one should use the fermionic particle masses as an input[2], identical to a QCD process, and it is customary to use the $\overline{\text{MS}}$ definition of Wilson coefficients. Despite this, not all parameters in the EW Lagrangian have an 'obvious' choice. In particular, the gauge couplings g_1 and g_2, and the Higgs VEV in the Lagrangian can be re-expressed in terms of a number of different experimentally measurable quantities. Some of these have already been introduced in Section 2.2.1, where the renormalisation conditions of Section 1.2.2 can be extended to dimension-six.

From here on in, when mentioning an input scheme, we refer to the EW input scheme, i.e. the set of three parameters to replace the variables g_1 and g_2 and the Higgs VEV in the Lagrangian and the definitions of counterterms.

Clearly, an important consideration for SMEFT predictions and fits is the choice of the EW input scheme. The investigation of NLO corrections in dimension-six SMEFT has been the focus of numerous recent studies: QCD corrections have been fully automated [49], NLO EW corrections and, in a few instances Next-to-Next-to-Leading-Order (NNLO) QCD corrections, have been calculated on a case-by-case basis for specific processes [29, 50–99]. Therefore, it is more pressing than ever to understand our choice of input scheme.

Ideally, the input parameters should be measured with very high accuracy such that the effect on SMEFT fits is subdominant or even negligible. However, even

[1] With regard to defining input parameters.
[2] Assuming one has not set them to zero.

beyond that, the choice of the input parameters influences perturbative convergence as well as the pattern of Wilson coefficients appearing in LO and NLO predictions.[1] Typical choices of the input parameters include the Fermi constant G_F, the mass of the W and Z bosons, M_W and M_Z, as well as the electromagnetic coupling constant α. Invariably, the NLO SMEFT calculations described above have been performed in one of three different schemes, which use either $\{M_W,\, M_Z,\, G_F\}$ (α_μ scheme), $\{M_W,\, M_Z,\, \alpha\}$ (α scheme), or $\{\alpha,\, M_Z,\, G_F\}$ (LEP scheme) as inputs. Some discussions of these input schemes can be found in [100,101]. However, there has been no systematic study which elucidates general features of these EW input schemes beyond LO in the SMEFT, much less a numerical exploration of benchmark results at NLO in the different schemes. The work presented in this thesis fills this gap.

Furthermore, in the SM, several studies have proposed EW input schemes which use the effective leptonic weak mixing angle $\sin\theta^\ell_{\text{eff}}$ as an input parameter [102–107].

In spite of this recent and past interest in EW input schemes involving $\sin\theta^\ell_{\text{eff}}$, a discussion in the context of SMEFT has not yet appeared in the literature. Again, the work of this thesis fills this gap by incorporating the $\{G_F, \sin\theta^\ell_{\text{eff}}, M_Z\}$ (v_μ^{eff} scheme) and $\{\alpha, \sin\theta^\ell_{\text{eff}}, M_Z\}$ (v_α^{eff} scheme) input schemes into the methodology in detail.

3.2 Assumptions and Work Flow

3.2.1 Lagrangian Assumptions and Flavour Scenarios

In order to reduce the calculational complexity of our Lagrangian, a number of beneficial assumptions must be made. The assumptions we make are common practice in recent developments for EW physics in SMEFT.

We reiterate the assumptions previously mentioned in Section 1.1.4 and extend them to the SMEFT. We work in the limit that all leptons and the light quarks are

[1] All will be seen in later chapters

massless, that being all quarks except the top. Therefore, the only masses which remain are those of the W, Z, and Higgs bosons, and that of the top quark.

Furthermore, we take the theory to be flavour diagonal. This has consequences on the SM, whereby the CKM matrix is set to the identity. Additionally, this restriction greatly reduces the number of Wilson coefficients, as two-fermion operators, cannot have differing flavour generations and so take the form,

$$\mathcal{C}_{ii}^{x}, \quad i = 1, 2, 3\,, \tag{3.2.1}$$

where we have labelled an arbitrary two fermion operator $\mathcal{C}_x$ and i is the flavour generation. It should be noted that for subscripts on Wilson coefficients, we are not using Einstein summation notation, unlike in the rest of this thesis. Therefore, in the above we have the operators $\mathcal{C}_{11}^{x}$, $\mathcal{C}_{22}^{x}$, and $\mathcal{C}_{33}^{x}$ and not a sum of them. For four-fermion operators, if the fermion representations are different a single flavour is associated with each representation,

$$\mathcal{C}_{iijj}^{xy}, \quad i, j = 1, 2, 3\,, \tag{3.2.2}$$

whereas for identical fermion representations an additional structure is allowed,

$$\begin{aligned} &\mathcal{C}_{iijj}^{xx}, \quad i, j = 1, 2, 3\,, \\ &\mathcal{C}_{ijji}^{xx}, \quad i, j = 1, 2, 3\,. \end{aligned} \tag{3.2.3}$$

Additionally, in an attempt to reduce the number of Wilson coefficients appearing in the processes, we also consider the assumption of $U(2)^2 \times U(3)^3$ flavour scenario. In the SM, the $U(3)^5$ symmetry for the SM fermions

$$U(3)^5 \equiv U(3)_q \times U(3)_l \times U(3)_u \times U(3)_d \times U(3)_e\,, \tag{3.2.4}$$

is broken only by the Yukawa couplings [108, 109]. The $U(2)^2 \times U(3)^3$ scenario extends this requirement to the SMEFT [110]. Since we consider all fermions except the top quark to be massless, we thus only allow the breaking of the $U(3)^5$ symmetry

by the top Yukawa coupling Y_t hence we have a

$$U(2)^2 \times U(3)^3 \equiv U(2)_q \times U(2)_u \times U(3)_l \times U(3)_d \times U(3)_e\,, \tag{3.2.5}$$

flavour symmetry. In the scenario case, we therefore distinguish Wilson coefficients involving the top quark from those involving first and second-generation up-type quarks.

We change from the flavour-general scenario to $U(2)^2 \times U(3)^3$ by making a set of replacements on the Wilson coefficients, see e.g. [96]. For operators with two flavour indices involving leptons or down-type quarks, we can suppress the flavour indices

$$C_{\substack{x\\ii}} \to C_x \quad \text{for} \quad C_x \in C_{He},\, C_{Hl}^{(1)},\, C_{Hl}^{(3)},\, C_{Hd}\,. \tag{3.2.6}$$

For the Wilson coefficients with two flavour indices involving up-type quark fields, we explicitly distinguish top-quark couplings

$$C_{\substack{x\\jj}} \to C_x \quad \text{for} \quad j \in 1,\,2\,, \quad C_{\substack{Hu\\33}} \to C_{Ht}, \quad C_{\substack{Hq\\33}}^{(1)} \to C_{HQ}^{(1)}, \quad C_{\substack{Hq\\33}}^{(3)} \to C_{HQ}^{(3)}\,. \tag{3.2.7}$$

For C_{uB} and C_{uW}, only Wilson coefficients with third-family indices contribute in the first place, so no replacement is necessary.

For four-fermion operators with two different fermion bilinears as well as C_{ee}, which is simplified by a Fierz identity, there is a single coefficient contributing under the $U(2)^2 \times U(3)^3$ assumption when no up-type quarks are involved

$$C_{\substack{x\\iijj}} \to C_x \quad \text{for} \quad C_x \in C_{ee},\, C_{le},\, C_{ld},\, C_{ed}\,. \tag{3.2.8}$$

For Wilson coefficients involving up-type quark fields we distinguish the third generation

$$\begin{aligned} &C_{\substack{x\\iijj}} \to C_x \quad \text{for} \quad j \in 1,\,2, \quad C_{\substack{lq\\ii33}}^{(1)} \to C_{lQ}^{(1)}, \quad C_{\substack{lq\\ii33}}^{(3)} \to C_{lQ}^{(3)}, \quad C_{\substack{lu\\ii33}} \to C_{lt}, \\ &C_{\substack{qe\\jjii}} \to C_{qe} \quad \text{for} \quad j \in 1,\,2, \quad C_{\substack{qe\\33ii}} \to C_{Qe} \quad . \end{aligned} \tag{3.2.9}$$

For C_{ll}, which involves two fermion currents of the same species and chirality, there

are two $U(3)^5$ symmetric combinations, which we distinguish with a prime

$$C_{\substack{ll\\iijj}} \to C_{ll}, \quad C_{\substack{ll\\ijji}} \to C'_{ll}, \quad C_{\substack{ll\\iiii}} \to C_{ll} + C'_{ll}. \tag{3.2.10}$$

3.2.2 Work Flow

We have carried out the calculations of this thesis using an in-house `FeynRules` [111] implementation of the SMEFT dimension-six Lagrangian and cross-checked our results with `SMEFTsim` [112, 113]. These model files were subsequently used with `FeynArts` and `FormCalc` [114–116] which we employed for the automated calculation of Feynman diagrams. The packages listed previously allowed the calculation of diagrams containing operators from classes 1-7 in the SMEFT. However, loop diagrams involving a class-8 operator cannot currently be implemented by this procedure. To calculate these, we used a 'by hand' approach, making use of `PackageX` [117] to extract analytic results for Feynman integrals. `DsixTools` [47] allowed for the quick implementation of Wilson coefficient renormalisation and the reduction of Wilson coefficient flavour indices. Finally, numerical results were obtained with `LoopTools` [115].

Chapter 4

Schemes in the SMEFT Literature

In this chapter, we introduce three of the five EW input schemes that we are considering in this thesis. The three schemes we introduce here are the α, α_μ and LEP schemes, which have common use in the SMEFT literature. For reference, the three input parameters that define each scheme are given in table 4.1 with the exact definition of the parameters given in the relevant sections.

We present definitions and derivations of counterterms necessary to complete EW NLO calculations in the SMEFT and print analytic results where appropriate.

However, in order to get into the specifics about the individual schemes, we necessitate having a common starting point for each scheme to treat them in a unified fashion. To achieve this we use the tree-level Lagrangian written in terms of v_T, M_W, and M_Z. In practice, this is obtained by transforming to the gauge-boson mass-basis using the field rotations defined in [42] and making the substitutions given in Eq. (2.2.18) and repeated here,

$$\bar{g}_1 = \frac{2M_W s_w}{c_w v_T}\left[1 - \frac{v_T^2}{4s_w^2}\left(C_{HD} + 4c_w s_w C_{HWB}\right)\right], \tag{4.0.1}$$

$$\bar{g}_2 = \frac{2M_W}{v_T}, \tag{4.0.2}$$

which are valid up to linear order in the Wilson coefficients. The sine and cosine of

scheme	inputs
α_μ	G_F, M_W, M_Z
α	α, M_W, M_Z
LEP	G_F, α, M_Z

Table 4.1: Nomenclature for the EW input schemes considered in this work.

the Weinberg angle are defined as,

$$s_w = \sqrt{1 - c_w^2}\,, \quad c_w = \frac{M_W}{M_Z}\,. \tag{4.0.3}$$

The renormalised Lagrangian in a given scheme is then obtained by interpreting the tree-level parameters and fields as bare ones, denoted with a subscript 0, and trading them for renormalised quantities through the addition of counterterms appropriate to that scheme much like Eq. (1.2.9) but extended to have counterterms of higher mass dimension.

Common to all schemes here is the fact we use the FJ renormalisation scheme [26] with definitions of the scheme and counterterms found in Section 3.1.6 of [24]. Additionally, in the same reference, alternative tadpole schemes are mentioned, but we make no comment on their use other than to highlight that they exist.

4.1 The α Scheme

To start our discussion of the three schemes which appear in current SMEFT literature, let's consider the α scheme. The α scheme uses the set of inputs $\{\alpha, M_W, M_Z\}$, where $\alpha = e^2/(4\pi)$ is the QED coupling constant defined in a given renormalisation scheme and M_W and M_Z are the masses of the W and Z bosons which are renormalised on-shell as described in Section 1.2.2.

For convenience, we introduce the derived parameter,

$$v_\alpha = \frac{2M_W s_w}{\sqrt{4\pi\alpha}}\,. \tag{4.1.1}$$

The bare quantity $v_{T,0}$ is then related to renormalised parameters and counterterms through

$$\frac{1}{v_{T,0}^2} = \frac{1}{v_\alpha^2}\left[1 - v_\alpha^2 \Delta v_\alpha^{(6,0,\alpha)} - \frac{1}{v_\alpha^2}\Delta v_\alpha^{(4,1,\alpha)} - \Delta v_\alpha^{(6,1,\alpha)}\right] . \tag{4.1.2}$$

The superscripts i and j in the counterterms $\Delta v_\alpha^{(i,j,\alpha)}$ label the operator dimension and the number of loops ($j = 0$ for tree-level and $j = 1$ for one-loop) respectively, while the superscript α refers to the fact that the expansion coefficients are multiplied by explicit factors of v_α. As is the case with many equations to follow, the dependence on the perturbative expansion parameter, which in this case is $1/v_\alpha^2 \sim \alpha$, has been made explicit.[1] The dependance on the expansion parameter has been factored out from each term. Consequently, the ΔX may be dimenesionful but the combination including the appropriate powers of the expansion parameter is dimensionless.

The expansion coefficients in Eq. (4.1.2) are determined by the counterterms for the input parameters M_W, M_Z, and the electric charge e. These are calculated from two-point functions, as in [29]. In the α scheme, we relate the bare and renormalised quantities up to NLO as,

$$\begin{aligned} X_0 &= X\left(1 + \frac{1}{v_\alpha^2}\Delta X^{(4,1,\alpha)} + \Delta X^{(6,1,\alpha)}\right) \\ &= X\left(1 + \frac{1}{v_\alpha^2}\Delta X^{(4,1)} + \Delta X^{(6,1)} - \Delta v_\alpha^{(6,0)}\Delta X^{(4,1)}\right) , \end{aligned} \tag{4.1.3}$$

where $X \in \{M_W, M_Z, e\}$ and X_0 are the corresponding bare parameters and in the final line we split the $(6,1)$ piece into the scheme dependent and independent parts. We have additionally suppressed the α superscript in the $(4,1)$ term, as it is independent of the expansion of the VEV. The quantities $\Delta M_W^{(6,1,\alpha)}$ and $\Delta M_Z^{(6,1,\alpha)}$ are calculated by extending the SM calculation of Section 1.2.2 to the SMEFT by including a single dimension-six operator in the loop whereas $\Delta e^{(6,1,\alpha)}$ requires

[1] There are a handful of exceptions to this in $\Delta v_\alpha^{(6,1,\alpha)}$; all appear in tadpoles, with the exception of the contribution from the Class-1 coefficient C_W.

modification and is given by [29],

$$\frac{\Delta e^{(6,1)}}{e} = \frac{1}{2}\frac{\partial \Sigma_T^{AA(6,1)}(k^2)}{\partial k^2}\bigg|_{k^2=0} + \frac{1}{M_Z^2}\left(\frac{c_w}{c_w}\Sigma_T^{AZ(6,1)}(0) - \frac{v_T^2}{4c_w s_w}C_{HD}\Sigma_T^{AZ(4)}(0)\right) . \tag{4.1.4}$$

We use the same notation for the expansion coefficients of the derived parameters c_w and s_w, so that, for instance,

$$\Delta s_w^{(i,1,\alpha)} = -\frac{c_w^2}{s_w^2}\left(\Delta M_W^{(i,1,\alpha)} - \Delta M_Z^{(i,1,\alpha)}\right) . \tag{4.1.5}$$

At tree level the relation between v_T and v_α is given by [29]

$$\frac{1}{v_T^2} = \frac{1}{v_\alpha^2}\left(1 + 2v_\alpha^2\frac{c_w}{s_w}\left[C_{HWB} + \frac{c_w}{4s_w}C_{HD}\right]\right) . \tag{4.1.6}$$

Interpreting this as a relation between the bare parameters, renormalising them as in Eq. (4.1.3), and matching with Eq. (4.1.2) we find

$$\Delta v_\alpha^{(6,0,\alpha)} = -2\frac{c_w}{s_w}\left[C_{HWB} + \frac{c_w}{4s_w}C_{HD}\right] , \tag{4.1.7}$$

$$\Delta v_\alpha^{(4,1,\alpha)} = 2\left(\Delta M_W^{(4,1)} + \Delta s_w^{(4,1)} - \Delta e^{(4,1)}\right) , \tag{4.1.8}$$

$$\begin{aligned}\Delta v_\alpha^{(6,1,\alpha)} =& 2\left(\Delta M_W^{(6,1,\alpha)} + \Delta s_w^{(6,1,\alpha)} - \Delta e^{(6,1,\alpha)}\right)\\ &+ \frac{2}{c_w s_w}\left[C_{HWB} + \frac{c_w}{2s_w}C_{HD}\right]\Delta s_w^{(4,1)}\\ &- 2v_\alpha^2\frac{c_w}{s_w}\left[\delta C_{HWB} + \frac{c_w}{4s_w}\delta C_{HD}\right] .\end{aligned} \tag{4.1.9}$$

where the δC_i are counterterms for the Wilson coefficients in the $\overline{\text{MS}}$ scheme, which are defined in Section 2.2.2 as

$$C_{i,0} = C_i + \delta C_i, \qquad \delta C_i \equiv \frac{1}{2\epsilon}\dot{C}_i \equiv \frac{1}{2\epsilon}\frac{dC_i}{d\ln\mu} , \tag{4.1.10}$$

where ϵ is the dimensional regulator in $d = 4 - 2\epsilon$ space-time dimensions. As mentioned, explicit results for the δC_i at one loop can be derived from [42, 45, 46].[1]

The counterterms ΔM_Z, ΔM_W and Δv_α as described here form the basis to perform any NLO calculation renormalised in the α scheme by replacing the bare parameters

[1] Practically, we use `DsixTools` [47] to extract them.

with the appropriate relation of Eq. (4.1.6) or Eq. (4.1.3).

A small stipulation which we neglected so far is in the implementation of the α scheme and the LEP scheme, to be introduced in Section 4.3, requires specifying the renormalisation scheme for α. Previously, we have defined α in an on-shell method. However, another possible choice is the $\overline{\text{MS}}$ definition $\overline{\alpha}(\mu)$ in five-flavour QED×QCD, where EW scale contributions are included through decoupling constants [29] and perturbative uncertainties can be estimated through scale variations.

In Chapter 5, when discussing these three schemes detailed in this chapter, we indeed choose this $\overline{\text{MS}}$ definition to take advantage of the scale uncertainty estimates. However, it should be noted that later, in Chapter 7, we change the scheme for α to the on-shell definition to be more in line with what is conventionally used in order to make just comparisons of results and potential EW fits with the current literature.

4.2 The α_μ Scheme

The second scheme we introduce in this section is the α_μ scheme. The α_μ scheme uses the set of inputs $\{G_F, M_W, M_Z\}$, where G_F is the Fermi constant as measured in muon decay.

In this scheme, the W-boson and Z-boson masses are again renormalised on-shell, identically to the α scheme. However, the renormalisation of v_T differs therefore we will expand in explicit powers of v_μ, as will be seen shortly, hence we have

$$M_{X,0} = M_X \left(1 + \frac{1}{v_\mu^2}\Delta M_X^{(4,1,\mu)} + \Delta M_X^{(6,1,\mu)}\right), \tag{4.2.1}$$

where the μ in the subscript indicates the expansion by explicit powers of v_μ and $X \in \{Z, W\}$. An equivalent expansion to that of Eq. (4.1.3) can be performed to obtain the counterterms in this scheme from previously calculated and soon to be calculated results.

The renormalisation of G_F in this scheme is implemented by modifying the coun-

terterms for v_T to read,

$$\frac{1}{v_{T,0}^2} = \frac{1}{v_\mu^2}\left[1 - v_\mu^2 \Delta v_\mu^{(6,0,\mu)} - \frac{1}{v_\mu^2}\Delta v_\mu^{(4,1,\mu)} - \Delta v_\mu^{(6,1,\mu)}\right] . \tag{4.2.2}$$

where

$$v_\mu \equiv \left(\sqrt{2}G_F\right)^{-\frac{1}{2}} \equiv \frac{2M_W s_w}{\sqrt{4\pi\alpha_\mu}} . \tag{4.2.3}$$

We have introduced the derived EW coupling α_μ in the final equality of the above equation. Using the PDG value of $G_F = 1.166 \times 10^{-5}$ GeV^{-2} [10] gives $\alpha_\mu \approx 1/132$. The counterterms, Δv_μ, in Eq. (4.2.2) are defined by the renormalisation condition that the relation in Eq. (4.2.3), $v_\mu = \left(\sqrt{2}G_F\right)^{-\frac{1}{2}}$, holds to all orders in perturbation theory. The Fermi constant G_F is a Wilson coefficient appearing in the effective Lagrangian

$$\mathcal{L}_{\text{eff}} = \mathcal{L}_{\text{QED}} + \mathcal{L}_{\text{QCD}} + \mathcal{L}_\mu , \tag{4.2.4}$$

where

$$\mathcal{L}_\mu = -\frac{4G_F}{\sqrt{2}}Q_\mu, \qquad Q_\mu = \left[\bar{\nu}_\mu \gamma_\mu P_L \mu\right] \times \left[\bar{e}\gamma^\mu P_L \nu_e\right] . \tag{4.2.5}$$

The four-fermion operator Q_μ mediates tree-level muon decay, and radiative corrections are obtained through Lagrangian insertions of a five-flavour version of QED×QCD, where the top-quark is integrated out. We will work only to NLO in the couplings, so QCD couplings will not appear, and we can drop the QCD Lagrangian in what follows.

The dimension-six term of the effective Lagrangian should be familiar, as it is identical to that of Eq. (2.1.6), the Lagrangian for Fermi Theory, and plays a vital role in the definition of the α_μ scheme.

The Fermi constant G_F is calculated by matching the SMEFT onto the effective Lagrangian above, by integrating out the heavy electroweak bosons and the top quark. In practice, this is done by ensuring that renormalised Green's functions match order by order in perturbation theory, to leading order in the EFT expansion

parameter $m_\mu/M_W \ll 1$. The matching can be performed with any convenient choice of external states. We work with massless fermions, and set all external momenta to zero. In that case, the loop corrections to the bare tree-level amplitude in the EFT are scaleless and vanish, so the renormalised amplitude is just given by the tree-level one plus UV counterterms. The main task is thus to evaluate the renormalised NLO matrix element for the muon decay in SMEFT.

To write the matrix element for the process $\mu \to \nu_\mu e \bar{\nu}_e$, we first define the spinor product

$$S_\mu = \left[\bar{u}(p_{\nu_\mu})\gamma_\nu P_L u(p_\mu)\right] \times \left[\bar{u}(p_e)\gamma^\nu P_L v(p_{\bar{\nu}_e})\right] , \tag{4.2.6}$$

where $P_L = (1-\gamma_5)/2$ and it is understood that the arguments of the Dirac spinors u and v are evaluated at $p_i = 0$. Furthermore, we define expansion coefficients of the bare one-loop amplitude in terms of the bare parameter $v_{T,0}$ as

$$\mathcal{A}_{\text{bare}} = -\frac{2}{v_{T,0}^2}\left(\mathcal{A}_{\text{bare}}^{(4,0)} + v_{T,0}^2\mathcal{A}_{\text{bare}}^{(6,0)} + \frac{1}{v_{T,0}^2}\mathcal{A}_{\text{bare}}^{(4,1)} + \mathcal{A}_{\text{bare}}^{(6,1)}\right) S_\mu + \dots . \tag{4.2.7}$$

The ... in the above equations refer either to spinor structures with different chirality structure, which we do not interfere with the tree-level SM result and can thus be neglected, or matrix elements of evanescent operators. Evanescent operators, which vanish in four dimensions as a result of their γ-matrix structure, no longer vanish in dimensional regularization where we work in d dimensions. The definition of the evanescent operators depends on the definition of the γ_5 matrix in d dimensions [118]. We choose to define γ_5 in naive dimensional regularization, where it anti-commutes with the other γ matrices, $\{\gamma_5, \gamma_\mu\} = 0$. For the muon decay only one evanescent operator appears in the one-loop diagrams with a four-fermion interaction and a boson connecting the two fermion bilinears. It is defined in the chiral basis as [119]

$$P_R\gamma^\mu\gamma^\nu\gamma^\lambda P_L \otimes P_R\gamma_\mu\gamma_\nu\gamma_\lambda P_L = 4(4-\epsilon)P_R\gamma^\mu P_L \otimes P_R\gamma_\mu P_L + E_{LL} , \tag{4.2.8}$$

where $P_R = (1+\gamma_5)/2$ and the $\otimes$ indicates a direct product of γ matrices (as in Eq. (4.2.6) after removing the external spinors). The scheme choice for the evanescent

operators impacts the finite pieces at one-loop when multiplied with $1/\epsilon$ terms. The evanescent operator E_{LL} itself can be removed by an appropriate counterterm.

The renormalised amplitude in the α_μ scheme to one-loop order then takes the form

$$\begin{aligned}\mathcal{A} &= -\frac{2}{v_\mu^2}\left(\mathcal{A}^{(4,0,\mu)} + v_\mu^2\mathcal{A}^{(6,0,\mu)} + \frac{1}{v_\mu^2}\mathcal{A}^{(4,1,\mu)} + \mathcal{A}^{(6,1,\mu)}\right) S_\mu + \dots \\ &\stackrel{!}{=} -\frac{2}{v_\mu^2} S_\mu + \dots \,. \end{aligned} \tag{4.2.9}$$

In the second line of Eq. (4.2.9) we have indicated that after imposing the renormalisation conditions in the α_μ scheme G_F does not receive any corrections at higher orders. Expanding $v_{T,0}^2$ in Eq. (4.2.7) using Eq. (4.2.2) and enforcing the above equality determines the expansion coefficients $\Delta v_\mu^{(i,j,\mu)}$ in Eq. (4.2.2). The tree-level results are

$$\mathcal{A}^{(4,0,\mu)} = 1\,, \tag{4.2.10}$$

$$\mathcal{A}^{(6,0,\mu)} = C^{(3)}_{\substack{Hl\\11}} + C^{(3)}_{\substack{Hl\\22}} - C_{\substack{ll\\1221}} - \Delta v_\mu^{(6,0,\mu)}\,. \tag{4.2.11}$$

This implies that

$$\Delta v_\mu^{(6,0,\mu)} = C^{(3)}_{\substack{Hl\\11}} + C^{(3)}_{\substack{Hl\\22}} - C_{\substack{ll\\1221}}\,. \tag{4.2.12}$$

At one loop, on the other hand, one finds that

$$\Delta v_\mu^{(4,1,\mu)} = \mathcal{A}^{(4,1)}_{\text{bare}} + \frac{1}{2}\Delta Z_f^{(4,1,\mu)}\,, \tag{4.2.13}$$

$$\begin{aligned}\Delta v_\mu^{(6,1,\mu)} =& \mathcal{A}^{(6,1)}_{\text{bare}} + \frac{1}{2}\Delta Z_f^{(6,1,\mu)} + \Delta v_\mu^{(6,0,\mu)}\left(\frac{1}{2}\Delta Z_f^{(4,1,\mu)} - 2\Delta v_\mu^{(4,1,\mu)}\right) \\ &+ \delta C^{(3)}_{\substack{Hl\\11}} + \delta C^{(3)}_{\substack{Hl\\22}} - \delta C_{\substack{ll\\1221}}\,. \end{aligned} \tag{4.2.14}$$

In the above, the δC are given in Eq. (4.1.10) and we have defined the combination of on-shell wavefunction renormalisation factors for the external fermions

$$\Delta Z_f = \Delta Z_\mu^L + \Delta Z_{\nu_\mu}^{L*} + \Delta Z_e^{L*} + \Delta Z_{\nu_e}^L\,, \tag{4.2.15}$$

where the superscript L has been used to indicate left-handed fermions and the ΔZ_f

are expanded as usual

$$\Delta Z_f = \frac{1}{v_\mu^2}\Delta Z_f^{(4,1,\mu)} + \Delta Z_f^{(6,1,\mu)}\,. \tag{4.2.16}$$

Much like the counterterms for the on-shell gauge boson masses, the counterterms $\Delta Z_f^{(6,1,\mu)}$ can be calculated in the same manner as in Section 1.2.2 and extending the two point functions to contain one dimension-six operator insertion. At one loop, ΔZ_f receives contributions from photon graphs, which vanish as the integrals are scaleless, and heavy-particle graphs (Z and W exchanges), which give finite contributions that must be taken into account. The explicit results for the one-loop coefficients in Eq. (4.2.2) are relatively compact, and we list them here. In the SM, one has

$$\begin{aligned}16\pi^2\,\Delta v_\mu^{(4,1,\mu)} = &-\frac{M_h^2}{2} - M_W^2 - \frac{M_Z^2}{2} + N_c m_t^2 + \frac{3M_W^2}{M_h^2 - M_W^2}A_0(M_h^2) - 2N_c A_0(m_t^2)\\ &+ \left(9 - \frac{3M_h^2}{M_h^2 - M_W^2}\right)A_0(M_W^2) + 3A_0(M_Z^2) + 3\frac{c_w^2}{s_w^2}\left[A_0(M_W^2) - A_0(M_Z^2)\right]\\ &+ 16\pi^2\Delta v_{\mu,\text{tad}}^{(4,1,\mu)}\,,\end{aligned} \tag{4.2.17}$$

where the tadpole contribution in unitary gauge is

$$\begin{aligned}16\pi^2 M_h^2\Delta v_{\mu,\text{tad}}^{(4,1,\mu)} = &\,8M_W^4 + 4M_Z^4 - 3M_h^2 A_0(M_h^2) + 8N_c m_t^2 A_0(m_t^2)\\ &- 12M_W^2 A_0(M_W^2) - 6M_Z^2 A_0(M_Z^2)\,,\end{aligned} \tag{4.2.18}$$

and

$$A_0(M^2) = M^2\left(\frac{1}{\epsilon} + 1 + \ln\frac{\mu^2}{M^2}\right)\,. \tag{4.2.19}$$

In SMEFT we find

$$\begin{aligned}16\pi^2\Delta v_\mu^{(6,1,\mu)} = \frac{1}{\epsilon}\Bigg[&M_W^2\left(\frac{2}{3}C_{H\Box} - \frac{28}{3}C_{\substack{Hl\\11}}^{(3)} - \frac{28}{3}C_{\substack{Hl\\22}}^{(3)} + \frac{8}{3}C_{\substack{Hl\\33}}^{(3)} + 8C_{\substack{Hq\\11}}^{(3)} + 8C_{\substack{Hq\\22}}^{(3)} + 8C_{\substack{Hq\\33}}^{(3)}\right.\\ &\left.+ 12\left(C_{\substack{ll\\1122}} - C_{\substack{ll\\1221}}\right)\right) + 6m_t^2\left(C_{\substack{Hl\\11}}^{(3)} + C_{\substack{Hl\\22}}^{(3)} - C_{\substack{lq\\1133}}^{(3)} - C_{\substack{lq\\2233}}^{(3)}\right)\\ &- 6M_Z^2 C_{\substack{ll\\1221}}\Bigg] + 16\pi^2\Delta v_\mu^{(4,1,\mu)}\left(-2\Delta v_\mu^{(6,0,\mu)} + \frac{C_{HD}}{2}\right)\end{aligned}$$

$$
\begin{aligned}
&+ M_h^2 \left(-C_{H\Box} + \frac{C_{HD}}{2} \right) + 5 M_Z^2 C_{\substack{ll \\ 1221}} \\
&+ M_W^2 \Bigg(- C_{H\Box} - \frac{3 C_{HD}}{2} - 12 \frac{s_w}{c_w} C_{HWB} + 10 C^{(3)}_{\substack{Hl \\ 11}} \\
&+ 10 C^{(3)}_{\substack{Hl \\ 22}} + 10 \left(C_{\substack{ll \\ 1122}} - C_{\substack{ll \\ 1221}} \right) \Bigg) \\
&+ 3 m_t^2 \left(- \frac{C_{HD}}{2} + C^{(3)}_{\substack{Hl \\ 11}} + C^{(3)}_{\substack{Hl \\ 22}} + 2 C^{(3)}_{\substack{Hq \\ 33}} - C^{(3)}_{\substack{lq \\ 1133}} - C^{(3)}_{\substack{lq \\ 2233}} \right) \\
&+ 6 M_W^2 \frac{A_0(M_h^2) - A_0(M_W^2)}{M_h^2 - M_W^2} \left(C_{H\Box} - \frac{C_{HD}}{2} \right) \\
&+ 6 A_0(M_W^2) \left(C^{(1)}_{\substack{Hl \\ 11}} + C^{(1)}_{\substack{Hl \\ 22}} + C^{(3)}_{\substack{Hl \\ 11}} + C^{(3)}_{\substack{Hl \\ 22}} + 2 C_{\substack{ll \\ 1122}} \right) \\
&+ 6 c_w^2 A_0(M_Z^2) \Bigg(- C_{HD} - C^{(1)}_{\substack{Hl \\ 11}} - C^{(1)}_{\substack{Hl \\ 22}} + C^{(3)}_{\substack{Hl \\ 11}} \\
&+ C^{(3)}_{\substack{Hl \\ 22}} + \left(-2 + \frac{1}{c_w^2} \right) C_{\substack{ll \\ 1221}} \Bigg) \\
&+ A_0(m_t^2) \left(3 C_{HD} - 6 C^{(3)}_{\substack{Hl \\ 11}} - 6 C^{(3)}_{\substack{Hl \\ 22}} - 12 C^{(3)}_{\substack{Hq \\ 33}} + 6 C^{(3)}_{\substack{lq \\ 1133}} + 6 C^{(3)}_{\substack{lq \\ 2233}} \right) \\
&+ 16 \pi^2 \Delta v^{(6,1,\mu)}_{\mu,\text{tad}} \,,
\end{aligned}
\tag{4.2.20}
$$

where the tadpole contribution in unitary gauge is

$$
\begin{aligned}
16\pi^2 M_h^2 \Delta v^{(6,1,\mu)}_{\mu,\text{tad}} = &+ 32\pi^2 M_h^2 \Delta v^{(4,1,\mu)}_{\mu,\text{tad}} C_{H\Box} - 8 M_W^4 \left(C_{HD} - 2 C_{HW} \right) \\
&- 8 M_W^2 M_Z^2 \left(C_{HB} - C_{HW} \right) + 2 M_Z^4 \left(4 C_{HB} - C_{HD} + 4 s_w c_w C_{HWB} \right) \\
&- M_h^2 A_0(M_h^2) \left(4 C_{H\Box} - 4 C_{HD} - 6 \frac{v_\mu^2}{M_h^2} C_H \right) \\
&+ 12 M_W^2 A_0(M_W^2) \left(C_{HD} - 2 C_{HW} \right) \\
&- 12 m_t^2 A_0(m_t^2) \left(2 C_{HD} + \frac{\sqrt{2} v_\mu}{m_t} C_{\substack{uH \\ 33}} \right) \\
&- M_Z^2 A_0(M_Z^2) \left(12 s_w^2 C_{HB} - 3 C_{HD} + 12 c_w^2 C_{HW} + 12 c_w s_w C_{HWB} \right) \,.
\end{aligned}
\tag{4.2.21}
$$

Note that the expansion coefficients are only gauge invariant when tadpoles are included – the split that we have given above is unique to unitary gauge. We have checked that our results are consistent with those in [70], a previous result using a simplified flavour structure for the SMEFT Wilson coefficients, and omitting tadpoles such that the results are gauge dependent and limited to R_ξ gauge - thus providing

a strong check on both sets of results.

4.2.1 Relation to the α scheme

Now we have been introduced to two schemes, the α and α_μ schemes, a logical next question to pose is how are the two related.

We can convert results in the α_μ scheme to the α scheme using the perturbative relation between v_μ and v_α. A useful quantity for this purpose is

$$\frac{v_\alpha^2}{v_\mu^2} \equiv 1 + \Delta r \,. \tag{4.2.22}$$

Two equivalent SMEFT expansions of this quantity are

$$\begin{aligned} \Delta r &= v_\alpha^2 \Delta r^{(6,0)} + \frac{1}{v_\alpha^2}\Delta r^{(4,1)} + \Delta r^{(6,1)} \,, \\ &= v_\mu^2 \Delta r^{(6,0)} + \frac{1}{v_\mu^2}\Delta r^{(4,1)} + \Delta r^{(6,1)} \,. \end{aligned} \tag{4.2.23}$$

The expansion coefficients are the same whether expanded in v_μ or v_α, so we use superscripts for operator dimension and loop order only.[1] They are obtained by equating the two expressions for $v_{T,0}$ given in Eq. (4.1.2) and Eq. (4.2.2) and performing a SMEFT expansion, yielding the result

$$\begin{aligned} \Delta r^{(6,0)} &= \Delta v_{\mu\alpha}^{(6,0)} \,, \\ \Delta r^{(4,1)} &= \Delta v_{\mu\alpha}^{(4,1)} \,, \\ \Delta r^{(6,1)} &= \Delta v_{\mu\alpha}^{(6,1)} + 2\Delta v_\mu^{(4,1,\mu)} \Delta v_{\mu\alpha}^{(6,0)} \,, \end{aligned} \tag{4.2.24}$$

where we have defined

$$\Delta v_{\mu\alpha}^{(i,j)} = \Delta v_\mu^{(i,j,\mu)} - \Delta v_\alpha^{(i,j,\alpha)} \,. \tag{4.2.25}$$

For two-body decays of heavy bosons, the SMEFT expansion coefficients in the α_μ

[1] It is understood that any implicit v_T dependence in the $(6,1)$ term is expressed in terms of v_α in the first line or v_μ in the second.

or α scheme take the form

$$\begin{aligned}\Gamma &= \frac{F}{v_\mu^2}\left[1 + v_\mu^2\Delta_\Gamma^{(6,0,\mu)} + \frac{1}{v_\mu^2}\Delta_\Gamma^{(4,1,\mu)} + \Delta_\Gamma^{(6,1,\mu)}\right] \\ &= \frac{F}{v_\alpha^2}\left[1 + v_\alpha^2\Delta_\Gamma^{(6,0,\alpha)} + \frac{1}{v_\alpha^2}\Delta_\Gamma^{(4,1,\alpha)} + \Delta_\Gamma^{(6,1,\alpha)}\right], \end{aligned} \tag{4.2.26}$$

where F does not depend on v_μ in the first line or v_α in the second. The relation between the expansion coefficients in the two schemes is

$$\begin{aligned}\Delta_\Gamma^{(6,0,\alpha)} &= \Delta_\Gamma^{(6,0,\mu)} + \Delta r^{(6,0)}, \\ \Delta_\Gamma^{(4,1,\alpha)} &= \Delta_\Gamma^{(4,1,\mu)} + \Delta r^{(4,1)}, \\ \Delta_\Gamma^{(6,1,\alpha)} &= \Delta_\Gamma^{(6,1,\mu)} + \Delta r^{(6,1)} + 2\Delta_\Gamma^{(4,1,\mu)}\Delta r^{(6,0)}. \end{aligned} \tag{4.2.27}$$

Conversions from the α to the α_μ scheme work in a similar manner. As a simple example, the expansion of counterterms X in Eq. (4.1.3) in the α_μ scheme is obtained by replacing $\alpha \to \mu$ in that equation, with expansion coefficients related through

$$\Delta X^{(4,1,\mu)} = \Delta X^{(4,1,\alpha)}, \qquad \Delta X^{(6,1,\mu)} = \Delta X^{(6,1,\alpha)} - \Delta r^{(6,0)}\Delta X^{(4,1,\alpha)}. \tag{4.2.28}$$

Here we can see explicitly that although both the α and the α_μ scheme use on-shell renormalisation for M_W and M_Z, the perturbative expansions of the counterterms differ at one-loop in SMEFT, yet the SM counterterms are the same - motivating the dropping of the index in Eq. (4.1.3).

4.3 The LEP Scheme

Finally, to conclude our introduction to the three common schemes in the literature, we have the LEP scheme. At LEP and in SMEFT analyses, one often considers the LEP scheme, where the on-shell W-boson mass is not used as an input, but is instead expressed as a SMEFT expansion in terms of the three independent input parameters $\{\alpha, G_F, M_Z\}$. Renormalised amplitudes in this scheme could be obtained similarly to previously, where one introduces counterterms for each of the input parameters. Here

however, we take an alternative tack and deduce the counterterms of the W-boson mass, a derived parameter in this scheme, from previously introduced relations. One may then use this derived parameter counterterm to achieve renormalisation in the LEP scheme alongside those for v_T and M_Z if one starts from our usual starting point of a Lagrangian written in terms of v_T, M_W, and M_Z.

The SMEFT expansion of the on-shell W-boson mass in this scheme is most easily obtained by re-arranging Eq. (4.2.22) and then expanding in Δr to find

$$M_W^2 = \hat{M}_W^2 \left[1 - \frac{\hat{s}_w^2}{\hat{c}_{2w}}\Delta r - \frac{\hat{c}_w^2 \hat{s}_w^4}{\hat{c}_{2w}^3}\Delta r^2\right] + \mathcal{O}\left(\Delta r^3\right) , \tag{4.3.1}$$

where

$$\hat{M}_W^2 = \frac{M_Z^2}{2}\left(1 + \sqrt{1 - \frac{4\pi\alpha v_\mu^2}{M_Z^2}}\right) , \quad \hat{c}_w^2 = \frac{\hat{M}_W^2}{M_Z^2} = 1 - \hat{s}_w^2 , \quad \hat{c}_{2w} = 2\hat{c}_w^2 - 1 . \tag{4.3.2}$$

In the LEP scheme, the appropriate SMEFT expansion of Δr depends only on the derived parameter $\hat{M}_W$. We therefore define expansion coefficients

$$\Delta r = v_\mu^2 \hat{\Delta} r^{(6,0)} + \frac{1}{v_\mu^2}\hat{\Delta} r^{(4,1)} + \hat{\Delta} r^{(6,1)} , \tag{4.3.3}$$

where the "hat" on the expansion coefficients $\hat{\Delta} r^{(i,j)}$ means that the dependence on the on-shell mass M_W in the $\Delta r^{(i,j)}$ in Eq. (4.2.23) has been eliminated in favour of $\hat{M}_W$ through iterative use of Eq. (4.3.1). A short calculation yields the following results:

$$\begin{aligned}
\hat{\Delta} r^{(6,0)} &= \Delta r^{(6,0)}\Big|_{M_W=\hat{M}_W} , \\
\hat{\Delta} r^{(4,1)} &= \Delta r^{(4,1)}\Big|_{M_W=\hat{M}_W} , \\
\hat{\Delta} r^{(6,1)} &= \Delta r^{(6,1)} - \frac{\hat{s}_w^2}{2\hat{c}_{2w}}\left[\Delta r^{(6,0)}\partial_W \Delta r^{(4,1)} + \Delta r^{(4,1)}\partial_W \Delta r^{(6,0)}\right]\Big|_{M_W=\hat{M}_W} ,
\end{aligned} \tag{4.3.4}$$

where the notation $\Big|_{M_W=\hat{M}_W}$ means that M_W is to be replaced by $\hat{M}_W$ and we have defined

$$\partial_W \equiv M_W \frac{\partial}{\partial M_W} . \tag{4.3.5}$$

Notice that the term $\hat{\Delta}r^{(6,1)}$ involves derivatives of Passarino-Veltmann functions, which at one-loop level are simple to evaluate. As a simple example, the derivative of the bubble function $A_0(M_W^2)$ is given by

$$\partial_W A_0(M_W^2) = 2M_W^2 \log \frac{\mu^2}{M_W^2} \,. \tag{4.3.6}$$

We can now write the SMEFT expansion of M_W in the LEP scheme as

$$M_W = \hat{M}_W \left[1 + v_\mu^2 \hat{\Delta}_W^{(6,0,\mu)} + \frac{1}{v_\mu^2}\hat{\Delta}_W^{(4,1,\mu)} + \hat{\Delta}_W^{(6,1,\mu)}\right], \tag{4.3.7}$$

where

$$\begin{aligned}
\hat{\Delta}_W^{(6,0,\mu)} &= -\frac{\hat{s}_w^2}{2\hat{c}_{2w}}\hat{\Delta}r^{(6,0)}, \\
\hat{\Delta}_W^{(4,1,\mu)} &= -\frac{\hat{s}_w^2}{2\hat{c}_{2w}}\hat{\Delta}r^{(4,1)}\,, \\
\hat{\Delta}_W^{(6,1,\mu)} &= -\frac{\hat{s}_w^2}{2\hat{c}_{2w}}\hat{\Delta}r^{(6,1)} - \frac{\hat{s}_w^4}{4\hat{c}_{2w}^2}\left(1 + \frac{4\hat{c}_w^2}{\hat{c}_{2w}}\right)\hat{\Delta}r^{(6,0)}\hat{\Delta}r^{(4,1)}\,.
\end{aligned} \tag{4.3.8}$$

The above expressions allows for the conversion of the SMEFT expansion of any quantity from the α_μ scheme to the LEP scheme by expressing the on-shell mass by the "hatted" version. The conversion for a general function of the on-shell W-boson mass takes the form

$$\begin{aligned}
&X(M_W)\left[1 + v_\mu^2 \Delta_X^{(6,0,\mu)} + \frac{1}{v_\mu^2}\Delta_X^{(4,1,\mu)} + \Delta_X^{(6,1,\mu)}\right] \\
&= X(\hat{M}_W)\left[1 + v_\mu^2 \hat{\Delta}_X^{(6,0,\mu)} + \frac{1}{v_\mu^2}\hat{\Delta}_X^{(4,1,\mu)} + \hat{\Delta}_X^{(6,1,\mu)}\right],
\end{aligned} \tag{4.3.9}$$

where the expansion coefficients Δ_X ($\hat{\Delta}_X$) are functions of M_W ($\hat{M}_W$). They are related through

$$\begin{aligned}
\hat{\Delta}_X^{(6,0,\mu)} &= \Delta_X^{(6,0,\mu)} + \hat{\Delta}_W^{(6,0,\mu)}\frac{\partial_W X}{X}, \\
\hat{\Delta}_X^{(4,1,\mu)} &= \Delta_X^{(4,1,\mu)} + \hat{\Delta}_W^{(4,1,\mu)}\frac{\partial_W X}{X}, \\
\hat{\Delta}_X^{(6,1,\mu)} &= \Delta_X^{(6,1,\mu)} + \hat{\Delta}_W^{(6,0,\mu)}\partial_W \Delta_X^{(4,1,\mu)} + \hat{\Delta}_W^{(4,1,\mu)}\partial_W \Delta_X^{(6,0,\mu)} \\
&\quad + \frac{1}{X}\left[\left(\hat{\Delta}_W^{(6,1,\mu)} + \Delta_X^{(4,1,\mu)}\hat{\Delta}_W^{(6,0,\mu)} + \Delta_X^{(6,0,\mu)}\hat{\Delta}_W^{(4,1,\mu)}\right)\partial_W X\right.
\end{aligned} \tag{4.3.10}$$

$$+ \hat{\Delta}_W^{(6,0,\mu)} \hat{\Delta}_W^{(4,1,\mu)} \partial_W^2 X \Big] ,$$

where $X = X(M_W)$, in a slight abuse of notation we have defined

$$\partial_W^2 \equiv M_W^2 \frac{\partial^2}{\partial M_W^2} , \tag{4.3.11}$$

and one is to set $M_W = \hat{M}_W$ on the right-hand side of the relations in Eq. (4.3.10).

Finally, to achieve our initial goal, we can relate the counterterm for M_W in the on-shell scheme to that in the LEP scheme, providing a framework of renormalisation in the LEP scheme. Setting $X = M_W$ in Eq. (4.3.9), and recalling that the on-shell definition of M_W has no tree-level dimension-six contributions, we can write

$$\begin{aligned} M_{W,0} &= M_W \left(1 + \frac{1}{v_\mu^2} \Delta M_W^{(4,1,\mu)} + \Delta M_W^{(6,1,\mu)} \right) \\ &= \hat{M}_W \left(1 + v_\mu^2 \hat{\Delta} \hat{M}_W^{(6,0,\mu)} + \frac{1}{v_\mu^2} \hat{\Delta} \hat{M}_W^{(4,1,\mu)} + \hat{\Delta} \hat{M}_W^{(6,1,\mu)} \right) . \end{aligned} \tag{4.3.12}$$

The terms on the second line as determined from Eq. (4.3.10) read

$$\hat{\Delta} \hat{M}_W^{(6,0,\mu)} = \hat{\Delta}_W^{(6,0,\mu)} , \tag{4.3.13}$$

$$\hat{\Delta} \hat{M}_W^{(4,1,\mu)} = \hat{\Delta}_W^{(4,1,\mu)} + \Delta M_W^{(4,1,\mu)} \Big|_{M_W = \hat{M}_W} , \tag{4.3.14}$$

$$\begin{aligned} \hat{\Delta} \hat{M}_W^{(6,1,\mu)} = \hat{\Delta}_W^{(6,1,\mu)} &+ \Delta M_W^{(6,1,\mu)} + \hat{\Delta}_W^{(6,0,\mu)} \Delta M_W^{(4,1,\mu)} \\ &+ \hat{\Delta}_W^{(6,0,\mu)} \partial_W \Delta M_W^{(4,1,\mu)} \Big|_{M_W = \hat{M}_W} . \end{aligned} \tag{4.3.15}$$

We emphasise, however, that the LEP scheme uses $\{\alpha, G_F, M_Z\}$ as input parameters, so the result is ultimately a function of these parameters and the associated counterterms $\{\hat{\Delta}e, \hat{\Delta}v_\mu, \hat{\Delta}M_Z\}$, which can be obtained from expansion coefficients in the α or α_μ scheme similarly to $\hat{\Delta}\hat{M}_W$.

Nonetheless, the counterterms $\hat{\Delta}\hat{M}_W$ alongside those for G_F, given in Eq. (4.2.2), and M_Z after eliminating the on-shell M_W for $\hat{M}_W$ using Eq. (4.3.1) will renormalise an amplitude in the LEP scheme.

Chapter 5

Analysis of Schemes in the Literature

In Chapter 4 we outlined implementation of three schemes: the α, α_μ, and LEP schemes. Derivations of counterterms were shown, which allows one to calculate any process to NLO in the EW coupling in the SMEFT.

In this chapter, we provide a comparison of the schemes and give note to their salient features. We are mainly interested in two features of the EW input schemes: the number of Wilson coefficients they introduce into physical observables through renormalisation, and perturbative convergence. One would assume it's advantageous for a small number of coefficients to appear, so that the finite parts of observables are dominated by process-specific Wilson coefficients rather than those related to the EW renormalisation scheme. Furthermore, one would like to avoid large corrections between orders, so that perturbation theory is well-behaved and can safely be truncated at a low order. We discuss these two issues in the following sections. This is then followed by an analysis of the derived parameters and the heavy boson decays, where we compare the three schemes. We finally suggest a set of universal replacements to account for large perturbative corrections for each of these schemes.

5.1 Numerical Values of Inputs

A numerical analysis of the different schemes requires specification of numerical values for the inputs. A somewhat important, but overlooked aspect of these values for the these three input schemes is the precision of these values extracted from measurements. In SM high precision calculation, where observables are predicted to many orders in perturbation theory, the uncertainties on the inputs may become significant to a point where one may wish to consider this effect further. However, for our purpose we have no such problem as uncertainties from truncation in perturbation theory, estimated in this section by scale uncertainties, by far dominate at LO and are in general larger at NLO. As a simple illustration, the value and uncertainty (solely from the precision on the inputs) for the prediction of G_F in the α scheme is given by

$$G_{F,\alpha}^{\text{NLO}} = (1.157 \pm 0.002) \times 10^{-5} \text{ GeV} \tag{5.1.1}$$

where we have taken the uncertainties on the input parameter from [10] and included the SM NLO correction to the LO result. This uncertainty is at the per-mille level and provides a negligible change to the uncertainties on the quoted results given later in this thesis for illustrative purposes. It is for that reason, the precision on the inputs has been dropped from the uncertainties quoted from results here on in. That being said

That all being said, Table 5.1 shows the numerical values of the inputs used in this work, where we take the values as given in [10]. The quantity $\overline{m}_b(M_h)$ takes the value shown only in the $h \to bb$ process, otherwise it is set to zero.

5.2 Number of Wilson coefficients

Probably the easiest comparison one can make between the schemes, and thus the one which we start with, is to compare the number of different Wilson coefficients each

M_h	125.1 GeV	$\overline{m}_b(M_h)$	3.0 GeV
m_t	172.9 GeV	$v_\alpha(M_h)$	241.7 GeV
M_W	80.38 GeV	v_μ	246.2 GeV
M_Z	91.19 GeV	$\alpha_s\,(M_h)$	0.1125

Table 5.1: Input parameters employed throughout this section. Note that v_α is a derived parameter.

scheme introduces through the renormalisation process. It is a simple matter to count the number of Wilson coefficients appearing in the finite parts of counterterms for the bare parameters $M_{Z,0}$, $M_{W,0}$ and $v_{T,0}$ in the different input schemes. The results at LO and NLO are listed in Table 5.2. Here and below we exclude Wilson coefficients which contribute only through tadpoles and therefore drop out of observables. This includes C_H and $C_{\substack{uH\\33}}$ in each of the three counterterms considered here. Note that although all schemes use the on-shell renormalisation scheme for M_Z, its dimension-six counterterm still differs between the schemes. To see this explicitly, we note that expansion coefficients in α_μ and α schemes can be written in the form

$$M_{Z,0} = M_Z \left(1 + \frac{1}{v_\sigma^2}\Delta M_Z^{(4,1)} + \Delta M_Z^{(6,1)} - \Delta v_\sigma^{(6,0,\sigma)} \Delta M_Z^{(4,1)}\right) , \tag{5.2.1}$$

where here and throughout the remainder of the chapter the choice of $\sigma \in \{\mu, \alpha\}$ selects between the α and α_μ schemes. An analogous equation holds for the counterterms for M_W. The coefficients $\Delta M_Z^{(4,1)}$ and $\Delta M_Z^{(6,1)}$ are the same in the two schemes, but differences in the dimension-six piece arise due to the renormalisation of v_T. In the LEP scheme, one must use $\sigma = \mu$ and in addition apply Eq. (4.3.7) to trade M_W for $\hat{M}_W$, which gives an additional scheme-dependent contribution.

The specific Wilson coefficients appearing in the various counterterms in the α scheme are determined by the two-point functions shown in Figure 5.1. The counterterm for the W-boson mass contains the following coefficients:

$$\Delta M_W^{(6,1,\alpha)}: \quad \{C_W, C_{H\Box}, C_{HD}, C_{HW}, C_{HWB}, C^{(3)}_{\substack{Hl\\ii}}, C^{(3)}_{\substack{Hq\\ii}}, C_{\substack{uW\\33}}\}\,, \quad i = 1,2,3\,. \tag{5.2.2}$$

$C_{H\Box}$ and C_{HW} contribute to the two left-most topologies in Figure 5.1, while C_{HWB}

		M_W	M_Z	v_T	Total # unique WC
α	LO	0	0	2	2
	NLO	12	29	29	29
α_μ	LO	0	0	3	3
	NLO	13	30	12	33
LEP	LO	5	0	3	5
	NLO	33	30	12	33

Table 5.2: Number of Wilson coefficients introduced in the dimension-six counterterms for the bare M_W, M_Z and v_T at LO and NLO, as well as the number of unique coefficients between them.

and C_W contribute to topologies three and four, which involve vertices with at least three gauge bosons. C_{HD} appears in all four purely bosonic diagrams. We see that 7 of the 12 coefficients appearing are due to flavour-specific W couplings to fermions, arising from the right-most graph in Figure 5.1. Since in the SM the W boson couples only to left-handed fermions, the SMEFT operators must also be left-handed unless they contain a top-quark loop (in which case a chirality flip is associated with a power of m_t), which explains the relatively small number appearing. For the Z-boson mass, on the other hand, both left and right-handed couplings are relevant even for massless fermions, and operators containing the field-strength tensor for the hypercharge field B_μ, namely C_{HB} and C_{uB}, contribute as well. This leads to a much larger number of coefficients compared to M_W. The full set is:

$$\begin{aligned}\Delta M_Z^{(6,1,\alpha)}: \quad & \{C_W, C_{H\Box}, C_{HD}, C_{HW}, C_{HB}, C_{HWB}, C^{(1)}_{\substack{Hl\\ii}}, C^{(1)}_{\substack{Hq\\ii}}, C^{(3)}_{\substack{Hl\\ii}}, C^{(3)}_{\substack{Hq\\ii}}, C_{\substack{uW\\33}}, C_{\substack{uB\\33}}, \\ & C_{\substack{He\\ii}}, C_{\substack{Hd\\ii}}, C_{\substack{Hu\\ii}}\}, \quad i = 1,2,3\,. \end{aligned} \tag{5.2.3}$$

The counterterm $\Delta v_\alpha^{(6,1,\alpha)}$ requires also the counterterm Δe, as shown in Eq. (4.1.9). Only those Wilson coefficients appearing in W, top-quark or Higgs loops contribute to the finite parts of the counterterm for electric charge renormalisation (through decoupling constants, as explained in [29]), which limits the result to the following 6 coefficients:

$$\Delta e^{(6,1,\alpha)}: \quad \{C_W, C_{HW}, C_{HB}, C_{HWB}, C_{\substack{uW\\33}}, C_{\substack{uB\\33}}\}\,. \tag{5.2.4}$$

Figure 5.1: Representative Feynman diagrams contributing to the WW, ZZ, γZ, and $\gamma\gamma$ two-point functions in SMEFT.

All of these are already contained in $\Delta M_Z^{(6,1,\alpha)}$, so the set of coefficients contributing to $\Delta v_\alpha^{(6,1,\alpha)}$ is the same as in Eq. (5.2.3).

In the α_μ scheme, one needs the counterterms $\Delta v_\mu^{(6,j,\mu)}$, which are calculated from muon decay in Section 4.2. In SMEFT, two kinds of coefficients appear at NLO – those that involve modified couplings of the external fermions, including four-fermion operators of the kind shown in Figure 5.2, or those that contribute to the W-boson two-point function at vanishing external momentum. The latter condition eliminates some operators compared to what is seen in ΔM_W itself (in the case of massless fermions or certain derivative couplings), while the former increases it mainly due to four-fermion operators. The end result is that the following set appears:

$$\Delta v_\mu^{(6,1,\mu)}: \quad \{C_{H\Box}, C_{HD}, C_{HWB}, C^{(1)}_{\substack{Hl\\jj}}, C^{(3)}_{\substack{Hl\\jj}}, C^{(3)}_{\substack{Hq\\33}}, C_{\substack{ll\\1221}}, C_{\substack{ll\\1122}}, C_{\substack{lq\\jj33}}\}, \quad j = 1, 2\,. \tag{5.2.5}$$

The counterterms for M_W and M_Z are also modified compared to the α scheme, as follows from Eq. (5.2.1); one finds that the α_μ scheme contains the four-fermion coefficient $C_{\substack{ll\\1221}}$ in addition to the α-scheme coefficients listed in Eqs. (5.2.2, 5.2.3). Finally, in the LEP scheme the counterterm $\hat{\Delta}\hat{M}_W^{(6,1,\mu)}$ (see Eq. (4.3.15)) is a function of those for e, M_Z, and v_T (renormalised in the α_μ scheme), and thus contains the full set of 33 unique coefficients that also appear in the α_μ scheme, while no additional coefficients appear in the counterterms for M_Z or v_T compared to the α_μ scheme.

The conclusion of this counting exercise is that there is a large overlap between the set of operators appearing in the NLO counterterms in the different schemes. The main difference is that a handful of four-fermion operators related to muon decay appear in the LEP and α_μ schemes but not in the α scheme.

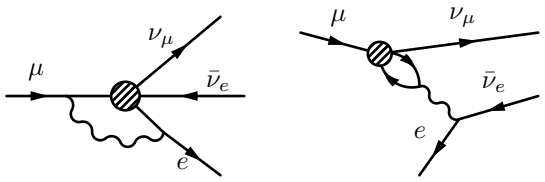

Figure 5.2: Representative Feynman diagrams contributing to the decay of the muon at one loop and involving four-fermion operators.

Although the direct comparison of the number of Wilson coefficients introduced by the specific counterterms in each scheme is instructive in understanding the potential number of Wilson coefficients introduced in a given calculation, ultimately the number of Wilson coefficients contributing to observables in the different schemes is process dependent and is determined by the structure of the LO amplitude. For instance, consider a process involving a $\gamma\ell\ell$ vertex, where ℓ is a charged lepton and γ is a photon. In the α scheme, the square of the bare vector-coupling vertex plus SMEFT counterterms (other than from field strength renormalisation) reads

$$\frac{4M_W^2 s_w^2}{v_\alpha^2}\left(1+\frac{2\Delta e^{(4,1,\alpha)}}{v_\alpha^2}+2\Delta e^{(6,1,\alpha)}\right). \tag{5.2.6}$$

In the α_μ scheme, on the other hand, the bare vertex plus associated counterterms read

$$\begin{aligned}&\frac{4M_W^2 s_w^2}{v_\mu^2}\left\{\frac{2\Delta e^{(4,1,\alpha)}}{v_\mu^2}+2\Delta e^{(6,1,\alpha)}-4\Delta e^{(4,1,\alpha)}\Delta r^{(6,0)}\right\}\\&+\frac{4M_W^2 s_w^2}{v_\mu^2}\left\{1-v_\mu^2\Delta r^{(6,0)}-\frac{1}{v_\mu^2}\Delta r^{(4,1)}-\Delta r^{(6,1)}+2\Delta r^{(6,0)}\Delta r^{(4,1)}\right\}.\end{aligned} \tag{5.2.7}$$

The two results are equal to each other if Eq. (4.2.22) is used to relate v_μ to v_α, but when the numerical value of v_μ is used as an input the terms on the second line of Eq. (5.2.7) contribute a large number of coefficients compared to what one has in the α scheme. The same set of coefficients contributes to muon decay calculated in the α scheme, or in the LEP scheme when M_W appears in a tree-level vertex.

5.3 Perturbative convergence

Next in our numerical analysis of these three commonly used input schemes we wish to discuss the perturbative convergence of each scheme, or more bluntly put, the finite corrections each scheme introduces to a given process. Generally speaking, one uses renormalisation schemes that avoid sensitivity to large logarithms of light fermion masses in fixed-order corrections, and also tadpole contributions to finite parts of observables in cases where some parameters are renormalised in the $\overline{\text{MS}}$ scheme and some in the on-shell scheme [29]. As long as those two issues are dealt with, top-quark loops are the main source of enhanced NLO corrections in the finite parts of counterterms. These can be especially important when associated with the counterterm Δs_w, since they involve inverse powers of $s_w^2 \sim 0.25$ through the relation

$$2\Delta s_w = -2\frac{c_w^2}{s_w^2}(\Delta M_W - \Delta M_Z) \approx -7(\Delta M_W - \Delta M_Z)\,, \tag{5.3.1}$$

where the factor of 2 is chosen to match that in Eq. (4.1.8).

In the SM, enhanced corrections from top-loop contributions to Δs_w related to the renormalisation scheme are easy to trace. First, by analysing the one-loop Feynman diagrams in the large-m_t limit, one can show that in the α_μ scheme

$$\Delta v_\mu^{(4,1,\mu)}\Big|_{m_t\to\infty} \equiv \Delta v_{\mu,t}^{(4,1,\mu)} = 2\Delta M_{W,t}^{(4,1,\mu)}\,. \tag{5.3.2}$$

The subscript "t" here and below refers to the large-m_t limit of the given quantity, i.e. the terms containing positive powers of m_t in the limit $m_t \to \infty$. Second, using Eqs. (4.1.8, 4.2.24), along with the fact that the SM contributions to Δe are subleading in the large-m_t limit, the α-scheme result is

$$\Delta v_{\alpha,t}^{(4,1,\alpha)} = -\Delta r_t^{(4,1)} + 2\Delta M_{W,t}^{(4,1,\alpha)}\,, \tag{5.3.3}$$

where Δr is defined in Eq. (4.2.22) such that

$$\frac{\Delta r_t^{(4,1)}}{v_\alpha^2} = -\frac{2\Delta s_{w,t}^{(4,1,\alpha)}}{v_\alpha^2} \equiv -\frac{c_w^2}{s_w^2}\frac{\Delta\rho_t^{(4,1)}}{v_\alpha^2} \approx -3.4\%\,, \tag{5.3.4}$$

and we have defined

$$\frac{\Delta\rho_t^{(4,1)}}{v_\alpha^2} \equiv \frac{3}{16\pi^2}\frac{m_t^2}{v_\alpha^2} \approx 1\% \,. \tag{5.3.5}$$

The numerical values above use $\mu = M_W$ to evaluate the running parameter v_α, along with the inputs in Table 5.1. Finally, using Eqs. (5.3.2, 5.3.3), the counterterms for v_T in the large-m_t limit in the two schemes can be written as

$$\left.\frac{1}{v_{T,0}^2}\right|_{m_t\to\infty} = \frac{1}{v_\sigma^2}\left[1 + \frac{1}{v_\sigma^2}\left(\Delta r_t^{(4,1)}\delta_{\alpha\sigma} - 2\Delta M_{W,t}^{(4,1)}\right)\right] , \tag{5.3.6}$$

where $\delta_{\alpha\sigma}$ is the Kronecker delta, and we have used that $\Delta M_W^{(4,1,\alpha)} = \Delta M_W^{(4,1,\mu)} = \Delta M_W^{(4,1)}$, see Eq. (5.2.1).

For the heavy boson decays considered in this work, the tree-level decay rates all scale as $1/v_T^2$. Therefore, Eq. (5.3.6) produces a simple pattern for the NLO corrections in the α and α_μ schemes. In the α_μ scheme, the tadpole and divergent contributions in $\Delta M_{W,t}^{(4,1)}$ cancel against other such contributions in physical observables, producing one-loop corrections proportional to $\Delta\rho_t^{(4,1)} \sim 1\%$ in the large-m_t limit. In the α scheme, the $\Delta M_{W,t}^{(4,1)}$ term is accompanied by a factor of $\Delta r_t^{(4,1)}$, which produces a correction of roughly -3.4% compared to the α_μ scheme. One indeed sees this pattern in the NLO SM corrections to W decays and Z decays, shown in Tables 5.3 and 5.5. Input-scheme dependent NLO corrections to weak vertices are thus better behaved in the α_μ scheme, and the numerical differences between the two schemes are nearly process independent.[1]

We now ask whether a simple relation between the dominant NLO corrections in the α and α_μ schemes also exists in SMEFT. To do this, we first define

$$\left.\frac{M_{W,0}^2}{v_{T,0}^2} z_W\right|_{m_t\to\infty} \equiv \frac{M_W^2}{v_\sigma^2}\left[1 + v_\sigma^2 K_W^{(6,0,\sigma)} + \frac{1}{v_\sigma^2}K_W^{(4,1,\sigma)} + K_W^{(6,1,\sigma)}\right] , \tag{5.3.7}$$

where z_W is the squared wavefunction renormalisation factor of the W-boson field. After replacing the bare quantities on the left-hand side by their renormalised coun-

[1] On the other hand, if the bare vertex contains a photon, then examining Eq. (5.2.7) shows that the situation is reversed and $+3.4\%$ correction is associated with the α_μ scheme.

terparts, it is straightforward to determine the $K_W^{(i,j,\sigma)}$ in terms of $\Delta M_{W,t}^{(i,j,\sigma)}$, $\Delta z_{W,t}^{(i,j,\sigma)}$, and $\Delta v_{\sigma,t}^{(i,j,\sigma)}$. This yields $K_W^{(6,0,\sigma)} = -\Delta v_{\sigma,t}^{(6,0,\sigma)}$ at tree level, and substituting in the explicit results for the counterterms leads to the following one-loop expressions in the α scheme:

$$\begin{aligned} K_W^{(4,1,\alpha)} &= \Delta r_t^{(4,1)}\,, \\ K_W^{(6,1,\alpha)} &= -\frac{1}{2}\dot{K}_W^{(6,0,\alpha)} \ln\frac{\mu^2}{m_t^2} + \Delta r_t^{(4,1)}\left[\frac{1}{s_w^2}C_{HD} + \frac{3}{c_w s_w}C_{HWB}\right. \\ &\quad \left. + 2C_{\substack{Hq\\33}}^{(3)} + \frac{2\sqrt{2}(1-2c_w^2)}{c_w^2}\frac{M_W}{m_t}C_{\substack{uW\\33}}\right], \end{aligned} \tag{5.3.8}$$

where

$$\begin{aligned} \dot{K}_W^{(6,0,\alpha)} = -4\Delta r_t^{(4,1)}\Bigg[& C_{HD} + \frac{2s_w}{c_w}C_{HWB} + 2C_{\substack{Hq\\33}}^{(1)} - 2C_{\substack{Hu\\33}} \\ & - \frac{2\sqrt{2}s_w}{c_w^2}\frac{M_W}{m_t}\left(c_w C_{\substack{uB\\33}} + \frac{5}{3}s_w C_{\substack{uW\\33}}\right)\Bigg]. \end{aligned} \tag{5.3.9}$$

In the α_μ scheme one has instead

$$\begin{aligned} K_W^{(4,1,\mu)} &= 0\,, \\ K_W^{(6,1,\mu)} &= -\frac{1}{2}\dot{K}_W^{(6,0,\mu)} \ln\frac{\mu^2}{m_t^2} + \Delta\rho_t^{(4,1)} \sum_{j=1,2}\left[C_{\substack{Hl\\jj}}^{(3)} - C_{\substack{lq\\jj33}}^{(3)}\right], \end{aligned} \tag{5.3.10}$$

where

$$\dot{K}_W^{(6,0,\mu)} = -4\Delta\rho_t^{(4,1)} \sum_{j=1,2}\left[C_{\substack{Hl\\jj}}^{(3)} - C_{\substack{lq\\jj33}}^{(3)}\right]. \tag{5.3.11}$$

One sees that the SMEFT expansion of K_W is tadpole free, finite, and independent of the renormalisation scale up to NLO. This is not an accident – it gives the flavour-independent part of the large-m_t limit of W decay into fermions. Furthermore, rearranging the above expressions yields the following result for the v_T counterterms:[1]

$$\begin{aligned} \Delta v_{\sigma,t}^{(4,1,\sigma)} &= -K_W^{(4,1,\sigma)} + 2\Delta M_{W,t}^{(4,1)}\,, \\ \Delta v_{\sigma}^{(6,0,\sigma)} &= -K_W^{(6,0,\sigma)}\,, \end{aligned}$$

[1] We omit here Wilson coefficient counterterms δC_i, which contribute only divergent parts and thus do not play a role in the discussion of perturbative convergence.

$$\Delta v_{\sigma,t}^{(6,1,\sigma)} = -K_W^{(6,1,\sigma)} + \left[2\Delta M_{W,t}^{(6,1,\sigma)} + 2\Delta M_{W,t}^{(4,1)} K_W^{(6,0,\sigma)} + \Delta z_{W,t}^{(6,1,\sigma)}\right] . \tag{5.3.12}$$

The SM part of Eq. (5.3.12) is identical to Eq. (5.3.6). The dimension-six parts are the generalisation to SMEFT. In each case, the counterterm for v_T is split into two distinct parts: a physical piece that is a finite, gauge and scale-independent quantity (the K_W), plus remaining terms which contain tadpoles and divergent parts that cancel against other such terms in physical observables. While at one-loop in the SM it was simple to identify the physical factor $\Delta r^{(4,1)}$ in the α scheme by studying the counterterm $v_\alpha^{(4,1,\alpha)}$ alone, in SMEFT it is helpful to choose an observable process in order to split the counterterm into the two distinct parts. While the choice of W decay is not unique, it leads directly to the SM results obtained from studying v_T alone.

We can now use our expressions for the counterterms for v_T in Eq. (5.3.12) to check whether, as in the SM, a simple pattern emerges for input-scheme dependent SMEFT corrections to weak vertices. As an example, consider the following expression, which gives a flavour-independent correction to Z-boson decays into fermions:

$$z_Z \frac{M_{Z,0}^2}{v_{T,0}^2}\left(1 - v_{T,0}^2 \frac{C_{HD}}{2}\right)\Bigg|_{m_t\to\infty} = \frac{M_Z^2}{v_\sigma^2}\left[1 + v_\sigma^2 k_Z^{(6,0,\sigma)} + \frac{1}{v_\sigma^2} k_Z^{(4,1,\sigma)} + k_Z^{(6,1,\sigma)}\right] , \tag{5.3.13}$$

where z_Z is the wavefunction renormalisation factor squared of the Z-boson field.[1] The expression on the right-hand side is finite, tadpole free, and scale-independent up to NLO. Writing the counterterms for v_T using Eq. (5.3.12), one has

$$\begin{aligned} k_Z^{(6,0,\sigma)} &= K_W^{(6,0,\sigma)} + k_Z^{(6,0)} , \\ k_Z^{(4,1,\sigma)} &= K_W^{(4,1,\sigma)} + k_Z^{(4,1)} , \\ k_Z^{(6,1,\sigma)} &= K_W^{(6,1,\sigma)} + 2k_Z^{(4,1)} K_W^{(6,0,\sigma)} + k_Z^{(6,1)} . \end{aligned} \tag{5.3.14}$$

Here we have split each term in the perturbative expansion further into scheme de-

[1] Compared to Eq. (5.3.7) an additional factor of C_{HD} arises for Z-boson decays. This arises from the relations between the W/Z-mass and the Lagrangian parameters in SMEFT and can be seen by considering the flavour independent part of Eq. (5.25) in addition to Eq. (5.27) in [42].

pendent and independent parts (the latter being denoted without the σ superscript). Both the scheme dependent and independent parts are separately scale independent and tadpole free. The results for the scheme-independent pieces are

$$\begin{aligned} k_Z^{(6,0)} &= -\frac{C_{HD}}{2}\,, \\ k_Z^{(4,1)} &= 2\left(\Delta M_Z^{(4,1)} - \Delta M_W^{(4,1)}\right) = \Delta\rho_t^{(4,1)}\,, \\ k_Z^{(6,1)} &= 2\Delta\rho_t^{(4,1)} C_{\substack{Hq\\33}}^{(3)} - \frac{\dot{k}_Z^{(6,0)}}{2}\ln\frac{\mu^2}{m_t^2}\,, \end{aligned} \tag{5.3.15}$$

where

$$\dot{k}_Z^{(6,0)} = -4\Delta\rho_t^{(4,1)}\left[C_{HD} + 2C_{\substack{Hq\\33}}^{(1)} - 2C_{\substack{Hu\\33}}\right]. \tag{5.3.16}$$

Inverse powers of s_w appear only in the α scheme and are absorbed into the factors $K_W^{(i,j,\alpha)}$, so the scheme-independent coefficients $k_Z^{(i,j)}$ have an expansion in $\Delta\rho_t^{(4,1)}$. In the SM, it is evident that the scheme-dependent corrections $k_Z^{(4,1,\sigma)}$ follow the pattern discussed after Eq. (5.3.6). In SMEFT, scheme-dependent corrections appear in the combination $K_W^{(6,1,\sigma)} + 2k_Z^{(4,1)}K_W^{(6,0,\sigma)}$ in the last line of Eq. (5.3.14). Moreover, the $K_W^{(6,1,\sigma)}$ pieces are explicitly μ-dependent, and one normally chooses the scale in a process-dependent way. For these reasons, the numerical pattern of scheme-dependent NLO corrections to weak vertices in SMEFT in the α and α_μ schemes is not nearly as regular as in the SM; this is best seen by comparing results for a range of processes, which we leave to Section 5.5.

We have focussed the above discussion on the α and α_μ schemes. Corrections in the LEP scheme are derived from those in the α_μ scheme by using Eq. (4.3.7) to eliminate M_W in favour of $\hat{M}_W$. The result simplifies considerably in the large-m_t limit. To derive it, we first note that the large-m_t limit of the expansion coefficients of Δr defined in Eq. (4.2.24) can be written in terms of the K_W from Eq. (5.3.7) according to

$$\Delta r_t^{(i,j)} = K_W^{(i,j,\alpha)} - K_W^{(i,j,\mu)}\,. \tag{5.3.17}$$

We can convert these into expansion coefficients of $\hat{\Delta} r_t$ using Eq. (4.3.4). The SM and tree level SMEFT pieces just involve evaluating the expression at $M_W = \hat{M}_W$. The only non-trivial SMEFT piece is the NLO coefficient, for which we find

$$\hat{\Delta} r_t^{(6,1)} = \Delta r_t^{(6,1)} + \frac{1}{c_{2w}} \left[\frac{c_w}{s_w} C_{HWB} - \Delta r^{(6,0)} - K_W^{(6,0,\alpha)} \right] K_W^{(4,1,\alpha)} \Big|_{M_W = \hat{M}_W} . \quad (5.3.18)$$

Inserting these results into Eq. (4.3.7) gives the following large-m_t corrections to the W-boson mass in the LEP scheme within the SM

$$\hat{\Delta}_{W,t}^{(4,1,\mu)} = \frac{1}{2} \frac{\hat{c}_w^2}{\hat{c}_{2w}} \Delta \rho_t^{(4,1)} , \quad (5.3.19)$$

while the SMEFT result is

$$\hat{\Delta}_{W,t}^{(6,0,\mu)} = \frac{s_w^2}{2c_{2w}} \left(K_W^{(6,0,\mu)} - K_W^{(6,0,\alpha)} \right) \quad (5.3.20)$$

$$\begin{aligned} \hat{\Delta}_{W,t}^{(6,1,\mu)} = & \frac{s_w^2}{2c_{2w}} \left(K_W^{(6,1,\mu)} - K_W^{(6,1,\alpha)} \right) \\ & + \frac{s_w^2}{2c_{2w}^2} \left[K_W^{(6,0,\alpha)} - \frac{c_w}{s_w} C_{HWB} + \left(1 - \frac{s_w^2}{2} - \frac{2c_w^2 s_w^2}{c_{2w}} \right) \Delta r^{(6,0)} \right] K_W^{(4,1,\alpha)} \Big|_{M_W = \hat{M}_W} . \end{aligned}$$

As an example, let us use this to write the factor of M_W^2 in Eq. (5.3.7) in terms of $\hat{M}_W^2$. Denoting the resulting LEP-scheme expansion coefficients as $\hat{K}_W^{(i,j,\mu)}$, one has the NLO SM result

$$\hat{K}_W^{(4,1,\mu)} = 2 \frac{1}{v_\mu^2} \hat{\Delta}_{W,t}^{(4,1,\mu)} \approx 1.5\% . \quad (5.3.21)$$

The tree-level SMEFT result is

$$v_\mu^2 \hat{K}_W^{(6,0,\mu)} = \frac{1}{c_{2w}} \left(c_w^2 K_W^{(6,0,\mu)} - s_w^2 K_W^{(6,0,\alpha)} \right) \approx 1.4 K_W^{(6,0,\mu)} - 0.4 K_W^{(6,0,\alpha)} , \quad (5.3.22)$$

while the NLO contribution is

$$\begin{aligned} \hat{K}_W^{(6,1,\mu)} = & \frac{1}{c_{2w}} \left(c_w^2 K_W^{(6,1,\mu)} - s_w^2 K_W^{(6,1,\alpha)} \right) + \frac{c_w^2}{c_{2w}^2} K_W^{(4,1,\alpha)} \Bigg\{ \left(1 - \frac{c_w^2 s_w^2}{c_{2w}} \right) C_{HD} \\ & + 3 \frac{s_w}{c_w} \left(1 - \frac{4}{3} \frac{c_w^2 s_w^2}{c_{2w}} \right) C_{HWB} - 2 s_w^2 \left(1 - \frac{s_w^2}{c_{2w}} \right) K_W^{(6,0,\mu)} \Bigg\} \Bigg|_{M_W = \hat{M}_W} . \quad (5.3.23) \end{aligned}$$

For other processes, the numerical factors multiplying the $\hat{\Delta}_W$ terms are dictated

by the dependence of the bare vertex on M_W, and are therefore rather process dependent, a point illustrated in Section 5.5.1.

5.4 Derived Parameters

Having an initial understanding on the perturbative behaviour of each scheme we next move onto some concrete examples of the simplest observables for any scheme which are "derived parameters", where an input parameter in one scheme is calculated as a SMEFT expansion in another. For the schemes considered here there are three such quantities: α in the α_μ scheme, G_F in the α scheme, or M_W in the LEP scheme. All of these are functions of the expansion coefficients (and their derivatives, in the case of the LEP scheme) of Δr defined in Eq. (4.2.22). In this section we briefly examine the latter two cases, and also define the procedure for estimating higher-order corrections in the SMEFT expansion through scale variations used throughout the remainder of the chapter.

The SMEFT expansion for G_F in the α scheme is obtained from Eq. (4.2.22) and yields

$$G_{F,\alpha} = \frac{1}{\sqrt{2}v_\alpha^2}\left[1 + v_\alpha^2\Delta r^{(6,0)} + \frac{1}{v_\alpha^2}\Delta r^{(4,1)} + \Delta r^{(6,1)}\right] . \tag{5.4.1}$$

The tree-level result (LO) evaluates to

$$\frac{G_{F,\alpha}^{\rm LO}}{G_F} = 1.034 + v_\alpha^2\left[3.859 C_{HWB} + 1.801 C_{HD} + 1.034 \sum_{j=1,2} C_{\substack{Hl\\jj}}^{(3)} - 1.034 C_{\substack{ll\\1221}}\right], \tag{5.4.2}$$

and the sum of tree-level and one-loop corrections (NLO) is

$$\begin{aligned}\frac{G_{F,\alpha}^{\rm NLO}}{G_F} =& 0.992 + v_\alpha^2 \Bigg[3.733 C_{HWB} + 1.756 C_{HD} + 1.064 \sum_{j=1,2} C^{(3)}_{\substack{Hl\\jj}} - 1.039 C_{\substack{ll\\1221}} \\ & - 0.167 C_{\substack{Hu\\33}} + 0.142 C^{(1)}_{\substack{Hq\\33}} - 0.083 C^{(3)}_{\substack{Hq\\33}} + 0.062 C_{\substack{uB\\33}} + 0.020 C_{\substack{uW\\33}} \\ & + 0.018 C_{\substack{ll\\1122}} - 0.016 \sum_{j=1,2} C^{(3)}_{\substack{lq\\jj22}} + 0.010 C_W - 0.006 \sum_{j=1,2} \left(C_{\substack{Hu\\jj}} + C^{(3)}_{\substack{Hq\\jj}} \right) \\ & + 0.004 \sum_{j=1,2} C^{(1)}_{\substack{Hl\\jj}} + 0.003 \left(C^{(1)}_{\substack{Hl\\33}} + \sum_{i=1,2,3} C_{\substack{He\\ii}} + \sum_{i=1,2,3} C_{\substack{Hd\\ii}} - \sum_{j=1,2} C^{(1)}_{\substack{Hq\\jj}} \right) \\ & + 0.002 \left(C_{HB} + C_{HW} + C_{H\Box} - C^{(3)}_{\substack{Hl\\33}} \right) \Bigg] ,\end{aligned} \tag{5.4.3}$$

where in both cases we have used $\mu = M_Z$, so that $v_\alpha = v_\alpha(M_Z)$ and $C_i = C_i(M_Z)$ in the above equations. In the SM, the LO prediction for G_F differs by 3.4% from the measured value while at NLO the difference is -0.8%. Evidently, the large-m_t limit contribution in Eq. (5.3.4) accounts for the bulk of the NLO correction. The LO SMEFT result contains 5 Wilson coefficients which alter the result, while the NLO one contains the full set of 33 Wilson coefficients identified in Table 5.2.

SMEFT expansions of physical quantities such as $G_{F,\alpha}$ contain a residual dependence on the renormalisation scale μ due to the truncation of the full series at a fixed order in perturbation theory. In the SM this is due to the running of α, while in SMEFT the Wilson coefficients C_i also run. It is often useful to use the stability of the results under variations of the scale μ about a default value as an estimate of uncalculated, higher-order corrections in the perturbative expansion. The Wilson coefficients are unknown numerical quantities that we wish to extract from data, so in order to implement their running we must calculate their value at arbitrary scales μ given their value at a default scale choice $\mu^{\rm def}$. For our purposes, it is sufficient to use the fixed-order solution to the RG equation in this calculation, which reads

$$C_i(\mu) = C_i(\mu^{\rm def}) + \ln\left(\frac{\mu}{\mu^{\rm def}}\right) \dot{C}_i(\mu^{\rm def}) \,, \tag{5.4.4}$$

where $\dot{C}_i$ was defined in Eq. (4.1.10). For the running of α we can also use the

fixed-order solution to the RG equation discussed in detail in Section 5.2 of [29] and is given as

$$\alpha(\mu) = \alpha(M_Z)\left(1 + 2\gamma_e(M_Z)\ln\frac{\mu}{M_Z}\right), \tag{5.4.5}$$

where $\gamma_e(M_Z) = \frac{\alpha(M_Z)}{\pi} \times \frac{20}{9}$. This equation is identical to that of Eq. (1.2.28) but where we have set the initial value of the scale to the Z-boson mass. Throughout the section, we estimate uncertainties from scale variations by using the afore mentioned equations to evaluate observables for the three scale choices $\mu \in \{\mu^{\rm def}, 2\mu^{\rm def}, \mu^{\rm def}/2\}$. Central values are given for $\mu = \mu^{\rm def}$, and upper and lower uncertainties are determined by values of the observables at the other two choices.[1]

Let us apply this method to the calculation of M_W in the LEP scheme, which is obtained by evaluating Eq. (4.3.7). Compared to $G_{F,\alpha}$, the W-mass is sensitive to a different combination of Δr as well as its derivatives with respect to M_W. The LO result with $\mu = M_Z$ as the default value and scale uncertainties estimated as described above yields

$$\begin{aligned} M_W^{\rm LO} =& 79.82^{+0.13}_{-0.13}\ {\rm GeV} + \hat{M}_W v_\mu^2 \Bigg[- 0.795^{+0.038}_{-0.038} C_{HWB} - 0.360^{+0.026}_{-0.026} C_{HD} \\ & - 0.220^{+0.008}_{-0.008} \sum_{j=1,2} C^{(3)}_{\substack{Hl \\ jj}} + 0.22^{+0.003}_{-0.003} C_{\substack{ll \\ 1221}} + 0.000^{+0.038}_{-0.038} C^{(1)}_{\substack{Hq \\ 33}} + 0.000^{+0.036}_{-0.036} C_{\substack{Hu \\ 33}} \\ & + 0.000^{+0.013}_{-0.013} C_{\substack{uB \\ 33}} + 0.000^{+0.012}_{-0.012} C_{\substack{uW \\ 33}} + 0.000^{+0.006}_{-0.006} \sum_{j=1,2} C^{(3)}_{\substack{lq \\ jj33}} + \dots \Bigg], \end{aligned} \tag{5.4.6}$$

where the ... indicate contributions where the difference between the upper and lower values obtained from scale variation is less that 1% of $\hat{M}_W$ when the numerical choice $C_i = v_\mu^{-2}$ is made. At NLO we find

$$\begin{aligned} M_W^{\rm NLO} =& 80.47^{+0.01}_{-0.00}\ {\rm GeV} + \hat{M}_W v_\mu^2 \Bigg[- 0.807^{+0.002}_{-0.000} C_{HWB} - 0.381^{+0.004}_{-0.000} C_{HD} \\ & - 0.228^{+0.000}_{-0.000} \sum_{j=1,2} C^{(3)}_{\substack{Hl \\ jj}} + 0.223^{+0.000}_{-0.000} C_{\substack{ll \\ 1221}} + 0.032^{+0.000}_{-0.010} C_{\substack{Hu \\ 33}} \end{aligned} \tag{5.4.7}$$

[1] At NLO a large number of $\dot{C}_i$ must be evaluated; we have employed `DsixTools` [47, 120] for this purpose.

$$- 0.028^{+0.009}_{-0.000} C^{(1)}_{\substack{Hq \\ 33}} + 0.016^{+0.000}_{-0.003} C^{(3)}_{\substack{Hq \\ 33}} + 0.012^{+0.000}_{-0.002} C_{\substack{uB \\ 33}} + \dots \Bigg] ,$$

where in this case the ... refer to contributions where both the central values and the difference in upper and lower scale uncertainties are both less than 1% in magnitude. For both the SM and SMEFT, the scale uncertainties are significantly larger at LO than at NLO. While the NLO corrections in SMEFT all lie within the scale uncertainties of the LO calculation, the same is not true of the SM, where scale variations in the SM at LO do not capture the behaviour of the higher-order corrections.

We can understand the qualitative features of these results by studying them in the large-m_t limit. Using Eqs. (5.3.19, 5.3.20) for the NLO corrections in this limit, the numerical result at the scale $\mu = M_Z$ is

$$\begin{aligned} M_{W,t}^{\rm NLO} =& 80.36^{+0.00}_{-0.00}\ \text{GeV} + \hat{M}_W v_\mu^2 \Bigg[- 0.799^{+0.001}_{-0.000} C_{HWB} - 0.373^{+0.002}_{-0.000} C_{HD} \\ & - 0.226^{+0.000}_{-0.000} \sum_{j=1,2} C^{(3)}_{\substack{Hl \\ jj}} + 0.222^{+0.000}_{-0.000} C_{\substack{ll \\ 1221}} + 0.035^{+0.000}_{-0.008} C_{\substack{Hu \\ 33}} \\ & - 0.035^{+0.007}_{-0.000} C^{(1)}_{\substack{Hq \\ 33}} + 0.014^{+0.000}_{-0.003} C^{(3)}_{\substack{Hq \\ 33}} + 0.012^{+0.000}_{-0.000} C_{\substack{uB \\ 33}} + \dots \Bigg] . \end{aligned} \tag{5.4.8}$$

This is clearly a good approximation to Eq. (5.4.7), where as in that equation we have not included contributions of less than 1%. The SM result is scale invariant in this limit, because the top quark is decoupled from the QED coupling $\alpha(\mu)$.

The NLO result for M_W in SMEFT generalises the previous result [81] to include the full flavour structure, and resums logarithms of light fermion masses related to the running of α; a more detailed comparison is given Appendix A.3. The current state-of-the-art in the SM [121] includes complete two-loop corrections as well as a partial set of even higher-order corrections. Adjusted to our numerical inputs, the result derived from the parametrisation in Eq. (6) of that paper, which we refer to as NNLO, reads

$$M_W^{\rm NNLO} = 80.36\ \text{GeV} , \tag{5.4.9}$$

which is outside the uncertainties in the NLO result Eq. (5.4.7). In order to gain insight into the structure of higher-order corrections, we have studied the split of the NNLO result into pure EW, and mixed EW-QCD components, which was given in [121] for the unphysical value $M_h = 100$ GeV. When adjusting our own inputs to that unphysical value, we find that the pure NNLO EW contributions are within our NLO uncertainty estimate, so that the discrepancy is due to mixed EW-QCD effects first appearing at NNLO and unrelated to the running of α. The large-m_t limit of these EW-QCD corrections can be obtained by making the following replacement in Eq. (5.3.19) [122]:

$$\Delta\rho_t^{(4,1)} \to \Delta\rho_t^{(4,1)} \left[1 - \frac{\alpha_s}{\pi}\frac{2}{3}\left(2\zeta_2 + 1\right)\right] , \tag{5.4.10}$$

where

$$\zeta_2 = \frac{\pi^2}{2} , \tag{5.4.11}$$

is the Riemann Zeta Function evaluated at 2. Including this correction changes the central value in Eq. (5.4.7) to 80.41 GeV, which agrees with the NNLO result to better than the per-mille level. Further improvements can be made through resummations of the type discussed in Section 5.6.

5.5 Heavy Boson Decays

While the previous sections elucidating some general features of the different input schemes, the aim of this section is to study in detail three benchmark observables to NLO in the SMEFT expansion in each scheme: W decay into leptons, Z decay into charged leptons, and Higgs decay into bottom quarks. For the numerical analysis we focus on $W \to \tau\nu$ and $Z \to \tau\tau$.

We write the expansion coefficients of the decay rates to NLO in SMEFT for boson

$X \in \{W, Z, h\}$ to fermion pair $f_1 f_2$ as

$$\Gamma^{\mathrm{s}}_{Xf_1f_2} = \Gamma^{\mathrm{s}(4,0)}_{Xf_1f_2} + \Gamma^{\mathrm{s}(4,1)}_{Xf_1f_2} + \Gamma^{\mathrm{s}(6,0)}_{Xf_1f_2} + \Gamma^{\mathrm{s}(6,1)}_{Xf_1f_2}\,, \tag{5.5.1}$$

where the superscript $s(i,j)$ refers to dimension-i, j-loop contributions in input scheme $s \in \{\alpha, \alpha_\mu, \mathrm{LEP}\}$. To study convergence, it is convenient to work instead with expansion coefficients of the decay rate normalised to the LO SM result, namely

$$\Delta^{\mathrm{s}(i,j)}_{Xf_1f_2} = \frac{\Gamma^{\mathrm{s}(i,j)}_{Xf_1f_2}}{\Gamma^{\mathrm{s}(4,0)}_{Xf_1f_2}}\,. \tag{5.5.2}$$

Throughout the section numerical values for the decay rates are evaluated using the default value $\mu^{\mathrm{def.}} = m_{\mathrm{decay}}$, where m_{decay} is the mass of the decaying particle, and scale uncertainties are obtained by varying the scale up and down by a factor of 2 about the default value, as in Section 5.4.

Obviously, results for three decays in three renormalisation schemes and involving a large number of SMEFT Wilson coefficients contain a plethora of information. We have organised it as follows:

- Figures 5.4, 5.5 and 5.6 show Eq. (5.5.2) for the NLO SM corrections as well as corrections appearing at LO and NLO in SMEFT when the choice $C_i = 1\,\mathrm{TeV}^{-2}$ is made. They also show the large-m_t limits of the NLO corrections in cases where top-loops contribute, and group the coefficients such that those appearing solely due to the choice of renormalisation scheme appear on the far right.

- In Tables 5.3, 5.4 and 5.5 we show the size of the NLO corrections to the SM and SMEFT coefficients which appear at tree-level in the different schemes, for the default scale choices.

- In Appendix A.4, we give results for the numerically most important contributions to the decay rates at LO and NLO in the SMEFT expansion, including uncertainties as estimated from scale variations.

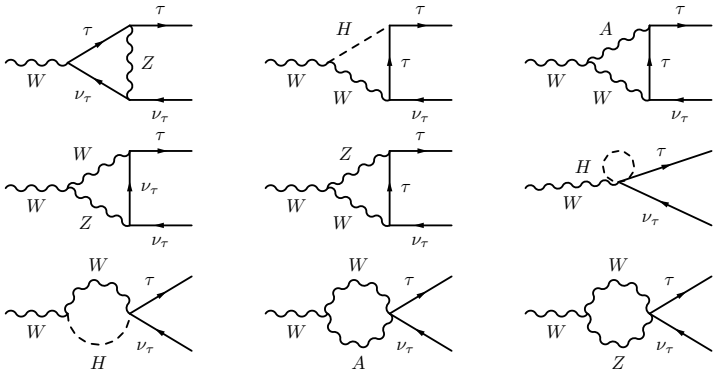

Figure 5.3: Representative virtual corrections for W decay into leptons at NLO.

The following subsections serve to explain and highlight the most noteworthy patterns emerging from these results.

5.5.1 $W \to \ell\nu$ decays

The tree-level decay rate for $W \to \tau\nu$ decays, written in terms of v_T, takes the form

$$\Gamma^{(4,0)}_{W\tau\nu} + \Gamma^{(6,0)}_{W\tau\nu} = \frac{M_W}{12\pi}\frac{M_W^2}{v_T^2}\left(1 + 2v_T^2 C^{(3)}_{\substack{Hl \\ 33}}\right) . \tag{5.5.3}$$

Renormalisation-scheme dependence thus enters the result through the counterterms for M_W and v_T.

The NLO decay rate is calculated by evaluating virtual corrections such as those shown in Figure 5.3, and then adding together with UV counterterms and real emission diagrams with an extra photon in the final state to get a finite result. The size of NLO SM corrections in the different schemes is easily understood using the large-m_t analysis in Section 5.3. In that limit, the NLO corrections in the α_μ scheme vanish, while those in α scheme are roughly -3.4%, a pattern which agrees well with the full results in Table 5.3. The SM LEP scheme corrections in the large-m_t limit are

$$\frac{\hat{M}_W}{12\pi}\frac{\hat{M}_W^2}{v_\mu^2}\left(1 + \frac{3}{2}\frac{\hat{c}_w^2}{\hat{c}_{2w}}\frac{\Delta\rho_t^{(4,1)}}{v_\mu^2}\right) \approx \frac{\hat{M}_W}{12\pi}\frac{\hat{M}_W^2}{v_\mu^2}\left(1 + 0.02\right) , \tag{5.5.4}$$

so that the NLO correction is again very close to the result in the table. Note that

in Eq. (5.5.4) we have consistently expressed all powers of the W mass in terms of $\hat{M}_W$, whether they come from the 2-body phase space or directly from the amplitude, which accounts the factor of 3/2 compared to Eq. (5.3.21). Absolute values of the decay rates at LO and NLO are given in Appendix A.4.1. In that notation, one finds the following ratios in the SM at NLO

$$\frac{\Gamma^{\alpha}_{W,\mathrm{NLO}}}{\Gamma^{\alpha_\mu}_{W,\mathrm{NLO}}} = 0.992\,, \qquad \frac{\Gamma^{\mathrm{LEP}}_{W,\mathrm{NLO}}}{\Gamma^{\alpha_\mu}_{W,\mathrm{NLO}}} = 1.003\,. \tag{5.5.5}$$

The first ratio agrees quite well with the estimate $G^{\mathrm{NLO}}_{F,\alpha}/G_F$ using Eq. (5.4.3), while the second is consistent with the estimate $(M^{\mathrm{NLO}}_W)^3/M^3_W$ using Eq. (5.4.7). Once the NLO corrections are included the results between the schemes show (better than) percent-level agreement.

In Figure 5.4 the corrections in SMEFT are shown. The absolute size of the SMEFT corrections is determined by the choice $C_i = \mathrm{TeV}^{-2}$. For that choice, SMEFT contributions are suppressed by $v_\sigma^2 \times \mathrm{TeV}^{-2} \approx 6\%$, and are anywhere between 10% to below per-mille level of the SM tree-level result depending on the coefficient. The NLO SMEFT results contain a large number of Wilson coefficients. We have organised the coefficients in Figure 5.4 such that those appearing only due to the renormalisation of v_T or M_W up to NLO are separated out onto the right part of the figure, while those appearing also in the bare matrix elements or wavefunction renormalisation factors and thus common to all schemes are on the left. In the α_μ scheme the coefficients $\Delta v_\mu^{(6,1,\mu)}$ appearing in Eq. (5.2.5) have a large overlap with those appearing in W-boson couplings, and as a result only four-fermion coefficients as well as those that modify Z couplings to leptons, $C^{(1)}_{\substack{Hl\\jj}}$, with $j = 1, 2$, are particular to that scheme. In the α scheme, on the other hand, the renormalisation of v_T brings in sensitivity to coefficients related to the renormalisation of M_Z and e, which are listed in Eqs. (5.2.3) and (5.2.4). The LEP scheme is sensitive to the full set of coefficients contained in Δr, through the renormalisation of M_W, and therefore contains the overlap of the coefficients in the other two schemes. Taken as a whole, the number of Wilson coefficients contributing at NLO for the central scale choice

is 39 in the LEP scheme, 35 in the α scheme and 25 in the α_μ scheme.

As in the SM, the numerically dominant NLO SMEFT corrections are related to top-quark loops. In the α and α_μ schemes, the scheme-dependent corrections in the large-m_t limit are nearly all contained in the factors K_W given in Eqs. (5.3.8, 5.3.10). For the default input choices, the SMEFT contributions evaluate to

$$\begin{aligned} v_\mu^2 K_W^{(6,0,\mu)} + K_W^{(6,1,\mu)} &= v_\mu^2 \Bigg[\sum_{j=1,2} \left(-C^{(3)}_{\substack{Hl \\ jj}} (1 + 0.0193) + 0.0193 C^{(3)}_{\substack{lq \\ jj33}} \right) + C_{\substack{ll \\ 1221}} (1 + 0.0) \Bigg], \\ v_\alpha^2 K_W^{(6,0,\alpha)} + K_W^{(6,1,\alpha)} &= v_\alpha^2 \Bigg[1.74 C_{HD} \left(1 - 0.0275\right) + 3.73 C_{HWB} \left(1 - 0.0354\right) \\ &\quad + 0.206 \left(C^{(1)}_{\substack{Hq \\ 33}} - C_{\substack{Hu \\ 33}} \right) - 0.0674 C^{(3)}_{\substack{Hq \\ 33}} - 0.0727 C_{\substack{uB \\ 33}} - 0.0334 C_{\substack{uW \\ 33}} \Bigg]. \end{aligned} \tag{5.5.6}$$

For coefficients appearing at LO, the NLO corrections are the second term in the parentheses, facilitating a comparison with Table 5.3. Results also for coefficients first appearing at NLO can be found in Eq. (A.4.3) and Eq. (A.4.5). We see the large-m_t limit corrections are a good approximation to the full ones. Interestingly, for the coefficients appearing at LO, there is no large hierarchy between the size of NLO corrections in the α scheme compared to the α_μ scheme, even though the analytic result for $K_W^{(6,1,\alpha)}$ contains 4 (3) inverse powers of s_w in the case of C_{HD} (C_{HWB}). In fact, the largest corrections are from $C^{(1)}_{\substack{Hq \\ 33}}$ and $C_{\substack{Hu \\ 33}}$, which appear only due to the scale-dependent logarithmic terms from Eq. (5.3.9). This illustrates the important point that, unlike the SM, the NLO corrections are strongly scale dependent in SMEFT.

The SMEFT corrections in the LEP scheme can be derived from results in the α_μ scheme using Eq. (4.3.7) to write M_W in terms of $\hat{M}_W$. The expansion coefficients arising after converting the factor of M_W^2 in the large-m_t limit, $\hat{K}_W^{(6,j,\mu)}$, were given in Eqs. (5.3.22, 5.3.23). In order to calculate the decay rate one must also write the factor of M_W arising from 2-body phase space in terms of $\hat{M}_W$. We have checked that after doing so the large-m_t limit corrections to the coefficients appearing in $\hat{K}_W$ are a good numerical approximation to the full ones.

In addition to the corrections related to the flavour-independent corrections, there

$W \to \tau\nu$	SM	C_{HD}	C_{HWB}	$C^{(3)}_{\substack{Hl \\ jj}}$	$C_{\substack{ll \\ 1221}}$	$C^{(3)}_{\substack{Hl \\ 33}}$
α	-4.2%	-1.7%	-3.0%	—	—	2.2%
α_μ	-0.3%	—	—	2.5%	-0.2%	2.2%
LEP	2.0%	8.1%	3.2%	5.1%	2.5%	4.6%

Table 5.3: NLO corrections to prefactors of LO Wilson coefficients in the three schemes. Negative corrections indicate a reduction in the magnitude of the numerical coefficient of a given Wilson coefficient. The flavour index j refers to $j \in 1, 2$.

are also contributions from the coefficient $C^{(3)}_{\substack{Hl \\ 33}}$, which specifically modifies the $\tau\nu W$ coupling. The large-m_t limit correction to $\Delta^{\mathrm{LEP}(6,1)}_{W,t}$ due to this coefficient is given by

$$-2\Delta\rho_t^{(4,1)} C^{(3)}_{\substack{Hl \\ 33}} \left(1 + 2\ln\frac{\mu^2}{m_t^2}\right)\left(1 + 3\hat{\Delta}^{(4,1,\mu)}_{W,t}\right) . \tag{5.5.7}$$

The corresponding results in the α and α_μ schemes are obtained from the above by setting $\hat{\Delta}^{(4,1,\mu)}_{W,t}$ to zero. Numerically, one finds that the NLO corrections to $C^{(3)}_{\substack{Hl \\ 33}}$ are about 4% in the LEP scheme, and 2% in the α and α_μ schemes, in rough agreement with Table 5.3. Compared to the other schemes, the NLO corrections to the coefficients appearing at tree-level in the LEP scheme show a rather irregular pattern due to the complicated dependence on the Weinberg angle.

While the size of the NLO corrections studied above is rather scale dependent, the sum of the LO and NLO contributions is independent of the scale (up to uncalculated NNLO terms in the SMEFT expansion) and is thus much less sensitive. To study this effect in detail, in Appendix A.4.1 we give numerical results in the three schemes including scale variations at LO and NLO. It is seen that in SMEFT, the dominant NLO corrections are typically within the uncertainties of the LO calculation as estimated through scale variations, and that the scale uncertainties in the NLO results are substantially smaller than in the LO ones.

$h \to b\bar{b}$		SM	$C_{H\Box}$	C_{HD}	$C_{\substack{dH \\ 33}}$	C_{HWB}	$C^{(3)}_{\substack{Hl \\ jj}}$	$C_{\substack{ll \\ 1221}}$
α	NLO QCD	20.3%	20.3%	20.3%	20.3%	20.3%	-	-
	NLO EW	-5.2 %	2.1%	-11.0%	4.2%	-6.7%	-	-
	NLO correction	15.1%	22.4%	9.3%	24.5%	13.6%	-	-
α_μ	NLO QCD	20.3%	20.3%	20.3%	20.3%	-	20.3%	20.3%
	NLO EW	-0.8 %	2.1%	2.0%	1.9%	-	0.9%	-0.8%
	NLO correction	19.5%	22.4%	22.3%	22.2%	-	21.2%	19.5%
LEP	NLO QCD	20.3%	20.3%	20.3%	20.3%	-	20.3%	20.3%
	NLO EW	-0.7 %	2.1%	1.6%	1.9%	-	0.7%	-0.9%
	NLO correction	19.5%	22.3%	21.9%	22.2%	-	21.0%	19.3%

Table 5.4: NLO corrections to prefactors of LO Wilson coefficients in the three schemes, split into QCD and EW corrections. The flavour index j refers to $j \in 1, 2$.

5.5.2 $h \to b\bar{b}$ decays

The tree-level decay rate for $h \to b\bar{b}$ decay is given by

$$\Gamma^{(4,0)}_{hb\bar{b}} + \Gamma^{(6,0)}_{hb\bar{b}} = \frac{3m_b^2 M_h}{8\pi v_T^2}\left[1 + v_T^2\left(2C_{H\Box} - \frac{1}{2}C_{HD} - \sqrt{2}\frac{v_T}{m_b}C_{\substack{dH \\ 33}}\right)\right]. \tag{5.5.8}$$

The decay $h \to b\bar{b}$ has two important differences with respect to the decays $W \to \ell\nu$ and $Z \to \ell\ell$ (to be discussed in Section 5.5.3). First, we retain the b-quark mass and, second, the strong coupling $\alpha_s(\mu)$ plays a role in the results already at NLO. The Higgs mass M_h is evaluated on-shell, but the NLO corrections do not involve its counterterm since it appears through phase space rather than through the amplitude. Therefore, the input-scheme dependence to NLO arises mainly through the counterterm for v_T.[1]

The decay $h \to b\bar{b}$ receives both QCD and EW corrections at NLO. The two effects are additive and to study the EW input scheme dependence of the results it is useful to quote the QCD and EW corrections separately, as in Table 5.4. To this order, the QCD corrections are scheme independent. In the α scheme the EW corrections are rather large and depend heavily on the Wilson coefficient considered, ranging

[1]Results in the α_μ and LEP scheme differ because one must eliminate M_W in favour of $\hat{M}_W$ in the NLO SM correction, but this is a small effect numerically.

from -11% to 4% and thus inducing significant shifts to QCD alone, while in the α_μ and LEP schemes the corrections are smaller are more uniform.

We can understand the qualitative features of the NLO EW corrections using the large-m_t limit. To this end, we use Eq. (5.3.12) to write the NLO decay rate in this limit as

$$\Gamma^s_{h b\bar{b}}\Big|_{m_t\to\infty} = \frac{3m_b^2 M_h}{8\pi v_\sigma^2}\left[1 + v_\sigma^2\left(K_h^{(6,0)} + K_W^{(6,0,\sigma)}\right) + \frac{1}{v_\sigma^2}\left(K_h^{(4,1)} + K_W^{(4,1,\sigma)}\right) + K_h^{(6,1)} + \Delta K_h^{(6,1,\sigma)}\right], \tag{5.5.9}$$

where $K_h^{(6,0)}$ is the SMEFT contribution in Eq. (5.5.8), and the scheme-dependent part of the NLO SMEFT correction is

$$\Delta K_h^{(6,1,\sigma)} = K_W^{(6,1,\sigma)} + 2K_h^{(4,1)}K_W^{(6,0,\sigma)} + \frac{1}{\sqrt{2}}\frac{v_\sigma}{m_b}K_W^{(4,1,\sigma)}C_{\substack{dH\\33}}\,. \tag{5.5.10}$$

Large-m_t limit results in the α scheme have been given previously in [29], while those in the α_μ scheme can be extracted from [58]. We make use of those results in what follows, thus employing the "vanishing gauge coupling limit", which in this case amounts to taking the limit $M_W \ll M_h$ in addition to $m_t \to \infty$. This is implemented to achieve simple results that are representative of the full calculation. The LEP and α_μ scheme results are identical in this limit.

In the SM, the scheme-independent NLO correction in the large-m_t limit is given by

$$\frac{1}{v_\sigma^2}K_h^{(4,1)} = \frac{1}{3v_\sigma^2}\Delta\rho_t^{(4,1)}\left(1 + \frac{7(N_c-3)}{3}\right) \approx 0.003\,. \tag{5.5.11}$$

It follows from the discussion in Section 5.3 that the large-m_t limit corrections in the α_μ scheme are tiny, while those in the α scheme are well approximated by $K_W^{(4,1,\alpha)} \approx -3.4\%$. Clearly, this mimics the features of the exact NLO EW corrections given in Table 5.4.

In SMEFT, the scheme-independent[1] NLO correction in the large-m_t limit is given

[1] In fact there is mild dependence on the scheme through the numerical value for v_σ.

by

$$\frac{K_h^{(6,1)}}{K_h^{(4,1)}} = C_{HD}\,(-1+6L_t) + 2\sqrt{2}\frac{M_W}{m_t}\,(-7+6L_t)\,C_{\underset{33}{uW}} + 4\,(1+6L_t)\,C^{(3)}_{\underset{33}{Hq}} + \frac{3}{2\sqrt{2}}\frac{v_\sigma}{m_b}\,(-1+10L_t)\,C_{\underset{33}{dH}} + \dots\,, \tag{5.5.12}$$

where $L_t = \ln\!\left(\mu^2/m_t^2\right)$ and we have set $N_c = 3$. The $\dots$ refer to Wilson coefficients which contain no overlap with those appearing in the scheme-dependent pieces in Eq. (5.5.10). In the α scheme the numerical value of the NLO corrections at $\mu = M_h$ is

$$\begin{aligned}\frac{1}{v_\alpha^2}\left(K_h^{(6,1)} + \Delta K_h^{(6,1,\alpha)}\right) = \Big\{ &- C_{HD}(1.6+9.7) + (0.0-17)C_{HWB} \\ &- (3.7+6.8)C^{(3)}_{\underset{33}{Hq}} + (0.0-8.8)(C_{\underset{33}{Hu}} - C^{(1)}_{\underset{33}{Hq}}) + (0.0-3.1)C_{\underset{33}{uB}} + (-4.6+0.42)C_{\underset{33}{uW}} \\ &- \frac{\sqrt{2}v_\alpha}{m_b}\,(1.8+1.7)\,C_{\underset{33}{dH}}\Big\} \times 10^{-2} + \dots\,,\end{aligned} \tag{5.5.13}$$

where the $\dots$ refer to coefficients not appearing in $\Delta K_W^{(6,1,\alpha)}$, and the order of the numbers inside the parentheses multiplying the Wilson coefficients on the right-hand side of the above equation matches the order of the two terms on the left-hand side. In most cases the scheme-dependent parts contained in $\Delta K_W^{(6,1,\alpha)}$ dominate over the scheme-independent ones. For coefficients not appearing already at NLO, one can verify that the results above are close to the exact NLO results in Eq. (A.4.12). Combined with the LO result in Eq. (A.4.11), one infers NLO EW corrections of -9% for C_{HD}, -5% for C_{HWB} in the α scheme. In the α_μ scheme, one has

$$\frac{1}{v_\mu^2}\Delta K_h^{(6,1,\mu)} = \left\{0.6C_{\underset{1221}{ll}} + \sum_{j=1,2}\left[-0.9C^{(3)}_{\underset{jj}{Hl}} + 0.3C^{(3)}_{\underset{jj33}{lq}}\right]\right\} \times 10^{-2}\,. \tag{5.5.14}$$

Contributions from C_{HWB} are completely absent in the α_μ scheme, while the NLO EW correction to C_{HD} from the above result and Eq. (A.4.13) is 3% in the large-m_t limit. This explains the pattern of results seen for these coefficients in Table 5.4. It makes clear that in this case factors of $K_W^{(i,j,\alpha)}$ work much the same in SMEFT as in the SM, producing sizeable NLO EW corrections compared to the α_μ scheme.

The full set of NLO corrections in the different schemes is shown in Figure 5.5. In

the numerical results in Appendix A.4.2 we follow [29] and leave in symbolic form enhancement factors of m_b/v_σ which disappear when $U(2)^2 \times U(3)^3$ is assumed. We have not done this in the figure, which explains, for instance, the very large contribution from $C_{\substack{dH \\ 33}}$. In contrast to the case of W decay, in some cases there are large differences between the large-m_t limit and full corrections; this occurs when a Wilson coefficient receives both EW and QCD corrections, the latter invariably being the larger effect. From the perspective of EW input-scheme dependent corrections, the most important feature of the figure is the number of Wilson coefficients appearing. In particular, there are far more in the α scheme, 42 in total, than in the α_μ or LEP schemes, both of which receive contributions from the same 29 Wilson coefficients. The main reason is that the renormalisation of v_T in the α scheme involves the large set of flavour-specific couplings to fermions identified given in Eq. (5.2.3), while in the α_μ and LEP schemes M_Z does not enter the tree-level amplitude and many of these coefficients are therefore absent.

5.5.3 $Z \to \ell\ell$ decays

The tree-level decay rate for $Z \to \tau\tau$ decay, written in terms of v_T, takes the form

$$\begin{aligned}\Gamma^{(4,0)}_{Z\tau\tau} + \Gamma^{(6,0)}_{Z\tau\tau} = \frac{M_Z}{24\pi}\Bigg\{ &\left[\frac{M_Z^2}{v_T^2}\left(1 - \frac{v_T^2}{2}C_{HD}\right)\right]\left(g_\tau^{(4,0)} + v_T^2 g_\tau^{(6,0)}\right) \\ &+ 2M_Z^2\left[c_{2w}\left(C^{(1)}_{\substack{Hl \\ 33}} + C^{(3)}_{\substack{Hl \\ 33}}\right) - 2s_w^2 C_{\substack{He \\ 33}}\right]\Bigg\}, \end{aligned} \tag{5.5.15}$$

where

$$\begin{aligned} g_\tau^{(4,0)} &= 1 - 4s_w^2 + 8s_w^4\,, \\ g_\tau^{(6,0)} &= 2\left(1 - 4s_w^2\right)\left(c_w^2 C_{HD} + 2c_w s_w C_{HWB}\right)\,. \end{aligned} \tag{5.5.16}$$

The term inside the square brackets in the first line of Eq. (5.5.15) is independent of the fermion species into which the Z decays and was considered in Eq. (5.3.13). The function g_τ depends on the charge and weak isospin of the τ lepton, and the terms on second line are specific to $Z\tau\tau$ couplings in SMEFT. The LO decay rate depends on

the full set of parameters M_W, M_Z, v_T, and so scheme-dependent corrections involve the full set of coefficients identified in Section 5.2.

The NLO decay rates in the three schemes are shown in Figure 5.6. In the α scheme the set of coefficients appearing in the renormalisation of v_T is the same as that for renormalising M_Z and M_W, so it does not introduce any unique coefficients at NLO. In the LEP and α_μ schemes, on the other hand, the renormalisation of v_T introduces a set of 4-fermion coefficients shown on the right-hand side of the figure that would not otherwise appear in the decay rate. In this case the number of coefficients appearing at NLO is quite large: 63 in the α scheme, and 67 in the α_μ and LEP schemes.

In order to understand the dominant corrections we study the large-m_t limit. Let us first consider the corrections to the SMEFT coefficients specific to $Z\tau\tau$ couplings, given in the second line of Eq. (5.5.15). In order to evaluate them in the three schemes, we can use

$$\Delta M_{Z,t}^{(4,1)} = \hat{\Delta} M_{Z,t}^{(4,1,\mu)} = -\Delta\rho_t^{(4,1)} \ln \frac{\mu^2}{m_t^2} + \dots \,, \tag{5.5.17}$$

where the $\dots$ signify tadpole contributions which cancel against those in the bare matrix elements. Along with the LEP scheme result

$$\hat{\Delta} s_{w,t}^{(4,1,\mu)} = -\frac{\hat{c}_w^2}{2\hat{c}_{2w}} \Delta\rho_t^{(4,1)} \approx -0.7 \Delta\rho_t^{(4,1)} \approx -0.4 \Delta s_{w,t}^{(4,1,\mu)} \,, \tag{5.5.18}$$

it is then easy to show that in the large-m_t limit we can replace the tree-level expressions involving $C_{\substack{He \\ 33}}$ by

$$\begin{aligned} M_Z^2 s_w^2 C_{\substack{He \\ 33}} &\to M_Z^2 s_w^2 C_{\substack{He \\ 33}} \left(1 + \frac{1}{v_\mu^2}\left[\frac{c_w^2}{s_w^2} - 2\ln\frac{\mu^2}{m_t^2}\right]\Delta\rho_t^{(4,1)}\right) \approx M_Z^2 s_w^2 C_{\substack{He \\ 33}} (1 + 0.06) \,, \\ M_Z^2 s_w^2 C_{\substack{He \\ 33}} &\to M_Z^2 \hat{s}_w^2 C_{\substack{He \\ 33}} \left(1 + \frac{1}{v_\mu^2}\left[-\frac{\hat{c}_w^2}{\hat{c}_{2w}} - 2\ln\frac{\mu^2}{m_t^2}\right]\Delta\rho_t^{(4,1)}\right) \approx M_Z^2 \hat{s}_w^2 C_{\substack{He \\ 33}} (1 + 0.01) \,, \end{aligned} \tag{5.5.19}$$

where the first result is for the α_μ (or α scheme after $\mu \to \alpha$) and the second line is for the LEP scheme. The results are a good approximation to the exact ones shown

in Table 5.5. The fairly large difference between the LEP and α_μ scheme makes clear that the corrections can be quite sensitive to the exact dependence on e.g. s_w in the tree-level results. We have checked that the corrections to the remaining coefficients appearing in the second line of Eq. (5.5.15) are also well-approximated by the large-m_t limit.

The NLO corrections related to the first line of Eq. (5.5.15) are more complicated. To study them, we first note that the large-m_t limit corrections to the function g_τ can be written in the α and α_μ schemes as

$$g_\tau = g_\tau^{(4,0)} + v_\sigma^2 g_\tau^{(6,0)} + \frac{1}{v_\sigma^2} g_\tau^{(4,1)} + g_\tau^{(6,1)} + \left(K_W^{(6,0,\sigma)} g_\tau^{(4,1)} - K_W^{(4,1,\sigma)} g_\tau^{(6,0)}\right) . \quad (5.5.20)$$

The scheme-independent function $g_\tau^{(4,1)}$ is obtained by replacing $s_w \to s_w(1 + \Delta s_w)$ and isolating the SM corrections; it thus reads

$$g_\tau^{(4,1)} = -4c_w^2(1 - 4s_w^2)\Delta\rho_t^{(4,1)} . \quad (5.5.21)$$

The function $g_\tau^{(6,1)}$ is obtained in the same way, except for in that case one must also include corrections from $Z - \gamma$ mixing to get a finite and tadpole-free result. The explicit result is

$$\begin{aligned} g_\tau^{(6,1)} = &-\frac{1}{2}\dot{g}_\tau^{(6,0)} \ln\frac{\mu^2}{m_t^2} + g_\tau^{(4,1)}\left(-\frac{C_{HWB}}{2c_w s_w} + 2C_{\substack{Hq\\33}}^{(3)} - 2\sqrt{2}\frac{M_W}{M_T}C_{\substack{uW\\33}}\right) \\ &- 12c_{2w}\Delta\rho_t^{(4,1)}\left(c_w^2 C_{HD} + 2c_w s_w C_{HWB}\right) , \end{aligned} \quad (5.5.22)$$

where

$$\dot{g}_\tau^{(6,0)} = -4g_\tau^{(4,1)}\left[C_{HD} + \frac{s_w}{c_w}C_{HWB} + 2C_{\substack{Hq\\33}}^{(1)} - 2C_{\substack{Hu\\33}} - \frac{\sqrt{2}s_w}{c_w^2}\frac{M_W}{m_t}\left(c_w C_{\substack{uB\\33}} + \frac{5}{3}s_w C_{\substack{uW\\33}}\right)\right] . \quad (5.5.23)$$

We can now obtain the NLO corrections to the first line of Eq. (5.5.15) in the large-m_t limit in the α scheme through the replacement

$$\frac{M_Z^2}{v_T^2}\left(1 - \frac{v_T^2}{2}C_{HD}\right)\left(g_\tau^{(4,0)} + v_T^2 g_\tau^{(6,0)}\right) \to \frac{M_Z^2}{v_\alpha^2}\left(g_\tau^{(4,0)} + v_\alpha^2 K_Z^{(6,0,\alpha)} + \frac{1}{v_\alpha^2}K_Z^{(4,1,\alpha)} + K_Z^{(6,1,\alpha)}\right) , \quad (5.5.24)$$

where the coefficients K_Z are obtained by expanding out Eqs. (5.3.13) and (5.5.20). The SM result in the α scheme is then given by

$$\begin{aligned} g_\tau^{(4,0)} + \frac{1}{v_\alpha^2} K_Z^{(4,1,\alpha)} &= g_\tau^{(4,0)} + \frac{1}{v_\alpha^2}\left(g_\tau^{(4,0)} K_W^{(4,1,\alpha)} + g_\tau^{(4,0)} k_Z^{(4,1)} + g_\tau^{(4,1)}\right) \\ &\approx g_\tau^{(4,0)}(1 - 0.034 + 0.009 - 0.006)\,, \end{aligned} \tag{5.5.25}$$

where the order of numerical terms on the second line matches the first, and $g_\tau^{(4,0)} \approx 0.51$. In the α_μ scheme $K_W^{(4,1,\mu)} = 0$, and in the LEP scheme one replaces $g_\tau^{(4,1)} \to -\frac{s_w^2}{c_{2w}} g_\tau^{(4,1)} \approx -0.40 g_\tau^{(4,1)}$. This accounts for the SM corrections in the α and α_μ schemes given in Table 5.5, which as in Higgs and W decay follows the pattern identified in Section 5.3.

Turning to SMEFT, the LO corrections in the α scheme are contained in

$$\begin{aligned} K_Z^{(6,0,\alpha)} &= g_\tau^{(4,0)} K_W^{(6,0,\alpha)} - g_\tau^{(4,0)} \frac{C_{HD}}{2} + g_\tau^{(6,0)} \\ &\approx g_\tau^{(4,0)} K_W^{(6,0,\alpha)} - 0.25 C_{HD} + (0.17 C_{HD} + 0.18 C_{HWB}) \\ &\approx 0.80 C_{HD} + 2.0 C_{HWB}\,, \end{aligned} \tag{5.5.26}$$

where the order of the terms on the second line matches that in the first. In the α_μ scheme one replaces $\alpha \to \mu$ in the above equation; in that case it is clear that the tree-level contributions from C_{HD} and C_{HWB} are quite small, since $K_W^{(6,0,\mu)}$ contains neither of these coefficients. At NLO in SMEFT, we can write

$$K_Z^{(6,1,\sigma)} = K_Z^{(6,1)} + \Delta K_Z^{(6,1,\sigma)}\,, \tag{5.5.27}$$

where the first term is independent of the scheme. In terms of component objects, one finds

$$\begin{aligned} \Delta K_Z^{(6,1,\sigma)} &= g_\tau^{(4,0)} K_W^{(6,1,\sigma)} + 2 g_\tau^{(4,0)} K_W^{(6,0,\sigma)} k_Z^{(4,1)} + 2 g_\tau^{(4,1)} K_W^{(6,0,\sigma)}\,, \\ K_Z^{(6,1)} &= g_\tau^{(4,0)} k_Z^{(6,1)} + g_\tau^{(6,1)} + g_\tau^{(6,0)} k_Z^{(4,1)} + g_\tau^{(4,1)} k_Z^{(6,0)}\,. \end{aligned} \tag{5.5.28}$$

One can use explicit expressions for the component functions given above to evaluate these numerically. As an example, let us consider the contributions from C_{HWB} and

C_{HD} in the α_μ scheme. These are contained solely in the scheme-independent factor, which at the scale $\mu = M_Z$

$$\frac{1}{v_\mu^2} K_Z^{(6,1)} = -0.049 C_{HD} - 0.042 C_{HWB} + \dots \tag{5.5.29}$$

where the ... refer to contributions from other C_i, which are less than 1% in the units above. Comparing with the second line of Eq. (5.5.26), this implies NLO corrections of 60% for C_{HD} and -20% for C_{HWB}, which are indeed close to the huge corrections in the exact results in Table 5.5. In the α scheme these coefficients also contribute through the scheme dependent piece. The numerical result is

$$\begin{aligned} \frac{1}{v_\alpha^2} \Delta K_Z^{(6,1,\alpha)} =& -0.027 C_{HD} - 0.064 C_{HWB} \\ &+ g_\tau^{(4,0)} \left[0.17 C_{\substack{Hq \\ 33}}^{(1)} - 0.17 C_{\substack{Hu \\ 33}} - 0.067 C_{\substack{Hq \\ 33}}^{(3)} - 0.061 C_{\substack{uB \\ 33}} - 0.023 C_{\substack{uW \\ 33}} \right] . \end{aligned} \tag{5.5.30}$$

Even though the contributions on the first line contain up to four (three) inverse powers of s_w in the case of C_{HD} (C_{HWB}), there is no clear hierarchy compared to the scheme-independent pieces in Eq. (5.5.29). Combining them with the LO numbers in Eq. (5.5.26), we account for the pattern seen in Table 5.5. Clearly, this pattern is quite complicated and is not driven by the scheme-dependent factors K_W as in the SM. On the other hand, the coefficients on the second line only appear through $K_W^{(6,1,\alpha)}$, and as seen from the exact results in Eq. (A.4.18) we see that this factor indeed absorbs the dominant corrections from them, much like $K_W^{(4,1,\alpha)}$ in the SM.

The LEP scheme results can be obtained from those in the α_μ scheme by employing Eq. (4.3.10). In the large-m_t limit the only non-trivial conversions are on the functions g_τ, which contain M_W dependence already at tree level. For instance, calling the LEP-scheme functions $\hat{g}_\tau$, we have the LO SMEFT result

$$\hat{g}_\tau^{(6,0)} = 4(1 - 4s_w^2) \frac{c_w^2 s_w^2}{c_{2w}} \left[\frac{1}{2} C_{HD} + \frac{1}{c_w s_w} C_{HWB} - K_W^{(6,0,\mu)} \right] , \tag{5.5.31}$$

and the LEP-scheme version of Eq. (5.5.26) becomes

$$\hat{K}_Z^{(6,0,\mu)} = \hat{g}_\tau^{(4,0)} K_W^{(6,0,\mu)} - \hat{g}_\tau^{(4,0)} \frac{C_{HD}}{2} + \hat{g}_\tau^{(6,0)}$$

$Z \to \tau\tau$	SM	C_{HD}	C_{HWB}	$C_{\substack{He \\ 33}}$	$C^{(1)}_{\substack{Hl \\ 33}}$	$C^{(3)}_{\substack{Hl \\ 33}}$	$C^{(3)}_{\substack{Hl \\ jj}}$	$C_{\substack{ll \\ 1221}}$
α	-4.0%	-10.6%	-5.4%	7.7%	0.3%	-0.5%	—	—
α_μ	$< 0.1\%$	71.1%	-27.2%	7.6%	0.1%	-0.4%	2.9%	0.6%
LEP	1.0%	7.8%	17.4%	2.0%	4.7%	4.2%	6.9%	4.5%

Table 5.5: NLO corrections to prefactors of LO Wilson coefficients in the three schemes. Negative corrections indicate a reduction in the magnitude of the numerical coefficient of a given Wilson coefficient, while $< 0.1\%$ indicates changes below 0.1%, both positive and negative. The flavour index j refers to $j \in 1, 2$.

$$\approx -0.29 C_{HD} - 0.21 C_{HWB} - 0.59 \left(\sum_{j=1,2} C^{(3)}_{\substack{Hl \\ jj}} - C_{\substack{ll \\ 1221}} \right) . \qquad (5.5.32)$$

Compared to the α_μ scheme, the LO result for the coefficient C_{HD} is significantly larger, and those from the operators contained in $K_W^{(6,0,\mu)}$ are slightly smaller, which roughly explains the pattern for those coefficients seen in LEP scheme results Table 5.5. The result for C_{HWB} is slightly increased, but remains small and for that reason still receives a substantial NLO correction.

We have derived the complete large-m_t limit results and verified that they provide a good approximation to the full one, but the explicit expression for the function $\hat{g}_\tau^{(6,1,\mu)}$ is somewhat lengthy and we do not reproduce it here. In Section A.4.3 we show detailed LO and NLO results including uncertainties estimated from scale variations. It is clear that in cases where the NLO corrections are large, namely for certain operators in the α_μ and the LEP schemes, the uncertainties are underestimated, while in the α-scheme the uncertainty estimates are more reliable. This example highlights very clearly that the issue of NLO corrections in SMEFT is considerably more scheme and process-dependent than in the SM. The general rule that NLO corrections to weak decays are smaller in the LEP and α_μ schemes than in the α scheme familiar from the SM does not transfer over to SMEFT.

5.6 Universal corrections in SMEFT

A recurring theme of the previous sections was that EW corrections are dominated by top loops. While the numerical patterns in EW input-scheme dependent top-loop corrections in the SM are quite regular, those in SMEFT are more process and Wilson-coefficient dependent. The purpose of this section is to show that the dominant scheme-dependent EW corrections in SMEFT can nonetheless be taken into account by a certain set of simple substitutions in the LO results, similarly to the well-studied case of the SM.

Let us begin the discussion with the SM, where an important feature is that weak vertices in the α scheme receive corrections proportional to $\Delta r_t^{(4,1)}$, related to the renormalisation of v_T. It is simple to resum such corrections to all orders in perturbation theory. Using the large-m_t limit result in Eq. (5.3.3), and keeping for the moment only the $\Delta r_t^{(4,1)}$ terms (i.e. terms enhanced in the limit $c_w^2/s_w^2 \gg 1$, in which case the $\Delta M_{W,t}$ piece is subleading), we have

$$\begin{aligned}\frac{1}{v_{T,0}^2} &\approx \frac{1}{v_\alpha^2}\left[1+\frac{1}{v_{T,0}^2}\Delta r_t^{(4,1)}\right] \approx \frac{1}{v_\alpha^2}\left[1+\frac{1}{v_\alpha^2}\Delta r_t^{(4,1)}+\frac{1}{v_\alpha^2 v_{T,0}^2}\left(\Delta r_t^{(4,1)}\right)^2+\dots\right] \\ &= \frac{1}{v_\alpha^2}\left[1-\frac{1}{v_\alpha^2}\Delta r_t^{(4,1)}\right]^{-1} \equiv \frac{1}{\tilde{v}_\alpha^2}\,. \end{aligned} \tag{5.6.1}$$

This resums the $\Delta r_t^{(4,1)}$ terms to all orders. Adding back the subleading terms away from the double limit m_t, $c_w^2/s_w^2 \gg 1$ by matching with the one-loop result yields

$$\frac{1}{v_{T,0}^2} = \frac{1}{\tilde{v}_\alpha^2}\left[1-\frac{1}{\tilde{v}_\alpha^2}\left(\Delta v_\alpha^{(4,1,\alpha)}+\Delta r_t^{(4,1)}\right)\right]. \tag{5.6.2}$$

Expressing the counterterm for v_T as an expansion in $\tilde{v}_\alpha$ rather than v_α will obviously lead to a quicker convergence between orders. For example, the SM prediction to NLO for the derived quantity G_F in such a "$\tilde{\alpha}$ scheme" is

$$G_{F,\tilde{\alpha}}^{\rm NLO} = \frac{1}{\sqrt{2}\tilde{v}_\alpha^2}\left[1+\frac{1}{\tilde{v}_\alpha^2}\left(\Delta r^{(4,1)}-\Delta r_t^{(4,1)}\right)\right]. \tag{5.6.3}$$

Numerically, including uncertainties from scale variation using the procedure de-

scribed in Section 5.4,

$$\frac{G_{F,\tilde{\alpha}}^{\mathrm{LO}}}{G_F} = 1.000^{+0.007}_{-0.007}\,, \qquad \frac{G_{F,\tilde{\alpha}}^{\mathrm{NLO}}}{G_F} = 0.994^{+0.000}_{-0.000}\,, \tag{5.6.4}$$

where $G_{F,\tilde{\alpha}}^{\mathrm{LO}}$ refers to the first term in Eq. (5.6.3). This shows considerably improved convergence compared to the fixed-order α scheme expression in Eq. (5.4.1), and scale variations in the LO result give a good estimate of the NLO corrections.

To the best of our knowledge, a resummation of the type described above was first derived in [123], at the level of the W-boson mass in the LEP scheme (and also including subleading two-loop terms in the limit $s_w \to 0$). In that case, similar reasoning using Eq. (4.2.22) as a starting point leads to the resummed LO prediction

$$\left(M_W^{\widetilde{\mathrm{LO}}}\right)^2 = \tilde{M}_W^2 \equiv \frac{M_Z^2}{2}\left(1 + \sqrt{1 - \frac{4\pi\alpha v_\mu^2}{M_Z^2\left(1 - \frac{1}{v_\mu^2}\Delta r_t^{(4,1)}\right)}}\right). \tag{5.6.5}$$

The NLO result within the resummation formalism, modified to avoid double counting, is

$$M_W^{\widetilde{\mathrm{NLO}}} = \tilde{M}_W\left[1 - \frac{1}{2}\frac{\hat{s}_w^2}{\hat{c}_{2w}}\frac{1}{v_\mu^2}\Delta\tilde{r}^{(4,1)}\right], \qquad \Delta\tilde{r}^{(4,1)} = \Delta r^{(4,1)} - \Delta r_t^{(4,1)}\,. \tag{5.6.6}$$

Evaluating numerically and including uncertainties from scale variation leads to

$$M_W^{\widetilde{\mathrm{LO}}} = 80.33^{+0.13}_{-0.13}\mathrm{GeV}\,, \qquad M_W^{\widetilde{\mathrm{NLO}}} = 80.44^{+0.01}_{-0.00}\mathrm{GeV}\,, \tag{5.6.7}$$

which again shows improved perturbative convergence compared to the fixed-order results in Eqs. (5.4.6, 5.4.7).

Resummations are especially useful for derived parameters, which are known to a high level of experimental and perturbative accuracy. However, when viewed as a subset of corrections to EW vertices contributing to scattering amplitudes or decay rates in a specific input scheme, the corrections beyond NLO contained in the resummed formulas are typically negligible compared to process-dependent experimental and perturbative uncertainties. For instance, the central values of the

LO resummed results in Eqs. (5.6.4, 5.6.7) can be split up as

$$\begin{aligned}\frac{G_{F,\tilde{\alpha}}^{\rm LO}}{G_F} &= 1.034 - 0.035 + 0.001 = 1.000\,,\\ \widetilde{M_W^{\rm LO}} &= (79.82 + 0.54 - 0.03)\ \text{GeV} = 80.33\,\text{GeV}\,,\end{aligned} \tag{5.6.8}$$

where in both cases the sequence of three numbers after the first equality are the fixed-order LO, the fixed-order NLO correction, and the beyond NLO corrections, respectively. Clearly, the NLO expansions of the resummed formulas approximate the full results at sub percent-level precision, so a fixed-order implementation suffices for practical applications.

Universal NLO corrections to weak vertices implied by resummation can be obtained through a procedure of substitutions on LO results. The remaining, non-universal NLO corrections need to be calculated on a case-by-case basis, but these are typically small compared to the ones already included at LO through the aforementioned substitutions. While such procedures for universal corrections are well known in the SM (see for instance [124]), we give here a first implementation within SMEFT. Step-by-step, it works as follows

(1) Write the LO amplitude in terms of v_T, M_W, and $M_Z = M_W/c_w$.

(2) Make EW-input scheme dependent replacements on the LO amplitudes. In the α or α_μ scheme, these read

$$\begin{aligned}\frac{1}{v_T^2} &\to \frac{1}{v_\sigma^2}\left[1 + v_\sigma^2 K_W^{(6,0,\sigma)} + \frac{K_W^{(4,1,\sigma)}}{v_\sigma^2} + K_W^{(6,1,\sigma)}\right],\\ s_w^2 &\to s_w^2\left(1 - \frac{1}{v_\sigma^2}\Delta r_t^{(4,1)} + \Delta v_\sigma^{(6,0,\sigma)}\Delta r_t^{(4,1)} - 2C_{\substack{Hq\\33}}^{(3)}\Delta r_t^{(4,1)}\right),\\ c_w^2 &\to c_w^2\left(1 - \frac{1}{v_\sigma^2}\Delta \rho_t^{(4,1)} + \Delta v_\sigma^{(6,0,\sigma)}\Delta \rho_t^{(4,1)} - 2C_{\substack{Hq\\33}}^{(3)}\Delta \rho_t^{(4,1)}\right),\end{aligned} \tag{5.6.9}$$

where as usual $\sigma \in \{\alpha, \mu\}$ and the K_W are given in Eqs. (5.3.8, 5.3.10).

In the LEP scheme, make the above replacements with $\sigma = \mu$ in the LO amplitude. Subsequently, eliminate M_W in favour of $\hat{M}_W$ using Eq. (4.3.7),

in both the replacements and everywhere else in the LO observable (so that factors of M_W related to phase space are also taken into account).

(3) Expand the resulting expressions to NLO in a fixed-order SMEFT expansion before evaluating numerically.

We shall refer to results obtained from the above procedure as "LO_K" accurate.

In the SM, the substitutions in Eq. (5.6.9) are sufficient to capture NLO corrections proportional to $\Delta r_t^{(4,1)}$. Beyond that, writing $M_Z = M_W/c_w$ before performing the shifts ensures that the large-m_t limits of both W and Z decay are reproduced. In SMEFT, the substitution for v_T is motivated by Eq. (5.3.12), which splits the counterterm for v_T into a "physical", μ-independent order-by-order in perturbation theory and tadpole free part, K_W, and an "unphysical" part, which is tadpole dependent and divergent. The physical part captures the most singular large-m_t corrections as $s_w \to 0$ in SMEFT, as well as μ-dependent logarithms. The substitutions for s_w also capture such pieces of its counterterm, including a piece proportional to $C_{\substack{Hq \\ 33}}^{(3)}$ which is easily shown to be proportional to the NLO SM result. Finally, in both SMEFT and the SM, the shift for c_w is chosen to maintain $s_w^2 + c_w^2 = 1$. While Eq. (5.6.9) is not unique, other reasonable choices would differ only by terms proportional to $\Delta\rho_t^{(4,1)}$ rather than $\Delta r_t^{(4,1)}$ and thus agree with the above to roughly the percent level.[1]

In Table 5.6, we compare various perturbative approximations to heavy-boson decay rates in the SM within the α and LEP schemes, in each case normalised to the NLO result in the α_μ scheme at the default scale choice. The LO and NLO results refer to fixed-order perturbation theory, NLO_t refers to the large-m_t limit of NLO, and LO_K refers to the sum of LO and NLO corrections obtained through the above procedure. For the case of W and Z decay in the α scheme, the convergence between LO_K and NLO is greatly improved compared to pure fixed order, and varying the scale in the

[1] Substitutions for SMEFT vertices involving photons need to be considered on a case-by-case basis. For instance, a QED-type vertex in the α and LEP schemes is proportional to e and spurious corrections would be generated through the substitution procedure outlined above.

	$W \to \tau\nu$		$Z \to \tau\tau$		$h \to b\bar{b}$	
	α	LEP	α	LEP	α	LEP
NLO	$0.992^{+0.001}_{-0.001}$	$1.003^{+0.000}_{-0.000}$	$0.992^{+0.001}_{-0.001}$	$1.002^{+0.000}_{-0.000}$	$0.991^{+0.001}_{-0.001}$	$1.000^{+0.000}_{-0.000}$
NLO_t	$1.001^{+0.007}_{-0.007}$	$1.003^{+0.005}_{-0.005}$	$1.002^{+0.007}_{-0.007}$	$1.003^{+0.002}_{-0.002}$	$1.013^{+0.007}_{-0.007}$	$1.011^{+0.001}_{-0.001}$
LO	$1.036^{+0.008}_{-0.008}$	$0.983^{+0.005}_{-0.005}$	$1.034^{+0.008}_{-0.008}$	$0.993^{+0.001}_{-0.001}$	$1.045^{+0.007}_{-0.007}$	$1.008^{+0.001}_{-0.001}$
LO_K	$1.001^{+0.007}_{-0.007}$	$1.003^{+0.005}_{-0.005}$	$1.002^{+0.007}_{-0.007}$	$1.003^{+0.002}_{-0.002}$	$1.010^{+0.007}_{-0.007}$	$1.008^{+0.001}_{-0.001}$

Table 5.6: SM results in the α and LEP schemes. For each process, the results are normalised to the SM NLO results in the α_μ scheme.

LO_K results gives a good estimate for the residual corrections contained in the full NLO result. Also in Higgs decay LO_K is a marked improvement over LO, although in that case the results in all schemes are subject to a roughly -1% scheme-independent correction which is unrelated to the large-m_t limit and not captured through scale variations.

We next turn to SMEFT, focusing on cases where LO_K results involve corrections proportional to $\Delta r_t^{(4,1)}$. In Table 5.7 we show heavy-boson decay rates in SMEFT in the α scheme, listing the prefactors of Wilson coefficients appearing in $K_W^{(6,1,\alpha)}$. In this case, the NLO_t (but not LO_K) results use the large-m_t limit of Eq. (5.4.4) for scale variations of the Wilson coefficients. We see that also in SMEFT, the LO_K description improves perturbative convergence compared to pure fixed order, taking into account especially the dominant scheme-dependent corrections. This works best for W decay, where the central values of LO_K reproduce the NLO_t results by construction, and perturbative uncertainties are reduced compared to LO while still showing a good overlap with the NLO results. In Higgs decay, Wilson coefficients that receive significant scheme-independent corrections as shown Eq. (5.5.12), such as $C_{\substack{uW \\ 33}}$, display the biggest deviations from the NLO_t and NLO results at LO_K accuracy, although scale variations generally give a good indication of the size of the missing pieces. The case of Z decay is similar, although in contrast to Higgs and W decay the form of the LO amplitude in Eq. (5.5.15) implies that the shifts

of s_w in Eq. (5.6.9) also play a role. This latter effect is even more important in Z decay in the α_μ scheme; as shown in Table 5.8, LO_K accuracy largely takes into account the very large corrections to C_{HD} and C_{HWB} (as well as the more moderate but still significant corrections to $C_{\substack{He\\33}}$) seen in Table 5.5. The LO_K results for Higgs and W decay in the α_μ scheme, and for all decays in the LEP scheme, show similar levels of improvement as the cases discussed above – detailed tables can be found in Appendix A.5.

$W \to \tau\nu$	C_{HD}	C_{HWB}	$C^{(3)}_{\substack{Hq \\ 33}}$	$C_{\substack{Hu \\ 33}}$	$C^{(1)}_{\substack{Hq \\ 33}}$	$C_{\substack{uB \\ 33}}$	$C_{\substack{uW \\ 33}}$
NLO	$1.713^{+0.000}_{-0.011}$	$3.621^{+0.000}_{-0.011}$	$-0.079^{+0.018}_{-0.012}$	$-0.195^{+0.038}_{-0.000}$	$0.172^{+0.000}_{-0.033}$	$-0.072^{+0.008}_{-0.000}$	$-0.032^{+0.005}_{-0.000}$
NLO_t	$1.694^{+0.000}_{-0.009}$	$3.601^{+0.001}_{-0.008}$	$-0.067^{+0.019}_{-0.004}$	$-0.206^{+0.034}_{-0.000}$	$0.206^{+0.000}_{-0.030}$	$-0.073^{+0.005}_{-0.000}$	$-0.033^{+0.004}_{-0.000}$
LO	$1.742^{+0.120}_{-0.120}$	$3.733^{+0.131}_{-0.131}$	$0.000^{+0.008}_{-0.008}$	$0.000^{+0.182}_{-0.182}$	$0.000^{+0.189}_{-0.189}$	$0.000^{+0.066}_{-0.066}$	$0.000^{+0.059}_{-0.059}$
LO_K	$1.694^{+0.016}_{-0.033}$	$3.601^{+0.021}_{-0.031}$	$-0.067^{+0.011}_{-0.000}$	$-0.206^{+0.029}_{-0.000}$	$0.206^{+0.000}_{-0.032}$	$-0.073^{+0.007}_{-0.000}$	$-0.033^{+0.005}_{-0.000}$

$h \to b\bar{b}$	C_{HD}	C_{HWB}	$C^{(3)}_{\substack{Hq \\ 33}}$	$C_{\substack{Hu \\ 33}}$	$C^{(1)}_{\substack{Hq \\ 33}}$	$C_{\substack{uB \\ 33}}$	$C_{\substack{uW \\ 33}}$
NLO	$1.106^{+0.002}_{-0.018}$	$3.482^{+0.005}_{-0.016}$	$-0.116^{+0.025}_{-0.000}$	$-0.079^{+0.033}_{-0.000}$	$0.058^{+0.000}_{-0.034}$	$-0.030^{+0.008}_{-0.000}$	$-0.040^{+0.009}_{-0.000}$
NLO_t	$1.129^{+0.002}_{-0.012}$	$3.560^{+0.005}_{-0.011}$	$-0.105^{+0.030}_{-0.000}$	$-0.088^{+0.028}_{-0.000}$	$0.088^{+0.000}_{-0.027}$	$-0.031^{+0.006}_{-0.000}$	$-0.042^{+0.006}_{-0.000}$
LO	$1.242^{+0.089}_{-0.089}$	$3.733^{+0.128}_{-0.128}$	$0.000^{+0.112}_{-0.112}$	$0.000^{+0.183}_{-0.183}$	$0.000^{+0.188}_{-0.188}$	$0.000^{+0.066}_{-0.066}$	$0.000^{+0.094}_{-0.094}$
LO_K	$1.134^{+0.004}_{-0.021}$	$3.536^{+0.014}_{-0.024}$	$-0.068^{+0.125}_{-0.110}$	$-0.088^{+0.034}_{-0.000}$	$0.088^{+0.000}_{-0.027}$	$-0.031^{+0.007}_{-0.000}$	$0.004^{+0.036}_{-0.029}$

$Z \to \tau\tau$	C_{HD}	C_{HWB}	$C^{(3)}_{\substack{Hq \\ 33}}$	$C_{\substack{Hu \\ 33}}$	$C^{(1)}_{\substack{Hq \\ 33}}$	$C_{\substack{uB \\ 33}}$	$C_{\substack{uW \\ 33}}$
NLO	$1.406^{+0.002}_{-0.021}$	$3.867^{+0.003}_{-0.016}$	$-0.074^{+0.014}_{-0.001}$	$-0.143^{+0.031}_{-0.000}$	$0.117^{+0.000}_{-0.032}$	$-0.065^{+0.007}_{-0.000}$	$-0.016^{+0.008}_{-0.000}$
NLO_t	$1.419^{+0.002}_{-0.015}$	$3.876^{+0.004}_{-0.011}$	$-0.061^{+0.016}_{-0.002}$	$-0.156^{+0.027}_{-0.000}$	$0.156^{+0.000}_{-0.026}$	$-0.067^{+0.006}_{-0.000}$	$-0.019^{+0.007}_{-0.000}$
LO	$1.573^{+0.109}_{-0.109}$	$4.088^{+0.144}_{-0.144}$	$0.000^{+0.008}_{-0.008}$	$0.000^{+0.163}_{-0.163}$	$0.000^{+0.172}_{-0.172}$	$0.000^{+0.072}_{-0.072}$	$0.000^{+0.064}_{-0.064}$
LO_K	$1.426^{+0.000}_{-0.013}$	$3.870^{+0.030}_{-0.040}$	$-0.061^{+0.008}_{-0.000}$	$-0.173^{+0.050}_{-0.002}$	$0.173^{+0.000}_{-0.042}$	$-0.061^{+0.012}_{-0.000}$	$-0.023^{+0.007}_{-0.000}$

Table 5.7: The numerical prefactors of the Wilson coefficients in the α scheme appearing in $K_W^{(6,1,\alpha)}$ for various perturbative approximations. The tree-level decay rate as well as v_α^2 have been factored out and the results have been evaluated at the scale of the process. We show the results for W decay (top), h decay (center) and Z decay (bottom).

$Z \to \tau\tau$	$C^{(3)}_{\substack{Hl \\ jj}}$	$C^{(3)}_{\substack{lq \\ jj33}}$	$C_{\substack{ll \\ 1221}}$	$C^{(3)}_{\substack{Hq \\ 33}}$	C_{HD}	C_{HWB}	$C_{\substack{He \\ 33}}$
NLO	$-1.029^{+0.001}_{-0.000}$	$0.015^{+0.000}_{-0.001}$	$1.006^{+0.000}_{-0.000}$	$0.006^{+0.000}_{-0.002}$	$-0.289^{+0.009}_{-0.007}$	$0.258^{+0.003}_{-0.008}$	$-1.897^{+0.006}_{-0.002}$
NLO_t	$-1.021^{+0.001}_{-0.000}$	$0.015^{+0.004}_{-0.005}$	$1.006^{+0.002}_{-0.002}$	$0.006^{+0.000}_{-0.002}$	$-0.266^{+0.006}_{-0.005}$	$0.272^{+0.002}_{-0.002}$	$-1.864^{+0.005}_{-0.001}$
LO	$-1.000^{+0.015}_{-0.015}$	$0.000^{+0.026}_{-0.026}$	$1.000^{+0.004}_{-0.004}$	$0.000^{+0.001}_{-0.001}$	$-0.169^{+0.011}_{-0.011}$	$0.355^{+0.012}_{-0.012}$	$-1.764^{+0.046}_{-0.046}$
LO_K	$-1.021^{+0.012}_{-0.010}$	$0.015^{+0.000}_{-0.001}$	$1.006^{+0.004}_{-0.004}$	$0.006^{+0.001}_{-0.000}$	$-0.260^{+0.017}_{-0.017}$	$0.267^{+0.009}_{-0.009}$	$-1.838^{+0.048}_{-0.048}$

Table 5.8: The numerical prefactors of the Z decay SMEFT Wilson coefficients in the α_μ scheme appearing leading to dominant corrections at various perturbative approximations. The tree-level decay rate as well as v_μ^2 have been factored out and the results have been evaluated at the scale of the process.

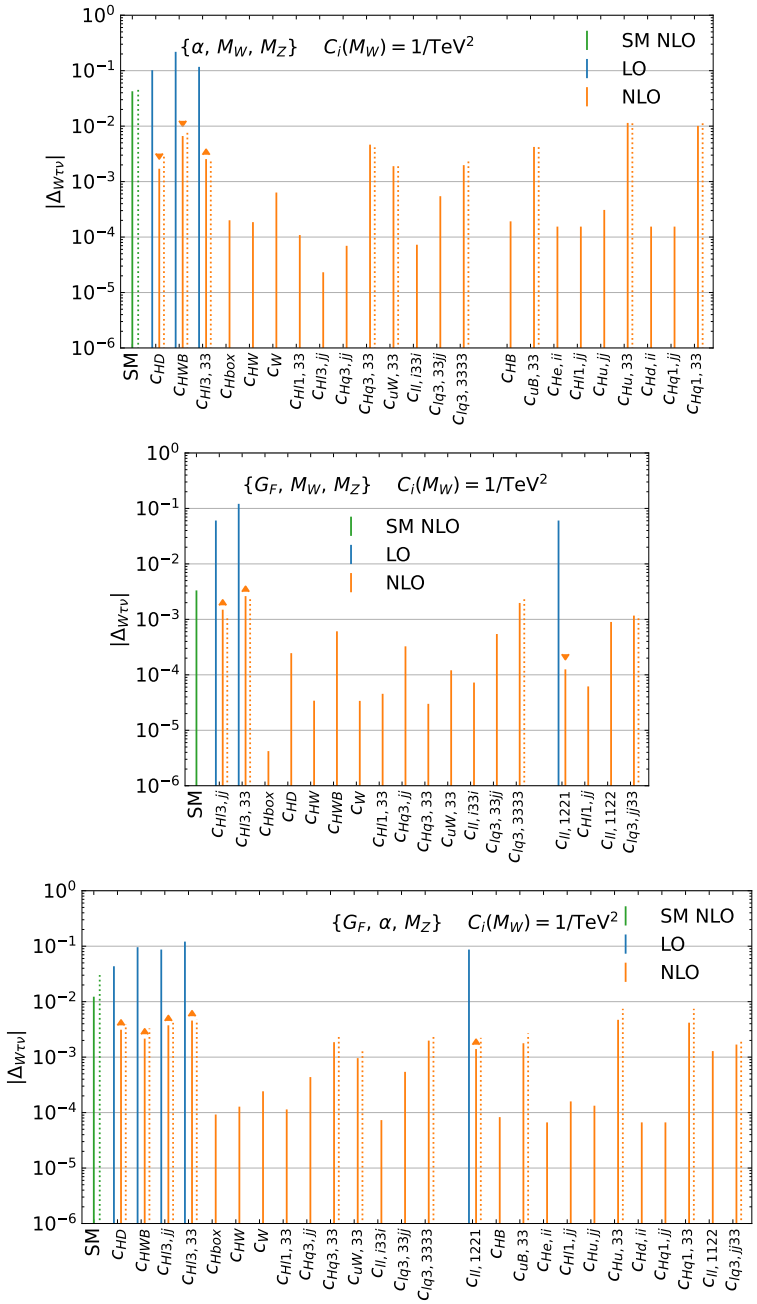

Figure 5.4: LO and NLO corrections $\Delta^{s(i,j)}_{W\tau\nu}$, as defined in Eq. (5.5.2), for the decay $W \to \tau\nu$ in the three schemes. Note that "NLO" in the legends only refers to the NLO corrections and that we write superscripts in the Wilson coefficient names as $C_{Hq3} \equiv C^{(3)}_{Hq}$. The flavour indices i and j run over values $j \in 1, 2$, and $i \in 1, 2, 3$. Operators which appear only through counterterms in a particular scheme are shown on the right. The dashed lines indicate the large-m_t limit of the NLO corrections. For operators appearing at LO the orange triangles indicate if the sign of the NLO correction is the same as (triangle pointing up) or different from (triangle pointing down) the sign of the LO contribution.

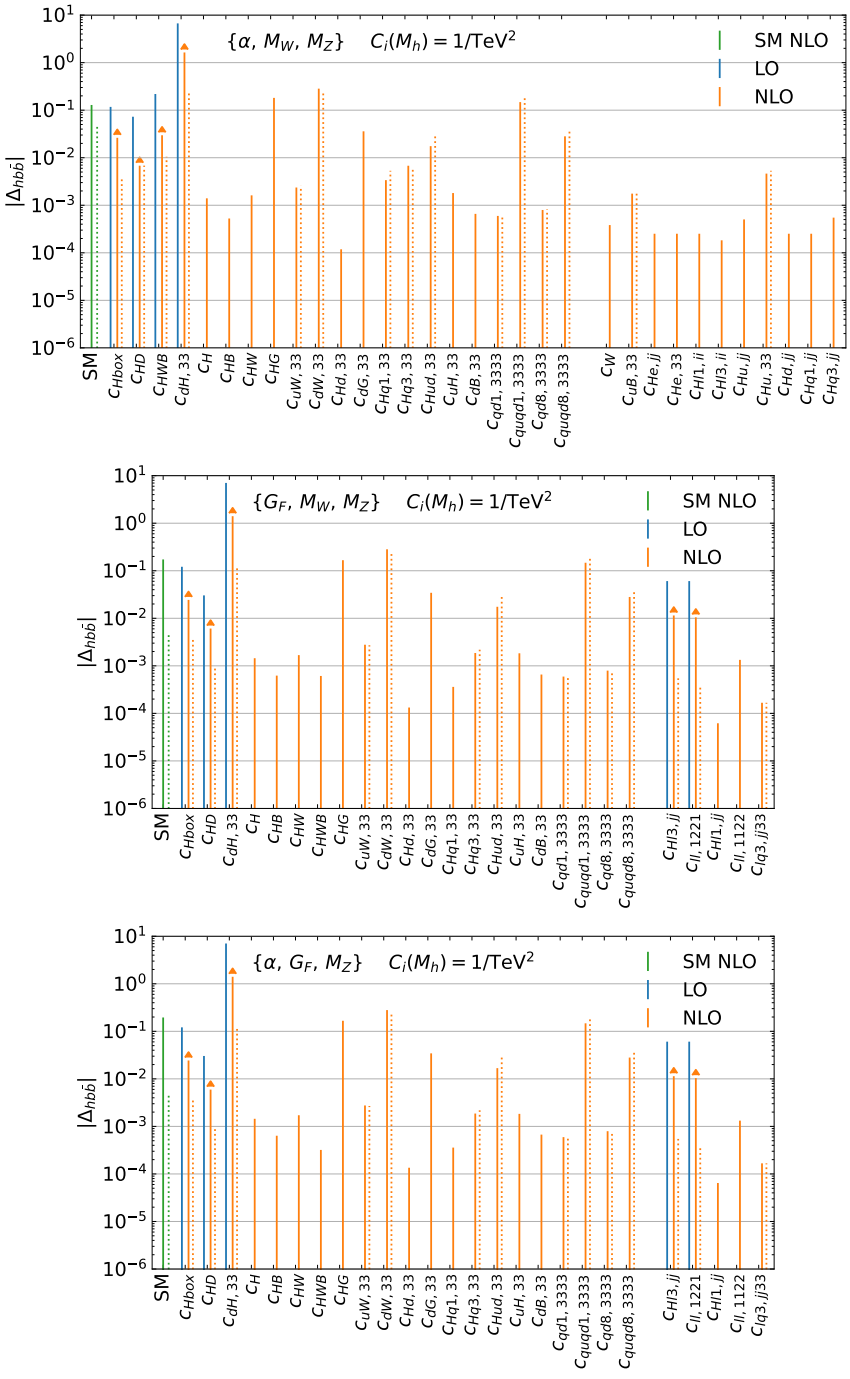

Figure 5.5: As in Figure 5.4, but for the decay $h \to b\bar{b}$.

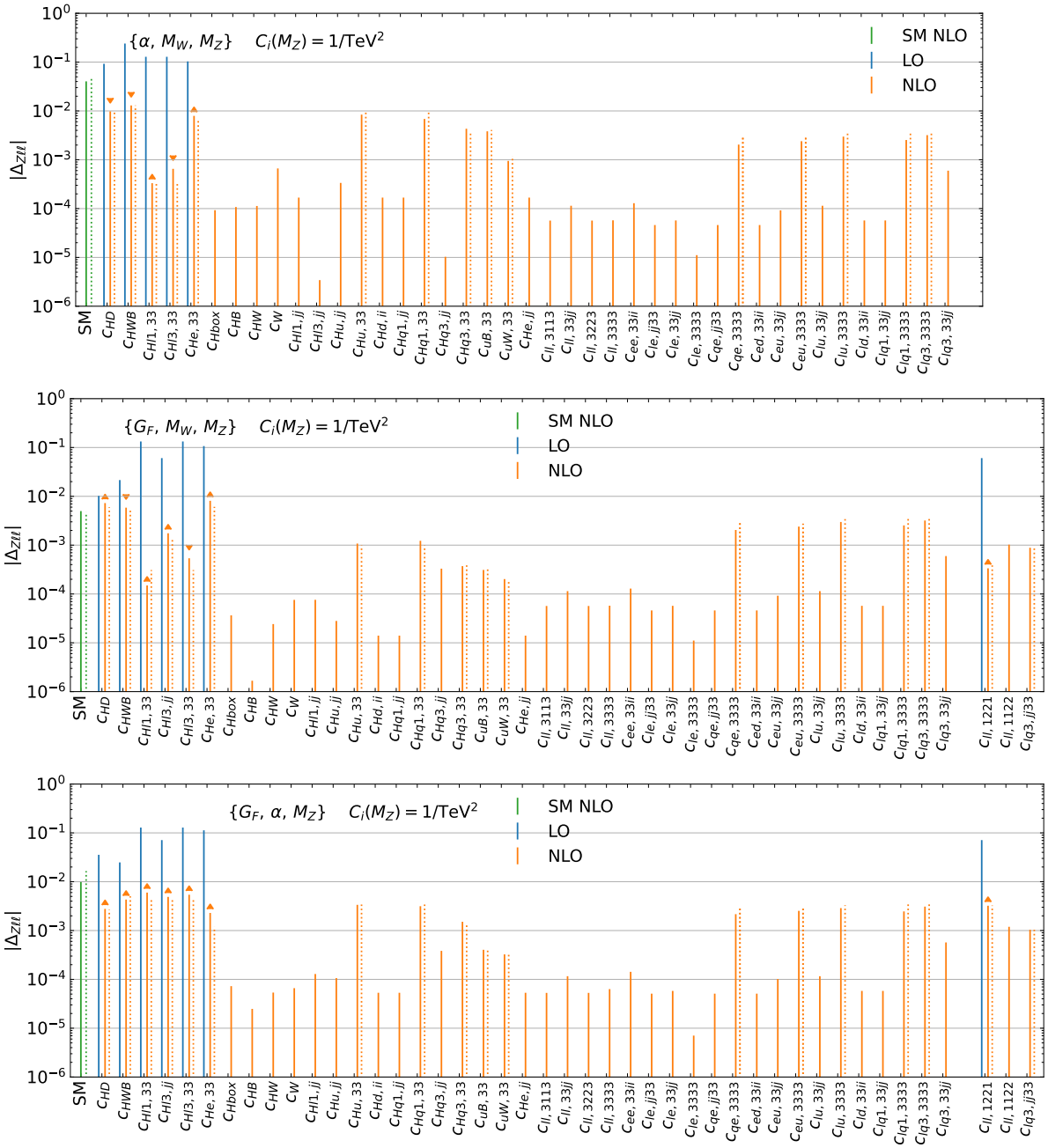

Figure 5.6: As in Figure 5.4, but for the decay $Z \to \tau\tau$.

Chapter 6

Introduction to the v_{σ}^{eff} Schemes in the SMEFT

In the previous sections, we mainly concerned ourselves with a review of three current EW input schemes that are used in the SMEFT. However, these three choices of input schemes are by no means the only choice, as a plethora of potential measurements are available to define an input scheme around.

In the SM, several studies have proposed EW input schemes which use the effective leptonic weak mixing angle $\sin\theta_{\text{eff}}^{\ell}$ as an input parameter [102–107]. The effective leptonic weak mixing angle has been measured with per-mille level precision at LEP [125], the Tevatron [126] and the LHC [127–130]. However, its numerical precision is (more than an order of magnitude) below that of other commonly used input values such as the mass of the W boson. This lack of precision potentially facilitated its exclusion from common use in the literature. However, future experiments, such as the P2 experiment at MESA [131], as well as the Møller [132] and SoLID [133,134] experiments at Jefferson Laboratory, will test this quantity with similar precision at lower energy scales. With potential improvements in precision of the measured value on the horizon, the arguments for using the weak mixing angle as an input in electroweak calculations is ever strengthening.

The aim of the next chapters introduce the $\{G_F, \sin\theta_{\text{eff}}^{\ell}, M_Z\}$ and $\{\alpha, \sin\theta_{\text{eff}}^{\ell}, M_Z\}$

input schemes which we collectively call the v_σ^{eff} schemes or individually the v_μ^{eff} and v_α^{eff} scheme respectively. We will provide a method of renormalisation in the one loop dimension-six SMEFT for the first time for these new input schemes.

6.1 Introduction to $\sin\theta_{\text{eff}}^{\ell}$

In order to implement the v_σ^{eff} schemes in a unified notation, we again write the tree-level Lagrangian in terms of $\{v_T, M_W, M_Z\}$ using Eq. (2.2.18). The renormalised Lagrangian is again obtained by interpreting the tree-level quantities as bare ones which are replaced by renormalised parameters plus counterterms in a particular scheme. For the inputs common to the two schemes, we relate the bare and renormalised parameters according to

$$\begin{aligned} M_{Z,0} &= M_Z\left(1+\Delta M_Z\right) , \\ s_{w,0} &= \sqrt{1-c_{w,0}^2} = \sin\theta_{\text{eff}}^{\ell}\left(1+\Delta s_{\text{eff}}\right) \equiv s_{\text{eff}}\left(1+\Delta s_{\text{eff}}\right) , \end{aligned} \tag{6.1.1}$$

where here, like previously, we indicate bare parameters with a subscript 0, and $c_{w,0} = M_{W,0}/M_{Z,0}$. The quantities ΔM_Z and Δs_{eff} appearing on the right-hand side of the above equations are counterterms, which are calculated in a SMEFT expansion in loops and operator dimension, including tadpoles in the FJ tadpole scheme [26].

It will often be convenient to work with the quantity

$$M_W^{\text{eff}} \equiv c_{\text{eff}} M_Z , \quad c_{\text{eff}} = \sqrt{1-s_{\text{eff}}^2} . \tag{6.1.2}$$

The relation between M_W^{eff} and the bare mass can be derived using Eq. (6.1.1). Writing

$$M_{W,0} = M_W^{\text{eff}}\left(1+\Delta M_W^{\text{eff}}\right) , \tag{6.1.3}$$

one finds

$$\Delta M_W^{\text{eff}} = \Delta M_Z - \frac{s_{\text{eff}}^2}{c_{\text{eff}}^2}\left[\Delta s_{\text{eff}} + \Delta M_Z \Delta s_{\text{eff}} + \frac{1}{2c_{\text{eff}}^2}\left(\Delta s_{\text{eff}}\right)^2\right] + \dots , \tag{6.1.4}$$

where the ... indicates terms not needed to NLO in the dimension-6 SMEFT expansion.

In addition to the counterterms for $s_{\rm eff}$ and M_Z, we also need those for v_T. In the $v_\mu^{\rm eff}$ scheme, one uses

$$\frac{1}{v_{T,0}^2} = \frac{1}{v_\mu^2}\left(1 - \Delta v_\mu^{\rm eff}\right), \tag{6.1.5}$$

while in the $v_\alpha^{\rm eff}$ scheme one has instead

$$\frac{1}{v_{T,0}^2} = \frac{1}{v_{\rm eff}^2}\left(1 - \Delta v_\alpha^{\rm eff}\right), \tag{6.1.6}$$

where we have defined

$$v_\mu \equiv \left(\sqrt{2}G_F\right)^{-\frac{1}{2}}, \qquad v_\alpha^{\rm eff} \equiv v_{\rm eff} \equiv \frac{2M_W^{\rm eff}s_{\rm eff}}{\sqrt{4\pi\alpha}}. \tag{6.1.7}$$

In the following two sections, we discuss renormalisation in the $v_\sigma^{\rm eff}$ schemes to NLO in SMEFT.

6.2 The $v_\mu^{\rm eff}$ Scheme

We start by giving results for the SMEFT expansion of the counterterms needed for renormalisation in the $v_\mu^{\rm eff}$ scheme, structuring the discussion in such a way that most results in the $v_\alpha^{\rm eff}$ scheme can be obtained by a simple set of substitutions.

We begin with the determination of the counterterm $\Delta s_{\rm eff}$. To this end, consider the amplitude for $Z \to \ell\ell$ decay, where $\ell \equiv \ell^i \in \{e, \mu, \tau\}$. We can write the bare amplitude to NLO in SMEFT in the form

$$\mathcal{A}_0(Z \to \ell\ell) = \mathcal{N}_0\left[\mathcal{A}_{L,0}^\ell S_L + \mathcal{A}_{R,0}^\ell S_R\right] + \dots, \tag{6.2.1}$$

where we have introduced the spinor structures

$$S_L = \left[\bar{u}(p_{\ell^-})\gamma^\nu P_L v(p_{\ell^+})\right]\epsilon_\nu^*(p_Z), \quad S_R = \left[\bar{u}(p_{\ell^-})\gamma^\nu P_R v(p_{\ell^+})\right]\epsilon_\nu^*(p_Z), \tag{6.2.2}$$

with $P_L = (1-\gamma_5)/2$ and $P_R = (1+\gamma_5)/2$. The ellipsis in Eq. (6.2.1) refers to spinor structures appearing beyond LO in the SMEFT expansion, which do not interfere with those above in the limit of vanishing lepton masses, and the overall factor $\mathcal{N}_0$ is defined by

$$\mathcal{N}_0 = \frac{M_{Z,0}}{v_{T,0}} \left(1 - \frac{v_{T,0}^2}{4} C_{HD,0}\right) \left(1 + \delta_{\text{QED}}\right) , \tag{6.2.3}$$

where δ_{QED} refers to QED corrections.

We can write the SMEFT expansion of the bare amplitudes as

$$\mathcal{A}^{\ell}_{L/R,0} = \mathcal{A}^{(4,0)}_{L/R,0} + v_{T,0}^2 \mathcal{A}^{\ell(6,0)}_{L/R,0} + \frac{1}{v_{T,0}^2} \mathcal{A}^{(4,1)}_{L/R,0} + \mathcal{A}^{\ell(6,1)}_{L/R,0} , \tag{6.2.4}$$

where the superscript (i,j) labels the operator dimension i contribution to the j-loop diagram, and we have pulled out explicit factors of $v_{T,0}$ such that the coefficients $\mathcal{A}^{(i,j)}$ do not depend on $v_{T,0}$.[1] The notation makes clear that the dimension-6 amplitudes depend on the lepton species ℓ while those in the SM do not.

The tree-level SM amplitudes read

$$\mathcal{A}^{(4,0)}_L = -1 + 2s_{w,0}^2 \equiv -c_{2w,0}, \quad \mathcal{A}^{(4,0)}_R = 2s_{w,0}^2 , \tag{6.2.5}$$

while in SMEFT

$$\mathcal{A}^{\ell(6,0)}_{L/R} = G^{(6,0)} + g^{\ell(6,0)}_{L/R} , \tag{6.2.6}$$

where the explicit results for decay into lepton species ℓ^i are

$$\begin{aligned} G^{(6,0)} &= -c_{w,0}^2 C_{HD} - 2c_{w,0}s_{w,0} C_{HWB} , \\ g_L^{\ell(6,0)} &= -C^{(1)}_{\substack{Hl \\ ii}} - C^{(3)}_{\substack{Hl \\ ii}} , \\ g_R^{\ell(6,0)} &= -C_{\substack{He \\ ii}} . \end{aligned} \tag{6.2.7}$$

[1] An implicit dependence on v_T in the $(6,1)$ coefficients occurs through the Class-1 coefficient C_W.

Consider now the definition of the effective weak mixing angle

$$\sin^2\theta_{\rm eff}^\ell = -\frac{1}{2}\,\mathrm{Re}\left(\frac{G_R^\ell(M_Z^2)}{G_L^\ell(M_Z^2)-G_R^\ell(M_Z^2)}\right), \tag{6.2.8}$$

where the $G_{L,R}^\ell$ are experimentally measured form factors at $q^2=M_Z^2$ [125–130]. The counterterm $\Delta s_{\rm eff}$ in Eq. (6.1.1) is determined to all orders in the SMEFT expansion through the renormalisation condition

$$\sin^2\theta_{\rm eff}^\ell = s_{\rm eff}^2\,. \tag{6.2.9}$$

To implement this renormalisation condition order by order in SMEFT, we first substitute the $G_L^\ell(G_R^\ell)$ in eq. (6.2.8) with the coefficients of $S_L(S_R)$ in Eq. (6.2.1), and replace the bare quantities with renormalised ones plus associated counterterms. We write the SMEFT expansions of $\Delta s_{\rm eff}$ and $\Delta v_\mu^{\rm eff}$ in the $v_\mu^{\rm eff}$ scheme as

$$\begin{aligned}\Delta s_{\rm eff} &= v_\mu^2\Delta s_{\rm eff}^{(6,0)} + \frac{1}{v_\mu^2}\Delta s_{\rm eff}^{(4,1)} + \Delta s_{\rm eff}^{(6,1,\mu)}\,,\\ \Delta v_\mu^{\rm eff} &= v_\mu^2\Delta v_\mu^{\rm eff(6,0)} + \frac{1}{v_\mu^2}\Delta v_\mu^{\rm eff(4,1)} + \Delta v_\mu^{\rm eff(6,1)}.\end{aligned} \tag{6.2.10}$$

The superscripts $(6,0)$ and $(4,1)$ have the same meaning as in Eq. (6.2.4), while the coefficient $\Delta s_{\rm eff}^{(6,1,\mu)}$ contains an extra superscript μ to indicate that v_T has been renormalised as in Eq. (6.1.5). Isolating the dependence on $\Delta v_\mu^{\rm eff}$ allows us to write

$$\Delta s_{\rm eff}^{(6,1,\mu)} = \Delta s_{\rm eff}^{(6,1)} - \Delta s_{\rm eff}^{(4,1)}\Delta v_\mu^{\rm eff(6,0)} + \Delta s_{\rm eff}^{(6,0)}\Delta v_\mu^{\rm eff(4,1)}\,, \tag{6.2.11}$$

where the coefficient $\Delta s_{\rm eff}^{(6,1)}$ does not depend on the renormalisation scheme for v_T.

The construction of renormalised $Z\to\ell\ell$ decay amplitudes also requires the on-shell wavefunction renormalisation factors of the external Z-boson and lepton fields. For the lepton fields, we can write the SMEFT expansion of the wavefunction renormalisation factors as

$$\begin{aligned}\ell_{L/R,0} &= \left[1+\frac{1}{2v_{T,0}^2}\Delta Z_{L/R,0}^{\ell(4,1)} + \frac{1}{2}\Delta Z_{L/R,0}^{\ell(6,1)}\right]\ell_{L/R}\\ &= \left[1+\frac{1}{2v_\mu^2}\Delta Z_{L/R}^{\ell(4,1)} + \frac{1}{2}\left(\Delta Z_{L/R}^{\ell(6,1)} - \Delta v_\mu^{(6,0)}\Delta Z_{L/R}^{\ell(4,1)}\right)\right]\ell_{L/R}\,.\end{aligned} \tag{6.2.12}$$

In the first line all terms are expressed in terms of the bare parameters $v_{T,0}, s_{w,0}$, while in the second renormalised parameters are used. The notation is such that

$$\begin{aligned}\Delta Z_{L/R}^{\ell(4,1)} &= \Delta Z_{L/R,0}^{\ell(4,1)}\Big|_{s_{w,0}\to s_{\text{eff}}}\,,\\ \Delta Z_{L/R}^{\ell(6,1)} &= \Delta s_{\text{eff}}^{(6,0)} s_{\text{eff}}\frac{\partial}{\partial s_{\text{eff}}}\Delta Z_{L/R}^{\ell(4,1)} + \Delta Z_{L/R,0}^{\ell(6,1)}\Big|_{s_{w,0}\to s_{\text{eff}}}\,,\end{aligned} \tag{6.2.13}$$

where the derivative in the SMEFT counterterm arises from replacing the implicit dependence on $s_{w,0}$ in the SM counterterm $\Delta Z_{L/R,0}^{\ell(4,1)}$ with the right-hand side of Eq. (6.2.10) and performing a SMEFT expansion. We emphasise that the $\Delta Z_{L/R}^{\ell}$ do *not* include QED corrections, which are instead contained in the factor δ_{QED} in Eq. (6.2.3). Wavefunction renormalisation graphs related to the Z-boson two-point function can be absorbed into the factor $\mathcal{N}_0$ in Eq. (6.2.1). Since $\mathcal{N}_0$ drops out of the ratio in Eq. (6.2.8) we do not discuss these two terms further. On the other hand, contributions from the $Z\gamma$ two-point function, where γ denotes the photon, are included in the definition of $\mathcal{A}_{L/R,0}^{\ell}$.

Performing a tree-level SMEFT expansion on Eq. (6.2.8) using the above equations yields

$$\begin{aligned}\Delta s_{\text{eff}}^{(6,0)} &= -\frac{1}{4s_{\text{eff}}^2}\left[G^{(6,0)} + 2s_{\text{eff}}^2 g_L^{\ell(6,0)} + c_{2\text{eff}} g_R^{\ell(6,0)}\right]\\ &= \frac{1}{4s_{\text{eff}}^2}\left[c_{\text{eff}}^2 C_{HD} + 2c_{\text{eff}}s_{\text{eff}}C_{HWB} + 2s_{\text{eff}}^2\left(C_{\substack{Hl\\ii}}^{(3)} + C_{\substack{Hl\\ii}}^{(1)}\right) + c_{2\text{eff}}C_{\substack{He\\ii}}\right]\,,\end{aligned} \tag{6.2.14}$$

while the one-loop result in the SM is

$$\Delta s_{\text{eff}}^{(4,1)} = -\frac{1}{2}\,\text{Re}\left[\mathcal{A}_{L,0}^{(4,1)} + \frac{c_{2\text{eff}}}{2s_{\text{eff}}^2}\mathcal{A}_{R,0}^{(4,1)} + c_{2\text{eff}}\left(\Delta Z_R^{\ell(4,1)} - \Delta Z_L^{\ell(4,1)}\right)\right]\,. \tag{6.2.15}$$

The part of the one-loop SMEFT result which is independent of the renormalisation scheme for v_T is

$$\begin{aligned}\Delta s_{\text{eff}}^{(6,1)} = &-\frac{1}{2}\,\text{Re}\left\{\mathcal{A}_{L,0}^{(6,1)} + \mathcal{A}_L^{(6,0)}\Delta Z_L^{\ell(4,1)} + \frac{c_{2\text{eff}}}{2s_{\text{eff}}^2}\left(\mathcal{A}_{R,0}^{(6,1)} + \mathcal{A}_R^{(6,0)}\Delta Z_R^{\ell(4,1)}\right)\right.\\ &\left. + c_{2\text{eff}}\left(\Delta Z_{R,0}^{\ell(6,1)} - \Delta Z_{L,0}^{\ell(6,1)}\right)\right\} + \frac{1}{2\epsilon}v_\mu^2\Delta\dot{s}_{\text{eff}}^{(6,0)}\end{aligned}$$

$$
\begin{aligned}
&- \Delta s_{\rm eff}^{(4,1)} \left(\Delta s_{\rm eff}^{(6,0)} + \frac{1}{2} C_{HD} - \frac{c_{2\rm eff}}{2 c_{\rm eff} s_{\rm eff}} C_{HWB} \right) \\
&+ \Delta s_{\rm eff}^{(6,0)} \left[s_{\rm eff} \frac{\partial}{\partial s_{\rm eff}} \Delta s_{\rm eff}^{(4,1)} - \frac{1}{2 s_{\rm eff}^2} \mathcal{A}_{R,0}^{(4,1)} - \Delta Z_R^{\ell(4,1)} \right] ,
\end{aligned} \tag{6.2.16}
$$

where we have defined

$$
c_{2\rm eff} = 1 - 2 s_{\rm eff}^2 \, . \tag{6.2.17}
$$

A couple of comments are in order concerning the form of this counterterm. First, the quantity $\Delta \dot{s}_{\rm eff}^{(6,0)}$ is obtained from $\Delta s_{\rm eff}^{(6,0)}$ through the replacement $C_i \to \dot{C}_i$, where $\dot{C}_i \equiv dC_i/d\ln\mu$; the term involving this quantity arises from $\overline{\rm MS}$ renormalisation of the Wilson coefficients in $d = 4 - 2\epsilon$ dimensions, and the $\dot{C}_i$ were calculated at one loop in [42, 45, 46].[1] Second, the final two lines are related to using Eq. (6.2.10) in the lower-order amplitudes and then performing the SMEFT expansion.

To evaluate the full NLO SMEFT result $\Delta s_{\rm eff}^{(6,1,\mu)}$ in Eq. (6.2.11) requires also the counterterm $\Delta v_\mu^{\rm eff}$. This counterterm, including tadpoles and without flavour assumptions, was determined at NLO in SMEFT in the α_μ scheme and given in Section 4.2. Their relation with the present work is

$$
\begin{aligned}
\Delta v_\mu^{\rm eff(6,0)} &= \Delta v_\mu^{(6,0)} = C_{\substack{Hl \\ 11}}^{(3)} + C_{\substack{Hl \\ 22}}^{(3)} - C_{\substack{ll \\ 1221}} \, , \\
\Delta v_\mu^{\rm eff(4,1)} &= \Delta v_\mu^{(4,1)} \Big|_{M_W \to M_W^{\rm eff}} \, , \\
\Delta v_\mu^{\rm eff(6,1)} &= \Delta s_{\rm eff}^{(6,0)} s_{\rm eff} \frac{\partial}{\partial s_{\rm eff}} \Delta v_\mu^{\rm eff(4,1)} + \Delta v_\mu^{(6,1)} \Big|_{M_W \to M_W^{\rm eff}} \, ,
\end{aligned} \tag{6.2.18}
$$

where to obtain the above results we have implicitly reexpressed the on-shell s_w in terms of $s_{\rm eff}$.

It will be useful later on to have an expression for the large-m_t limit of the loop corrections to the counterterm $\Delta s_{\rm eff}$. As a reminder, the large-m_t limit of a given quantity means the approximation where only terms proportional to positive powers of the top-quark mass m_t in the limit $m_t \to \infty$ are kept. In the SM, top-quark loops

[1] The $\dot{C}_i$ typically depend on a large number of Wilson coefficients, so again we mention the convenient electronic implementation in `DsixTools` [47, 120]. As they are one-loop corrections they thus scale as $1/v_\mu^2$ and so the counterterm is independent of v_μ.

contribute to $\Delta s_{\rm eff}^{(4,1)}$ in Eq. (6.2.15) only through the $Z\gamma$-mixing contribution to the bare amplitudes $\mathcal{A}_{L/R,0}^{(4,1)}$. It is easy to show, however, that this two-point function vanishes in the large-m_t limit, so

$$\Delta s_{{\rm eff},t}^{(4,1)} = 0\,, \tag{6.2.19}$$

where here and below the subscript t refers to the large-m_t limit of a given quantity. In SMEFT, there are three contributions in the large-m_t limit, which arise from $Z\gamma$ mixing, top-loop corrections from four-fermion operators, and a scheme-dependent correction proportional to $\Delta v_{\mu,t}^{(4,1)}$. The result can be written in the form

$$\Delta s_{{\rm eff},t}^{(6,1,\mu)} = \Delta s_{{\rm eff},t}^{Z\gamma(6,1)} + \Delta s_{{\rm eff},t}^{4f(6,1)} + \Delta s_{\rm eff}^{(6,0)} \Delta v_{\mu,t}^{{\rm eff}(4,1,\mu)} + \dots\,, \tag{6.2.20}$$

where the $\dots$ refers to divergent and tadpole contributions, which drop out of physical observables. An explicit calculation yields

$$\begin{aligned}
\Delta s_{{\rm eff},t}^{Z\gamma(6,1)} &= \frac{\sqrt{2} c_{\rm eff}}{3 s_{\rm eff}} \frac{M_Z}{m_t} \Delta\rho_t^{(4,1)} \left[c_{\rm eff} C_{\substack{uB \\ 33}} \left(-3 + 16 s_{\rm eff}^2\right) + s_{\rm eff} C_{\substack{uW \\ 33}} \left(-11 + 16 s_{\rm eff}^2\right) \right] \ln\left(\frac{\mu^2}{m_t^2}\right)\,, \\
\Delta s_{{\rm eff},t}^{4f(6,1)} &= \Delta\rho_t^{(4,1)} \left[C^{(3)}_{\substack{lq \\ ii33}} - C^{(1)}_{\substack{lq \\ ii33}} + C_{\substack{lu \\ ii33}} + \frac{c_{2{\rm eff}}}{2 s_{\rm eff}^2} \left(C_{\substack{eu \\ ii33}} - C_{\substack{qe \\ 33ii}} \right) \right] \ln\left(\frac{\mu^2}{m_t^2}\right)\,, \\
\Delta v_{\mu,t}^{{\rm eff}(4,1)} &= -\Delta\rho_t^{(4,1)} \left[1 + 2 \ln\left(\frac{\mu^2}{m_t^2}\right) \right]\,,
\end{aligned} \tag{6.2.21}$$

where, as above, we omitted divergent and tadpole contributions, and quoted the results in units of

$$\Delta\rho_t^{(4,1)} \equiv \frac{3}{16\pi^2} m_t^2\,. \tag{6.2.22}$$

6.3 The $v_\alpha^{\rm eff}$ Scheme

The $v_\alpha^{\rm eff}$ scheme differs from the $v_\mu^{\rm eff}$ scheme through the renormalisation of v_T, which is performed as in Eq. (6.1.6). The SMEFT expansion coefficients of that counterterm, as well as those of $\Delta s_{\rm eff}$ in this scheme, are defined as in Eq. (6.2.10) after the replacement $\mu \to \alpha$.

In order to calculate the expansion coefficients of $\Delta v_\alpha^{\rm eff}$, we will need those for M_Z

and electric charge renormalisation. We define these in the v_α^{eff} scheme as

$$\begin{aligned} M_{Z,0} &= M_Z \left(1 + \frac{1}{v_{\text{eff}}^2}\Delta M_Z^{(4,1)} + \Delta M_Z^{(6,1)} - \Delta v_\alpha^{\text{eff}(6,0)} \Delta M_Z^{(4,1)}\right) , \\ e_0 &= e \left(1 + \frac{1}{v_{\text{eff}}^2}\Delta e^{(4,1)} + \Delta e^{(6,1)} - \Delta v_\alpha^{\text{eff}(6,0)} \Delta e^{(4,1)}\right) , \end{aligned} \tag{6.3.1}$$

where the coefficients with superscript $(6,1)$ are calculated as in Eq. (4.1.3) from two point functions whilst replacing the implicit dependence on $s_{w,0}$ in the SM counterterm as in Eq. (6.2.13). It will also be useful to work with expansion coefficients of the derived counterterm ΔM_W^{eff}. We define these coefficients as

$$M_{W,0} = M_W^{\text{eff}} \left[1 + v_{\text{eff}}^2 \Delta M_W^{\text{eff}(6,0)} + \frac{1}{v_{\text{eff}}^2}\Delta M_W^{\text{eff}(4,1)} + \Delta M_W^{\text{eff}(6,1,\alpha)}\right] . \tag{6.3.2}$$

Performing a SMEFT expansion on Eq. (6.1.4) leads to

$$\begin{aligned} \Delta M_W^{\text{eff}(6,0)} &= -\frac{s_{\text{eff}}^2}{c_{\text{eff}}^2}\Delta s_{\text{eff}}^{(6,0)} , \\ \Delta M_W^{\text{eff}(4,1)} &= \Delta M_Z^{(4,1)} - \frac{s_{\text{eff}}^2}{c_{\text{eff}}^2}\Delta s_{\text{eff}}^{(4,1)} , \\ \Delta M_W^{\text{eff}(6,1,\alpha)} &= \Delta M_W^{\text{eff}(6,1)} - \Delta M_W^{\text{eff}(4,1)} \Delta v_\alpha^{\text{eff}(6,0)} + \Delta M_W^{\text{eff}(6,0)} \Delta v_\alpha^{\text{eff}(4,1)} , \end{aligned} \tag{6.3.3}$$

where

$$\Delta M_W^{\text{eff}(6,1)} = \Delta M_Z^{(6,1)} - \frac{s_{\text{eff}}^2}{c_{\text{eff}}^2}\left[\Delta s_{\text{eff}}^{(6,1)} + \Delta s_{\text{eff}}^{(6,0)} \Delta M_Z^{(4,1)} + \frac{1}{c_{\text{eff}}^2}\Delta s_{\text{eff}}^{(6,0)} \Delta s_{\text{eff}}^{(4,1)}\right] . \tag{6.3.4}$$

With this notation at hand, we can present a compact result for the expansion coefficients of $\Delta v_\alpha^{\text{eff}}$. They read

$$\begin{aligned} \Delta v_\alpha^{\text{eff}(6,0)} &= \Delta v_\alpha^{(6,0)} - \frac{2c_{2\text{eff}}}{s_{\text{eff}}^2}\Delta M_W^{\text{eff}(6,0)} , \\ \Delta v_\alpha^{\text{eff}(4,1)} &= 2\left(\Delta M_W^{\text{eff}(4,1)} + \Delta s_{\text{eff}}^{(4,1)} - \Delta e^{(4,1)}\right) , \\ \Delta v_\alpha^{\text{eff}(6,1)} &= 2\left(\Delta M_W^{\text{eff}(6,1)} + \Delta s_{\text{eff}}^{(6,1)} - \Delta e^{(6,1)}\right) - \Delta v_\alpha^{\text{eff}(6,0)} \Delta v_\alpha^{\text{eff}(4,1)} \\ &\quad + \frac{2}{c_{\text{eff}} s_{\text{eff}}}\left[C_{HWB} + \frac{c_{\text{eff}}}{2s_{\text{eff}}} C_{HD}\right] \Delta s_{\text{eff}}^{(4,1)} \\ &\quad + \frac{2}{s_{\text{eff}}^2}\left[-s_{\text{eff}}^2 \Delta M_W^{\text{eff}(4,1)} + c_{\text{eff}}^2 \Delta s_{\text{eff}}^{(4,1)}\right] \Delta M_W^{\text{eff}(6,0)} \\ &\quad - v_{\text{eff}}^2 \frac{c_{\text{eff}}}{s_{\text{eff}}} \frac{1}{\epsilon}\left[\dot{C}_{HWB} + \frac{c_{\text{eff}}}{4s_{\text{eff}}} \dot{C}_{HD}\right] . \end{aligned} \tag{6.3.5}$$

In the above, we have the tree-level α-scheme result

$$\Delta v_\alpha^{(6,0)} = -2\frac{c_{\text{eff}}}{s_{\text{eff}}}\left[C_{HWB} + \frac{c_{\text{eff}}}{4s_{\text{eff}}}C_{HD}\right], \tag{6.3.6}$$

which leads to the following tree-level results in the v_α^{eff} scheme:

$$\Delta v_\alpha^{\text{eff}(6,0)} = -\frac{1}{2}C_{HD} - \frac{1}{c_{\text{eff}}s_{\text{eff}}}C_{HWB} - \frac{c_{2\text{eff}}}{c_{\text{eff}}^2}\left(g_L^{\ell(6,0)} + \frac{c_{2\text{eff}}}{2s_{\text{eff}}^2}g_R^{\ell(6,0)}\right). \tag{6.3.7}$$

One should note that unlike in Chapter 5, the QED coupling e from here on is given by the more conventional on-shell definition [10] as opposed to the $\overline{\text{MS}}$ definition of Chapters 4 and 5. This is done with the foresight of potential comparison with other results in the literature at the order of decay rate calculations and fits of Wilson coefficients. Even when discussing the α and LEP schemes from now on, we refer to their counterparts with this on-shell definition of the QED coupling.

It is simple to convert between these two schemes using the perturbative relation

$$\begin{aligned}\overline{\alpha}(\mu) &= \alpha(M_Z)\left[1 + \frac{\alpha(M_Z)}{\pi}\sum_{f\neq t}\frac{N_c^f}{3}Q_f^2\left(\frac{5}{3} + \ln\frac{\mu^2}{M_Z^2}\right)\right] \\ &= \alpha(M_Z)\left[1 + \frac{\alpha(M_Z)}{\pi}\left(\frac{100}{27} + \frac{20}{9}\ln\frac{\mu^2}{M_Z^2}\right)\right],\end{aligned} \tag{6.3.8}$$

where Q_f is the charge of the fermion and $N_c^f = 3$ ($N_c^f = 1$) for quarks (leptons).

6.3.1 Relation to the v_μ^{eff} scheme

In Section 4.2.1 we outlined a method to convert between the α and α_μ scheme or vice versa. Here we follow a similar structure to relate the v_μ^{eff} and v_α^{eff} schemes.

We again start with the useful quantity

$$\frac{v_{\text{eff}}^2}{v_\mu^2} \equiv 1 + \Delta r^{\text{eff}}. \tag{6.3.9}$$

The SMEFT expansion coefficients are the same whether v_μ or v_{eff} is used.

$$\Delta r^{\text{eff}} = v_{\text{eff}}^2\Delta r^{\text{eff}(6,0)} + \frac{1}{v_{\text{eff}}^2}\Delta r^{\text{eff}(4,1)} + \Delta r^{\text{eff}(6,1)}$$

$$= v_\mu^2 \Delta r^{\rm eff(6,0)} + \frac{1}{v_\mu^2}\Delta r^{\rm eff(4,1)} + \Delta r^{\rm eff(6,1)} \,. \tag{6.3.10}$$

The expansion coefficients are calculated similarly to those for M_W. The results are

$$\begin{aligned}
\Delta r^{\rm eff(6,0)} &= \Delta v_\mu^{\rm eff(6,0)} - \Delta v_\alpha^{\rm eff(6,0)} \,, \\
\Delta r^{\rm eff(4,1)} &= \Delta v_\mu^{\rm eff(4,1)} - \Delta v_\alpha^{\rm eff(4,1)} \\
\Delta r^{\rm eff(6,1)} &= \Delta v_\mu^{\rm eff(6,1)} - \Delta v_\alpha^{\rm eff(6,1)} + 2\Delta v_\mu^{\rm eff(4,1)} \Delta r^{\rm eff(6,0)} \,.
\end{aligned} \tag{6.3.11}$$

We do not write it, but relations between terms in a perturbative expansion of a decay rate between the two schemes are given by an equivalent relation to that of Eq. (4.2.27) where the logical replacement of the appropriate terms for those relevant for these two schemes has taken place.

In lieu of giving full analytic expressions as to not print long expressions, we write the results in the large-m_t limit in the form

$$\Delta r_t^{\rm eff(i,j)} = K_\alpha^{\rm eff(i,j)} - K_\mu^{\rm eff(i,j)} \,. \tag{6.3.12}$$

Results for the $K_\mu^{\rm eff}$ can be read off from Section 5.3 as they are identical to the K_μ given there, while the results for $K_\alpha^{\rm eff}$ are new. The one-loop result in the SM is

$$K_\sigma^{\rm eff(4,1)} = -\Delta\rho_t^{(4,1)} \delta_{\alpha\sigma} \,. \tag{6.3.13}$$

The SMEFT answer takes the form

$$\begin{aligned}
K_\sigma^{\rm eff(6,0)} &= -\Delta v_\sigma^{\rm eff(6,0)} \,, \\
K_\sigma^{\rm eff(6,1)} &= -\frac{1}{2} v_\sigma^2 \dot{K}_{\sigma,t}^{\rm eff(6,0)} \ln\frac{\mu^2}{m_t^2} + k_\sigma^{\rm eff(6,1)} \,.
\end{aligned} \tag{6.3.14}$$

One has, for the non-logarithmic pieces

$$\begin{aligned}
k_\mu^{\rm eff(6,1)} &= \Delta\rho_t^{(4,1)} \sum_{j=1,2} \left[C_{\substack{Hl \\ jj}}^{(3)} - C_{\substack{lq \\ jj33}}^{(3)} \right] , \\
k_\alpha^{\rm eff(6,1)} &= 2K_\alpha^{\rm eff(4,1)} \left(K_\alpha^{\rm eff(6,0)} + C_{\substack{Hq \\ 33}}^{(3)} \right) \,,
\end{aligned} \tag{6.3.15}$$

whereas the dependence on the renormalisation scale μ is governed by

$$v_\sigma^2 \dot{K}_{\mu,t}^{\text{eff}(6,0)} = -4\Delta\rho_t^{(4,1)} \sum_{j=1,2} \left[C_{\substack{Hl \\ jj}}^{(3)} - C_{\substack{lq \\ jj33}}^{(3)} \right],$$
$$v_\sigma^2 \dot{K}_{\alpha,t}^{\text{eff}(6,0)} = \frac{1}{2}\dot{C}_{HD,t} + \frac{1}{c_{\text{eff}}\, s_{\text{eff}}}\dot{C}_{HWB,t} + \frac{c_{2\text{eff}}}{c_{\text{eff}}^2}\left(\dot{g}_{L,t}^{\ell(6,0)} + \frac{c_{2\text{eff}}}{2s_{\text{eff}}^2}\dot{g}_{R,t}^{\ell(6,0)} \right). \tag{6.3.16}$$

All components needed to evaluate the latter result were given in Eq. (6.3.26). Although not exercised here, the previous form of the results alludes to a potential set of universal corrections to be defined synonymous with those in Section 5.6 but for the schemes in consideration here.

6.3.2 Relation to the α and α_μ schemes

Finally, to tie all schemes considered in this thesis together, the determination of relations between one of the v_σ^{eff} schemes and one of the three previous schemes is necessary. Doing so allows predictions in any one scheme to be related to another through a series of replacements, potentially in multiple steps.

We follow the same course as relating the α_μ and LEP schemes and obtain shifts of the W-boson mass which then relates the schemes using an on-shell (M_W) and effective (M_W^{eff}) W-boson mass.

We write the SMEFT expansion of M_W in the v_σ^{eff} scheme, where $\sigma \in \{\alpha, \mu\}$, as[1]

$$M_W = M_W^{\text{eff}} \left(1 + v_\sigma^2 \Delta_W^{\text{eff}(6,0)} + \frac{1}{v_\sigma^2}\Delta_W^{\text{eff}(4,1)} + \Delta_W^{\text{eff}(6,1,\sigma)} \right). \tag{6.3.17}$$

Identically to deriving the expansion of $\hat{M}_W$, a simple way to derive Δ_W^{eff} is to use the bare mass $M_{W,0}$ as an intermediary

$$M_{W,0} = M_W^{\text{eff}} \left(1 + \Delta M_W^{\text{eff}} \right) = M_W \left(1 + \Delta M_W \right). \tag{6.3.18}$$

After expressing the expansion coefficients of the on-shell counterterm ΔM_W in

[1] remembering that when $\sigma = \alpha$ we have the notation that $v_\sigma = v_\alpha^{\text{eff}} \equiv v_{\text{eff}}$

terms of M_W^{eff} following the notation of Eq. (6.2.13), one finds

$$\begin{aligned}
\Delta_W^{\text{eff}(6,0)} &= \Delta M_W^{\text{eff}(6,0)}\,, \\
\Delta_W^{\text{eff}(4,1)} &= \Delta M_W^{\text{eff}(4,1)} - \Delta M_W^{(4,1)}\,, \\
\Delta_W^{\text{eff}(6,1,\sigma)} &= \Delta_W^{\text{eff}(6,1)} - \Delta_W^{\text{eff}(4,1)}\Delta v_\sigma^{\text{eff}(6,0)} + \Delta_W^{\text{eff}(6,0)}\left(\Delta v_\sigma^{\text{eff}(4,1)} - 2\Delta M_W^{(4,1)}\right)\,,
\end{aligned} \tag{6.3.19}$$

with

$$\Delta_W^{\text{eff}(6,1)} = \Delta M_W^{\text{eff}(6,1)} - \Delta M_W^{(6,1)} + \Delta_W^{\text{eff}(6,0)}\Delta M_W^{(4,1)}\,. \tag{6.3.20}$$

In contrast to the counterterms themselves, the quantities Δ_W^{eff} are finite and tadpole free. As is now customary at this point, we study the large-m_t corrections to this quantity in the two schemes. To do so, we first note that

$$\begin{aligned}
\Delta s_{\text{eff},t}^{(4,1)} &= \Delta e_t^{(4,1)} = 0\,, \\
\Delta v_{\alpha,t}^{\text{eff}(4,1)} &= 2\Delta M_{W,t}^{\text{eff}(4,1)} = 2\Delta M_{Z,t}^{(4,1)}\,, \\
\Delta v_{\mu,t}^{\text{eff}(4,1)} &= 2\Delta M_{W,t}^{(4,1)}\,.
\end{aligned} \tag{6.3.21}$$

It follows that the SM result is

$$\Delta_{W,t}^{\text{eff}(4,1)} = \Delta M_{Z,t}^{(4,1)} - \Delta M_{W,t}^{(4,1)} = \frac{1}{2}\Delta\rho_t^{(4,1)}\,. \tag{6.3.22}$$

Moreover, the result in SMEFT can be written in the form

$$\Delta_W^{\text{eff}(6,1,\sigma)} = \Delta_{W,t}^{\text{eff}(6,1)} + \Delta_{W,t}^{\text{eff}(4,1)}\left(2\Delta_W^{\text{eff}(6,0)}\delta_{\sigma\alpha} - \Delta v_\sigma^{\text{eff}(6,0)}\right)\,, \tag{6.3.23}$$

where $\delta_{\sigma\alpha}$ is the Kronecker delta. An explicit calculation shows that

$$\Delta_{W,t}^{\text{eff}(6,1)} = 2\Delta_{W,t}^{\text{eff}(4,1)}\left[C_{\substack{Hq\\33}}^{(3)} - \frac{\sqrt{2}M_W^{\text{eff}}}{m_t}C_{\substack{uW\\33}} - \frac{1}{2}\Delta_W^{(6,0)}\right] - \dot{\Delta}_{W,t}^{\text{eff}(6,0)}\ln\frac{\mu}{m_t}\,, \tag{6.3.24}$$

where the logarithmic dependence is governed by

$$\dot{\Delta}_{W,t}^{\text{eff}(6,0)} = -\frac{1}{4}\dot{C}_{HD,t} - \frac{s_{\text{eff}}}{2c_{\text{eff}}}\dot{C}_{HWB,t} + \frac{s_{\text{eff}}^2}{2c_{\text{eff}}^2}\dot{g}_{L,t}^{\ell(6,0)} + \frac{c_{2\text{eff}}}{4c_{\text{eff}}^2}\dot{g}_{R,t}^{\ell(6,0)}\,, \tag{6.3.25}$$

with

$$\begin{aligned}
\dot{C}_{HD,t} &= 8\Delta\rho_t^{(4,1)}\left[C_{HD} + 2C^{(1)}_{\substack{Hq\\33}} - 2C_{\substack{Hu\\33}}\right], \\
\dot{C}_{HWB,t} &= 4\Delta\rho_t^{(4,1)}\left[C_{HWB} - \sqrt{2}\frac{M_Z}{m_t}\left(c_{\text{eff}}C_{\substack{uB\\33}} + \frac{5}{3}s_{\text{eff}}C_{\substack{uW\\33}}\right)\right], \\
\dot{g}^{\ell(6,0)}_{L,t} &= 4\Delta\rho_t^{(4,1)}\left[g_L^{\ell(6,0)} - C^{(1)}_{\substack{lq\\ii33}} + C^{(3)}_{\substack{lq\\ii33}} + C_{\substack{lu\\33ii}}\right], \\
\dot{g}^{\ell(6,0)}_{R,t} &= 4\Delta\rho_t^{(4,1)}\left[g_R^{\ell(6,0)} + C_{\substack{eu\\ii33}} - C_{\substack{qe\\33ii}}\right].
\end{aligned} \tag{6.3.26}$$

where the $g^{\ell(6,0)}_{L/R}$ are defined in Eq. (6.2.7).

The re-expression of the on-shell M_W in an α or α_μ scheme expression using Eq. (6.3.17) with $\sigma \in \{\alpha, \mu\}$ and expanding in SMEFT produces the result in the v_α^{eff} or v_μ^{eff} scheme, respectively. The expansion in SMEFT is equivalent to that of Eq. (4.3.9), after one replace the "hatted" quantities with the corresponding "eff" quantities.

Chapter 7

Numerical Analysis of the v_{σ}^{eff} schemes

With results of the previous chapters in hand, we now have the framework available to calculate electroweak processes to one loop in the SMEFT in five different input schemes.[2] In this chapter, we provide discussion of the attributes of the v_{α}^{eff} and v_{μ}^{eff} schemes. However, as opposed to the approach of Chapter 5 whereby a detailed breakdown of the schemes in question was undertaken, we focus more on comparison with the three commonly used schemes previously mentioned in this thesis, discussing all important attributes.

7.1 Numerical Values of Inputs

We begin this section on numerical analysis identically to the last, with the specification of the numerical values used for the inputs. For the analysis of the v_{α}^{eff} and v_{μ}^{eff} schemes we employ the use of the numerical values given in table 7.1. Comments about the precision of the values made in Section 5.1 are applicable again here. Values for the inputs of the α, α_{μ}, and LEP schemes used in this section for com-

[2] Potentially, one could argue eight different schemes if one counts double for each scheme involving the input α due to the choice of renormalising on-shell or in $\overline{\text{MS}}$.

m_t	172.9 GeV	v_μ	246.2 GeV
M_W	80.38 GeV	v_α^{eff}	246.5 GeV
M_Z	91.19 GeV	$(\sin\theta_{\text{eff}}^e)^2$	0.23166
m_H	125.1 GeV	$\alpha(M_Z)$	1/128.946

Table 7.1: Input parameters employed throughout this section. Note that v_α^{eff} is a derived parameter.

parison, can also be taken from table 7.1. These are identical to those specified in table 5.1 except the QED coupling as we use an on-shell definition here. A numerical value of the derived parameter v_α can be obtained by using its definition given in Eq. (4.1.1) and substituting in the numerical values. Again, numerical values are taken from [10].

One comment we make here is that the choice of a value for $\sin\theta_{\text{eff}}^\ell$ is somewhat problematic, especially in the SMEFT. Experimentally, $\sin^2\theta_{\text{eff}}^\ell$ is typically averaged over measurements involving electrons and muons. In SMEFT, using an average leads to some difficulties because it would require a combination of first and second-generation Wilson coefficients entering the counterterms, depending on the ratio of electron and muon data entering the combination. To avoid this issue, we use the most precise available measurement of $\sin\theta_{\text{eff}}^\ell$ from the couplings to electrons only, namely the ATLAS measurement with one central and one forward electron [128].

7.2 Number of Wilson coeffficients

The discussion of the number of Wilson coefficients appearing in each of the counterterms in the v_α^{eff} and v_μ^{eff} schemes follows mainly the same path as that of Section 5.2. The quantities Δe, ΔM_Z and Δv_μ were discussed in detail there, and so we do not repeat it here. That being said, a slight comment is needed as a few additional counterterms may be present. The expansion of each of the counterterms in the v_σ^{eff} will have an explicit dependence on v_σ^{eff}, and so there will be a direct contribution from $\Delta v_\sigma^{\text{eff}}$. As we have done many times before, we can write the counterterm for a

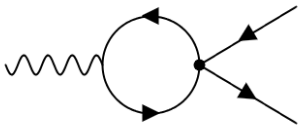

Figure 7.1: Representative Feynman diagrams contributing to the decay of a Z boson via a four fermion operator.

quantity X as

$$\begin{aligned} X_0 &= X\left(1+\frac{1}{v_\mu^2}\Delta X^{(4,1,\mu)}+\Delta X^{(6,1,\mu)}\right) \\ &= X\left(1+\frac{1}{v_\mu^2}\Delta X^{(4,1)}+\Delta X^{(6,1)}-\Delta v_\mu^{\text{eff}(6,0)}\Delta X^{(4,1)}\right), \end{aligned} \tag{7.2.1}$$

in the v_μ^{eff} scheme, and analogously for the v_α^{eff} scheme. Therefore, Wilson coefficients appearing in the quantities $\Delta v_\sigma^{\text{eff}(6,0)}$ will additionally appear, if not already so, in the set of Wilson coefficients for each counterterm.

The counterterm Δs_{eff} defined in a particular scheme, is a new quantity unique to these two schemes. Defined through Z decay, it contains numerous Wilson coefficient previously unseen in counterterms, the majority of which arise from four fermion operator insertions, such as in Figure 7.1. Overall, the following 62 coefficients appear

$$\begin{aligned} \Delta s_{\text{eff}}^{(6,1,\mu)} : \{&C_{HB}, C_{HD}C_{HW}, C_{HWB}, C_W, C_{\substack{uW\\33}}, C_{\substack{uB\\33}}, C_{\substack{Hd\\ii}}, C_{\substack{Hu\\ii}}, \\ &C_{\substack{He\\ii}}, C^{(1)}_{\substack{Hl\\ii}}, C^{(3)}_{\substack{Hl\\ii}}, C^{(1)}_{\substack{Hq\\ii}}, C^{(3)}_{\substack{Hq\\ii}}, C_{\substack{ee\\11ii}}, C_{\substack{eu\\11ii}}, C_{\substack{ld\\11ii}}, C_{\substack{lu\\11ii}}, \\ &C_{\substack{le\\11ii}}, C_{\substack{le\\ii11}}, C_{\substack{ll\\ii11}}, C_{\substack{ll\\1ii1}}, C^{(1)}_{\substack{lq\\11ii}}, C^{(3)}_{\substack{lq\\11ii}}, C_{\substack{qe\\ii11}}\}, \quad i=1,2,3, \end{aligned} \tag{7.2.2}$$

where one should take care as some Wilson coefficients appear twice (e.g. $C_{\substack{ll\\1111}}$) for compactness.

The large number of Wilson coefficients in this counterterm has a noticeable impact on the numbers appearing for any observable. To this end, we find it instructive here to look at the derived parameters (by proxy through looking at the finite quantities Δr, Δr^{eff}, $\hat{\Delta}\hat{M}_W$, and ΔM_W^{eff}).

Table 7.2 shows the number of Wilson coefficients entering the important quantities

	Δr		Δr^{eff}		$\hat{\Delta}_W$		Δ_W^{eff}	
	gen	$U(2)^2 \times U(3)^3$	gen	$U(2)^2 \times U(3)^3$	gen	$U(2)^2 \times U(3)^3$	gen	$U(2)^2 \times U(3)^3$
LO	5	4	7	6	5	4	5	5
NLO	33	21	64	34	33	21	63	34

Table 7.2: Number of Wilson coefficients appearing in the derived parameters of each scheme under general flavour assumptions and $U(2)^2 \times U(3)^3$. The LO row represents the (6,0) piece of the corresponding quantity, whereas NLO represents the (6,1) piece.

Δr, Δr^{eff}, $\hat{\Delta}\hat{M}_W$ and ΔM_W^{eff}. These quantities, through the use of the relevant equations to be outlined in Section 7.3.1, are the key ingredient to the simplest of the predictions in each scheme, the derived parameters.

It is seen that the quantities $\hat{\Delta}\hat{M}_W$ and Δr contain exactly the same number of Wilson coefficients, which is not surprising as they can be easily related to each other, as shown in Section 4.3. Both quantities are functions of the counterterms ΔM_W, ΔM_Z, Δe and Δv_μ, hence, will contain the combined set of all coefficient appearing in those counterterms.

More noticeably however is the large number of coefficients appearing in the "eff" quantities as compared to their equivalent counterparts for both the general flavour and $U(2)^2 \times U(3)^3$ assumptions. As mentioned, these are mainly due to additional four fermion operators arising from Z decay introduced through the counterterm to s_{eff}. As we would ideally keep the number of scheme dependant Wilson coefficients to a minimum, this is much an undesirable property of the v_μ^{eff} and v_α^{eff} schemes.

The pattern of predictions in the v_σ^{eff} schemes containing more Wilson coefficients continues to the more involved calculation of the heavy gauge boson decays. Table 7.3 shows the counting for such process at LO and NLO for a general flavour assumption and $U(2)^2 \times U(3)^3$.

For the general flavour assumption, there are no surprises in what is seen, there are many additional Wilson coefficients appearing in the v_μ^{eff} and v_α^{eff} schemes at NLO, with the exception being for the decay $Z \to ee$ where we have an overlap between the four fermion operators of the matrix element and those in Δs_{eff}.

		$\Gamma_{W\tau\nu}$		$\Gamma_{Z\tau\tau}$ (Γ_{Zee})		Total # unique WC	
		gen	$U(2)^2 \times U(3)^3$	gen	$U(2)^2 \times U(3)^3$	gen	$U(2)^2 \times U(3)^3$
v_μ^{eff}	LO	8	6	9 (6)	4	10	6
	NLO	69	34	93 (63)	33	93	34
v_α^{eff}	LO	6	5	7 (4)	4	8	5
	NLO	68	34	92 (63)	34	92	34
α_μ	LO	4	1	8 (7)	6	8	6
	NLO	25	14	67 (64)	34	67	34
α	LO	3	3	5 (5)	5	5	5
	NLO	35	22	63 (63)	34	63	34
LEP	LO	6	4	8 (7)	6	8	6
	NLO	39	22	67 (64)	34	67	34

Table 7.3: Number of Wilson coefficients appearing in heavy boson decay rates under general flavour assumptions and $U(2)^2 \times U(3)^3$. Note that assuming $U(2)^2 \times U(3)^3$ the number of operators appearing in $\Gamma_{Z\tau\tau}$ and Γ_{Zee} is the same and hence only one value is given.

Under the $U(2)^2 \times U(3)^3$ assumption as described in Section 3.2.1, a lot of flavour structure is removed. Consequently, the four fermion operators appearing in the $Z \to ee$ and $Z \to \tau\tau$ processes are now identical. An overlap between the Wilson coefficients in counterterms of s_{eff} and the matrix element for the decays to any charged lepton is observed, giving an identical count. For W decay additional Wilson coefficients remain in the v_μ^{eff} and v_α^{eff} schemes in contrast to the other three, although fewer than for the general flavour case, as Wilson coefficients involving right-handed particles are still introduced through the counterterms to s_{eff}.

In a full analysis of electroweak precision observables including gauge-boson decays to quarks and Z decay to neutrinos, the total number of Wilson coefficients that can appear is further increased through contributions from four-quark operators. For the $U(2)^2 \times U(3)^3$ assumption, the total number of operators appearing grows from 34 in the leptonic Z and W decays considered here to 56 in the full set of electroweak precision observables [96].

scheme	inputs
v_μ^{eff}	G_F, $\sin\theta_{\text{eff}}^\ell$, M_Z
v_α^{eff}	α, $\sin\theta_{\text{eff}}^\ell$, M_Z
α_μ	G_F, M_W, M_Z
α	α, M_W, M_Z
LEP	G_F, α, M_Z

Table 7.4: Nomenclature for the EW input schemes considered in this work.

		$\frac{M_W^s}{M_W}-1$	$\frac{\alpha^s}{\alpha}-1$	$\frac{G_F^s}{G_F}-1$	$\frac{\sin^2\theta_{\text{eff}}^{\ell,s}}{\sin^2\theta_{\text{eff}}^\ell}-1$
v_μ^{eff}	LO	-0.56%	0.21%	–	–
	NLO	0.05%	0.23%	–	–
v_α^{eff}	LO	-0.56%	–	-0.21%	–
	NLO	0.04%	–	-0.23%	–
α_μ	LO	–	-2.44%	–	-3.72%
	NLO	–	0.51%	–	0.34%
α	LO	–	–	2.50%	-3.72%
	NLO	–	–	-0.67%	0.45%
LEP	LO	-0.51%	–	–	-0.30%
	NLO	0.09%	–	–	-0.32%

Table 7.5: SM results for derived parameters in scheme s relative to the experimental values in table 7.1.

7.3 Numerical Analysis

In this section, we present a brief numerical analysis of the v_σ^{eff} schemes, covering derived input parameters in Section 7.3.1 before turning to heavy EW boson decays in Section 7.3.2. Like the numerical analysis of Chapter 5, we study the perturbative convergence associated with these schemes. Moreover, here we make qualitative and quantitative comparisons of the v_σ^{eff} schemes with the widely used α, α_μ, and LEP schemes. As a reminder, we put all inputs of the five schemes in table 7.4

7.3.1 Derived parameters

In each of the five input schemes in table 7.4, two parameters in the set $\{M_W, \alpha, G_F, \sin\theta_{\text{eff}}^\ell\}$ are derived parameters which can be calculated in a SMEFT expansion. For instance,

in the $v_\sigma^{\rm eff}$ schemes, the on-shell W-boson mass M_W is given by

$$M_W = M_W^{\rm eff}\left(1+\Delta_W^{\rm eff}\right) = M_W^{\rm eff}\left(1+v_\sigma^2\Delta_W^{\rm eff(6,0)}+\frac{1}{v_\sigma^2}\Delta_W^{\rm eff(4,1)}+\Delta_W^{\rm eff(6,1,\sigma)}\right), \quad (7.3.1)$$

where $\Delta_W^{\rm eff}$ is a finite shift. Similarly, the v_μ and $v_{\rm eff}$ are related according to

$$\frac{1}{v_\mu^2} = \frac{1}{v_{\rm eff}^2}\left[1+\Delta r^{\rm eff}\right] = \frac{1}{v_{\rm eff}^2}\left[1+v_{\rm eff}^2\Delta r^{\rm eff(6,0)}+\frac{1}{v_{\rm eff}^2}\Delta r^{\rm eff(4,1)}+\Delta r^{\rm eff(6,1)}\right]. \quad (7.3.2)$$

The form above allows to determine G_F in the $v_\alpha^{\rm eff}$ scheme, whereas α in the $v_\mu^{\rm eff}$ scheme is easily obtained after inverting the equation. We have derived the SMEFT expansions for $\Delta_W^{\rm eff}$ and $\Delta r^{\rm eff}$, including explicit results in the large-m_t limit, in Section 6.3.2 and 6.3.1 respectively. Results for $\sin\theta_{\rm eff}^\ell$ in the α, α_μ and LEP schemes are obtained by evaluating Eq. (6.2.8), while results for all other derived parameters have been given in Section 5.4.[1]

The derived parameters are useful for two reasons. First, from a practical perspective, they are the simplest examples of EW precision observables and therefore play an important role in global analyses of data. Second, they are the key ingredients for converting results and understanding differences between EW input schemes. For example, if one calculates a quantity in the α_μ scheme, one can convert it to the $v_\mu^{\rm eff}$ scheme by substituting M_W with Eq. (7.3.1) with $\sigma = \mu$ and performing a SMEFT expansion. In the SM, if the derived value of M_W in the $v_\mu^{\rm eff}$ agrees well with the measured value at a given order, then results for other observables in the α_μ and $v_\mu^{\rm eff}$ scheme will show similar level of numerical agreement. This should also be true in SMEFT, but in that case the derived value of M_W depend on the Wilson coefficients, whose values are not precisely known and are left symbolic. Differences in observables between schemes show up in non-trivial patterns of Wilson coefficients and the level of agreement between schemes is less obvious. In the remainder of this section we examine derived parameters in the SM across all schemes, and use the prediction of M_W in the $v_\sigma^{\rm eff}$ schemes to illustrate some of their important features.

[1] We have converted factors of $\overline{\alpha}(\mu)$ used previously to the on-shell definition $\alpha(M_Z)$ using Eq. (6.3.8).

SM. In table 7.5 we show LO and NLO results for derived parameters in the SM, where NLO is defined as LO plus the NLO correction. In all cases, the NLO and measured values agree to roughly half a percent or better. In the $v_\sigma^{\rm eff}$ schemes, the deviation between the derived parameters and the experimental values is already below the per-mille level at LO, while the α and α_μ schemes involve percent-level NLO corrections to $\sin\theta_{\rm eff}^\ell$, α or G_F. Such corrections originate mainly from large-m_t corrections to the counterterm for s_w in those schemes; for instance, in the α_μ scheme the one-loop SM result is

$$s_{w,0}^2 = s_w^2 \left[1 + \left(\frac{c_w}{s_w}\right)^2 \frac{\Delta\rho_t^{(4,1)}}{v_\mu^2} + \dots\right] \approx s_w^2 \left[1 + 3.3\% + \dots\right] , \tag{7.3.3}$$

where the $\dots$ refers to terms which are subleading in the large-m_t limit, and $c_w = M_W/M_Z$. The same result holds in the α scheme after the replacement $v_\mu \to 2M_W s_w/\sqrt{4\pi\alpha}$.

A noticeable feature of the $v_\sigma^{\rm eff}$ schemes is that the NLO corrections to G_F or α are extremely small. These corrections are related to $\Delta r^{\rm eff(4,1)}$ in Eq. (7.3.2), and an estimate from the top-loop contribution in Eq. (6.3.12) gives $-\Delta\rho_t^{(4,1)}/v_\sigma^2 \approx -1\%$. To understand why this estimate breaks down, we split the one-loop SM correction into component parts according to

$$\begin{aligned}\frac{1}{v_\alpha^2}\Delta r^{\rm eff(4,1)} &= \frac{1}{v_\alpha^2}\Delta r_t^{\rm eff(4,1)} + \frac{1}{v_\alpha^2}\Delta r_{\rm rem}^{\rm eff(4,1)} + \frac{\alpha(M_Z)}{\pi}\frac{100}{27} \\ &= (-0.9348 + 0.0049 + 0.9143)\,\% = -0.0156\% , \end{aligned} \tag{7.3.4}$$

where the ordering of the numerical terms on the second line matches those of the analytic expressions above. We note an accidental cancellation between the large-m_t limit result and that related to the running of α in the on-shell scheme[1]; the latter correction can be eliminated by converting to the $\overline{\rm MS}$ definition as in Eq. (6.3.8). By contrast, the NLO corrections to M_W in the $v_\sigma^{\rm eff}$ scheme do not depend on the

[1] A similar cancellation occurs in the NLO correction to $\sin^2\theta_{\rm eff}^\ell$ in the LEP scheme, whose large-m_t correction is obtained from Eq. (7.3.3) by the replacement $c_w^2/s_w^2 \to -c_{2w}/c_w^2$ and is roughly -1.5% numerically.

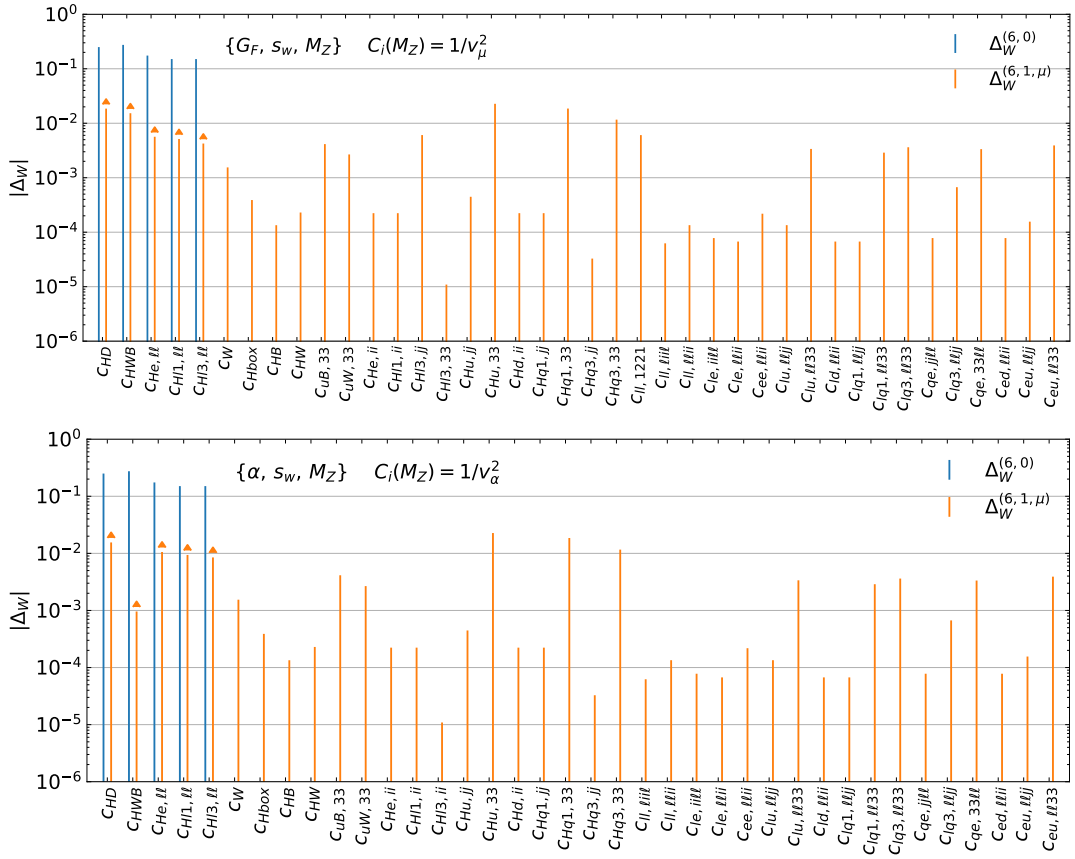

Figure 7.2: SMEFT corrections to the W boson mass in the v_μ^{eff} (top) and v_α^{eff} (bottom) schemes, with Δs_w determined from $Z \to ee$ decay, so that $\ell = 1$. The Wilson coefficients are evaluated at $C_i = 1/v_\sigma^2$. The flavour indices i and j run over values $j \in 1, 2$, and $i \in 1, 2, 3$.

counterterm for α. The top-loop contribution in Eq. (6.3.22) is a good estimate for the NLO correction, as seen in the result

$$\begin{aligned} M_W^{v_\sigma^{\text{eff}}} &= M_W^{\text{eff}} \left[1 + \frac{1}{v_\sigma^2}\left(\frac{1}{2}\Delta\rho_t^{(4,1)} + \Delta_{W,\text{rem.}}^{\text{eff}(4,1)}\right)\right] \\ &= 79.93\,\text{GeV}\,\left[1 + 0.00468 + 0.00137\right] = 80.42\,\text{GeV}\,, \end{aligned} \tag{7.3.5}$$

where the order of numerical contributions in the second line matches that on the first and we set $v_\sigma = v_\mu$ to obtain the numerical value.

SMEFT. Results for derived parameters in SMEFT depend on a number of Wilson coefficients and are thus quite lengthy. For brevity, we focus the discussion on M_W in the v_σ^{eff} schemes, leaving a comparison of observables across schemes to the heavy-

		C_{HWB}	C_{HD}	$C_{\substack{He\\11}}$	$C^{(3)}_{\substack{Hl\\11}}$
LO	v_σ^{eff}	$-0.275^{+0.009}_{-0.009}$	$-0.250^{+0.017}_{-0.017}$	$-0.175^{+0.004}_{-0.004}$	$-0.151^{+0.003}_{-0.003}$
NLO	v_μ^{eff}	$-0.290^{+0.001}_{-0.000}$	$-0.269^{+0.003}_{-0.000}$	$-0.180^{+0.000}_{-0.000}$	$-0.161^{+0.000}_{-0.000}$
	v_α^{eff}	$-0.276^{+0.000}_{-0.000}$	$-0.266^{+0.002}_{-0.000}$	$-0.185^{+0.000}_{-0.000}$	$-0.159^{+0.000}_{-0.000}$
NLO_t	v_μ^{eff}	$-0.280^{+0.003}_{-0.002}$	$-0.261^{+0.006}_{-0.003}$	$-0.178^{+0.000}_{-0.000}$	$-0.158^{+0.001}_{-0.001}$
	v_α^{eff}	$-0.272^{+0.002}_{-0.002}$	$-0.261^{+0.006}_{-0.003}$	$-0.183^{+0.000}_{-0.000}$	$-0.158^{+0.001}_{-0.001}$
		$C^{(1)}_{\substack{Hl\\11}}$	$C_{\substack{Hu\\33}}$	$C^{(1)}_{\substack{Hq\\33}}$	$C^{(3)}_{\substack{Hq\\33}}$
LO	v_σ^{eff}	$-0.151^{+0.004}_{-0.004}$	$0.000^{+0.026}_{-0.026}$	$0.000^{+0.026}_{-0.026}$	$0.000^{+0.001}_{-0.001}$
NLO	v_μ^{eff}	$-0.156^{+0.000}_{-0.000}$	$0.023^{+0.000}_{-0.007}$	$-0.019^{+0.006}_{-0.000}$	$0.012^{+0.000}_{-0.002}$
	v_α^{eff}	$-0.160^{+0.000}_{-0.000}$	$0.023^{+0.000}_{-0.006}$	$-0.019^{+0.006}_{-0.000}$	$0.012^{+0.000}_{-0.002}$
NLO_t	v_μ^{eff}	$-0.154^{+0.000}_{-0.000}$	$0.024^{+0.000}_{-0.005}$	$-0.024^{+0.005}_{-0.000}$	$0.009^{+0.000}_{-0.002}$
	v_α^{eff}	$-0.158^{+0.000}_{-0.000}$	$0.024^{+0.000}_{-0.005}$	$-0.024^{+0.005}_{-0.000}$	$0.009^{+0.000}_{-0.002}$

Table 7.6: The numerical prefactors of the Wilson coefficients in the v_μ^{eff} and v_α^{eff} schemes contributing to Δ_W for the LO, NLO and NLO_t (large-m_t limit) perturbative approximations. The SM tree-level approximation along with v_μ^2 has been factored out. The results have been evaluated at $\mu = M_Z$ and varied up and down by a factor of 2 to give the uncertainties. Only Wilson coefficients whose numerical prefactor is greater than 1% at NLO have been included.

boson decay rates presented in Section 7.3.2.

We show in figure 7.2 the LO and NLO SMEFT corrections to M_W in the v_σ^{eff} schemes. The numerical contribution from each Wilson coefficient at the scale $\mu = M_Z$ is obtained by making the choice $C_i(M_Z) = 1/v_\sigma^2$, and the results are given in units of M_W^{eff}; in other words, we are quoting results for the expansion coefficients of Δ_W as defined in Eq. (7.3.1).

It is clear from figure 7.2 that many of the NLO SMEFT corrections to M_W are numerically small when all Wilson coefficients are set to a common value. In table 7.6, we give numerical results at LO and NLO (defined as the sum of LO plus the NLO correction) for those SMEFT operators whose NLO contribution is larger than 1% for the default choice $C_i(M_Z) = 1/v_\sigma^2$. All of these coefficients receive NLO corrections from top loops, and to show their significance we give results where only the large-m_t limit of these corrections is used (NLO$_t$ in the table). In each case, we include scale uncertainties obtained by evaluating the prediction for the three scale choices $\mu \in [M_Z,\, 2M_Z,\, M_Z/2]$, using Eq. (5.4.4) to express the results in terms of $C_i(M_Z)$. In most cases there is a good convergence between LO and NLO when scale uncertainties are included. The large-m_t limit results are generally an improvement for central values, but come with small scale uncertainties which do not always overlap with the complete NLO result.

7.3.2 Heavy boson decays at NLO

To analyse $W \to \tau\nu$ and $Z \to \tau\tau$ decays we define SMEFT expansion coefficients for the decay $X \to f_1 f_2$ in input scheme s as

$$\Gamma(X \to f_1 f_2) = \Gamma^{s(4,0)}_{Xf_1f_2} + \Gamma^{s(6,0)}_{Xf_1f_2} + \Gamma^{s(4,1)}_{Xf_1f_2} + \Gamma^{s(6,1)}_{Xf_1f_2}\,. \tag{7.3.6}$$

Moreover, we write LO and NLO results as

$$\begin{aligned}\Gamma^{s}_{Xf_1f_2,\text{LO}} &\equiv \Gamma^{s(4,0)}_{Xf_1f_2} + \Gamma^{s(6,0)}_{Xf_1f_2}\,,\\ \Gamma^{s}_{Xf_1f_2,\text{NLO}} &\equiv \Gamma^{s}_{Xf_1f_2s,\text{LO}} + \Gamma^{s(4,1)}_{Xf_1f_2} + \Gamma^{s(6,1)}_{Xf_1f_2}\,.\end{aligned} \tag{7.3.7}$$

		$\Gamma^s_{W\ell\nu}/\ \Gamma^{\rm exp}_{W\ell\nu} - 1$	$\Gamma^s_{Z\ell\ell}/\Gamma^{\rm exp}_{Z\ell\ell} - 1$
$v_\mu^{\rm eff}$	LO	-1.30%	-0.70%
	NLO	0.16%	0.12%
$v_\alpha^{\rm eff}$	LO	-1.51%	-0.91%
	NLO	-0.06%	-0.11%
α_μ	LO	0.37%	-0.08%
	NLO	0.03%	-0.07%
α	LO	2.87%	2.41%
	NLO	-0.66%	-0.74%
LEP	LO	-1.17%	-0.66%
	NLO	0.31%	0.16%

Table 7.7: Deviations of the SM predictions for $Z \to \ell\ell$ and $W \to \ell\nu$ decay rates in scheme s from the experimental measurements of $\Gamma^{\rm exp}_{Z\ell\ell} = 83.98$ MeV and $\Gamma^{\rm exp}_{W\ell\nu} = 226.4$ MeV [10].

The LO results for $s \in \{v_\mu^{\rm eff}, v_\alpha^{\rm eff}\}$ are given by

$$\Gamma^s_{W\tau\nu,\rm LO} = \frac{M_W^{\rm eff}}{12\pi}\left\{\left(\frac{M_W^{\rm eff}}{v_\sigma}\right)^2 + (M_W^{\rm eff})^2\left[2C^{(3)}_{\substack{Hl\\33}} + 3\Delta_W^{\rm eff(6,0)} - \Delta v_\sigma^{\rm eff(6,0)}\right]\right\},$$

$$\begin{aligned}\Gamma^s_{Z\tau\tau,\rm LO} = \frac{M_Z}{24\pi}\Bigg\{&\frac{M_Z^2}{v_\sigma^2}\left(1 - \frac{v_\sigma^2}{2}C_{HD}\right)g^{(4,0)} + M_Z^2\Big[\left(2\left(g_R^{\ell(6,0)} - g_L^{\ell(6,0)}\right) - \Delta v_\sigma^{\rm eff(6,0)}\right)g^{(4,0)}\\ &+ 2c_{2\rm eff}\left(g_L^{\tau(6,0)} - g_L^{\ell(6,0)}\right) + 4s^2_{\rm eff}\left(g_R^{\tau(6,0)} - g_R^{\ell(6,0)}\right)\Big]\Bigg\},\end{aligned} \tag{7.3.8}$$

where $\ell \equiv \ell^i$ is the charged lepton species used in the definition of $\Delta s_{\rm eff}$ and

$$g^{(4,0)} = 1 - 4s^2_{\rm eff} + 8s^4_{\rm eff}\,. \tag{7.3.9}$$

As a reminder, the LO results in the other three schemes are given in Chapter 5. To derive the result for W decay we have written W-mass dependence arising both through two-body phase-space and in the matrix element squared in terms of $M_W^{\rm eff}$. Note that in Z decay the flavour-independent coupling $G^{(6,0)}$ given in Eq. 6.2.7 has dropped out of the decay rate due to a cancellation against $\Delta s_{\rm eff}^{(6,0)}$. Further simplifications occur only if $\ell = \tau$ or a flavour symmetry such as $U(2)^2 \times U(3)^3$ is imposed, in which case the contribution in the final line vanishes.

The LO and NLO results for W and Z decay in the SM are shown in table 7.7, where we have normalised the results to the experimentally measured values. The

		C_{HD}	C_{HWB}	$C_{\substack{He\\33}}$	$C_{\substack{Hu\\33}}$	$C^{(3)}_{\substack{Hq\\33}}$
v_μ^{eff}	LO	$-0.500^{+0.033}_{-0.033}$	$0.000^{+0.000}_{-0.000}$	$-1.843^{+0.048}_{-0.048}$	$0.000^{+0.052}_{-0.052}$	$0.000^{+0.000}_{-0.000}$
	NLO	$-0.527^{+0.005}_{-0.000}$	$0.004^{+0.000}_{-0.000}$	$-1.905^{+0.004}_{-0.000}$	$0.048^{+0.000}_{-0.013}$	$0.022^{+0.000}_{-0.004}$
v_α^{eff}	LO	$0.000^{+0.000}_{-0.000}$	$2.370^{+0.081}_{-0.081}$	$-1.843^{+0.050}_{-0.050}$	$0.000^{+0.003}_{-0.003}$	$0.000^{+0.005}_{-0.005}$
	NLO	$-0.001^{+0.000}_{-0.000}$	$2.439^{+0.000}_{-0.006}$	$-1.903^{+0.004}_{-0.000}$	$0.005^{+0.000}_{-0.001}$	$0.002^{+0.000}_{-0.000}$
α_μ	LO	$-0.169^{+0.011}_{-0.011}$	$0.355^{+0.012}_{-0.012}$	$-1.764^{+0.046}_{-0.046}$	$0.000^{+0.018}_{-0.018}$	$0.000^{+0.001}_{-0.001}$
	NLO	$-0.289^{+0.009}_{-0.007}$	$0.258^{+0.003}_{-0.004}$	$-1.897^{+0.006}_{-0.002}$	$0.018^{+0.011}_{-0.016}$	$0.006^{+0.000}_{-0.002}$
α	LO	$1.573^{+0.108}_{-0.108}$	$4.088^{+0.143}_{-0.143}$	$-1.764^{+0.050}_{-0.050}$	$0.000^{+0.162}_{-0.162}$	$0.000^{+0.008}_{-0.008}$
	NLO	$1.408^{+0.002}_{-0.019}$	$3.869^{+0.002}_{-0.013}$	$-1.898^{+0.006}_{-0.002}$	$-0.142^{+0.030}_{-0.000}$	$-0.073^{+0.014}_{-0.000}$
LEP	LO	$-0.600^{+0.040}_{-0.040}$	$-0.474^{+0.016}_{-0.016}$	$-1.837^{+0.048}_{-0.048}$	$0.000^{+0.062}_{-0.062}$	$0.000^{+0.001}_{-0.001}$
	NLO	$-0.631^{+0.005}_{-0.000}$	$-0.475^{+0.001}_{-0.000}$	$-1.899^{+0.004}_{-0.000}$	$0.057^{+0.000}_{-0.015}$	$0.025^{+0.000}_{-0.005}$

Table 7.8: Selected SMEFT contributions to the $Z \to \tau\tau$ decay rate including scale variation in the five schemes.

NLO corrections in the SM bring results from all five schemes into close numerical agreement. These corrections are at the 1.5% level for W decay in the v_σ^{eff} and LEP schemes, where M_W is not an input and hence factors of $3\Delta_W^{s(4,1)}/v_\sigma^2$ arise compared to the α_μ scheme. Corrections of around -3% arise in the α scheme, which are mainly due to the top-loop corrections to s_w shown in Eq. (7.3.3) and in Chapter 5. As explained in Section 7.3.1, the close agreement between decay rates at NLO different schemes is a direct consequence of the predictions of the derived parameters matching the experimental inputs as seen in table 7.5.

However, the situation in SMEFT is different. The relations between input parameters in different schemes depend on the unknown Wilson coefficients. Therefore, in general, although the numerical prefactor multiplying a particular Wilson coefficient stemming from the matrix element is consistent across schemes, the somewhat arbitrary relations between schemes can result in the numerical prefactor of a given Wilson coefficient being very different across schemes. This point is seen in table 7.8, where the LO and NLO contributions for an illustrative sample of Wilson coefficients are shown for the decay $Z \to \tau\tau$, using $\ell^i = e$ to determine the Δs_{eff} counterterm in

the v_σ^{eff} schemes. The results include perturbative uncertainties obtained by varying the default scale choice $\mu_{\text{def}} = M_Z$ up and down by a factor of two. We note the following features:

- The contributions from the coefficients C_{HD} and C_{HWB} have rather different prefactors in each scheme, and convergence between LO and NLO also differs markedly from case to case – especially in the α_μ scheme the NLO corrections are large and well outside the LO scale uncertainties.

- By contrast, at LO the coefficient $C_{\substack{He\\33}}$ appears only in the $Z \to \tau\tau$ matrix element. The dominant NLO corrections arise from SM counterterms on this LO vertex, and tend to push the NLO results in different schemes to similar values. The NLO corrections in the α and α_μ schemes are outside the LO scale uncertainties.

- The coefficients $C_{\substack{Hu\\33}}$ and $C^{(3)}_{\substack{Hq\\33}}$ first appear at NLO for fixed μ. The contribution of the former is well estimated by LO scale uncertainties through the running of C_{HD} (driven by the top-loop contribution shown in Eq. (6.3.26)), while that of the latter is unrelated to RG running and requires a genuine NLO calculation.

Regarding the first two points, NLO corrections in the v_σ^{eff} schemes tend to be milder than in the α or α_μ schemes because in the latter case Δs_w gets scale-independent corrections of the type shown in Eq. (7.3.3). In that case including universal corrections from the large-m_t limit using the procedure outlined in Section 5.6 can improve convergence between orders.[1]

We conclude by stating that the specific pattern of contributions described above is specific to Z decay, but the important point that the size of SMEFT contributions related to a particular Wilson coefficient is highly scheme specific in general.

[1] A similar procedure could be followed for the v_σ^{eff} schemes using eq. (6.3.12) as a starting point.

Chapter 8

Conclusions

Throughout this thesis, we have devoted our efforts into understanding the qualitative and quantitative features of numerous different choices of Electroweak (EW) input schemes in the Standard Model Effective Field Theory (SMEFT). We have provided definitions and expressions for counterterms in each of the schemes, which for schemes involving the weak mixing angle is a first implementation in the SMEFT. Furthermore, we used the derived parameters and the decays of the heavy gauge bosons in each scheme, making use of large-m_t analysis, to illucidate the salient features of each of the schemes.

In Chapters 1 and 2 we gave an introduction to the relevant background information for this thesis. The former concerned the Standard Model (SM), mainly focusing on the form of the Lagrangian and one-loop renormalisation, while the latter introduced Effective Field Theories (EFTs) and most importantly, the SMEFT, discussing the main changes to SM parameters. This culminated in the relation expressing the Lagrangian parameters g_1, and g_2 in terms of the bare parameters v_T, $M_{W,0}$, and $M_{Z,0}$ giving a unified starting point for our discussions on input schemes. In Chapter 3 we gave preliminary information useful to motivate and understand the ideas presented in the subsequent chapters.

Chapter 4 began our review of the EW input schemes and introduced the α, α_μ, and LEP schemes, the most common choices in the literature. Counterterms for all

input parameters in the schemes were defined and expressions were given. However, we found it instructive to define the quantities v_α in the α scheme and $\hat{M}_W$ in the LEP scheme and derive their associated counterterms, thus giving replacements for our unified starting Lagrangian. We presented how analytic predictions for derived parameters in each scheme can be obtained. Furthermore, it was shown that the analytic expressions for the derived parameters were precisely the relations which relate the schemes, allowing any analytic results in the literature in one scheme to be converted into another.

In Chapter 5 we provided analysis of the three schemes of Chapter 4. We started with counting the number of unique Wilson coefficients which appear in each counterterms. However, this counting is not everything, as the specific form of the calculation can lead to cancellations, drastically reducing the number of Wilson coefficients appearing. We showed that the source of the largest corrections can be associated to top loops in the finite parts of the counterterms. If then coupled with inverse powers of $s_w^2 \sim 0.25$ the effects are accentuated. These largest corrections were shown to be well approximated by the large-m_t limit for the schemes as defined. In the SM, by writing the counterterms for v_T in a unified way in the large-m_t limit, it was manifest that corrections associated with the VEV in the α_μ or LEP scheme go approximately as $\Delta\rho_t^{(4,1)} \sim 1\%$, whereas those in the α scheme go with $\Delta r^{(4,1)} = -\frac{c_w^2}{s_w^2}\Delta\rho_t^{(4,1)} \sim 3.4\%$. In SMEFT, the dominant corrections related to the renormalisation of v_T still arise from top loops, but these involve μ-dependent logarithmic corrections related to the running of Wilson coefficients, in addition to more complicated dependence on the Weinberg angle than in the SM. Consequently, the numerical results across Wilson coefficients and processes are not nearly as regular. Nonetheless, we used the decay of the W boson to leptons as a benchmark process to define the finite, gauge, and scale independent K factors, $K_W^{(i,j,\sigma)}$. The K factors allowed us to write further processes as a combination of scheme dependent parts involving K_W, which accounted for the large correction of the counterterms, and scheme independent parts. This identification of scheme dependent corrections enabled the creation of a set of

universal replacement rules, allowing for the largest scheme dependent correction to be introduced into the Leading-Order (LO) result. The consequences of such replacements were to bring all the three schemes into closer alignment with each other, with the remaining Next-to-Leading-Order (NLO) corrections, for a Wilson coefficient, all being of a similar, smaller size.

Chapter 6 saw the introduction of two new schemes, those involving the effective weak mixing angle as an input, the v_α^{eff} and the v_μ^{eff} schemes. We extended the already established implementation of these schemes in the SM to the SMEFT, giving expressions of necessary counterterms in a compact notation. The notation conveyed that the large-m_t counterterms to the weak mixing angle was proportional to $\Delta\rho_t^{(4,1)}$, a notable feature of these schemes. The connection between the two schemes was made, and analytic conversion factors were derived and presented. To finish, and to make the connection with the initially presented schemes, expressions for the W mass predictions in the v_σ^{eff} schemes were given, relating these schemes to either the α or α_μ schemes thus allowing analytic results in the literature to be expressed in terms of any one of five schemes with minimal effort.

Chapter 7 again started with a counting exercise; counterterms for the weak mixing angle involved numerous Wilson coefficients, most of which previously uninvolved in EW counterterms. By considering the definition of the weak mixing angle, this is of little surprise, as all Wilson coefficients involved in Z decay to leptons are present, which involves many four-fermion operators. A numerical analysis of the schemes showed that, in general, corrections in the SM in the v_σ^{eff} schemes are smaller, a fact already established. Moreover, for certain predictions in the v_α^{eff} scheme, these corrections can be even smaller than a large-m_t analysis would suggest due to an accidental cancellation between corrections to the VEV and the on-shell running of α. For processes in the SMEFT, it was seen that, somewhat surprisingly on first sight, the prefactors to Wilson coefficients of the predictions in different schemes don't necessarily align as higher orders in perturbation theory are calculated. Scheme dependent corrections can drive these prefactors to independent values, which can

result in large differences with a non-trivial pattern of perturbative convergence across all the schemes.

We end this thesis by asking whether there is a preferred input scheme for SMEFT calculations. After including universal corrections, the perturbative convergence in the different schemes presented here is expected to be similar. With the schemes on equal footing and conversions amongst them unchallenging, there is little reason to prefer one over the other, a fact we can exploit. Differences in theoretical predictions in the SMEFT between different input schemes arise from unknown uncalculated higher order corrections in perturbation theory, much like in the SM. If we wish to concern ourselves with constraining the Wilson coefficients, the non-trivial pattern of perturbative convergence across all the schemes has the capacity to be advantageous. Fits of the Wilson coefficients performed in different schemes may provide a valuable consistency check, alongside potential improvement in the constraints of some Wilson coefficients. No input scheme is perfect, each has beneficial properties over the others. Including multiple input schemes into our arsenal of tools to constrain Wilson coefficients, facilitated by the work presented here, has the potential to be highly fruitful.

Appendix A

Appendix

A.1 Warsaw Basis

$1:X^3$	
Q_G	$f^{ABC}G_\mu^{A\nu}G_\nu^{B\rho}G_\rho^{C\mu}$
$Q_{\widetilde{G}}$	$f^{ABC}\widetilde{G}_\mu^{A\nu}G_\nu^{B\rho}G_\rho^{C\mu}$
Q_W	$\epsilon^{IJK}W_\mu^{I\nu}W_\nu^{J\rho}W_\rho^{K\mu}$
$Q_{\widetilde{W}}$	$\epsilon^{IJK}\widetilde{W}_\mu^{I\nu}W_\nu^{J\rho}W_\rho^{K\mu}$

$2:H^6$	
Q_H	$(H^\dagger H)^3$

$3:H^4D^2$	
$Q_{H\Box}$	$(H^\dagger H)\Box(H^\dagger H)$
Q_{HD}	$\left(H^\dagger D_\mu H\right)^*\left(H^\dagger D_\mu H\right)$

$4:X^2H^2$	
Q_{HG}	$H^\dagger H\, G_{\mu\nu}^A G^{A\mu\nu}$
$Q_{H\widetilde{G}}$	$H^\dagger H\, \widetilde{G}_{\mu\nu}^A G^{A\mu\nu}$
Q_{HW}	$H^\dagger H\, W_{\mu\nu}^I W^{I\mu\nu}$
$Q_{H\widetilde{W}}$	$H^\dagger H\, \widetilde{W}_{\mu\nu}^I W^{I\mu\nu}$
Q_{HB}	$H^\dagger H\, B_{\mu\nu}B^{\mu\nu}$
$Q_{H\widetilde{B}}$	$H^\dagger H\, \widetilde{B}_{\mu\nu}B^{\mu\nu}$
Q_{HWB}	$H^\dagger\sigma^I H\, W_{\mu\nu}^I B^{\mu\nu}$
$Q_{H\widetilde{W}B}$	$H^\dagger\sigma^I H\, \widetilde{W}_{\mu\nu}^I B^{\mu\nu}$

$5:\psi^2H^3+\text{h.c.}$	
Q_{eH}	$(H^\dagger H)(\bar{l}_p e_r H)$
Q_{uH}	$(H^\dagger H)(\bar{q}_p u_r \widetilde{H})$
Q_{dH}	$(H^\dagger H)(\bar{q}_p d_r H)$

$6:\psi^2XH+\text{h.c.}$	
Q_{eW}	$(\bar{l}_p\sigma^{\mu\nu}e_r)\sigma^I H W_{\mu\nu}^I$
Q_{eB}	$(\bar{l}_p\sigma^{\mu\nu}e_r)H B_{\mu\nu}$
Q_{uG}	$(\bar{q}_p\sigma^{\mu\nu}T^A u_r)\widetilde{H}\, G_{\mu\nu}^A$
Q_{uW}	$(\bar{q}_p\sigma^{\mu\nu}u_r)\sigma^I\widetilde{H}\, W_{\mu\nu}^I$
Q_{uB}	$(\bar{q}_p\sigma^{\mu\nu}u_r)\widetilde{H}\, B_{\mu\nu}$
Q_{dG}	$(\bar{q}_p\sigma^{\mu\nu}T^A d_r)H\, G_{\mu\nu}^A$
Q_{dW}	$(\bar{q}_p\sigma^{\mu\nu}d_r)\sigma^I H\, W_{\mu\nu}^I$
Q_{dB}	$(\bar{q}_p\sigma^{\mu\nu}d_r)H\, B_{\mu\nu}$

$7:\psi^2H^2D$	
$Q_{Hl}^{(1)}$	$(H^\dagger i\overleftrightarrow{D}_\mu H)(\bar{l}_p\gamma^\mu l_r)$
$Q_{Hl}^{(3)}$	$(H^\dagger i\overleftrightarrow{D}_\mu^I H)(\bar{l}_p\sigma^I\gamma^\mu l_r)$
Q_{He}	$(H^\dagger i\overleftrightarrow{D}_\mu H)(\bar{e}_p\gamma^\mu e_r)$
$Q_{Hq}^{(1)}$	$(H^\dagger i\overleftrightarrow{D}_\mu H)(\bar{q}_p\gamma^\mu q_r)$
$Q_{Hq}^{(3)}$	$(H^\dagger i\overleftrightarrow{D}_\mu^I H)(\bar{q}_p\sigma^I\gamma^\mu q_r)$
Q_{Hu}	$(H^\dagger i\overleftrightarrow{D}_\mu H)(\bar{u}_p\gamma^\mu u_r)$
Q_{Hd}	$(H^\dagger i\overleftrightarrow{D}_\mu H)(\bar{d}_p\gamma^\mu d_r)$
$Q_{Hud}+\text{h.c.}$	$i(\widetilde{H}^\dagger D_\mu H)(\bar{u}_p\gamma^\mu d_r)$

$8:(\bar{L}L)(\bar{L}L)$		$8:(\bar{R}R)(\bar{R}R)$	
Q_{ll}	$(\bar{l}_p\gamma_\mu l_r)(\bar{l}_s\gamma^\mu l_t)$	Q_{ee}	$(\bar{e}_p\gamma_\mu e_r)(\bar{e}_s\gamma^\mu e_t)$
$Q_{qq}^{(1)}$	$(\bar{q}_p\gamma_\mu q_r)(\bar{q}_s\gamma^\mu q_t)$	Q_{uu}	$(\bar{u}_p\gamma_\mu u_r)(\bar{u}_s\gamma^\mu u_t)$
$Q_{qq}^{(3)}$	$(\bar{q}_p\gamma_\mu\sigma^I q_r)(\bar{q}_s\gamma^\mu\sigma^I q_t)$	Q_{dd}	$(\bar{d}_p\gamma_\mu d_r)(\bar{d}_s\gamma^\mu d_t)$
$Q_{lq}^{(1)}$	$(\bar{l}_p\gamma_\mu l_r)(\bar{q}_s\gamma^\mu q_t)$	Q_{eu}	$(\bar{e}_p\gamma_\mu e_r)(\bar{u}_s\gamma^\mu u_t)$
$Q_{lq}^{(3)}$	$(\bar{l}_p\gamma_\mu\sigma^I l_r)(\bar{q}_s\gamma^\mu\sigma^I q_t)$	Q_{ed}	$(\bar{e}_p\gamma_\mu e_r)(\bar{d}_s\gamma^\mu d_t)$
		$Q_{ud}^{(1)}$	$(\bar{u}_p\gamma_\mu u_r)(\bar{d}_s\gamma^\mu d_t)$
		$Q_{ud}^{(8)}$	$(\bar{u}_p\gamma_\mu T^A u_r)(\bar{d}_s\gamma^\mu T^A d_t)$

$8:(\bar{L}L)(\bar{R}R)$	
Q_{le}	$(\bar{l}_p\gamma_\mu l_r)(\bar{e}_s\gamma^\mu e_t)$
Q_{lu}	$(\bar{l}_p\gamma_\mu l_r)(\bar{u}_s\gamma^\mu u_t)$
Q_{ld}	$(\bar{l}_p\gamma_\mu l_r)(\bar{d}_s\gamma^\mu d_t)$
Q_{qe}	$(\bar{q}_p\gamma_\mu q_r)(\bar{e}_s\gamma^\mu e_t)$
$Q_{qu}^{(1)}$	$(\bar{q}_p\gamma_\mu q_r)(\bar{u}_s\gamma^\mu u_t)$
$Q_{qu}^{(8)}$	$(\bar{q}_p\gamma_\mu T^A q_r)(\bar{u}_s\gamma^\mu T^A u_t)$
$Q_{qd}^{(1)}$	$(\bar{q}_p\gamma_\mu q_r)(\bar{d}_s\gamma^\mu d_t)$
$Q_{qd}^{(8)}$	$(\bar{q}_p\gamma_\mu T^A q_r)(\bar{d}_s\gamma^\mu T^A d_t)$

$8:(\bar{L}R)(\bar{R}L)+\text{h.c.}$	
Q_{ledq}	$(\bar{l}_p^j e_r)(\bar{d}_s q_{tj})$

$8:(\bar{L}R)(\bar{L}R)+\text{h.c.}$	
$Q_{quqd}^{(1)}$	$(\bar{q}_p^j u_r)\epsilon_{jk}(\bar{q}_s^k d_t)$
$Q_{quqd}^{(8)}$	$(\bar{q}_p^j T^A u_r)\epsilon_{jk}(\bar{q}_s^k T^A d_t)$
$Q_{lequ}^{(1)}$	$(\bar{l}_p^j e_r)\epsilon_{jk}(\bar{q}_s^k u_t)$
$Q_{lequ}^{(3)}$	$(\bar{l}_p^j\sigma_{\mu\nu} e_r)\epsilon_{jk}(\bar{q}_s^k\sigma^{\mu\nu} u_t)$

Table A.1: The 59 independent baryon number conserving dimension-six operators built from Standard Model fields, in the notation of [45]. The subscripts p, r, s, t are flavour indices, and σ^I are Pauli matrices.

A.2 Phase Space Integrals

Here we outline the steps needed to perform the phase space integrals necessary to compute the decays of the Heavy bosons to fermions at LO and NLO. These are the 2-body phase space integrals where the final state is just massless fermions and the 3-body phase space integrals where we additionally have an emission of a massless gauge boson. We shall present the result for a massive Z boson of four momentum P_Z and mass M_Z decaying to two massless electrons (and a massless gauge boson). Results for other decays are easily obtained by substitutions. We will work in dimensional regularisation where we have $d = 4 - 2\epsilon$ space-time dimensions. Our calculations start from the differential cross-section given by,

$$d\sigma = \frac{1}{F}|\mathcal{M}|^2 d\Phi_{1\to n}, \tag{A.2.1}$$

where F is a flux factor and $d\Phi_{1\to n}$ is the differential Lorentz invariant phase space for an n particle final state,

$$d\Phi_{1\to n}\left(P_Z; p_1, ..., p_n\right) = \prod_{i=1}^{n}\left[\frac{d^d p_i}{(2\pi)^d}\left(2\pi\right)\delta^+(p_i^2)\right]\left(2\pi\right)^d \delta^d\left(\sum_{i=1}^{n} p_i - P_Z\right), \tag{A.2.2}$$

where we have

$$\delta^+(p_i^2 - m_i^2) = \delta(p_i^2 - m_i^2)\Theta(E_i)\,, \tag{A.2.3}$$

which ensures final state particles are on-shell with positive energy. For a particle decay, we have $F = 2E_0$, where E_0 is the energy of the decaying particle, which in our case is M_Z. We can integrate out the delta functions which ensures the final states are on shell,

$$d\Phi_{1\to n}\left(P_Z; p_1, ..., p_n\right) = \prod_{i=1}^{n}\left[\frac{d^{d-1}\vec{p}_i}{(2\pi)^{d-1}\,2p_i^0}\right]\left(2\pi\right)^d \delta^d\left(\sum_{i=1}^{n} p_i - P_Z\right). \tag{A.2.4}$$

A.2.1 Two-body phase space

The decay rate of the Z boson to electrons can be written as

$$\Gamma_{Z\to ee} = \frac{1}{2M_Z}\int \frac{d^{d-1}\vec{p}_1}{(2\pi)^{d-1}\,2p_1^0}\frac{d^{d-1}\vec{p}_2}{(2\pi)^{d-1}\,2p_2^0}\,(2\pi)^d\,\delta^d\left(p_1+p_2-P_Z\right)|\mathcal{M}_{Zee}|^2\,. \quad \text{(A.2.5)}$$

In the center of mass frame,

$$P_Z = (M_Z,\vec{0}),\quad p_1 = (p_1^0,\vec{p_1}),\quad p_2 = (p_2^0,\vec{p_2})\,. \quad \text{(A.2.6)}$$

We can write the d-dimension delta functon as a product of a (d-1)-dimensional spacial delta function and a temporal delta function

$$\delta^d\left(p_1+p_2-P_Z\right) = \delta\left(p_1^0+p_2^0-M_Z\right)\delta^{d-1}\left(\vec{p}_1+\vec{p}_2-\vec{0}\right)\,. \quad \text{(A.2.7)}$$

Hence, performing the integral over $\vec{p}_2$ imposes $\vec{p}_2 = -\vec{p}_1$,

$$\Gamma_{Z\to ee} = \frac{1}{2M_Z}\int \frac{d^{d-1}\vec{p}_1}{(2\pi)^{d-2}\,4|\vec{p}_1|^2}\delta\left(2|\vec{p}_1|^2-M_Z\right)|\mathcal{M}_{Zee}|^2\Big|_{\vec{p}_2\to-\vec{p}_1}\,. \quad \text{(A.2.8)}$$

We choose to write the final (d-1)-dimensional integral in spherical coordinates

$$d^{d-1}\vec{p}_1 = |\vec{p_1}|^{d-2}d|\vec{p}_1|d\Omega_{d-1}\,, \quad \text{(A.2.9)}$$

where

$$d\Omega_{d-1} = \sin^{d-2}(\phi_{d-1})\sin^{d-3}(\phi_{d-2})...\sin(\phi_1)d\phi_1...d\phi_{d-1}, \quad \text{(A.2.10)}$$

and we have defined the range of ϕ_1 to be $[0,2\pi]$ and all other angles ranges to be $[0,\pi]$. For the decays we consider in this thesis, the two body matrix elements are angle independent. Therefore, we can use

$$\int d\Omega_{d-1} = \frac{2\pi^{\frac{d-1}{2}}}{\Gamma\left(\frac{d-1}{2}\right)} \quad \text{(A.2.11)}$$

when integrating over all angles such that

$$\Gamma_{Z\to ee} = \frac{\pi^{\frac{3-d}{2}}}{2^d M_Z\Gamma\left(\frac{d-1}{2}\right)}\int d|\vec{p}_1||\vec{p}_1|^{d-4}\delta\left(2|\vec{p}_1|^2-M_Z\right)|\mathcal{M}_{Zee}|^2\Big|_{\vec{p}_2\to-\vec{p}_1}\,. \quad \text{(A.2.12)}$$

Performing the integral over $\vec{p_1}$ using

$$\delta\left(f(x)\right) = \sum_{x_0 \in \text{roots}} \frac{\delta\left(x - x_0\right)}{f'(x_0)}\,, \tag{A.2.13}$$

gives us

$$\begin{aligned}\Gamma_{Z\to ee} &= \frac{2^{3-2d}\pi^{\frac{3-d}{2}} M_Z^{d-5}}{\Gamma\left(\frac{d-1}{2}\right)} |\mathcal{M}_{Zee}|^2 \\ &= \frac{1}{8\pi} |\mathcal{M}_{Zee}|^2\,. \end{aligned} \tag{A.2.14}$$

In the second line we are free to take the limit $d \to 4$ as the result contains no poles in epsilon.

A.2.2 Three-body phase space

Now we move on to the process with a three body final state, where, in our example, we include a photon into the final state additional to the two electrons. To tackle this problem, we separate the three body phase space into two two-body phase spaces through the use of

$$d\Phi_{1\to 3}\left(P_Z; p_1, p_2, p_\gamma\right) = \frac{dQ^2}{2\pi} d\Phi_{1\to 2}\left(P_Z; Q, p_\gamma\right) d\Phi_{1\to 2}\left(Q; p_1, p_2\right), \tag{A.2.15}$$

we can write

$$\Gamma_{Zee\gamma} = \frac{1}{2M_Z} I_3\,, \tag{A.2.16}$$

where we have defined the integral

$$\begin{aligned} I_3 &= \int d\Phi_{1\to 3}\left(P_Z; p_1, p_2, p_\gamma\right) |\mathcal{M}_{Zee\gamma}|^2 \\ &= \int \frac{dQ^2}{2\pi} d\Phi_{1\to 2}\left(P_Z; Q, p_\gamma\right) d\Phi_{1\to 2}\left(Q; p_1, p_2\right) |\mathcal{M}_{Zee\gamma}|^2. \end{aligned} \tag{A.2.17}$$

The first step is to solve the integral

$$I_{\text{PS1}} = \int d\Phi_{1\to 2}\left(Q; p_1, p_2\right) |\mathcal{M}_{Zee\gamma}|^2\,, \tag{A.2.18}$$

which we have named phase space 1. This integral can be solved in any frame, and so we choose to use the rest frame of Q, parameterising the momenta of the particles as

$$\begin{aligned} Q &= (Q^0, \vec{0}) \,, \\ P_Z &= (E_Z, 0, ..., 0, |\vec{p_Z}|) \,, \\ p_1 &= (|\vec{p}_1|, 0, ..., |\vec{p}_1| \sin\theta, |\vec{p}_1| \cos\theta) \,, \\ p_2 &= (|\vec{p}_2|, 0, ..., |\vec{p}_2| \sin\theta, -|\vec{p}_2| \cos\theta) \,, \\ p_\gamma &= (|\vec{p_\gamma}|, 0, ..., 0, |\vec{p_\gamma}|) \,. \end{aligned} \tag{A.2.19}$$

In general, for a three body decay, there will be some angular dependence between outgoing particles, so when performing the angular integrals, we keep dependence on a single angle through

$$\int d\Omega_{d-1} = \frac{2\pi^{\frac{d-2}{2}}}{\Gamma\left(\frac{d-2}{2}\right)} \int_0^\pi d\phi \sin^{d-3}(\phi) \,, \tag{A.2.20}$$

yielding

$$I_{\rm PS1} = \frac{2^{4-3d}\pi^{\frac{2-d}{2}}(Q^2)^{\frac{d-4}{2}}}{\Gamma\left(\frac{d-2}{2}\right)} \int_0^\pi d\phi \sin^{d-3}(\phi) |\mathcal{M}_{Zee\gamma}|^2. \tag{A.2.21}$$

Next, we move on to the second phase space integral

$$\begin{aligned} I_{\rm PS2} &= \int d\Phi_{1\to 2}\left(P_Z; Q, p_\gamma\right) I_{\rm PS1} \\ &= \frac{d^{d-1}\vec{Q}}{(2\pi)^{d-1}\, 2Q^0} \frac{d^{d-1}\vec{p}_\gamma}{(2\pi)^{d-1}\, 2p_\gamma^0} (2\pi)^d \, \delta^d\left(P_Z - Q - p_\gamma\right) I_{\rm PS1} \,. \end{aligned} \tag{A.2.22}$$

As $I_{\rm PS1}$ is written in terms of Lorentz invariant quantities, and an angle which we integrate over, changing frames is trivial, hence we evaluate phase space two in the rest frame of the Z boson. This introduces no new difficulties. First we integrate over $d^{d-1}\vec{p}_\gamma$, perform a change to spherical coordinates and integrate over all the sphere as the angular dependence is already in phase space one. Doing so we find

$$I_{\rm PS2} = \frac{2^{5-3d}\pi^{2-d} M_Z^{2-d}}{\Gamma(d-2)} (Q^2)^{\frac{d-4}{2}} \left(M_Z^2 - Q^2\right)^{d-3} \int_0^\pi d\phi \sin^{d-3}\phi |\mathcal{M}_{Zee\gamma}|^2. \tag{A.2.23}$$

Finally, interpreting the quantity Q^2 as the energy imparted to the electron pair, we see that, for the case of massless electrons, we integrate Q^2 from zero upto M_Z^2. The end result is the phase space integral evaluates as

$$I_3 = \frac{2^{4-3d}\pi^{1-d}M_Z^{2-d}}{\Gamma(d-2)}\int_0^{M_Z^2} dQ^2(Q^2)^{\frac{d-4}{2}}\left(M_Z^2-Q^2\right)^{d-3}\int_0^{\pi} d\phi\sin^{d-3}\phi|\mathcal{M}_{Zee\gamma}|^2. \tag{A.2.24}$$

A.3 Comparison with previous literature

Electroweak precision observables at NLO in SMEFT have been calculated previously in [81, 135]. In this section we compare the LEP-scheme results for M_W and the $Z \to \ell\ell$ decay rate with results given in that work.[1] In order to do so, we must take into account some differences in calculational set-ups.

First, in contrast to the present work, those works use $\alpha^{\text{O.S.}}(0)$ as an input, so that large logarithms of lepton masses and hadronic contributions appear in fixed order. We can convert our results to that renormalisation scheme by eliminating $\alpha(M_Z)$ through use of Eq. (6.3.8) and

$$\alpha^{\text{O.S.}}(M_Z) = \frac{\alpha^{\text{O.S.}}(0)}{1-\Delta\alpha} \approx \alpha^{\text{O.S.}}(0)(1+\Delta\alpha)\,, \tag{A.3.1}$$

where

$$\Delta\alpha = \Delta\alpha_{\text{lep}} + \Delta\alpha^{(5)}_{\text{had}} = 0.03142 + 0.02764\,. \tag{A.3.2}$$

Expanding observables to linear order in $\alpha^{\text{O.S.}}(0)$ and $\Delta\alpha$ then yields SM predictions as given in [81, 135]. After making this conversion and using a common set of input parameters also for heavy-particle masses, we can exactly reproduce the SM values for the W mass at LO and NLO:

$$M_W^{\text{LO}} = 80.939\text{ GeV}, \qquad M_W^{\text{NLO}} = 80.548\text{ GeV}\,. \tag{A.3.3}$$

[1] The decay rate for the W boson has not been compared since a leptonic partial branching fraction is not provided in the previous literature.

The SMEFT results for the W-boson mass also agree, when the same set of flavour assumptions is made.

For the $Z \to \ell\ell$ decay rate, we agree with an analytic result in the α_μ scheme provided to us by the authors of [81, 135] (after using the flavour assumptions of those papers). This forms the basis for LEP-scheme results. In our case these are obtained by using Eqs. (4.3.7) and (4.3.9) to express the result in terms of $\hat{M}_W$, while [81,135] re-organise the SM part of the loop expansion in a way that is specified in [96]. Taking into account these differences, as well as the renormalisation of α discussed above, we find numerical agreement with [81, 135].

A.4 Numerical results for the decay rates

Here we present numerical results for the decay rates considered in Section 5.5 in the three schemes. We use the notation

$$\begin{aligned}\Gamma^s_{X,\mathrm{LO}} &\equiv \Gamma^{s(4,0)}_{Xf_1f_2} + \Gamma^{s(6,0)}_{Xf_1f_2}\,,\\ \Gamma^s_{X,\mathrm{NLO}} &\equiv \Gamma^s_{X,\mathrm{LO}} + \Gamma^{s(4,1)}_{Xf_1f_2} + \Gamma^{s(6,1)}_{Xf_1f_2}\,,\end{aligned} \tag{A.4.1}$$

where the quantities appearing on the right-hand side are defined in Eq. (5.5.1). Scale uncertainties are obtained as explained in Section 5.4. For brevity, we show only those coefficients which have an absolute numerical prefactor or absolute difference between the upper and lower scale uncertainties of greater than 1% of the LO SM result after factoring out the appropriate v_σ^2; results omitted for this reason are indicated by ... in the equations that follow.

A.4.1 $W \to \tau\nu$ decay

For W decay in the α-scheme we find

$$\Gamma^\alpha_{W,\mathrm{LO}} = 234.6^{+1.8}_{-1.8}\ \mathrm{MeV} + v_\alpha^2\Gamma^{\alpha(4,0)}_{W\tau\nu_\tau}\Big\{3.733^{+0.132}_{-0.132}C_{HWB} + 2.000^{+0.034}_{-0.034}C^{(3)}_{\substack{Hl\\33}} + 1.742^{+0.120}_{-0.120}C_{HD}$$

$$+ 0.000^{+0.189}_{-0.189} C^{(1)}_{\substack{Hq \\ 33}} + 0.000^{+0.182}_{-0.182} C_{\substack{Hu \\ 33}} + 0.000^{+0.066}_{-0.066} C_{\substack{uB \\ 33}} + 0.000^{+0.059}_{-0.059} C_{\substack{uW \\ 33}}$$
$$+ 0.000^{+0.046}_{-0.046} C^{(3)}_{\substack{lq \\ 3333}} + 0.000^{+0.008}_{-0.008} \left(C_{HB} + C_{HW} + C_W + \sum_{i=1,2,3} C^{(3)}_{\substack{Hq \\ ii}} + \sum_{j=1,2} C^{(3)}_{\substack{lq \\ 33jj}} \right)$$
$$+ 0.000^{+0.007}_{-0.007} C_{H\Box} + 0.000^{+0.005}_{-0.005} \sum_{j=1,2} C_{\substack{Hu \\ jj}} + \dots \Bigg\}, \tag{A.4.2}$$

$$\Gamma^{\alpha}_{W,\mathrm{NLO}} = 224.6^{+0.1}_{-0.2}\ \mathrm{MeV} + v_\alpha^2 \Gamma^{\alpha(4,0)}_{W\tau\nu_\tau} \Bigg\{ 3.620^{+0.000}_{-0.011} C_{HWB} + 2.043^{+0.000}_{-0.002} C^{(3)}_{\substack{Hl \\ 33}}$$
$$+ 1.713^{+0.000}_{-0.011} C_{HD} - 0.195^{+0.038}_{-0.000} C_{\substack{Hu \\ 33}} + 0.172^{+0.000}_{-0.033} C^{(1)}_{\substack{Hq \\ 33}} - 0.079^{+0.018}_{-0.002} C^{(3)}_{\substack{Hq \\ 33}}$$
$$- 0.072^{+0.008}_{-0.000} C_{\substack{uB \\ 33}} - 0.034^{+0.002}_{-0.000} C^{(3)}_{\substack{lq \\ 3333}} - 0.032^{+0.005}_{-0.000} C_{\substack{uW \\ 33}} - 0.011^{+0.000}_{-0.000} C_W$$
$$+ 0.000^{+0.001}_{-0.026} C_{\substack{uu \\ 3333}} + 0.000^{+0.000}_{-0.023} C^{(1)}_{\substack{qq \\ 3333}} + 0.000^{+0.020}_{-0.000} C^{(1)}_{\substack{qu \\ 3333}}$$
$$+ 0.000^{+0.003}_{-0.012} C^{(3)}_{\substack{qq \\ 3333}} + \dots \Bigg\}, \tag{A.4.3}$$

For the α_μ-scheme we obtain

$$\Gamma^{\alpha_\mu}_{W,\mathrm{LO}} = 227.2^{+0.0}_{-0.0}\ \mathrm{MeV} + v_\mu^2 \Gamma^{\mu(4,0)}_{W\tau\nu_\tau} \Bigg\{ 2.000^{+0.031}_{-0.031} C^{(3)}_{\substack{Hl \\ 33}} - 1.000^{+0.015}_{-0.015} \sum_{j=1,2} C^{(3)}_{\substack{Hl \\ jj}}$$
$$+ 1.000^{+0.004}_{-0.004} C_{\substack{ll \\ 1221}} + 0.000^{+0.044}_{-0.044} C^{(3)}_{\substack{lq \\ 3333}} + 0.000^{+0.026}_{-0.026} \sum_{j=1,2} C^{(3)}_{\substack{lq \\ jj33}} + 0.000^{+0.011}_{-0.011} C_{\substack{ll \\ 1122}}$$
$$+ 0.000^{+0.007}_{-0.007} \sum_{j=1,2} C^{(3)}_{\substack{lq \\ 33jj}} + \dots \Bigg\}, \tag{A.4.4}$$

$$\Gamma^{\alpha_\mu}_{W,\mathrm{NLO}} = 226.5^{+0.0}_{-0.0}\ \mathrm{MeV} + v_\mu^2 \Gamma^{\mu(4,0)}_{W\tau\nu_\tau} \Bigg\{ 2.043^{+0.000}_{-0.001} C^{(3)}_{\substack{Hl \\ 33}} - 1.025^{+0.001}_{-0.000} \sum_{j=1,2} C^{(3)}_{\substack{Hl \\ jj}}$$
$$+ 0.998^{+0.000}_{-0.000} C_{\substack{ll \\ 1221}} - 0.033^{+0.001}_{-0.000} C^{(3)}_{\substack{lq \\ 3333}} + 0.019^{+0.000}_{-0.001} \sum_{j=1,2} C^{(3)}_{\substack{lq \\ jj33}}$$
$$- 0.015^{+0.000}_{-0.000} C_{\substack{ll \\ 1122}} + 0.010^{+0.000}_{-0.000} C_{HWB} + \dots \Bigg\}. \tag{A.4.5}$$

And finally for the LEP scheme, we find

$$\Gamma^{\mathrm{LEP}}_{W,\mathrm{LO}} = 222.7^{+1.1}_{-1.1}\ \mathrm{MeV} + v_\mu^2 \Gamma^{\mathrm{LEP}(4,0)}_{W\tau\nu_\tau} \Bigg\{ - 2.379^{+0.102}_{-0.102} C_{HWB} + 2.000^{+0.019}_{-0.019} C^{(3)}_{\substack{Hl \\ 33}}$$
$$- 1.656^{+0.032}_{-0.032} \sum_{j=1,2} C^{(3)}_{\substack{Hl \\ jj}} + 1.656^{+0.001}_{-0.001} C_{\substack{ll \\ 1221}} - 1.078^{+0.073}_{-0.073} C_{HD} + 0.000^{+0.114}_{-0.114} C^{(1)}_{\substack{Hq \\ 33}}$$
$$+ 0.000^{+0.109}_{-0.109} C_{\substack{Hu \\ 33}} + 0.000^{+0.045}_{-0.045} C^{(3)}_{\substack{lq \\ 3333}} + 0.000^{+0.043}_{-0.043} \sum_{j=1,2} C^{(3)}_{\substack{lq \\ jj33}} + 0.000^{+0.040}_{-0.040} C_{\substack{uB \\ 33}}$$

$$+ 0.000^{+0.037}_{-0.037} C_{\substack{uW \\ 33}} + 0.000^{+0.018}_{-0.018} C_{\substack{ll \\ 1122}} + 0.000^{+0.007}_{-0.007} \sum_{j=1,2} C^{(3)}_{\substack{lq \\ 33jj}} + \dots \Bigg\}, \tag{A.4.6}$$

$$\begin{aligned}
\Gamma^{\text{LEP}}_{W,\text{NLO}} =& 227.2^{+0.0}_{-0.0}\ \text{MeV} + v_\mu^2 \Gamma^{\text{LEP}(4,0)}_{W\tau\nu_\tau} \Bigg\{ - 2.455^{+0.008}_{-0.000} C_{HWB} + 2.091^{+0.001}_{-0.001} C^{(3)}_{\substack{Hl \\ 33}} \\
& - 1.742^{+0.002}_{-0.000} \sum_{j=1,2} C^{(3)}_{\substack{Hl \\ jj}} + 1.697^{+0.000}_{-0.001} C_{\substack{ll \\ 1221}} - 1.165^{+0.012}_{-0.001} C_{HD} + 0.116^{+0.002}_{-0.031} C_{\substack{Hu \\ 33}} \\
& - 0.103^{+0.029}_{-0.002} C^{(1)}_{\substack{Hq \\ 33}} - 0.033^{+0.002}_{-0.002} C^{(3)}_{\substack{lq \\ 3333}} + 0.046^{+0.001}_{-0.010} C^{(3)}_{\substack{Hq \\ 33}} + 0.044^{+0.000}_{-0.008} C_{\substack{uB \\ 33}} \\
& - 0.024^{+0.001}_{-0.000} C_{\substack{ll \\ 1122}} + 0.019^{+0.000}_{-0.006} C_{\substack{uW \\ 33}} + 0.032^{+0.001}_{-0.003} \sum_{j=1,2} C^{(3)}_{\substack{lq \\ jj33}} \\
& + 0.000^{+0.015}_{-0.001} C_{\substack{uu \\ 3333}} + 0.000^{+0.014}_{-0.000} C^{(1)}_{\substack{qq \\ 3333}} + 0.000^{+0.000}_{-0.011} C^{(1)}_{\substack{qu \\ 3333}} + \dots \Bigg\}.
\end{aligned} \tag{A.4.7}$$

A.4.2 $h \to b\bar{b}$ decay

To evaluate scale uncertainties for $h \to b\bar{b}$ we also require the running of $m_b(\mu)$ and $\alpha_s(\mu)$. As with the running of $\alpha(\mu)$, we again use a one-loop fixed-order solution to the RG equations for $m_b(\mu)$ and $\alpha_s(\mu)$ which are given by

$$m_b(\mu) = m_b(M_h)\left[1 + \gamma_b(M_h) \ln\left(\frac{\mu}{M_h}\right)\right], \tag{A.4.8}$$

$$\alpha_s(\mu) = \alpha_s(M_h)\left[1 - \frac{\alpha_s(M_h)}{2\pi}\beta_0 \ln\left(\frac{\mu}{M_h}\right)\right], \tag{A.4.9}$$

where

$$\gamma_b(\mu) = -\frac{3}{2\pi}\left[\alpha_s(\mu) C_F + \alpha(\mu) Q_b^2\right], \qquad \beta_0 = \frac{11}{3} C_A - \frac{4}{3} T_F\, n_f\,, \tag{A.4.10}$$

with

$$C_F = \frac{4}{3}\,, \quad C_A = 3\,, \quad T_F = \frac{1}{2}\,, \quad \text{and} \quad n_f = 5\,.$$

In the α scheme we find

$$\Gamma^{\alpha}_{hbb,\text{LO}} = 2.300^{+0.209}_{-0.209}\ \text{MeV} + v_\alpha^2 \Gamma^{\alpha(4,0)}_{hbb} \Bigg\{ - 1.414^{+0.099}_{-0.099} \frac{v_\alpha}{m_b} C_{\substack{dH \\ 33}} + 3.733^{+0.243}_{-0.243} C_{HWB}$$

$$
\begin{aligned}
&+ 2.000^{+0.084}_{-0.084} C_{H\Box} + 1.242^{+0.034}_{-0.034} C_{HD} + 0.000^{+0.078}_{-0.078} \frac{v_\alpha}{m_b} C^{(1)}_{\substack{quqd \\ 3333}} + 0.000^{+0.067}_{-0.067} \frac{v_\alpha}{m_b} C_{\substack{dW \\ 33}} \\
&+ 0.000^{+0.015}_{-0.015} \frac{v_\alpha}{m_b} C^{(8)}_{\substack{quqd \\ 3333}} + 0.000^{+0.008}_{-0.008} \frac{v_\alpha}{m_b} C_{\substack{Hud \\ 33}} + 0.000^{+0.397}_{-0.397} C_{HG} + 0.000^{+0.213}_{-0.213} C_{\substack{dB \\ 33}} \\
&+ 0.000^{+0.189}_{-0.189} C^{(1)}_{\substack{Hq \\ 33}} + 0.000^{+0.183}_{-0.183} C_{\substack{Hu \\ 33}} + 0.000^{+0.112}_{-0.112} C^{(3)}_{\substack{Hq \\ 33}} + 0.000^{+0.094}_{-0.094} C_{\substack{uW \\ 33}} \\
&+ 0.000^{+0.066}_{-0.066} C_{\substack{uB \\ 33}} + 0.000^{+0.027}_{-0.027} C_{HW} + 0.000^{+0.027}_{-0.027} C_{\substack{uH \\ 33}} + 0.000^{+0.013}_{-0.013} C^{(8)}_{\substack{qd \\ 3333}} \\
&+ 0.000^{+0.011}_{-0.011} C_{\substack{Hd \\ 33}} + 0.000^{+0.009}_{-0.009} C^{(1)}_{\substack{qd \\ 3333}} + 0.000^{+0.008}_{-0.008} \sum_{j=1,2} C^{(3)}_{\substack{Hq \\ jj}} + 0.000^{+0.008}_{-0.008} C_W \\
&+ 0.000^{+0.006}_{-0.006} C_{HB} + 0.000^{+0.005}_{-0.005} \sum_{j=1,2} C_{\substack{Hu \\ jj}} + \dots \Bigg\}, \qquad \text{(A.4.11)}
\end{aligned}
$$

$$
\begin{aligned}
\Gamma^{\alpha}_{hbb,\mathrm{NLO}} =& 2.647^{+0.036}_{-0.119}\ \mathrm{MeV} + v_\alpha^2 \Gamma^{\alpha(4,0)}_{hbb} \Bigg\{ - 1.761^{+0.072}_{-0.030} \frac{v_\alpha}{m_b} C_{\substack{dH \\ 33}} - 0.060^{+0.012}_{-0.020} \frac{v_\alpha}{m_b} C_{\substack{dW \\ 33}} \\
&+ 4.239^{+0.055}_{-0.159} C_{HWB} + 3.094^{+0.704}_{-0.953} C_{HG} + 0.031^{+0.031}_{-0.000} \frac{v_\alpha}{m_b} C^{(1)}_{\substack{quqd \\ 3333}} \\
&+ 2.448^{+0.031}_{-0.083} C_{H\Box} + 1.358^{+0.013}_{-0.042} C_{HD} + 0.009^{+0.003}_{-0.000} \frac{v_\alpha}{g_s m_b} C_{\substack{dG \\ 33}} \\
&+ 0.006^{+0.005}_{-0.001} \frac{v_\alpha}{m_b} C^{(8)}_{\substack{quqd \\ 3333}} - 0.004^{+0.003}_{-0.001} \frac{v_\alpha}{m_b} C_{\substack{Hud \\ 33}} - 0.116^{+0.014}_{-0.024} C^{(3)}_{\substack{Hq \\ 33}} \\
&- 0.079^{+0.012}_{-0.032} C_{\substack{Hu \\ 33}} + 0.058^{+0.035}_{-0.013} C^{(1)}_{\substack{Hq \\ 33}} - 0.040^{+0.004}_{-0.025} C_{\substack{uW \\ 33}} - 0.031^{+0.005}_{-0.011} C_{\substack{uH \\ 33}} \\
&- 0.030^{+0.001}_{-0.015} C_{\substack{uB \\ 33}} + 0.028^{+0.007}_{-0.013} C_{HW} + 0.024^{+0.000}_{-0.000} C_H - 0.014^{+0.010}_{-0.000} C^{(8)}_{\substack{qd \\ 3333}} \\
&- 0.011^{+0.022}_{-0.079} C_{\substack{dB \\ 33}} - 0.010^{+0.007}_{-0.001} C^{(1)}_{\substack{qd \\ 3333}} + 0.000^{+0.072}_{-0.049} \frac{1}{g_s} C_{\substack{uG \\ 33}} \\
&+ 0.000^{+0.000}_{-0.020} C^{(3)}_{\substack{qq \\ 3333}} + 0.000^{+0.000}_{-0.018} C_{\substack{uu \\ 3333}} + 0.000^{+0.016}_{-0.000} C^{(1)}_{\substack{qu \\ 3333}} + 0.000^{+0.000}_{-0.016} C^{(1)}_{\substack{qq \\ 3333}} \\
&+ \dots \Bigg\}. \qquad \text{(A.4.12)}
\end{aligned}
$$

Here and in other numerical results for $h \to b\bar{b}$, we have left enhancement factors such as v_α/m_b symbolic, with the exception of $C_{\substack{dB \\ 33}}$. Scale variations of the LO SMEFT results fail to include the NLO results of the operators first appearing at LO in all schemes, where only one operator is within 2σ region. However, for operators first appearing at NLO the NLO result is typically included in the LO scale-variation band. More reliable uncertainty estimates can be made by varying the renormalisation scales of the b-quark mass and Wilson coefficients independently as in [29].

In the α_μ scheme one finds

$$\begin{aligned}\Gamma^{\alpha_\mu}_{hbb,\mathrm{LO}} =& 2.217^{+0.221}_{-0.221}\ \mathrm{MeV} + v_\mu^2 \Gamma^{\alpha_\mu(4,0)}_{hbb} \Bigg\{ -1.414^{+0.095}_{-0.095} \frac{v_\mu}{m_b} C_{\substack{dH\\33}} + 2.000^{+0.095}_{-0.095} C_{H\Box} \\ &+ 1.000^{+0.104}_{-0.104} C_{\substack{ll\\1221}} - 1.000^{+0.086}_{-0.086} \sum_{j=1,2} C^{(3)}_{\substack{Hl\\jj}} - 0.500^{+0.021}_{-0.021} C_{HD} \\ &+ 0.000^{+0.074}_{-0.074} \frac{v_\mu}{m_b} C^{(1)}_{\substack{quqd\\3333}} + 0.000^{+0.063}_{-0.063} \frac{v_\mu}{m_b} C_{\substack{dW\\33}} + 0.000^{+0.014}_{-0.014} \frac{v_\mu}{m_b} C^{(8)}_{\substack{quqd\\3333}} \\ &+ 0.000^{+0.007}_{-0.007} \frac{v_\mu}{m_b} C_{\substack{Hud\\33}} + 0.000^{+0.397}_{-0.397} C_{HG} + 0.000^{+0.206}_{-0.206} C_{\substack{dB\\33}} + 0.000^{+0.115}_{-0.115} C^{(3)}_{\substack{Hq\\33}} \\ &+ 0.000^{+0.034}_{-0.034} C_{\substack{uW\\33}} + 0.000^{+0.034}_{-0.034} C_{HW} + 0.000^{+0.026}_{-0.026} C_{\substack{uH\\33}} + 0.000^{+0.026}_{-0.026} \sum_{j=1,2} C^{(3)}_{\substack{lq\\jj33}} \\ &+ 0.000^{+0.012}_{-0.012} C^{(8)}_{\substack{qd\\3333}} + 0.000^{+0.011}_{-0.011} C_{\substack{ll\\1122}} + 0.000^{+0.009}_{-0.009} C^{(1)}_{\substack{qd\\3333}} + 0.000^{+0.008}_{-0.008} C_{\substack{Hd\\33}} + ... \Bigg\},\end{aligned} \tag{A.4.13}$$

$$\begin{aligned}\Gamma^{\alpha_\mu}_{hbb,\mathrm{NLO}} =& 2.650^{+0.043}_{-0.129}\ \mathrm{MeV} + v_\mu^2 \Gamma^{\alpha_\mu(4,0)}_{hbb} \Bigg\{ -1.728^{+0.068}_{-0.029} \frac{v_\mu}{m_b} C_{\substack{dH\\33}} - 0.057^{+0.009}_{-0.018} \frac{v_\mu}{m_b} C_{\substack{dW\\33}} \\ &+ 3.094^{+0.698}_{-0.946} C_{HG} + 2.447^{+0.035}_{-0.084} C_{H\Box} + 0.030^{+0.028}_{-0.000} \frac{v_\mu}{m_b} C^{(1)}_{\substack{quqd\\3333}} \\ &- 1.212^{+0.054}_{-0.020} \sum_{j=1,2} C^{(3)}_{\substack{Hl\\jj}} + 1.195^{+0.019}_{-0.060} C_{\substack{ll\\1221}} - 0.612^{+0.020}_{-0.008} C_{HD} \\ &+ 0.009^{+0.003}_{-0.000} \frac{v_\mu}{g_s m_b} C_{\substack{dG\\33}} + 0.006^{+0.005}_{-0.001} \frac{v_\mu}{m_b} C^{(8)}_{\substack{quqd\\3333}} - 0.004^{+0.002}_{-0.001} \frac{v_\mu}{m_b} C_{\substack{Hud\\33}} \\ &- 0.046^{+0.001}_{-0.008} C_{\substack{uW\\33}} - 0.031^{+0.008}_{-0.038} C^{(3)}_{\substack{Hq\\33}} - 0.030^{+0.004}_{-0.010} C_{\substack{uH\\33}} \\ &+ 0.028^{+0.006}_{-0.015} C_{HW} + 0.024^{+0.000}_{-0.000} C_H - 0.022^{+0.007}_{-0.002} C_{\substack{ll\\1122}} - 0.013^{+0.009}_{-0.000} C^{(8)}_{\substack{qd\\3333}} \\ &- 0.011^{+0.016}_{-0.073} C_{\substack{dB\\33}} + 0.010^{+0.001}_{-0.001} C_{HB} - 0.010^{+0.001}_{-0.001} C_{HWB} \\ &+ 0.003^{+0.010}_{-0.000} \sum_{j=1,2} C^{(3)}_{\substack{lq\\jj33}} + 0.000^{+0.059}_{-0.083} \frac{1}{g_s} C_{\substack{uG\\33}} + 0.000^{+0.000}_{-0.010} C^{(3)}_{\substack{qq\\3333}} + ... \Bigg\}.\end{aligned} \tag{A.4.14}$$

In the LEP scheme one finds

$$\begin{aligned}\Gamma^{\mathrm{LEP}}_{hbb,\mathrm{LO}} =& 2.217^{+0.221}_{-0.221}\ \mathrm{MeV} + v_\mu^2 \Gamma^{\mathrm{LEP}(4,0)}_{hbb} \Bigg\{ -1.414^{+0.095}_{-0.095} \frac{v_\mu}{m_b} C_{\substack{dH\\33}} + 2.000^{+0.095}_{-0.095} C_{H\Box} \\ &+ 1.000^{+0.104}_{-0.104} C_{\substack{ll\\1221}} - 1.000^{+0.085}_{-0.085} \sum_{j=1,2} C^{(3)}_{\substack{Hl\\jj}} - 0.500^{+0.020}_{-0.020} C_{HD} \\ &+ 0.000^{+0.074}_{-0.074} \frac{v_\mu}{m_b} C^{(1)}_{\substack{quqd\\3333}} + 0.000^{+0.062}_{-0.062} \frac{v_\mu}{m_b} C_{\substack{dW\\33}} + 0.000^{+0.014}_{-0.014} \frac{v_\mu}{m_b} C^{(8)}_{\substack{quqd\\3333}}\end{aligned}$$

$$+ 0.000^{+0.008}_{-0.008}\frac{v_\mu}{m_b}C_{\substack{Hud\\33}} + 0.000^{+0.397}_{-0.397}C_{HG} + 0.000^{+0.207}_{-0.207}C_{\substack{dB\\33}}$$
$$+ 0.000^{+0.115}_{-0.115}C^{(3)}_{\substack{Hq\\33}} + 0.000^{+0.034}_{-0.034}C_{\substack{uW\\33}} + 0.000^{+0.033}_{-0.033}C_{HW}$$
$$+ 0.000^{+0.026}_{-0.026}C_{\substack{uH\\33}} + 0.000^{+0.026}_{-0.026}\sum_{j=1,2}C^{(3)}_{\substack{lq\\jj33}} + 0.000^{+0.012}_{-0.012}C^{(8)}_{\substack{qd\\3333}}$$
$$+ 0.000^{+0.011}_{-0.011}C_{\substack{ll\\1122}} + 0.000^{+0.009}_{-0.009}C^{(1)}_{\substack{qd\\3333}} + 0.000^{+0.008}_{-0.008}C_{\substack{Hd\\33}} + ...\Bigg\}, \quad \text{(A.4.15)}$$

$$\Gamma^{\text{LEP}}_{hbb,\text{NLO}} = 2.650^{+0.049}_{-0.124}\ \text{MeV} + v_\mu^2\Gamma^{\text{LEP}(4,0)}_{hbb}\Bigg\{ - 1.728^{+0.068}_{-0.029}\frac{v_\mu}{m_b}C_{\substack{dH\\33}} - 0.056^{+0.009}_{-0.018}\frac{v_\mu}{m_b}C_{\substack{dW\\33}}$$
$$+ 3.094^{+0.698}_{-0.946}C_{HG} + 2.447^{+0.035}_{-0.084}C_{H\Box} + 0.030^{+0.028}_{-0.000}\frac{v_\mu}{m_b}C^{(1)}_{\substack{quqd\\3333}}$$
$$- 1.210^{+0.054}_{-0.020}\sum_{j=1,2}C^{(3)}_{\substack{Hl\\jj}} + 1.193^{+0.019}_{-0.060}C_{\substack{ll\\1221}} - 0.609^{+0.020}_{-0.008}C_{HD}$$
$$+ 0.009^{+0.003}_{-0.000}\frac{v_\mu}{m_b}C_{\substack{dG\\33}} + 0.006^{+0.005}_{-0.001}\frac{v_\mu}{m_b}C^{(8)}_{\substack{quqd\\3333}} - 0.003^{+0.002}_{-0.001}\frac{v_\mu}{m_b}C_{\substack{Hud\\33}}$$
$$- 0.045^{+0.001}_{-0.008}C_{\substack{uW\\33}} - 0.031^{+0.008}_{-0.038}C^{(3)}_{\substack{Hq\\33}} - 0.030^{+0.004}_{-0.010}C_{\substack{uH\\33}}$$
$$+ 0.028^{+0.006}_{-0.015}C_{HW} + 0.024^{+0.000}_{-0.000}C_H - 0.022^{+0.007}_{-0.002}C_{\substack{ll\\1122}} - 0.013^{+0.009}_{-0.000}C^{(8)}_{\substack{qd\\3333}}$$
$$- 0.011^{+0.016}_{-0.074}C_{\substack{dB\\33}} + 0.003^{+0.010}_{-0.000}\sum_{j=1,2}C^{(3)}_{\substack{lq\\jj33}} + 0.011^{+0.001}_{-0.001}C_{HB}$$
$$+ 0.000^{+0.059}_{-0.083}C_{\substack{uG\\33}} + 0.000^{+0.000}_{-0.010}C^{(3)}_{\substack{qq\\3333}} + ...\Bigg\}. \quad \text{(A.4.16)}$$

A.4.3 $Z \to \tau\tau$ decay

We present results for Z-boson decay in the three different schemes, using $\mu = M_Z$ as the central scale. In the α-scheme we find

$$\Gamma^{\alpha}_{Z,\text{LO}} = 86.75^{+0.067}_{-0.067}\ \text{MeV} + v_\alpha^2\Gamma^{\alpha(4,0)}_{Z\tau\tau}\Bigg\{4.088^{+0.144}_{-0.144}C_{HWB} + 2.190^{+0.056}_{-0.056}C^{(1)}_{\substack{Hl\\33}}$$
$$+ 2.190^{+0.038}_{-0.038}C^{(3)}_{\substack{Hl\\33}} - 1.764^{+0.051}_{-0.051}C_{\substack{He\\33}} + 1.573^{+0.109}_{-0.109}C_{HD} + 0.000^{+0.172}_{-0.172}C^{(1)}_{\substack{Hq\\33}}$$
$$+ 0.000^{+0.163}_{-0.163}C_{\substack{Hu\\33}} + 0.000^{+0.072}_{-0.072}C_{\substack{uB\\33}} + 0.000^{+0.064}_{-0.064}C_{\substack{uW\\33}} + 0.000^{+0.060}_{-0.060}C^{(1)}_{\substack{lq\\3333}}$$
$$+ 0.000^{+0.057}_{-0.057}C_{\substack{lu\\3333}} + 0.000^{+0.050}_{-0.050}C^{(3)}_{\substack{lq\\3333}} + 0.000^{+0.048}_{-0.048}C_{\substack{qe\\3333}} + 0.000^{+0.046}_{-0.046}C_{\substack{eu\\3333}}$$
$$+ 0.000^{+0.008}_{-0.008}\left(\sum_{j=1,2}C^{(3)}_{\substack{lq\\33jj}} + \sum_{i=1,2,3}C^{(3)}_{\substack{Hq\\ii}} + C_{HW} + C_{HB}\right) + 0.000^{+0.008}_{-0.008}C_W$$

$$+ 0.000^{+0.007}_{-0.007} C_{H\Box} + 0.000^{+0.006}_{-0.006} \sum_{j=1,2} C_{\substack{Hu \\ jj}} + \dots \Big\}, \tag{A.4.17}$$

$$\begin{aligned}
\Gamma^{\alpha}_{Z,\mathrm{NLO}} = 83.25^{+0.04}_{-0.06}\ \mathrm{MeV} + v_\alpha^2 \Gamma^{\alpha(4,0)}_{Z\tau\tau} \Big\{ & 3.867^{+0.003}_{-0.016} C_{HWB} + 2.196^{+0.000}_{-0.004} C^{(1)}_{\substack{Hl \\ 33}} \\
& + 2.179^{+0.000}_{-0.001} C^{(3)}_{\substack{Hl \\ 33}} - 1.899^{+0.008}_{-0.002} C_{\substack{He \\ 33}} + 1.406^{+0.002}_{-0.021} C_{HD} - 0.143^{+0.031}_{-0.000} C_{\substack{Hu \\ 33}} \\
& + 0.117^{+0.000}_{-0.032} C^{(1)}_{\substack{Hq \\ 33}} - 0.074^{+0.014}_{-0.001} C^{(3)}_{\substack{Hq \\ 33}} - 0.065^{+0.007}_{-0.000} C_{\substack{uB \\ 33}} - 0.054^{+0.001}_{-0.001} C^{(3)}_{\substack{lq \\ 3333}} \\
& - 0.051^{+0.004}_{-0.000} C_{\substack{lu \\ 3333}} + 0.043^{+0.000}_{-0.003} C^{(1)}_{\substack{lq \\ 3333}} + 0.041^{+0.002}_{-0.006} C_{\substack{eu \\ 3333}} - 0.035^{+0.007}_{-0.002} C_{\substack{qe \\ 3333}} \\
& - 0.016^{+0.008}_{-0.000} C_{\substack{uW \\ 33}} - 0.011^{+0.001}_{-0.000} C_W - 0.010^{+0.000}_{-0.000} \sum_{j=1,2} C^{(3)}_{\substack{lq \\ 33jj}} + 0.000^{+0.000}_{-0.021} C_{\substack{uu \\ 3333}} \\
& + 0.000^{+0.000}_{-0.019} C^{(1)}_{\substack{qq \\ 3333}} + 0.000^{+0.016}_{-0.000} C^{(1)}_{\substack{qu \\ 3333}} + 0.000^{+0.002}_{-0.010} C^{(3)}_{\substack{qq \\ 3333}} + \dots \Big\}.
\end{aligned} \tag{A.4.18}$$

In the α_μ-scheme we obtain

$$\begin{aligned}
\Gamma^{\alpha_\mu}_{Z,\mathrm{LO}} = 83.91^{+0.00}_{-0.00}\ \mathrm{MeV} + v_\mu^2 \Gamma^{\mu(4,0)}_{Z\tau\tau} \Big\{ & 2.190^{+0.057}_{-0.057} C^{(1)}_{\substack{Hl \\ 33}} + 2.190^{+0.034}_{-0.034} C^{(3)}_{\substack{Hl \\ 33}} - 1.764^{+0.046}_{-0.046} C_{\substack{He \\ 33}} \\
& - 1.000^{+0.015}_{-0.015} \sum_{j=1,2} C^{(3)}_{\substack{Hl \\ jj}} + 1.000^{+0.004}_{-0.004} C_{\substack{ll \\ 1221}} + 0.355^{+0.012}_{-0.012} C_{HWB} - 0.169^{+0.011}_{-0.011} C_{HD} \\
& + 0.000^{+0.058}_{-0.058} C^{(1)}_{\substack{lq \\ 3333}} + 0.000^{+0.055}_{-0.055} C_{\substack{lu \\ 3333}} + 0.000^{+0.049}_{-0.049} C^{(3)}_{\substack{lq \\ 3333}} + 0.000^{+0.046}_{-0.046} C_{\substack{qe \\ 3333}} \\
& + 0.000^{+0.045}_{-0.045} C_{\substack{eu \\ 3333}} + 0.000^{+0.026}_{-0.026} \sum_{j=1,2} C^{(3)}_{\substack{lq \\ jj33}} + 0.000^{+0.018}_{-0.018} C_{\substack{Hu \\ 33}} + 0.000^{+0.017}_{-0.017} C^{(1)}_{\substack{Hq \\ 33}} \\
& + 0.000^{+0.011}_{-0.011} C_{\substack{ll \\ 1122}} + 0.000^{+0.008}_{-0.008} \sum_{j=1,2} C^{(3)}_{\substack{lq \\ 33jj}} + 0.000^{+0.006}_{-0.006} C_{\substack{uB \\ 33}} \\
& + 0.000^{+0.005}_{-0.005} C_{\substack{uW \\ 33}} + \dots \Big\},
\end{aligned} \tag{A.4.19}$$

$$\begin{aligned}
\Gamma^{\alpha_\mu}_{Z,\mathrm{NLO}} = 83.92^{+0.00}_{-0.00}\ \mathrm{MeV} + v_\mu^2 \Gamma^{\mu(4,0)}_{Z\tau\tau} \Big\{ & 2.193^{+0.000}_{-0.003} C^{(1)}_{\substack{Hl \\ 33}} + 2.181^{+0.000}_{-0.001} C^{(3)}_{\substack{Hl \\ 33}} - 1.897^{+0.006}_{-0.002} C_{\substack{He \\ 33}} \\
& - 1.029^{+0.001}_{-0.000} \sum_{j=1,2} C^{(3)}_{\substack{Hl \\ jj}} + 1.006^{+0.000}_{-0.000} C_{\substack{ll \\ 1221}} - 0.289^{+0.009}_{-0.007} C_{HD} + 0.258^{+0.003}_{-0.004} C_{HWB} \\
& - 0.053^{+0.001}_{-0.001} C^{(3)}_{\substack{lq \\ 3333}} - 0.049^{+0.003}_{-0.000} C_{\substack{lu \\ 3333}} + 0.042^{+0.000}_{-0.002} C^{(1)}_{\substack{lq \\ 3333}} + 0.040^{+0.002}_{-0.005} C_{\substack{eu \\ 3333}} \\
& - 0.034^{+0.006}_{-0.002} C_{\substack{qe \\ 3333}} - 0.020^{+0.016}_{-0.012} C^{(1)}_{\substack{Hq \\ 33}} + 0.018^{+0.011}_{-0.016} C_{\substack{Hu \\ 33}} - 0.017^{+0.000}_{-0.000} C_{\substack{ll \\ 1122}} \\
& + 0.015^{+0.000}_{-0.001} \sum_{j=1,2} C^{(3)}_{\substack{lq \\ jj33}} + \dots \Big\},
\end{aligned} \tag{A.4.20}$$

and in the LEP-scheme we find

$$\begin{aligned}\Gamma^{\rm LEP}_{Z,\rm LO} =& 83.30^{+0.11}_{-0.11}\ \text{MeV} + v_\mu^2\Gamma^{\rm LEP(4,0)}_{Z\tau\tau}\Big\{2.121^{+0.035}_{-0.035}C^{(1)}_{\substack{Hl\\33}} + 2.121^{+0.012}_{-0.012}C^{(3)}_{\substack{Hl\\33}}\\ &- 1.863^{+0.069}_{-0.069}C_{\substack{He\\33}} + 1.173^{+0.031}_{-0.031}C_{\substack{ll\\1221}} - 1.173^{+0.008}_{-0.008}\sum_{j=1,2}C^{(3)}_{\substack{Hl\\jj}} - 0.587^{+0.026}_{-0.026}C_{HD}\\ &- 0.410^{+0.046}_{-0.046}C_{HWB} + 0.000^{+0.061}_{-0.061}C^{(1)}_{\substack{Hq\\33}} + 0.000^{+0.060}_{-0.060}C_{\substack{Hu\\33}} + 0.000^{+0.056}_{-0.056}C^{(1)}_{\substack{lq\\3333}}\\ &+ 0.000^{+0.053}_{-0.053}C_{\substack{lu\\3333}} + 0.000^{+0.049}_{-0.049}C_{\substack{qe\\3333}} + 0.000^{+0.047}_{-0.047}C^{(3)}_{\substack{lq\\3333}} + 0.000^{+0.047}_{-0.047}C_{\substack{eu\\3333}}\\ &+ 0.000^{+0.030}_{-0.030}\sum_{j=1,2}C^{(3)}_{\substack{lq\\jj33}} + 0.000^{+0.013}_{-0.013}C_{\substack{ll\\1122}} + 0.000^{+0.008}_{-0.008}\sum_{j=1,2}C^{(3)}_{\substack{lq\\33jj}}\\ &+ 0.000^{+0.007}_{-0.007}C_{\substack{uB\\33}} + 0.000^{+0.006}_{-0.006}C_{\substack{uW\\33}} + ...\Big\},\end{aligned} \tag{A.4.21}$$

$$\begin{aligned}\Gamma^{\rm LEP}_{Z,\rm NLO} =& 84.12^{+0.00}_{-0.03}\ \text{MeV} + v_\mu^2\Gamma^{\rm LEP(4,0)}_{Z\tau\tau}\Big\{2.219^{+0.003}_{-0.004}C^{(1)}_{\substack{Hl\\33}} + 2.210^{+0.002}_{-0.001}C^{(3)}_{\substack{Hl\\33}}\\ &- 1.901^{+0.005}_{-0.000}C_{\substack{He\\33}} - 1.254^{+0.000}_{-0.004}\sum_{j=1,2}C^{(3)}_{\substack{Hl\\jj}} + 1.227^{+0.002}_{-0.000}C_{\substack{ll\\1221}} - 0.633^{+0.004}_{-0.003}C_{HD}\\ &- 0.481^{+0.000}_{-0.012}C_{HWB} + 0.055^{+0.002}_{-0.013}C_{\substack{Hu\\33}} - 0.052^{+0.011}_{-0.002}C^{(1)}_{\substack{Hq\\33}} - 0.051^{+0.000}_{-0.002}C^{(3)}_{\substack{lq\\3333}}\\ &- 0.048^{+0.004}_{-0.002}C_{\substack{lu\\3333}} + 0.042^{+0.000}_{-0.004}C_{\substack{eu\\3333}} + 0.041^{+0.002}_{-0.003}C^{(1)}_{\substack{lq\\3333}} - 0.036^{+0.005}_{-0.000}C_{\substack{qe\\3333}}\\ &+ 0.025^{+0.000}_{-0.005}C^{(3)}_{\substack{Hq\\33}} - 0.020^{+0.002}_{-0.000}C_{\substack{ll\\1122}} + 0.017^{+0.003}_{-0.001}\sum_{j=1,2}C^{(3)}_{\substack{lq\\jj33}} + ...\Big\}.\end{aligned} \tag{A.4.22}$$

A.5 Numerical results using universal corrections in SMEFT

For completeness, we present here numerical results for the prefactors of the Wilson coefficients at different perturbative orders for W, h and Z decay which have not been shown in Section 5.6 yet. Table A.2 shows the results for W and h decay in the α scheme. For the LEP scheme, Table A.3 shows the results for W, and Z decay, respectively. The h decay results for the LEP scheme have been omitted since they only have very small (numerical) differences with respect to the numbers in the α_μ scheme, which are presented in Table A.2.

$W \to \tau\nu$	$C^{(3)}_{\substack{Hl \\ jj}}$	$C^{(3)}_{\substack{lq \\ jj33}}$	$C_{\substack{ll \\ 1221}}$
NLO	$-1.025^{+0.001}_{-0.000}$	$0.019^{+0.000}_{-0.001}$	$0.998^{+0.000}_{-0.000}$
NLO_t	$-1.019^{+0.001}_{-0.000}$	$0.019^{+0.004}_{-0.005}$	$1.000^{+0.002}_{-0.002}$
LO	$-1.000^{+0.015}_{-0.015}$	$0.000^{+0.026}_{-0.026}$	$1.000^{+0.004}_{-0.004}$
LO_K	$-1.019^{+0.011}_{-0.010}$	$0.019^{+0.000}_{-0.001}$	$1.000^{+0.004}_{-0.004}$

$h \to b\bar{b}$	$C^{(3)}_{\substack{Hl \\ jj}}$	$C^{(3)}_{\substack{lq \\ jj33}}$	$C_{\substack{ll \\ 1221}}$
NLO	$-1.009^{+0.001}_{-0.000}$	$0.003^{+0.000}_{-0.000}$	$0.992^{+0.000}_{-0.000}$
NLO_t	$-1.009^{+0.002}_{-0.001}$	$0.003^{+0.003}_{-0.005}$	$1.006^{+0.002}_{-0.002}$
LO	$-1.000^{+0.014}_{-0.014}$	$0.000^{+0.026}_{-0.026}$	$1.000^{+0.005}_{-0.005}$
LO_K	$-1.003^{+0.013}_{-0.012}$	$0.003^{+0.000}_{-0.001}$	$1.000^{+0.005}_{-0.005}$

Table A.2: The numerical prefactors of the Wilson coefficients in the α_μ scheme appearing in $K_W^{(6,1,\mu)}$ for various perturbative approximations. The tree-level decay rate as well as v_μ^2 have been factored out and the results have been evaluated at the scale of the process. We show the results for W decay (left) and Higgs decay (right).

For results in the α scheme and Z decay in the α_μ scheme, we refer to Tables 5.7 and 5.8 in Section 5.6.

$W \to \tau\nu$	C_{HD}	C_{HWB}	$C^{(3)}_{\substack{Hq\\33}}$	$C_{\substack{Hu\\33}}$	$C^{(1)}_{\substack{Hq\\33}}$	$C_{\substack{uB\\33}}$	$C_{\substack{uW\\33}}$
NLO	$-1.165^{+0.012}_{-0.001}$	$-2.455^{+0.008}_{-0.000}$	$0.046^{+0.001}_{-0.010}$	$0.116^{+0.002}_{-0.031}$	$-0.103^{+0.029}_{-0.002}$	$0.044^{+0.000}_{-0.008}$	$0.019^{+0.000}_{-0.006}$
NLO_t	$-1.143^{+0.009}_{-0.002}$	$-2.434^{+0.024}_{-0.019}$	$0.040^{+0.002}_{-0.011}$	$0.124^{+0.002}_{-0.028}$	$-0.124^{+0.026}_{-0.002}$	$0.045^{+0.000}_{-0.005}$	$0.023^{+0.000}_{-0.004}$
LO	$-1.078^{+0.073}_{-0.073}$	$-2.379^{+0.102}_{-0.102}$	$0.000^{+0.005}_{-0.005}$	$0.000^{+0.109}_{-0.109}$	$0.000^{+0.114}_{-0.114}$	$0.000^{+0.040}_{-0.040}$	$0.000^{+0.037}_{-0.037}$
LO_K	$-1.143^{+0.027}_{-0.018}$	$-2.434^{+0.045}_{-0.039}$	$0.040^{+0.000}_{-0.005}$	$0.124^{+0.000}_{-0.025}$	$-0.124^{+0.027}_{-0.004}$	$0.045^{+0.000}_{-0.007}$	$0.023^{+0.000}_{-0.005}$
	$C^{(3)}_{\substack{Hl\\jj}}$	$C^{(3)}_{\substack{lq\\jj33}}$	$C_{\substack{ll\\1221}}$	$C^{(3)}_{\substack{Hl\\33}}$			
NLO	$-1.742^{+0.002}_{-0.000}$	$0.032^{+0.001}_{-0.003}$	$1.697^{+0.000}_{-0.001}$	$2.091^{+0.001}_{-0.001}$			
NLO_t	$-1.725^{+0.007}_{-0.005}$	$0.032^{+0.007}_{-0.010}$	$1.693^{+0.003}_{-0.003}$	$2.079^{+0.007}_{-0.009}$			
LO	$-1.173^{+0.008}_{-0.008}$	$0.000^{+0.030}_{-0.030}$	$1.656^{+0.001}_{-0.001}$	$2.000^{+0.019}_{-0.019}$			
LO_K	$-1.725^{+0.011}_{-0.009}$	$0.032^{+0.001}_{-0.003}$	$1.693^{+0.001}_{-0.001}$	$2.040^{+0.020}_{-0.020}$			

$Z \to \tau\tau$	C_{HD}	C_{HWB}	$C^{(3)}_{\substack{Hq\\33}}$	$C_{\substack{Hu\\33}}$	$C^{(1)}_{\substack{Hq\\33}}$	$C_{\substack{uB\\33}}$	$C_{\substack{uW\\33}}$
NLO	$-0.633^{+0.004}_{-0.003}$	$-0.481^{+0.000}_{-0.012}$	$0.025^{+0.000}_{-0.005}$	$0.055^{+0.002}_{-0.013}$	$-0.052^{+0.011}_{-0.002}$	$0.007^{+0.002}_{-0.000}$	$0.005^{+0.002}_{-0.000}$
NLO_t	$-0.631^{+0.012}_{-0.009}$	$-0.493^{+0.055}_{-0.057}$	$0.022^{+0.000}_{-0.005}$	$0.056^{+0.001}_{-0.013}$	$-0.056^{+0.012}_{-0.002}$	$0.006^{+0.001}_{-0.000}$	$0.006^{+0.001}_{-0.000}$
LO	$-0.587^{+0.026}_{-0.026}$	$-0.410^{+0.046}_{-0.046}$	$0.000^{+0.001}_{-0.001}$	$0.000^{+0.060}_{-0.060}$	$0.000^{+0.061}_{-0.061}$	$0.000^{+0.007}_{-0.007}$	$0.000^{+0.006}_{-0.006}$
LO_K	$-0.619^{+0.011}_{-0.013}$	$-0.496^{+0.056}_{-0.060}$	$0.022^{+0.000}_{-0.001}$	$0.027^{+0.031}_{-0.034}$	$-0.027^{+0.031}_{-0.034}$	$0.010^{+0.004}_{-0.002}$	$0.004^{+0.003}_{-0.002}$
	$C^{(3)}_{\substack{Hl\\jj}}$	$C^{(3)}_{\substack{lq\\jj33}}$	$C_{\substack{ll\\1221}}$	$C_{\substack{He\\33}}$	$C^{(1)}_{\substack{Hl\\33}}$	$C^{(3)}_{\substack{Hl\\33}}$	
NLO	$-1.254^{+0.000}_{-0.004}$	$0.017^{+0.003}_{-0.001}$	$1.227^{+0.002}_{-0.000}$	$-1.901^{+0.005}_{-0.000}$	$2.219^{+0.003}_{-0.004}$	$2.210^{+0.002}_{-0.001}$	
NLO_t	$-1.244^{+0.025}_{-0.024}$	$0.017^{+0.006}_{-0.006}$	$1.227^{+0.027}_{-0.027}$	$-1.882^{+0.024}_{-0.019}$	$2.197^{+0.016}_{-0.020}$	$2.197^{+0.017}_{-0.020}$	
LO	$-1.174^{+0.008}_{-0.008}$	$0.000^{+0.030}_{-0.030}$	$1.174^{+0.031}_{-0.031}$	$-1.863^{+0.069}_{-0.069}$	$2.121^{+0.035}_{-0.035}$	$2.121^{+0.012}_{-0.012}$	
LO_K	$-1.244^{+0.037}_{-0.037}$	$0.017^{+0.001}_{-0.001}$	$1.227^{+0.030}_{-0.030}$	$-1.855^{+0.069}_{-0.069}$	$2.166^{+0.037}_{-0.037}$	$2.166^{+0.013}_{-0.013}$	

Table A.3: The numerical prefactors of the Wilson coefficients in the LEP scheme appearing in $K_W^{(6,1,\mu)}$ and $\hat{\Delta}_{W,t}^{(6,1,\mu)}$ for various perturbative approximations. The tree-level decay rate as well as v_μ^2 have been factored out and the results have been evaluated at the scale of the process. We show the results for W decay (top) and Z decay (bottom).

Bibliography

[1] M. D. Schwartz, *Quantum Field Theory and the Standard Model*. Cambridge University Press, 2013.

[2] S. L. Glashow, *Partial-symmetries of weak interactions*, *Nuclear Physics* **22** (1961) 579–588.

[3] A. Salam and J. Ward, *Electromagnetic and weak interactions*, *Physics Letters* **13** (1964) 168–171.

[4] S. Weinberg, *A model of leptons*, *Phys. Rev. Lett.* **19** (Nov, 1967) 1264–1266.

[5] J. Goldstone, A. Salam and S. Weinberg, *Broken symmetries*, *Phys. Rev.* **127** (Aug, 1962) 965–970.

[6] O. W. Greenberg, *Spin and unitary-spin independence in a paraquark model of baryons and mesons*, *Phys. Rev. Lett.* **13** (Nov, 1964) 598–602.

[7] M. Y. Han and Y. Nambu, *Three-triplet model with double* SU(3) *symmetry*, *Phys. Rev.* **139** (Aug, 1965) B1006–B1010.

[8] P. W. Higgs, *Broken symmetries and the masses of gauge bosons*, *Phys. Rev. Lett.* **13** (Oct, 1964) 508–509.

[9] F. Englert and R. Brout, *Broken symmetry and the mass of gauge vector mesons*, *Phys. Rev. Lett.* **13** (Aug, 1964) 321–323.

[10] Particle Data Group collaboration, R. L. Workman et al., *Review of Particle Physics*, *PTEP* **2022** (2022) 083C01.

[11] Y. Nambu, *Axial vector current conservation in weak interactions*, *Phys. Rev. Lett.* **4** (Apr, 1960) 380–382.

[12] J. Goldstone, *Field Theories with Superconductor Solutions*, *Nuovo Cim.* **19** (1961) 154–164.

[13] G. Feinberg and S. Weinberg, *Law of Conservation of Muons*, *Phys. Rev. Lett.* **6** (1961) 381–383.

[14] N. Cabibbo, *Unitary Symmetry and Leptonic Decays*, *Phys. Rev. Lett.* **10** (1963) 531–533.

[15] M. Kobayashi and T. Maskawa, *CP Violation in the Renormalizable Theory of Weak Interaction*, *Prog. Theor. Phys.* **49** (1973) 652–657.

[16] L. Wolfenstein, *Parametrization of the Kobayashi-Maskawa Matrix*, *Phys. Rev. Lett.* **51** (1983) 1945.

[17] M. E. Peskin and D. V. Schroeder, *An Introduction to quantum field theory*. Addison-Wesley, Reading, USA, 1995.

[18] A. Zee, *Quantum field theory in a nutshell*. 2003.

[19] J. C. Romao and J. P. Silva, *A resource for signs and Feynman diagrams of the Standard Model*, *Int. J. Mod. Phys. A* **27** (2012) 1230025, [1209.6213].

[20] T. Appelquist and J. Carazzone, *Infrared singularities and massive fields*, *Phys. Rev. D* **11** (May, 1975) 2856–2861.

[21] T. Kinoshita, *Mass singularities of Feynman amplitudes*, *J. Math. Phys.* **3** (1962) 650–677.

[22] T. D. Lee and M. Nauenberg, *Degenerate Systems and Mass Singularities*, *Phys. Rev.* **133** (1964) B1549–B1562.

[23] *Regularization and renormalization of gauge fields*, *Nuclear Physics B* **44** (1972) 189–213.

[24] A. Denner and S. Dittmaier, *Electroweak Radiative Corrections for Collider Physics*, *Phys. Rept.* **864** (2020) 1–163, [1912.06823].

[25] A. Denner and S. Dittmaier, *Electroweak radiative corrections for collider physics*, *Physics Reports* **864** (04, 2020) .

[26] J. Fleischer and F. Jegerlehner, *Radiative Corrections to Higgs Decays in the Extended Weinberg-Salam Model*, *Phys. Rev. D* **23** (1981) 2001–2026.

[27] C. G. Callan, *Broken scale invariance in scalar field theory*, *Phys. Rev. D* **2** (Oct, 1970) 1541–1547.

[28] K. Symanzik, *Small distance behavior in field theory and power counting*, *Commun. Math. Phys.* **18** (1970) 227–246.

[29] J. M. Cullen, B. D. Pecjak and D. J. Scott, *NLO corrections to $h \to b\bar{b}$ decay in SMEFT*, *JHEP* **08** (2019) 173, [1904.06358].

[30] H. Georgi, *Effective field theory*, *Annual Review of Nuclear and Particle Science* **43** (1993) 209–252.

[31] C. N. Leung, S. T. Love and S. Rao, *Low-Energy Manifestations of a New Interaction Scale: Operator Analysis*, *Z. Phys. C* **31** (1986) 433.

[32] S. Weinberg, *Phenomenological Lagrangians*, *Physica A* **96** (1979) 327–340.

[33] W. Buchmuller and D. Wyler, *Effective Lagrangian Analysis of New Interactions and Flavor Conservation*, *Nucl. Phys. B* **268** (1986) 621–653.

[34] K. G. Wilson, *Renormalization group and critical phenomena. 1. Renormalization group and the Kadanoff scaling picture*, *Phys. Rev. B* **4** (1971) 3174–3183.

[35] K. G. Wilson, *Renormalization group and critical phenomena. 2. Phase space cell analysis of critical behavior*, *Phys. Rev. B* **4** (1971) 3184–3205.

[36] D. Skinner, *Quantum Field Theory II*, 2018.

[37] E. Fermi, *Tentativo di una teoria dei raggi β*, *Il Nuovo Cimento (1924-1942)* **11** (1934) 1–19.

[38] I. Brivio and M. Trott, *The standard model as an effective field theory*, *Physics Reports* **793** (2019) 1–98.

[39] G. Isidori, F. Wilsch and D. Wyler, *The Standard Model effective field theory at work*, 2303.16922.

[40] B. Grzadkowski, M. Iskrzynski, M. Misiak and J. Rosiek, *Dimension-Six Terms in the Standard Model Lagrangian*, *JHEP* **10** (2010) 085, [1008.4884].

[41] S. Weinberg, *Varieties of Baryon and Lepton Nonconservation*, *Phys. Rev. D* **22** (1980) 1694.

[42] R. Alonso, E. E. Jenkins, A. V. Manohar and M. Trott, *Renormalization Group Evolution of the Standard Model Dimension Six Operators III: Gauge Coupling Dependence and Phenomenology*, *JHEP* **04** (2014) 159, [1312.2014].

[43] B. Grinstein and M. B. Wise, *Operator analysis for precision electroweak physics*, *Physics Letters B* **265** (1991) 326–334.

[44] I. Stewart, *Effective Field Theory 8.851*, 2013.

[45] E. E. Jenkins, A. V. Manohar and M. Trott, *Renormalization Group Evolution of the Standard Model Dimension Six Operators I: Formalism and lambda Dependence*, *JHEP* **10** (2013) 087, [1308.2627].

[46] E. E. Jenkins, A. V. Manohar and M. Trott, *Renormalization Group Evolution of the Standard Model Dimension Six Operators II: Yukawa Dependence*, *JHEP* **01** (2014) 035, [1310.4838].

[47] J. Fuentes-Martin, P. Ruiz-Femenia, A. Vicente and J. Virto, *DsixTools 2.0: The Effective Field Theory Toolkit*, *Eur. Phys. J. C* **81** (2021) 167, [2010.16341].

[48] J. Aebischer, J. Kumar and D. M. Straub, *Wilson: a Python package for the running and matching of Wilson coefficients above and below the electroweak scale*, *Eur. Phys. J. C* **78** (2018) 1026, [1804.05033].

[49] C. Degrande, G. Durieux, F. Maltoni, K. Mimasu, E. Vryonidou and C. Zhang, *Automated one-loop computations in the standard model effective field theory*, *Phys. Rev. D* **103** (2021) 096024, [2008.11743].

[50] C. Zhang and F. Maltoni, *Top-quark decay into Higgs boson and a light quark at next-to-leading order in QCD*, *Phys. Rev. D* **88** (2013) 054005, [1305.7386].

[51] A. Crivellin, S. Najjari and J. Rosiek, *Lepton Flavor Violation in the Standard Model with general Dimension-Six Operators*, *JHEP* **04** (2014) 167, [1312.0634].

[52] C. Zhang, *Effective field theory approach to top-quark decay at next-to-leading order in QCD*, *Phys. Rev. D* **90** (2014) 014008, [1404.1264].

[53] G. M. Pruna and A. Signer, *The $\mu \to e\gamma$ decay in a systematic effective field theory approach with dimension 6 operators*, *JHEP* **10** (2014) 014, [1408.3565].

[54] R. Grober, M. Muhlleitner, M. Spira and J. Streicher, *NLO QCD Corrections to Higgs Pair Production including Dimension-6 Operators*, *JHEP* **09** (2015) 092, [1504.06577].

[55] C. Hartmann and M. Trott, *On one-loop corrections in the standard model effective field theory; the $\Gamma(h \to \gamma\,\gamma)$ case*, *JHEP* **07** (2015) 151, [1505.02646].

[56] M. Ghezzi, R. Gomez-Ambrosio, G. Passarino and S. Uccirati, *NLO Higgs effective field theory and κ-framework*, *JHEP* **07** (2015) 175, [1505.03706].

[57] C. Hartmann and M. Trott, *Higgs Decay to Two Photons at One Loop in the Standard Model Effective Field Theory*, *Phys. Rev. Lett.* **115** (2015) 191801, [1507.03568].

[58] R. Gauld, B. D. Pecjak and D. J. Scott, *One-loop corrections to $h \to b\bar{b}$ and $h \to \tau\bar{\tau}$ decays in the Standard Model Dimension-6 EFT: four-fermion operators and the large-m_t limit*, *JHEP* **05** (2016) 080, [1512.02508].

[59] J. Aebischer, A. Crivellin, M. Fael and C. Greub, *Matching of gauge invariant dimension-six operators for $b \to s$ and $b \to c$ transitions*, *JHEP* **05** (2016) 037, [1512.02830].

[60] C. Zhang, *Single Top Production at Next-to-Leading Order in the Standard Model Effective Field Theory*, *Phys. Rev. Lett.* **116** (2016) 162002, [1601.06163].

[61] O. Bessidskaia Bylund, F. Maltoni, I. Tsinikos, E. Vryonidou and C. Zhang, *Probing top quark neutral couplings in the Standard Model Effective Field Theory at NLO in QCD*, *JHEP* **05** (2016) 052, [1601.08193].

[62] F. Maltoni, E. Vryonidou and C. Zhang, *Higgs production in association with a top-antitop pair in the Standard Model Effective Field Theory at NLO in QCD*, *JHEP* **10** (2016) 123, [1607.05330].

[63] R. Gauld, B. D. Pecjak and D. J. Scott, *QCD radiative corrections for $h \to b\bar{b}$ in the Standard Model Dimension-6 EFT*, *Phys. Rev. D* **94** (2016) 074045, [1607.06354].

[64] C. Degrande, B. Fuks, K. Mawatari, K. Mimasu and V. Sanz, *Electroweak Higgs boson production in the standard model effective field theory beyond leading order in QCD*, *Eur. Phys. J. C* **77** (2017) 262, [1609.04833].

[65] C. Hartmann, W. Shepherd and M. Trott, *The Z decay width in the SMEFT: y_t and λ corrections at one loop*, *JHEP* **03** (2017) 060, [1611.09879].

[66] M. Grazzini, A. Ilnicka, M. Spira and M. Wiesemann, *Modeling BSM effects on the Higgs transverse-momentum spectrum in an EFT approach*, *JHEP* **03** (2017) 115, [1612.00283].

[67] D. de Florian, I. Fabre and J. Mazzitelli, *Higgs boson pair production at NNLO in QCD including dimension 6 operators*, *JHEP* **10** (2017) 215, [1704.05700].

[68] N. Deutschmann, C. Duhr, F. Maltoni and E. Vryonidou, *Gluon-fusion Higgs production in the Standard Model Effective Field Theory*, *JHEP* **12** (2017) 063, [1708.00460].

[69] J. Baglio, S. Dawson and I. M. Lewis, *An NLO QCD effective field theory analysis of W^+W^- production at the LHC including fermionic operators*, *Phys. Rev. D* **96** (2017) 073003, [1708.03332].

[70] S. Dawson and P. P. Giardino, *Higgs decays to ZZ and $Z\gamma$ in the standard model effective field theory: An NLO analysis*, *Phys. Rev. D* **97** (2018) 093003, [1801.01136].

[71] C. Degrande, F. Maltoni, K. Mimasu, E. Vryonidou and C. Zhang, *Single-top associated production with a Z or H boson at the LHC: the SMEFT interpretation*, *JHEP* **10** (2018) 005, [1804.07773].

[72] E. Vryonidou and C. Zhang, *Dimension-six electroweak top-loop effects in Higgs production and decay*, *JHEP* **08** (2018) 036, [1804.09766].

[73] A. Dedes, M. Paraskevas, J. Rosiek, K. Suxho and L. Trifyllis, *The decay $h \to \gamma\gamma$ in the Standard-Model Effective Field Theory*, *JHEP* **08** (2018) 103, [1805.00302].

[74] M. Grazzini, A. Ilnicka and M. Spira, *Higgs boson production at large transverse momentum within the SMEFT: analytical results*, *Eur. Phys. J. C* **78** (2018) 808, [1806.08832].

[75] S. Dawson and P. P. Giardino, *Electroweak corrections to Higgs boson decays to $\gamma\gamma$ and W^+W^- in standard model EFT*, *Phys. Rev. D* **98** (2018) 095005, [1807.11504].

[76] S. Dawson and A. Ismail, *Standard model EFT corrections to Z boson decays*, *Phys. Rev. D* **98** (2018) 093003, [1808.05948].

[77] S. Dawson, P. P. Giardino and A. Ismail, *Standard model EFT and the Drell-Yan process at high energy*, *Phys. Rev. D* **99** (2019) 035044, [1811.12260].

[78] T. Neumann and Z. E. Sullivan, *Off-Shell Single-Top-Quark Production in the Standard Model Effective Field Theory*, *JHEP* **06** (2019) 022, [1903.11023].

[79] A. Dedes, K. Suxho and L. Trifyllis, *The decay $h \to Z\gamma$ in the Standard-Model Effective Field Theory*, *JHEP* **06** (2019) 115, [1903.12046].

[80] R. Boughezal, C.-Y. Chen, F. Petriello and D. Wiegand, *Top quark decay at next-to-leading order in the Standard Model Effective Field Theory*, *Phys. Rev. D* **100** (2019) 056023, [1907.00997].

[81] S. Dawson and P. P. Giardino, *Electroweak and QCD corrections to Z and W pole observables in the standard model EFT*, *Phys. Rev. D* **101** (2020) 013001, [1909.02000].

[82] J. Baglio, S. Dawson and S. Homiller, *QCD corrections in Standard Model EFT fits to WZ and WW production*, *Phys. Rev. D* **100** (2019) 113010, [1909.11576].

[83] U. Haisch, M. Ruhdorfer, E. Salvioni, E. Venturini and A. Weiler, *Singlet night in Feynman-ville: one-loop matching of a real scalar*, *JHEP* **04** (2020) 164, [2003.05936].

[84] J. M. Cullen and B. D. Pecjak, *Higgs decay to fermion pairs at NLO in SMEFT*, *JHEP* **11** (2020) 079, [2007.15238].

[85] A. David and G. Passarino, *Use and reuse of SMEFT*, 2009.00127.

[86] S. Dittmaier, S. Schuhmacher and M. Stahlhofen, *Integrating out heavy fields in the path integral using the background-field method: general formalism*, *Eur. Phys. J. C* **81** (2021) 826, [2102.12020].

[87] S. Dawson and P. P. Giardino, *New physics through Drell-Yan standard model EFT measurements at NLO*, *Phys. Rev. D* **104** (2021) 073004, [2105.05852].

[88] R. Boughezal, E. Mereghetti and F. Petriello, *Dilepton production in the SMEFT at O(1/Λ4)*, *Phys. Rev. D* **104** (2021) 095022, [2106.05337].

[89] M. Battaglia, M. Grazzini, M. Spira and M. Wiesemann, *Sensitivity to BSM effects in the Higgs p_T spectrum within SMEFT*, *JHEP* **11** (2021) 173, [2109.02987].

[90] J. Kley, T. Theil, E. Venturini and A. Weiler, *Electric dipole moments at one-loop in the dimension-6 SMEFT*, *Eur. Phys. J. C* **82** (2022) 926, [2109.15085].

[91] H. E. Faham, F. Maltoni, K. Mimasu and M. Zaro, *Single top production in association with a WZ pair at the LHC in the SMEFT*, *JHEP* **01** (2022) 100, [2111.03080].

[92] U. Haisch, D. J. Scott, M. Wiesemann, G. Zanderighi and S. Zanoli, *NNLO event generation for $pp \to Zh \to \ell^+\ell^- b\bar{b}$ production in the SM effective field theory*, *JHEP* **07** (2022) 054, [2204.00663].

[93] G. Heinrich, J. Lang and L. Scyboz, *SMEFT predictions for $gg \to hh$ at full NLO QCD and truncation uncertainties*, *JHEP* **08** (2022) 079, [2204.13045].

[94] A. Bhardwaj, C. Englert and P. Stylianou, *Implications of the muon anomalous magnetic moment for the LHC and MUonE*, *Phys. Rev. D* **106** (2022) 075031, [2206.14640].

[95] K. Asteriadis, S. Dawson and D. Fontes, *Double insertions of SMEFT operators in gluon fusion Higgs boson production*, *Phys. Rev. D* **107** (2023) 055038, [2212.03258].

[96] L. Bellafronte, S. Dawson and P. P. Giardino, *The importance of flavor in SMEFT Electroweak Precision Fits*, *JHEP* **05** (2023) 208, [2304.00029].

[97] N. Kidonakis and A. Tonero, *SMEFT chromomagnetic dipole operator contributions to $t\bar{t}$ production at approximate NNLO in QCD*, 2309.16758.

[98] R. Gauld, U. Haisch and L. Schnell, *SMEFT at NNLO+PS: Vh production*, 2311.06107.

[99] G. Heinrich and J. Lang, *Combining chromomagnetic and four-fermion operators with leading SMEFT operators for $gg \to hh$ at NLO QCD*, 2311.15004.

[100] I. Brivio and M. Trott, *Scheming in the SMEFT... and a reparameterization invariance!*, *JHEP* **07** (2017) 148, [1701.06424].

[101] I. Brivio, S. Dawson, J. de Blas, G. Durieux, P. Savard, A. Denner et al., *Electroweak input parameters*, 2111.12515.

[102] D. C. Kennedy and B. W. Lynn, *Electroweak Radiative Corrections with an Effective Lagrangian: Four Fermion Processes*, *Nucl. Phys. B* **322** (1989) 1–54.

[103] F. M. Renard and C. Verzegnassi, *A Z peak subtracted representation of four fermion processes at future e+ e- colliders*, *Phys. Rev. D* **52** (1995) 1369–1376.

[104] A. Ferroglia, G. Ossola and A. Sirlin, *Scale independent calculation of sin**2 theta(eff)**lept*, *Phys. Lett. B* **507** (2001) 147–152, [hep-ph/0103001].

[105] A. Ferroglia, G. Ossola, M. Passera and A. Sirlin, *Simple formulae for sin**2 Theta (eff)(lept), M(W), Gamma(l), and their physical applications*, *Phys. Rev. D* **65** (2002) 113002, [hep-ph/0203224].

[106] M. Chiesa, F. Piccinini and A. Vicini, *Direct determination of* $\sin^2\theta^{\ell}_{eff}$ *at hadron colliders*, *Phys. Rev. D* **100** (2019) 071302, [1906.11569].

[107] S. Amoroso, M. Chiesa, C. L. Del Pio, K. Lipka, F. Piccinini, F. Vazzoler et al., *Probing the weak mixing angle at high energies at the LHC and HL-LHC*, *Phys. Lett. B* **844** (2023) , [2302.10782].

[108] J. M. Gerard, *FERMION MASS SPECTRUM IN SU(2)-L x U(1)*, *Z. Phys. C* **18** (1983) 145.

[109] R. S. Chivukula and H. Georgi, *Composite Technicolor Standard Model*, *Phys. Lett. B* **188** (1987) 99–104.

[110] G. D'Ambrosio, G. F. Giudice, G. Isidori and A. Strumia, *Minimal flavor violation: An Effective field theory approach*, *Nucl. Phys. B* **645** (2002) 155–187, [hep-ph/0207036].

[111] A. Alloul, N. D. Christensen, C. Degrande, C. Duhr and B. Fuks, *FeynRules 2.0 - A complete toolbox for tree-level phenomenology*, *Comput. Phys. Commun.* **185** (2014) 2250–2300, [1310.1921].

[112] I. Brivio, Y. Jiang and M. Trott, *The SMEFTsim package, theory and tools*, *JHEP* **12** (2017) 070, [1709.06492].

[113] I. Brivio, *SMEFTsim 3.0 — a practical guide*, *JHEP* **04** (2021) 073, [2012.11343].

[114] T. Hahn, S. Paßehr and C. Schappacher, *FormCalc 9 and Extensions*, *PoS* **LL2016** (2016) 068, [1604.04611].

[115] T. Hahn and M. Perez-Victoria, *Automatized one loop calculations in four-dimensions and D-dimensions*, *Comput. Phys. Commun.* **118** (1999) 153–165, [hep-ph/9807565].

[116] T. Hahn, *Generating Feynman diagrams and amplitudes with FeynArts 3*, *Comput. Phys. Commun.* **140** (2001) 418–431, [hep-ph/0012260].

[117] H. H. Patel, *Package-X: A Mathematica package for the analytic calculation of one-loop integrals*, *Comput. Phys. Commun.* **197** (2015) 276–290, [1503.01469].

[118] S. Herrlich and U. Nierste, *Evanescent operators, scheme dependences and double insertions*, *Nucl. Phys. B* **455** (1995) 39–58, [hep-ph/9412375].

[119] W. Dekens and P. Stoffer, *Low-energy effective field theory below the electroweak scale: matching at one loop*, *JHEP* **10** (2019) 197, [1908.05295].

[120] A. Celis, J. Fuentes-Martin, A. Vicente and J. Virto, *DsixTools: The Standard Model Effective Field Theory Toolkit*, *Eur. Phys. J. C* **77** (2017) 405, [1704.04504].

[121] M. Awramik, M. Czakon, A. Freitas and G. Weiglein, *Precise prediction for the W boson mass in the standard model*, *Phys. Rev. D* **69** (2004) 053006, [hep-ph/0311148].

[122] F. Halzen and B. A. Kniehl, Δr *beyond one loop*, *Nucl. Phys. B* **353** (1991) 567–590.

[123] M. Consoli, W. Hollik and F. Jegerlehner, *The Effect of the Top Quark on the M(W)-M(Z) Interdependence and Possible Decoupling of Heavy Fermions from Low-Energy Physics*, *Phys. Lett. B* **227** (1989) 167–170.

[124] A. Denner, *Techniques for calculation of electroweak radiative corrections at the one loop level and results for W physics at LEP-200*, *Fortsch. Phys.* **41** (1993) 307–420, [0709.1075].

[125] ALEPH, DELPHI, L3, OPAL, SLD, LEP Electroweak Working Group, SLD Electroweak Group, SLD Heavy Flavour Group collaboration, S. Schael et al., *Precision electroweak measurements on the Z resonance*, *Phys. Rept.* **427** (2006) 257–454, [hep-ex/0509008].

[126] CDF, D0 collaboration, T. A. Aaltonen et al., *Tevatron Run II combination of the effective leptonic electroweak mixing angle*, *Phys. Rev. D* **97** (2018) 112007, [1801.06283].

[127] ATLAS collaboration, G. Aad et al., *Measurement of the forward-backward asymmetry of electron and muon pair-production in pp collisions at $\sqrt{s}$ = 7 TeV with the ATLAS detector*, *JHEP* **09** (2015) 049, [1503.03709].

[128] ATLAS collaboration, *Measurement of the effective leptonic weak mixing angle using electron and muon pairs from Z-boson decay in the ATLAS experiment at $\sqrt{s} = 8$ TeV*, .

[129] CMS collaboration, A. M. Sirunyan et al., *Measurement of the weak mixing angle using the forward-backward asymmetry of Drell-Yan events in pp collisions at 8 TeV*, *Eur. Phys. J. C* **78** (2018) 701, [1806.00863].

[130] LHCb collaboration, R. Aaij et al., *Measurement of the forward-backward asymmetry in $Z/\gamma^* \to \mu^+\mu^-$ decays and determination of the effective weak mixing angle*, *JHEP* **11** (2015) 190, [1509.07645].

[131] N. Berger et al., *Measuring the weak mixing angle with the P2 experiment at MESA*, *J. Univ. Sci. Tech. China* **46** (2016) 481–487, [1511.03934].

[132] MOLLER collaboration, J. Benesch et al., *The MOLLER Experiment: An Ultra-Precise Measurement of the Weak Mixing Angle Using Møller Scattering*, 1411.4088.

[133] SoLID collaboration, J. P. Chen, H. Gao, T. K. Hemmick, Z. E. Meziani and P. A. Souder, *A White Paper on SoLID (Solenoidal Large Intensity Device)*, 1409.7741.

[134] Jefferson Lab SoLID collaboration, J. Arrington et al., *The solenoidal large intensity device (SoLID) for JLab 12 GeV*, *J. Phys. G* **50** (2023) 110501, [2209.13357].

[135] S. Dawson and P. P. Giardino, *Flavorful electroweak precision observables in the Standard Model effective field theory*, *Phys. Rev. D* **105** (2022) 073006, [2201.09887].